SMART URBAN ENVIRONMENTAL HEALTH FROM MULTI-SCALE, MULTIMEDIA, MULTI-EXPOSURE, MULTI-TARGET PERSPECTIVES

EDITED BY: Hongtao Yi, Chuanrong Zhang, Min Chen and Fei Li

PUBLISHED IN: Frontiers in Public Health

frontiers Research Topics

frontiers

ISSN 1664-8714
ISBN 978-2-83250-454-3
DOI 10.3389/978-2-83250-454-3

About Frontiers

Frontiers is more than just an open-access publisher of scholarly articles: it is a pioneering approach to the world of academia, radically improving the way scholarly research is managed. The grand vision of Frontiers is a world where all people have an equal opportunity to seek, share and generate knowledge. Frontiers provides immediate and permanent online open access to all its publications, but this alone is not enough to realize our grand goals.

Frontiers Journal Series

The Frontiers Journal Series is a multi-tier and interdisciplinary set of open-access, online journals, promising a paradigm shift from the current review, selection and dissemination processes in academic publishing. All Frontiers journals are driven by researchers for researchers; therefore, they constitute a service to the scholarly community. At the same time, the Frontiers Journal Series operates on a revolutionary invention, the tiered publishing system, initially addressing specific communities of scholars, and gradually climbing up to broader public understanding, thus serving the interests of the lay society, too.

Dedication to Quality

Each Frontiers article is a landmark of the highest quality, thanks to genuinely collaborative interactions between authors and review editors, who include some of the world's best academicians. Research must be certified by peers before entering a stream of knowledge that may eventually reach the public - and shape society; therefore, Frontiers only applies the most rigorous and unbiased reviews.
Frontiers revolutionizes research publishing by freely delivering the most outstanding research, evaluated with no bias from both the academic and social point of view. By applying the most advanced information technologies, Frontiers is catapulting scholarly publishing into a new generation.

What are Frontiers Research Topics?

Frontiers Research Topics are very popular trademarks of the Frontiers Journals Series: they are collections of at least ten articles, all centered on a particular subject. With their unique mix of varied contributions from Original Research to Review Articles, Frontiers Research Topics unify the most influential researchers, the latest key findings and historical advances in a hot research area! Find out more on how to host your own Frontiers Research Topic or contribute to one as an author by contacting the Frontiers Editorial Office: frontiersin.org/about/contact

SMART URBAN ENVIRONMENTAL HEALTH FROM MULTI-SCALE, MULTIMEDIA, MULTI-EXPOSURE, MULTI-TARGET PERSPECTIVES

Topic Editors:
Hongtao Yi, The Ohio State University, United States
Chuanrong Zhang, University of Connecticut, United States
Min Chen, Nanjing Normal University, China
Fei Li, Zhongnan University of Economics and Law, China

Citation: Yi, H., Zhang, C., Chen, M., Li, F., eds. (2022). Smart Urban Environmental Health From Multi-Scale, Multimedia, Multi-Exposure, Multi-Target Perspectives. Lausanne: Frontiers Media SA. doi: 10.3389/978-2-83250-454-3

Table of Contents

04 ***Editorial: Smart Urban Environmental Health From Multi-Scale, Multimedia, Multi-Exposure, Multi-Target Perspectives***
Fei Li, Chuanrong Zhang, Min Chen and Hongtao Yi

06 ***Investigation and Systematic Risk Assessment in a Typical Contaminated Site of Hazardous Waste Treatment and Disposal***
Wenhui Zhu, Xintong Yang, Jun He, Xiahui Wang, Ran Lu and Zheng Zhang

18 ***The Status Quo and Attribution of Wildlife Crimes: A Study of Cases in China From the Perspective of Ecological Economic Ethics***
Zhongmin Zhang, Yuting Zeng and Danqi Xie

30 ***Trace Metal Lead Exposure in Typical Lip Cosmetics From Electronic Commercial Platform: Investigation, Health Risk Assessment and Blood Lead Level Analysis***
Yanan Li, Yanyan Fang, Zehua Liu, Yahan Zhang, Kangli Liu, Luping Jiang, Boyuan Yang, Yongdie Yang, Yongwei Song and Chaoyang Liu

43 ***Spatio-Temporal Variation of Health Production Efficiency Considering Environmental Pollution in China Based on Modified EBM and Spatial Econometric Model***
Fan Liu, Gen Li, Ying Zhou, Yinghui Ma and Tao Wang

58 ***Estimation of Relative Risk of Mortality and Economic Burden Attributable to High Temperature in Wuhan, China***
Si Chen, Junrui Zhao, Soo-Beom Lee and Seong Wook Kim

69 ***Policy Effects of Ecological Red Lines on Industrial Upgrading and Health Promotion: Evidence From China Based on DID Model***
Penghao Ye

83 ***Exploring the Spatiotemporal Evolution and Socioeconomic Determinants of PM2.5 Distribution and Its Hierarchical Management Policies in 366 Chinese Cities***
Minli Zhu, Jinyuan Guo, Yuanyuan Zhou and Xiangyu Cheng

97 ***Prediction for Origin-Destination Distribution of Dockless Shared Bicycles: A Case Study in Nanjing City***
Min Cao, Ying Liang, Yanhui Zhu, Guonian Lü and Zaiyang Ma

111 ***Green Space Cooling Effect and Contribution to Mitigate Heat Island Effect of Surrounding Communities in Beijing Metropolitan Area***
Wei Liu, Haiyue Zhao, Shibo Sun, Xiyan Xu, Tingting Huang and Jianning Zhu

127 ***Conflict or Coordination? Spatiotemporal Coupling of Urban Population–Land Spatial Patterns and Ecological Efficiency***
Ling Shan, Yuehua Jiang, Cuicui Liu, Jing Zhang, Guanghong Zhang and Xufeng Cui

145 ***The Provincial Baseline of $PM_{2.5}$ in China and Its Hierarchical Management Strategy***
Doudou Jin, Shaojie Kong, Changhong Ou, Anwei Chen and Fei Li

frontiers | Frontiers in Public Health

TYPE Editorial
PUBLISHED 27 September 2022
DOI 10.3389/fpubh.2022.989922

OPEN ACCESS

EDITED AND REVIEWED BY
Dimirios Nikolopoulos,
University of West Attica, Greece

*CORRESPONDENCE
Fei Li
lifei@zuel.edu.cn

SPECIALTY SECTION
This article was submitted to Environmental health and Exposome, a section of the journal Frontiers in Public Health

RECEIVED 09 July 2022
ACCEPTED 09 September 2022
PUBLISHED 27 September 2022

CITATION
Li F, Zhang C, Chen M and Yi H (2022) Editorial: Smart urban environmental health from multi-scale, multimedia, multi-exposure, multi-target perspectives.
Front. Public Health 10:989922.
doi: 10.3389/fpubh.2022.989922

Editorial: Smart urban environmental health from multi-scale, multimedia, multi-exposure, multi-target perspectives

Fei Li[1]*, Chuanrong Zhang[2], Min Chen[3] and Hongtao Yi[4]

[1]Research Center for Environment and Health, Zhongnan University of Economics and Law, Wuhan, China, [2]Department of Geography, Center for Environmental Sciences and Engineering, University of Connecticut, Stamford, CT, United States, [3]Key Laboratory of Virtual Geographic Environment (Ministry of Education of PRC), Nanjing Normal University, Nanjing, China, [4]John Glenn College of Public Affairs, The Ohio State University, Columbus, OH, United States

KEYWORDS

multimedia environmental risk, environmental monitoring, health geography, urban modeling and simulation, exposure management

Editorial on the Research Topic
Smart urban environmental health from multi-scale, multimedia, multi-exposure, multi-target perspectives

Over half of the global population live in urbanized areas. These areas have become the geographic focus of resource consumption and chemical emissions. Pollutants in the urban environmental multi-media (including water, soil, air, etc.) are intensifying, causing chronic public health risk and hazard increases *via* multi-exposure pathways and multi-scale distribution differences. This Research Topic aims to provide a platform for researchers committed to the related progress on urban environmental health and sustainable development. As a result, our Research Topic has generated a great deal of interests and generated 11 multi-disciplinary articles in total.

The environmental monitoring and risk management research covered within this Research Topic includes studies about atmospheric pollution, soil pollution and cosmetic toxin. Contributors included a team from Chinese Academy for Environmental Planning published their systematic risk assessment in a typical contaminated site of a hazardous waste disposal center based on soil boreholes and groundwater monitoring wells investigation (Zhu et al.). Based on the chemical element analysis of lead (Pb) in the selected 34 popular lip cosmetics from Chinese e-commerce market, Li et al. found that there was no significant (non-)carcinogenic risk and blood Pb risk caused by adults and children's exposure to those lip cosmetics. The study by Zhu et al. proposed a hierarchical urban PM2.5 management policy by exploring the PM2.5 spatiotemporal evolution and its socioeconomic driver analysis. Further, the provincial baseline of PM2.5 in China was calculated by Jin et al., and their findings may help decision-makers to establish the differentiated control rules based on the classified cities.

The urban environmental health and sustainable development covered in this Research Topic also comprises a series of interdisciplinary studies, which explore this topic using methods from econometrics, landscape ecology, and environmental hygiene. The study by Chen et al. found that the economic losses of high temperature on the health of Wuhan residents were 156.1 billion RMB (95% CI: 92.28–211.40 billion RMB) during 2013–2019, accounting for 1.81% (95% CI: 1.14–2.45%) of Wuhan's annual GDP. Further, the findings of Liu et al. may help planners and government to understand the current cooling condition of green spaces, improve their cooling capacity, mitigate the urban heat island effect, and create a comfortable and healthy thermal environment during summer. Shan et al. analyzed the coordinated relationship between urban population–land spatial patterns (UPLSPs) and ecological efficiency (EE) in 12 Hubei cities as case studies. Their results indicated that the related departments should coordinate human and land resources and the ecological environment, and narrow regional development differences. By using the difference-in-differences (DID) method, Ye et al. found that the Ecological Red Lines (ERL)'s pilot scheme in four provinces of China hardly drove any promotion effects on the ratio of the tertiary industry to secondary industry while the residents' health was significantly improved by 1.029%. The study by Liu et al. analyzed the spatio-temporal variation of health production efficiency (HPE) of each province across China and highlighted the significant socioeconomic driving factors on health production efficiency, then targeted policies to accelerate the overall HPE development were proposed.

In this Research Topic, the environmental health law and geography studies have also been covered. The research by Zhang et al. highlighted the importance of knowledge on analyzing the subject and the subjective, incidence, and sentencing factors of wildlife crimes from legal and ethical perspectives, and uses the ecological economic ethical model to measure wildlife crimes. Cao et al. proposed a combining long short-term memory (LSTM) and quantum particle swarm optimization (QPSO) method to forecast the demand for shared bicycles in different urban regions, through which to reduce chemical emissions and improve public health by increasing user experiences.

The high diversity of the urban environment and public health studies on sustainability theme is likely to be of interest to a broad audience for upcoming decades. This Research Topic provides not just a timely reference source for academics, but also practical use for decision-makers, environmental engineers, and land planners concerned with environment-public health-sustainable development.

It is a pleasure to thank the members of the Editorial Board, all authors and co-authors and all referees for their valuable contributions to this Research Topic. Furthermore, these interesting publications would not be possible without the efficient support from the Journal Office.

Author contributions

FL wrote the first draft of this manuscript. CZ, MC, and HY critically reviewed and approved the final paper. All authors contributed to the article and approved the submitted version.

Conflict of interest

The authors declare that the research was conducted in the absence of any commercial or financial relationships that could be construed as a potential conflict of interest.

Publisher's note

frontiers in Public Health

ORIGINAL RESEARCH
published: 27 October 2021
doi: 10.3389/fpubh.2021.764788

Investigation and Systematic Risk Assessment in a Typical Contaminated Site of Hazardous Waste Treatment and Disposal

Wenhui Zhu, Xintong Yang, Jun He, Xiahui Wang, Ran Lu and Zheng Zhang*

Soil Environmental Protection Center, Research Center of Heavy Metal Pollution Prevention and Control, Chinese Academy for Environmental Planning, Beijing, China

A total of 214 sampling sites of a hazardous waste disposal center were surveyed in a two-stage pollution investigation, including soil boreholes and groundwater monitoring wells. Results showed that chemical oxygen demand (COD) (4.00–2930.00 mg/L), fluoride (0.07–9.08 mg/L), chromium (0.12–1.20 μg/L), nickel (0.15–459.00 μg/L), lead (0.10–10.20 μg/L), cadmium (Cd) (0.05–16.40 μg/L), and beryllium (0.06–3.48 μg/L) were detected in groundwater samples. For soils, Cd in soil (78.7 mg/kg) exceeded the risk screening value (65 mg/kg) for soil contamination of the second type of development land (GB36600-2018), and there remained the risk of leakage in the landfill detection investigation. Then, a health risk assessment was carried out. Based on the definitions of the groundwater exposure pathway (HJ 25.3-2019) and the pollution investigation of groundwater, the carcinogenic and non-carcinogenic risks of groundwater were generally considered to be negligible. The carcinogenic risk and non-carcinogenic risk of the concerned pollutant in soil for risk assessment (Cd) under the condition of reutilization exceeded the corresponding acceptable levels (1E-06 and 1). The (non-)carcinogenic risk of Cd mainly came from oral intake of soil and inhalation of soil particles under two conditions of reutilization and non-utilization, so on-site workers and surrounding residents should be properly protected from the mouth and nose to minimize the intake of pollutants from the soil and soil particles. The area of soil contaminated by Cd was about 630.58 m^2, and the amount of pollution was about 1261.16 m^3. The heavy metal pollution was only distributed in the depth range of 0–2 m, and the suggested risk control value of soil pollutants under the condition of reutilization for Cd was 56 mg/kg. Based on different pollution characteristics of soil, groundwater, and the landfill, targeted control measures were proposed.

Keywords: heavy metals, waste disposal site, simulative diffusion assessment, health risk assessment, contaminated site

OPEN ACCESS

Edited by:
Fei Li,
Zhongnan University of Economics and Law, China

Reviewed by:
Xingrun Wang,
Chinese Research Academy of Environmental Sciences, China
Mengxue Wan,
Chinese Research Academy of Environmental Sciences, China

****Correspondence:***
Xiahui Wang
wangxh@caep.org.cn

Specialty section:
This article was submitted to Environmental health and Exposome, a section of the journal Frontiers in Public Health

Received: *26 August 2021*
Accepted: *22 September 2021*
Published: *27 October 2021*

Citation:
Zhu W, Yang X, He J, Wang X, Lu R and Zhang Z (2021) Investigation and Systematic Risk Assessment in a Typical Contaminated Site of Hazardous Waste Treatment and Disposal. Front. Public Health 9:764788. doi: 10.3389/fpubh.2021.764788

INTRODUCTION

A contaminated site, also known as a "brown field," refers to a site that is contaminated by the production, management, treatment, and storage of toxic and harmful substances, the stacking or treatment and disposal of hazardous wastes, as well as mining activities, and is harmful to human health or the ecological environment. With the deterioration of terrestrial

ecosystem and the reduction of land productivity, pollution in soil and groundwater becomes increasingly serious, which poses threats and challenges to the ecological environment, food safety, drinking water safety, regional ecological environment, human settlement environment health, sustainable economic and social development, and even social stability (1, 2), which need to be paid close attention to. The hazardous waste treatment and disposal center is a typical contaminated site. The main treatment and disposal methods of hazardous waste produced in the industrial production process include incineration and sanitary landfill, during which pollutants such as organic matter, fluoride, and heavy metals are produced (3–5). Chromium, nickel, lead, cadmium (Cd), and beryllium are known to cause various health effects, such as certain cancers, respiratory diseases, gastrointestinal disorders, and skin allergies (6–8). In the process of disposal, some pollutants can migrate *via* the atmosphere, water, and other media, so pollutants will enter the soil, accumulate in the soil, and diffuse in underground water (9–12), causing some adverse effects on the ecological environment and the health of residents around the disposal center. It is urgent to assess the environmental risks of contaminated sites in order to provide early warning for the development of these risks.

Risk assessment of contaminated sites is an important part of the framework system of site environmental management. On the one hand, it can guide the environmental investigation and monitoring of pollutants in contaminated sites and obtain key parameters of soil and groundwater. In addition, risk assessment can determine whether the risks are worthy of attention and calculate the remediation targets and pollution scope of specific sites. Pollutants migrate in soil, groundwater, and others in the contaminated site. Therefore, many scholars are studying the quality of soil and water environment around hazardous waste disposal sites and other contaminated sites. Surface pollutants can enter groundwater through leaching, leakage, runoff, and other ways, posing a threat to the nearby ecological environment and human health. The toxicity, bioaccumulation, and persistence of trace metal pollution in groundwater have been widely studied by researchers all over the world (13–16). In addition to affecting aquatic systems, trace metals also affect human health through consumption and skin contact with polluted water (7, 17). In recent years, more pieces of research on the characterization of space pollution level and potential health risk assessment come out, including pollution characteristics, key pollutants and regions, and current health risk level analysis (18–20). However, there are few studies on the adverse effects of groundwater migration in contaminated sites. In recent years, numerous research has been done in the field of soil heavy metal pollution and health risk assessment in contaminated sites at home and abroad (21–26). However, due to different technical and budgetary constraints, climate and environment, regional soil heterogeneity, receptor exposure characteristics, and other factors, there is no international agreement on the quantitative risk management framework of contaminated land (27–29). In particular, the contaminated sites of hazardous waste treatment and disposal may have a variety of contaminated sources, rich types of pollutants, and unknown degrees of toxicity and harmful effects, and there is a transmission of pollutants between the soil and water. Therefore, it is of great significance to explore the evaluation and management of these hazardous waste disposal centers in China, find out the deficiencies in the process of local technical guidance, and put forward corresponding suggestions.

The objectives of this study were: (1) to investigate the current characteristics (concentration) and affected areas of pollution in soil and groundwater in a typical contaminated site of hazardous waste treatment and disposal, identify characteristic pollutants, determine the causes and potential sources of pollution, and quantify the risk of landfill leakage; (2) evaluate the spatial carcinogenic and non-carcinogenic risks caused by each exposure pathways of characteristic pollutants under the condition of reutilization or non-utilization, and simulate the groundwater migration of pollutants of concern; (3) comprehensively analyze the spatial distribution, health risks, local background values and soil remediation cases at home and abroad of heavy metals in soil and groundwater, determine the areas and soil depth, earthwork volume and area that need remediation, and put forward comprehensive and feasible control values of polluted heavy metals in soil and targeted control measures based on different pollution characteristics of soil, groundwater and the landfill, so as to provide reference for pollution risk control of hazardous waste treatment and disposal sites.

MATERIALS AND METHODS

Study Area and Pollution Identification

The typical Hazardous Waste Disposal Center (HWDC) is located in a province in southern China. The HWDC is about 600 acres, of which the production and management area is about 175 acres, the unused land is about 380 acres, and the landfill area is about 45 acres, as shown in **Supplementary Figure S1** in the support information S7. Geological and hydrogeological surveys (as shown in **Figure 1**) showed that the elevation of the HWDC was high in the north and low in the south. The stratigraphic structure was classified according to the sedimentary age and genetic type of the strata, and the top-down strata were divided into the artificial fill (Q_4^{ml}), silty clay (Q_2^{dl+pl}), and argillaceous siltstone (N). The groundwater type in the HWDC was pore phreatic water in loose rock, which mainly occurred in the Q_4^{ml} pore. The groundwater flowed from the northeast to the southwest. The main lithology of this layer was silty clay, with weak permeability and continuous but irregular spatial distribution. Pore groundwater in this layer was poor, with poor mobility. According to the measured groundwater level elevation, the average hydraulic gradient of groundwater is about 0.018. According to the geotechnical laboratory test results, the range of permeability coefficient (recommended value) is 9.70E-06–5.22E-05 cm/s, and the range of groundwater seepage velocity (recommended value) is 1.51E-04–8.12E-04 m/day.

Samples Collection and Detection

In the preliminary investigation, based on the principle of "systematized layout and professional judgment," sampling

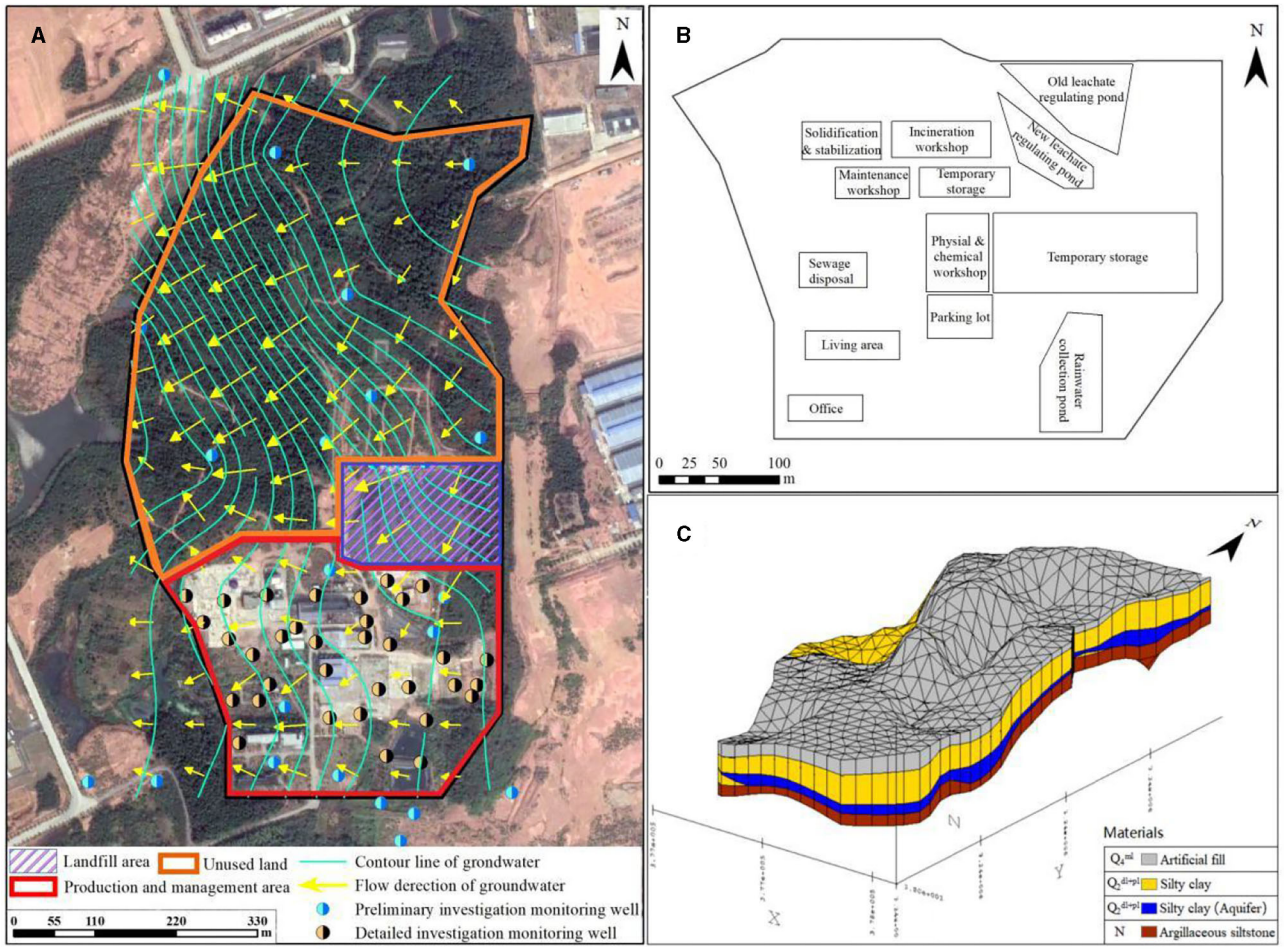

FIGURE 1 | Flow direction of groundwater **(A)**, production and management area **(B)**, and strata classifications **(C)**.

points were set in unused land and production and management area. Soil sampling holes were arranged according to 40 × 40 m grid density in the production and management area. A total of 73 soil sampling points (including one background point) were arranged, and 384 soil samples were collected. Twenty-four groundwater monitoring wells (including three original monitoring wells and two civil wells in the disposal center) were arranged according to the grid density of 80 × 80 m, and 27 groundwater samples (including three groundwater quality control samples) were collected in production and management area. For unused land, the preliminary investigation had a total of 81 soil sampling points. For groundwater sampling points, 12 groundwater monitoring wells (including one groundwater quality control sample) were arranged in the unused land according to the grid density of 150 × 150 m (the grid density of 40 × 40 m in the suspected pollution area in the unused land). A total of 266 samples were collected in unused land in the preliminary investigation, including 252 soil samples (including 28 quality control samples) and 14 groundwater samples (including two quality control samples). The distribution of sampling points in unused land and the production and management area is shown in **Figure 2A**.

According to the preliminary investigation results, the scope of the pollution survey had been significantly narrowed, and a further detailed investigation was carried out. A total of 141 sampling points were surveyed, including 90 soil boreholes and 51 groundwater monitoring wells. A total of 518 samples were collected in a detailed investigation, including 461 soil samples (including 45 quality control samples) and 57 groundwater samples (including 37 newly built groundwater monitoring wells, 14 original groundwater monitoring wells, and six quality control samples). Detailed investigation points are shown in **Figure 2B**.

In addition, the landfill was the key pollution source of the HWDC, and there remained a risk of pollution leakage after several years of discard. So, the corresponding site investigation was carried out in a detailed investigation. The landfill had a complete anti-seepage structure, so the traditional drilling survey was not suitable for the landfill. Therefore, the leakage detection equipment of the double electrode method was used to investigate the leakage risk of landfills. The

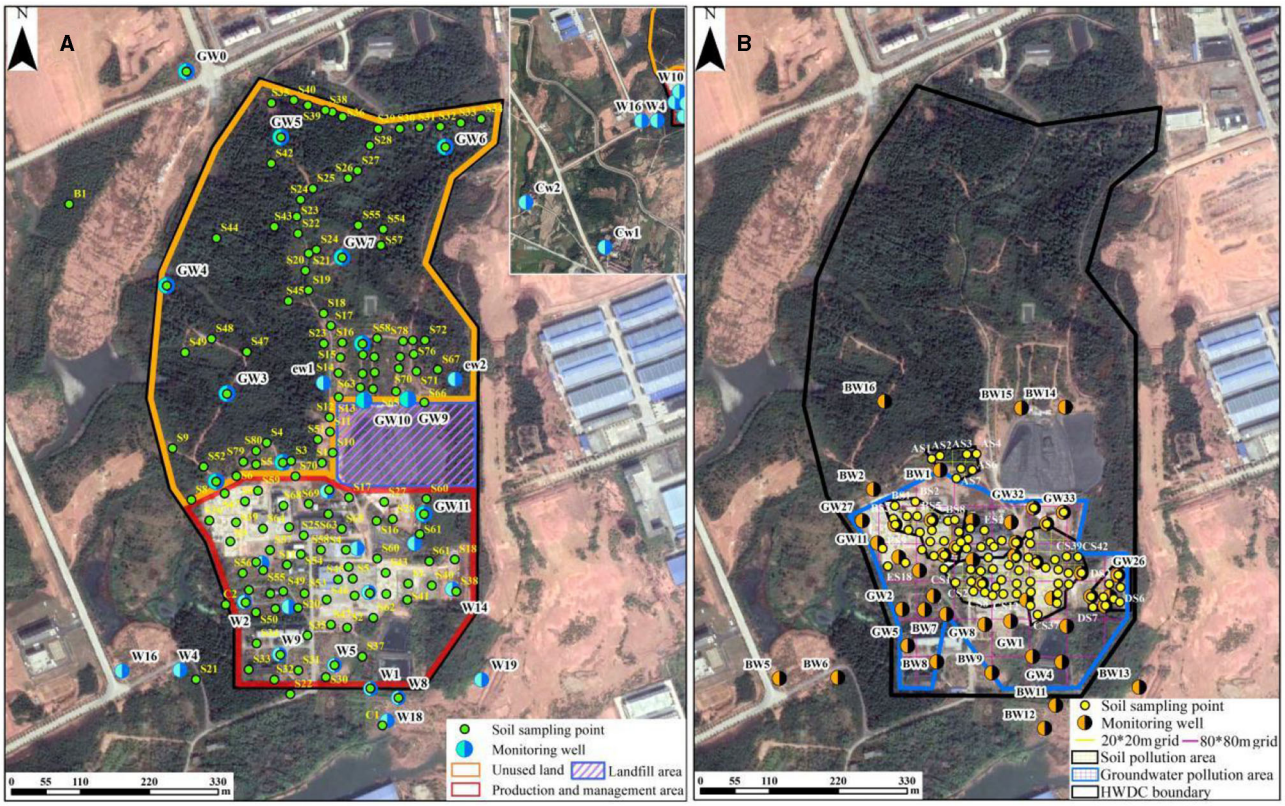

FIGURE 2 | Sampling points distribution in the preliminary survey **(A)** and detailed investigation **(B)**.

double electrode method used two electrodes with an applied voltage to qualitatively determine whether there was leakage in the impervious layer of the landfill according to the circuit impedance. The field signal source of leakage detection with the double electrode method was 100–300 V, and the detection current was 100–500 mA. According to the 2–4 m point spacing, a total of 151 electrodes were arranged with five lines and a total length of 390 m.

Health Risk Assessment

Two land-use plans, namely, the reutilization scenario and the non-utilization scenario, were considered. Then, hazard identification, exposure assessment, toxicity assessment, and risk characterization were carried out to determine whether the human health risk caused by soil and groundwater pollution exceeded the acceptable level. The risk control value of soil and groundwater pollution was calculated, and the quantity of contaminated soil to be remediated was estimated, which lays a solid foundation for the risk control and remediation scheme in the next step. *Technical guidelines for risk assessment of soil contamination of land for construction* (HJ 25.3-2019) stipulate 9 exposure pathways. The contaminants of concern identified by the preliminary and detailed investigation, heavy metals and fluoride, are not volatile. Therefore, the exposure pathways under the condition of reutilization were as follows: oral intake of soil, skin contact with soil, inhalation of indoor soil particles, and inhalation of outdoor soil particles. Correspondingly, the exposure pathways under the condition of non-utilization were oral intake of soil, skin contact with soil, and inhalation of outdoor soil particles.

First, the exposure dose of the identified contaminant is quantified. For carcinogenic pollutants, the exposure dose *via* the oral intake of soil for adults is calculated as Formula (1).

$$OISER_{ca} = \frac{OSIR_a \times ED_a \times EF_a \times ABS_o}{BW_a \times AT_{ca}} \times 10^{-6} \quad (1)$$

where $OISER_{ca}$ is the exposure dose *via* the oral intake of soil (carcinogenic effect), kg (soil)·kg^{-1} (body weight)·day^{-1}; $OSIR_a$ is the daily intake of soil for adults, mg·day^{-1}; BW_a is the adult average weight, kg; EF_a is the adult exposure frequency, day·a^{-1}; ED_a is the adult exposure cycle, a; ABS_o is the absorption efficiency factor of oral intake, dimensionless; AT_{ca} is the average time of carcinogenic effect, days. The recommended values of $OSIR_a$, BW_a, EF_a, ED_a, ABS_o, and AT_{ca} are shown in **Supplementary Table S1**.

For non-carcinogenic pollutants, Formula (2) is used to calculate the exposure dose *via* the oral intake of soil for adults.

$$OISER_{nc} = \frac{OSIR_a \times ED_a \times EF_a \times ABS_o}{BW_a \times AT_{nc}} \times 10^{-6} \quad (2)$$

where $OISER_{nc}$ is the exposure dose *via* the oral intake of soil (non-carcinogenic effect), kg (soil)·kg^{-1} (body weight)·day^{-1}; AT_{nc} is the average time of non-carcinogenic effect, days. The recommended value of AT_{nc} is shown in **Supplementary Table S1**. Formula (1) shows the meaning of $OSIR_a$, BW_a, EF_a, ED_a, ABS_o. The exposure dose of (non-)carcinogenic pollutants *via* other pathways to be exposed to soil or groundwater can be found in the support information S1. Then, based on the toxicity parameters (as shown in the support information S2), the carcinogenic and non-carcinogenic risks were characterized. The carcinogenic risk of a single pollutant in soil *via* oral intake was calculated as Formula (3).

$$CR_{ois} = OISER_{ca} \times C_{sur} \times SF_o \tag{3}$$

where CR_{ois} is carcinogenic risk *via* oral exposure to contaminated soil, dimensionless; C_{sur} is the concentration of pollutants in surface soil, mg·kg^{-1}. C_{sur} values must be obtained according to site investigation. The meaning of $OISER_{ca}$ and SF_o i is shown in Formula (1) and Formula (S7). The carcinogenic risks of a single pollutant *via* other exposure pathways for soil or groundwater are shown in support information S3. The hazard quotient of a single pollutant in contaminated soil *via* oral intake was calculated as Formula (4).

$$HQ_{ois} = \frac{OISER_{nc} \times C_{sur}}{RfD_o \times SAF} \tag{4}$$

where HQ_{ois} is the hazard quotient *via* oral exposure to contaminated soil, dimensionless; SAF is the distribution coefficient of reference dose when exposed to soil, dimensionless. The meaning of $OISER_{nc}$, C_{sur}, and RfD_o is shown in Formula (3) and Formula (S8). The hazard quotients of a single pollutant *via* other exposure pathways for soil or groundwater are shown in support information S4. Based on the carcinogenic risk (total carcinogenic risk) or hazard quotient (hazard index) of various pollutants *via* different exposure pathways to soil or groundwater above, the carcinogenic risk and hazard index of all pollutants are calculated. The carcinogenic risk of all pollutants of concern *via* all exposure pathways is calculated as Formula (5).

$$CR_{sum} = \sum_{i=1}^{n} CR_i \tag{5}$$

where CR_{sum} is the total carcinogenic risk of all pollutants (the number of kind is n) of concern, dimensionless. The definition of CR_i is shown in Formula (S11). The hazard index of all pollutants of concern *via* all exposure pathways is calculated as Formula (6).

$$HQ_{sum} = \sum_{i=1}^{n} HI_i \tag{6}$$

where HQ_{sum} is the hazard index of all pollutants (the number of kind is n) of concern, dimensionless. The definition of HI_i is shown in Formula (S14).

Simulation and Prediction Model of Pollutants in Groundwater

Groundwater modeling system (GMS 10.4) is a visual three-dimensional groundwater simulation software package. Modflow is a three-dimensional finite-difference groundwater flow model. MT3DMS is the most widely used three-dimensional groundwater solute transport simulation model. In the GMS software package, MT3DMS can be seamlessly connected with Modflow, supporting all hydrological and discrete characteristics of Modflow, which is the most widely used numerical model of solute transport at home and abroad. According to the pollution distribution of each pollutant and groundwater flow model, aquifer parameters, initial conditions, and boundary conditions are substituted into the water quality model; permeability coefficient is 0.05 m/d, the rainfall recharge rate is 3.22E-04 m/day, effective porosity is 3.00E-01, boundary discharge is 1.299 m^3/day, dispersion is 4.4 m, and heavy metal soil-water allocation coefficients (Kd) are 1.50E+02 L/kg for fluoride, 1.50E+01 L/kg for Cd, and 1.60E+01 L/kg for a nickel. Modflow and MT3DMS models are used to jointly run the water flow and water quality model, and the prediction results of pollutant migration and transmission are obtained.

Multivariate and Geostatistical Methods

SPSS 16.0 software (IBM, Armonk, NY, USA) was used for logging data and calculation. In order to analyze the characteristics of heavy metals, the basic statistical parameters such as average value, extreme value, detection rate, exceeding the rate, and exceeding time were calculated. Using a geographic information system (GIS) (ArcGIS 9.3 software), the concentration of toxic metals at each sampling point of groundwater in the disposal center on the plane map and the spatial distribution characteristics of toxic metals pollution in the soil of the whole region were demonstrated. IDW (inverse distance weighted) uses a specific number of nearest points and is then weighted according to their distance to the interpolated point (30–32). IDW method was used to draw the spatial distribution map of the toxic metals in the soil of the disposal center, so as to clearly show the spatial variation and spatial pattern of heavy metal concentrations in the study area.

RESULTS AND DISCUSSION

Pollutant Concentrations in the Groundwater and Soil

Groundwater

Detailed investigation showed that chemical oxygen demand (COD) (4.00–2930.00 mg/L), fluoride (0.07–9.08 mg/L), chromium (0.12–1.20 μg/L), nickel (0.15–459.00 μg/L), lead (0.10–10.20 μg/L), Cd (0.05–16.40 μg/L), and beryllium (0.06–3.48 μg/L) were detected in groundwater samples, and the detection rate ranged from 6 to 100%. Among them, COD, fluoride, nickel, and Cd exceeded the corresponding Class IV water quality standards in *Standard for groundwater quality* (GB/T 14848-2017) (10 mg/L for COD, 2 mg/L for fluoride, 100 μg/L for nickel, and 10 μg/L for Cd). The pH value of the GW14

sample was 5.47, slightly lower than the standard value of 5.5. The groundwater samples exceeded the COD standard (GB/T 14848-2017) (10 mg/L) by 81%, and the maximum detectable concentration was 2,930 mg/L, which exceeded 10 mg/L by 292 times. The exceeding rates of fluoride and nickel samples were 8%, and the maximum exceeding times were 3.54 times and 3.59 times, respectively. Cd only has a single exceeding point, GW29 (16.40 μg/L), and the exceeding time was 0.64 times.

The sampling points exceeding the Class IV water quality standards of COD (GB/T 14848-2017) and spatial distribution of groundwater COD are shown in **Figure 3A**. **Figure 3A** shows that the COD of the upper, middle, and lower reaches of the groundwater in the disposal center generally exceeded the standard. COD increased significantly in the middle reaches of the production management area, especially high in the original physical and chemical workshop (GW23), the north side of the physical and chemical workshop (GW20 and GW24) and the east side of the original temporary storage area (GW3 and GW14), and the exceeding ratio was more than 100 times. The COD concentration of BW5 and BW6 monitoring wells downstream slightly exceeded the standard, <10 times. The historical hazardous waste management activities of the disposal center may contribute to the excessive COD in groundwater. There was also a certain excessive COD upstream of groundwater. The disposal center is located in the gathering area of three leading industries which are textile and clothing, electronic information, and new energy and new materials. The exceeding standard of COD may also be a regional problem in the gathering area. However, the significant high concentration of COD in the production and management area also indicated the possibility of organic pollution in the groundwater of the HWDC, including volatile organic compounds (VOCs), semi-volatile organic compounds (SVOCs), and total petroleum hydrocarbons (TPH), which is worthy of attention in the future risk control strategies.

The sampling points exceeding Class IV water quality standards of fluoride in *Standard for groundwater quality* (GB/T 14848-2017) and spatial distribution of groundwater fluoride are shown in **Figure 3B**. **Figure 3B** shows that fluoride mainly slightly exceeded the standard, which was mainly distributed in the incineration workshop (GW31), the original temporary storage in the north of the physical and chemical workshop (GW20), the temporary storage in the east of the physical and chemical workshop (GW14), and the local area around the initial rainwater collection pool (GW4). The sampling points exceeding Cd standard (GB/T 14848-2017) and spatial distribution of groundwater Cd are shown in **Figure 3C**. **Figure 3C** shows that Cd pollution was mainly distributed in the surrounding area of the original solidification/stabilization workshop (GW29), exceeding Cd standard slightly. The sampling points exceeding nickel standard (GB/T 14848-2017) and spatial distribution of groundwater Cd are shown in **Figure 3D**. **Figure 3D** shows that the nickel-contaminated area was mainly concentrated in the northern side of the original temporary storage (GW20), the physical and chemical workshop (GW23), and the eastern side of the physical and chemical workshop temporary storage (GW3 and GW14). In the sewage treatment system of the disposal center, the unqualified discharge of production wastewater and domestic wastewater may lead to heavy metal pollution in water ponds. In addition, hazardous landfills may have a history of leakage, which may cause heavy metal pollution to groundwater downstream.

Soil

The preliminary investigation found that in the production and management area, for the soil, the total chromium of the site S10 located in the stabilization/solidification workshop area exceeded the standard. The total chromium evaluation standard refers to the Dutch soil and groundwater intervention value standard which was 380 mg/kg. But the maximum concentration of total chromium in this study was 1,170 mg/kg, far below the soil screening value (2,500 mg/kg) published in China. Thus, it was appropriate to consider the total chromium below the standard. In the unutilized area, Cd only in the surface S3 (0.5 m) (78.7 mg/kg) exceeded the risk screening value (65 mg/kg) for soil contamination of the second type of development land in *Soil environmental quality-Risk control standard for soil contamination of development land* (GB36600-2018) 0.21 times, and it was below the intervention value (172 mg/kg). According to the statistical analysis of the test results of soil samples, the excessive Cd samples only exist at 0.5 m sampling depth in the surface soil layer. According to the sampling depth of soil samples, the IDW method was used in ArcGIS to hierarchically characterize the spatial distribution of exceeding Cd pollution in soil, shown in **Figure 3E**. It can be seen from **Figure 3E** that Cd pollution in the 0.5 m soil layer was only distributed at the junction of the production management area and unused land on the north side. The pollution may come from road transport litter or dust. Incineration workshops were used to incinerate waste, and atmospheric emissions may lead to heavy metal pollution in the surrounding soil. For the production and management area, production workshops (incineration, material/chemical, and stabilization/solidification workshops) and temporary storage are directly exposed to hazardous waste, whereas facilities and equipment, site walls, and ground can be clung to a small amount of residual hazardous waste. In addition, varying degrees of damage can happen to buildings, and rainwater helps the leaching and infiltration of hazardous waste, causing heavy metal pollution of soil.

Detailed investigation showed that fluoride (331–2,060 mg/kg), chromium (24–394 mg/kg), nickel (7–546 mg/kg), lead (3.3–204 mg/kg), Cd (0.01–51.3 mg/kg), and beryllium (0.82–6.83 mg/kg) were detected in soil samples, and the detection rate ranged from 97.84 to 100%. The detection rate of Cd was 97.84%, and the detection rates of nickel, lead, Cd, and beryllium were all 100%. Chromium, nickel, lead, Cd, and beryllium contents were all below their corresponding standards.

Leakage Risk of Landfill

According to the landfill leakage detection method and parameters in section Samples Collection and Detection, the impedance test distribution of landfill leakage detection was calculated, as shown in **Supplementary Figure S2** in support information S8. Test results in **Supplementary Figure S2** showed

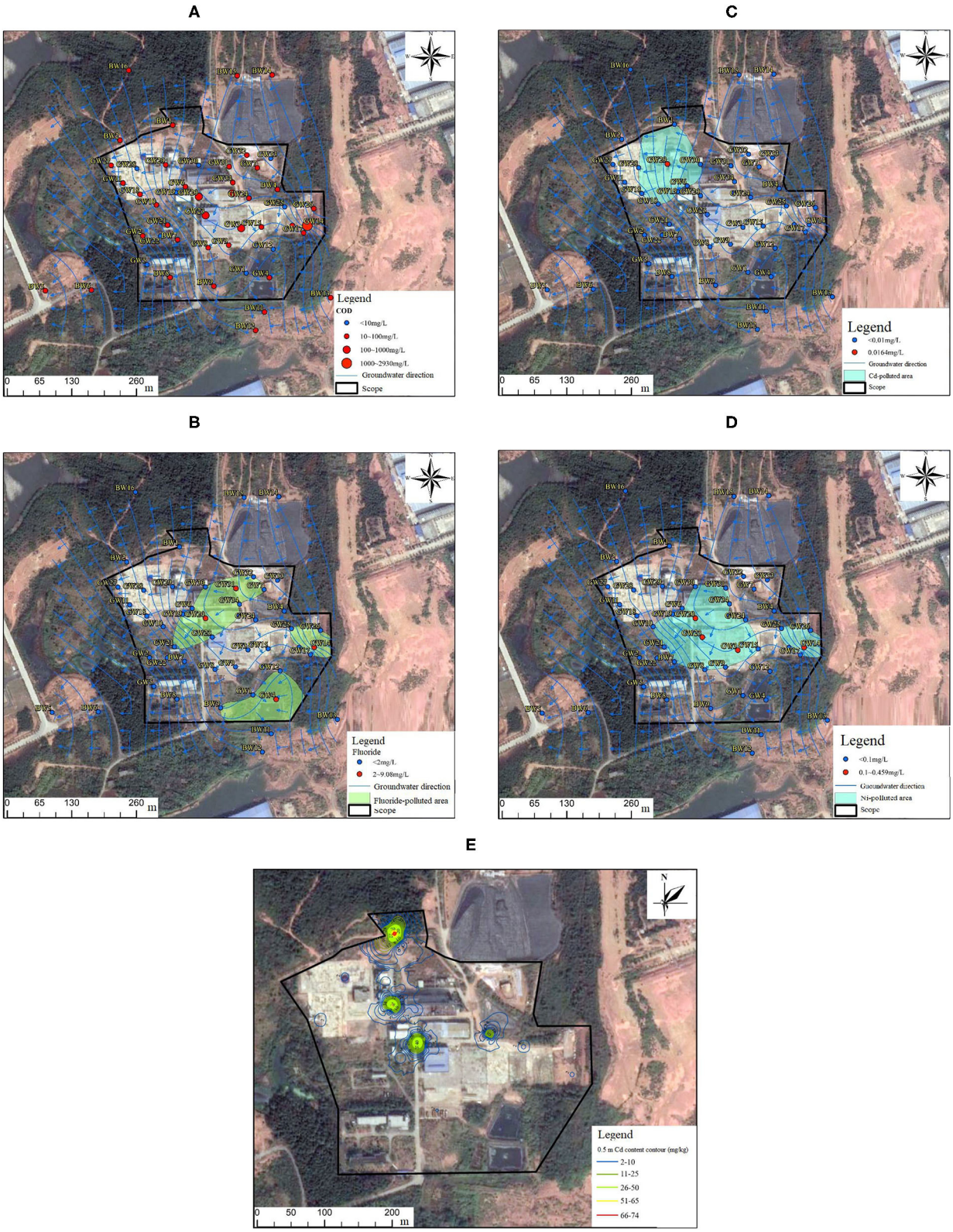

FIGURE 3 | Spatial characterization of the sampling points exceeding COD **(A)**, fluoride **(B)**, Cd **(C)**, and nickel **(D)** standard in groundwater (GB/T 14848-2017) and spatial distribution of Cd pollution in 0.5 m soil (GB36600-2018) **(E)**.

that the field signal source was 100–300 V, the detection current was 100–500 mA, and the impedance between the two electrodes of the landfill impervious layer was 1.1 k−1.2 k. There was a good electrical conductivity between the impervious layers, and the high-density polyethylene (HDPE) film of the impervious layer might have been damaged. In addition, **Supplementary Figure S2** also showed that the overall conductivity of the landfill area on the east side was stronger than that on the west side, and the leakage risk of the impervious layer on the east side was higher than that on the west side. Groundwater monitoring data in section Groundwater showed that no significant pollution leakage was observed in the landfill, which may be due to the implementation of the surface coverage with HDPE membrane in this landfill, blocking the downward migration of pollutants resulting from the infiltration of large amounts of rainwater.

Multi-Scenario Health Risk Assessment of Heavy Metals

Groundwater

Fluoride was the concern pollutant in groundwater that needs risk assessment, and the exceeding points were GW4, GW14, GW20, and GW31. The other two contaminants of concern were nickel, with excessive points GW3, GW14, GW20, and GW23 and Cd with GW29. The above pollutants are not volatile, therefore, according to the *Technical guidelines for risk assessment of soil contamination of land for construction* (HJ 25.3-2019), there was no corresponding exposure pathway, and the probability of human health risk caused by pollutants in groundwater *via* drinking groundwater was rather small. Therefore, it was considered that the carcinogenic risk and non-carcinogenic risk under the condition of reutilization or non-utilization were 0, so it was not necessary to consider the risk control value. But the risk of groundwater migration and diffusion must be paid attention to.

Soils

The concern pollutant for risk assessment was Cd, and the corresponding sampling point was S3.

(1) Risk characterization results under the condition of reutilization

The health risks of the pollutants in the soil under the condition of reutilization are shown in **Tables 1**, **2**. It can be seen from **Tables 1**, **2** that under the condition of reutilization, the total carcinogenic risk of soil in the disposal center was 1.02E-06, and the non-carcinogenic hazard index reaches 1.41E+00. Soil carcinogenic risk exceeded the acceptable level of 1E-06 required by the *Technical guidelines for risk assessment of soil contamination of land for construction* (HJ 25.3-2019). The non-carcinogenic hazard index exceeded the acceptable level hazard quotient 1 required by the *Technical guidelines for risk assessment of soil contamination of land for construction* (HJ 25.3-2019). Thus, under the condition of reutilization, the risk control value of Cd in the soil needed to be further discussed.

(2) Risk characterization results under the condition of non-utilization

The health risks of the pollutants in the soil under the condition of non-utilization are shown in **Tables 3**, **4**. It can be seen from **Tables 3**, **4** that under the condition of non-utilization, the total carcinogenic risk of soil in the disposal center was 1.77E-07, and the non-carcinogenic hazard index reached 6.91E-01. Soil carcinogenic risk does not exceed the acceptable level of 1E-06 required by the *Technical*

TABLE 1 | Soil risk results under the condition of reutilization (carcinogenic risk).

Sampling point	Depth	Pollutant	CR_s^{ing}	CR_s^{der}	CR_s^{ip}	CR_s^{op}	CR_s^{iv}	$CR_s^{sur\text{-}ov}$	$CR_s^{sub\text{-}ov}$	$CR_s^{T\text{-}on}$
S3	0.5 m	Cd	-	-	8.47E-07	1.77E-07	-	-	-	1.02E-06

TABLE 2 | Soil risk results under the condition of reutilization (non-carcinogenic hazard index).

Sampling point	Depth	Pollutant	HQ_s^{ing}	HQ_s^{der}	HQ_s^{ip}	HQ_s^{op}	HQ_s^{iv}	$HQ_s^{sur\text{-}ov}$	$HQ_s^{sub\text{-}ov}$	HI_s^{on}
S3	0.5 m	Cd	4.36E-01	1.05E-01	7.16E-01	1.49E-01	-	-	-	1.41E+00

TABLE 3 | Soil risk results under the condition of non-utilization (carcinogenic risk).

Sampling point	Depth	Pollutant	CR_s^{ing}	CR_s^{der}	CR_s^{op}	$CR_s^{sur\text{-}ov}$	$CR_s^{sub\text{-}ov}$	$CR_s^{T\text{-}on}$
S3	0.5 m	Cd	-	-	1.77E-07	-		1.77E-07

TABLE 4 | Soil risk results under the condition of non-utilization (non-carcinogenic hazard index).

Sampling point	Depth	Pollutant	HQ_s^{ing}	HQ_s^{der}	HQ_s^{op}	$HQ_s^{sur\text{-}ov}$	$HQ_s^{sub\text{-}ov}$	HI_s^{on}
S3	0.5 m	Cd	4.36E-01	1.05E-01	1.49E-01	-		6.91E-01

guidelines for risk assessment of soil contamination of land for construction (HJ 25.3-2019). The non-carcinogenic hazard index did not exceed the acceptable level hazard quotient 1 required by the *Technical guidelines for risk assessment of soil contamination of land for construction* (HJ 25.3-2019). The carcinogenic risk and non-carcinogenic risk of Cd were acceptable under the condition of non-utilization.

Contributive Rates of Exposure Pathways

The risk contribution rates of soil pollutants *via* different exposure pathways under the two conditions of reutilization and non-utilization were calculated, and the results are shown in **Supplementary Tables S3–S6**. It can be seen from **Supplementary Tables S3, S4** that, the carcinogenic and non-carcinogenic risks of Cd mainly came from the oral intake of soil and inhalation of indoor soil particles under the condition of reutilization. It can be seen from **Supplementary Tables S5, S6** that the carcinogenic and non-carcinogenic risks of Cd mainly came from oral intake of soil and inhalation of outdoor soil particles under the condition of non-utilization.

Migration Effects of Heavy Metals and Fluoride in Groundwater

According to the models and parameters in section Simulation and Prediction Model of Pollutants in Groundwater, the migration of heavy metals and fluoride exceeding groundwater standards (GB/T 14848-2017) was simulated. The migration results of heavy metals (Ni and Cd) and fluoride in the 50-year simulation period are shown in **Figure 4**. From **Figure 4**, it can be seen that heavy metals (nickel and Cd) and fluoride plumes were unlikely to migrate and diffuse out of the western and southern site boundaries within 50 years. Fluoride, nickel, and Cd may be greatly affected by the adsorption of soil.

Risk Management Suggestions

Pollutants that exceeded the corresponding environmental standard values in a single medium in the preliminary and detailed investigation were considered pollutants of concern, which were further subject to health risk assessments under the two land-use plans. For the pollutant whose health risk exceeds the corresponding risk limit, further regulatory measures are necessary, so the recommended control values need to be calculated. The risk control value was not necessary for groundwater, but the risk of groundwater migration and diffusion must be paid attention to. For soil under the condition of non-utilization, there was no need to calculate the recommended risk control values for pollutants. Therefore, the recommended risk control values for pollutants in soil are discussed under the condition of reutilization.

For greater rationality of the calculated risk control value to be directly considered as the risk control value in the disposal center, the calculated risk control value (56 mg/kg for Cd) and the values of the soil control point (0.04 mg/kg for Cd), domestic relevant standards (screening value of 65 mg/kg and intervention value of 172 mg/kg for Cd in the second type of land for construction), and domestic existing cases (65 mg/kg) were compared to put forward the suggested risk control value of soil pollutants under the condition of reutilization-−56 mg/kg for Cd. Under the condition of non-utilization, based on key information of sampling points exceeding standard (GB36600-2018), the engineering quantity of soil risk control in the disposal center was estimated and characterized. The area of soil contaminated by Cd was about 630.58 m^2, and the amount of pollution was about 1261.16 m^3. The heavy metal pollution was only distributed in the depth range of 0–2 m, which was between the screening value and the intervention value.

Under the condition of reutilization, the risk of soil Cd was unacceptable and the single area and volume were relatively small, so the control strategy of ectopic excavation and barrier landfill is recommended. For polluted groundwater, the simulation results of pollution migration showed that the speed of pollution migration was very slow, so the control strategy of "monitoring the natural attenuation and long-term monitoring" is suggested. For the landfill, there was no significant leakage in the landfill, but there remained the risk of leakage in the landfill detection investigation. It is suggested that the landfill should be closed and greened as soon as possible, and drainage measures should be taken to avoid the downward migration of pollution caused by rainwater leaching and infiltration.

CONCLUSIONS

In the pollution investigation of groundwater and soils, COD, fluoride, nickel, Cd, lead, and beryllium exceeded the corresponding environmental standard in a single medium. However, whether the contents of pollutants in a single medium exceed the standard or not is not enough for management decisions. It is necessary to further carry out the risk assessment of these pollutants of concern to evaluate the harmful effects. Among them, the carcinogenic and non-carcinogenic risks of Cd in soil exceeded the corresponding risk assessment limits, so Cd needed to be managed specifically, and the recommended control value of Cd is further proposed. Based on concern contaminants identification in preliminary and detailed investigation and further health risk assessment under two land use plans, the area of soil contaminated by Cd was evaluated to be about 630.58 m^2, and the amount of pollution was about 1261.16 m^3. The heavy metal pollution was only distributed in the depth range of 0–2 m, which was between the screening value and the intervention value. The suggested risk control value of soil pollutants under the condition of reutilization was 56 mg/kg for Cd. Under the condition of reutilization, the risk of soil Cd was unacceptable and the single area and volume were relatively small, so the control strategy of ectopic excavation and barrier landfill is recommended. Contributive rates analyze of exposure pathways showed that oral intake of soil and inhalation of indoor soil particles were the main pathways contributing to the carcinogenic and non-carcinogenic risks under the two conditions of reutilization and non-utilization. The contaminants of concern identified by the preliminary and detailed investigation, heavy metals and fluoride, are not volatile. Therefore, it was considered that there were no vapor

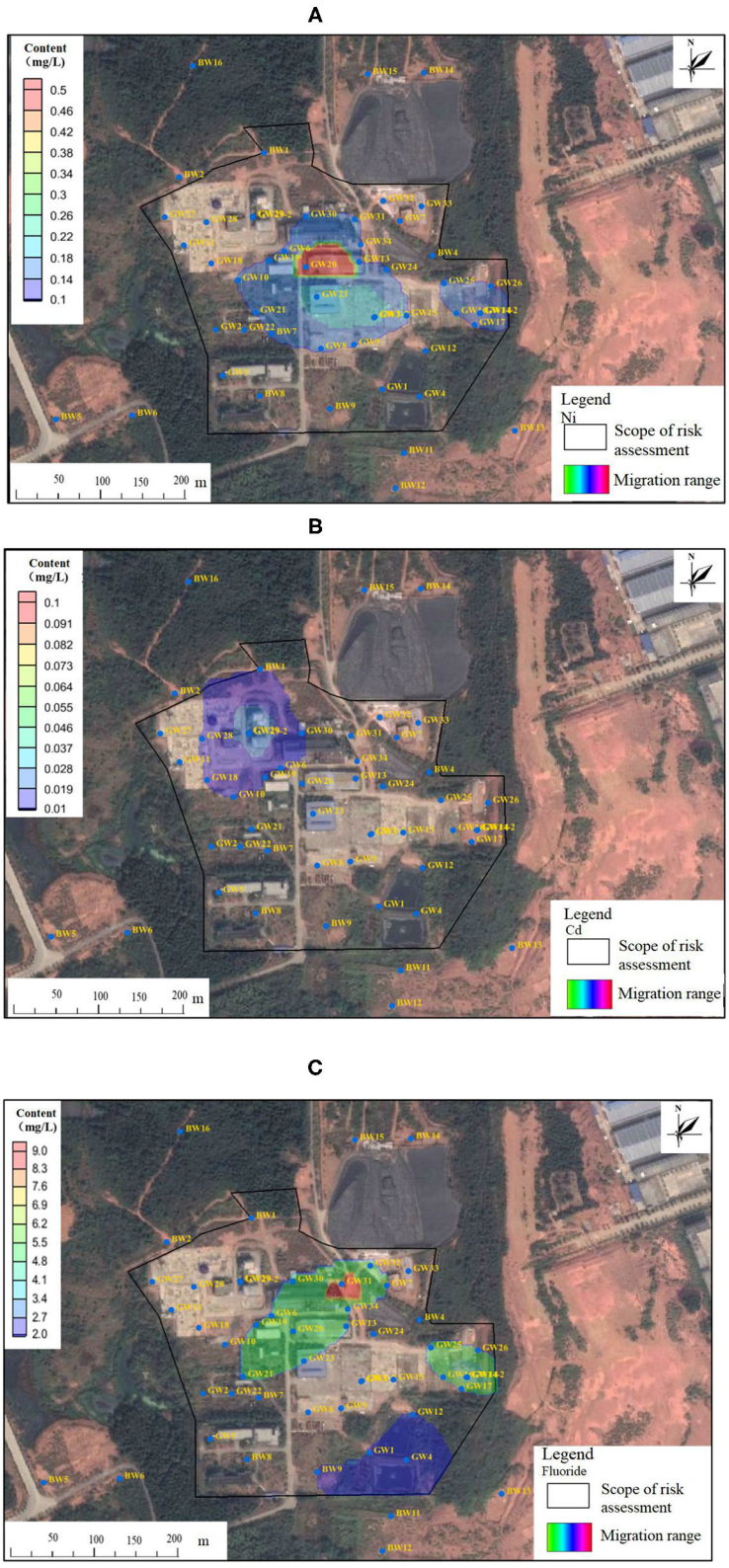

FIGURE 4 | Nickel **(A)**, Cd **(B)**, and fluoride **(C)** plume simulation in the next 50 years.

exposure pathways for soil and groundwater to the human body. The risk control value was not necessary for groundwater, but the risk of groundwater migration and diffusion must be paid attention to. The migration of heavy metals and fluoride exceeding groundwater standard (GB36600-2018) were simulated. The migration speed of fluoride, nickel, and Cd in groundwater was slow, and the pollution range of each pollutant changes little in 50 years. For polluted groundwater, the simulation results of pollution migration showed that the speed of pollution migration was very slow, so the control strategy of "monitoring the natural attenuation and long-term monitoring" is suggested. For the landfill leakage risk, the landfill should be closed and greened with drainage measures to avoid the downward migration of pollution caused by rainwater leaching and infiltration.

DATA AVAILABILITY STATEMENT

The raw data supporting the conclusions of this article will be made available by the authors, without undue reservation.

AUTHOR CONTRIBUTIONS

WZ and XW contributed to the conception of the study. WZ and XY performed the experiment. WZ, XY, and JH contributed significantly to analysis and manuscript preparation. WZ and XY performed the data analyses and wrote the manuscript. JH, RL, and ZZ helped perform the analysis with constructive discussions. All authors have read and agreed to the published version of the manuscript.

FUNDING

This work was supported by the National Key Research and Development Program of China (2018YFC1800205 and 2018YFC1800200).

SUPPLEMENTARY MATERIAL

The Supplementary Material for this article can be found online at: https://www.frontiersin.org/articles/10.3389/fpubh.2021.764788/full#supplementary-material

REFERENCES

1. Barcelos DA, Pontes FVM, Silva FANG, Castro DC, Anjos NOA, et al. Gold mining tailing: Environmental availability of metals and human health risk assessment. *J Hazard Mater.* (2020) 397:122721. doi: 10.1016/j.jhazmat.2020.122721
2. Wei L, Wang K, Noguera DR, Jiang J, Oyserman B, Zhao N, et al. Transformation and speciation of typical heavy metals in soil aquifer treatment system during long time recharging with secondary effluent: Depth distribution and combination. *Chemosphere.* (2016) 165:100–9. doi: 10.1016/j.chemosphere.2016.09.027
3. Maleki A, Hajizadeh Z, Sharifi V, Emdadi Z. A green, porous and eco-friendly magnetic geopolymer adsorbent for heavy metals removal from aqueous solutions. *J Clean Prod.* (2019) 215:1233–45. doi: 10.1016/j.jclepro.2019.01.084
4. Pan Y, Ding L, Xie S, Zeng M, Zhang J, Peng H. Spatiotemporal simulation, early warning, and policy recommendations of the soil heavy metal environmental capacity of the agricultural land in a typical industrial city in China: Case of Zhongshan City. *J Clean Prod*. (2020) 2020:124849. doi: 10.1016/j.jclepro.2020.124849
5. Xiao R, Guo D, Ali A, Mi S, Liu T, Ren C, et al. Accumulation, ecological-health risks assessment, and source apportionment of heavy metals in paddy soils: A case study in Hanzhong, Shaanxi, China. *Environ Poll.* (2019) 248:349–57. doi: 10.1016/j.envpol.2019.02.045
6. He ZL, Yang XE, Stofella PJ. Trace elements in agroecosystems and impacts on the environment. *J Trace Elem Med Biol.* (2005) 19:125–40. doi: 10.1016/j.jtemb.2005.02.010
7. Bhutiani R, Kulkarni DB, Khanna DR, Gautam A. Water quality, pollution source apportionment and health risk assessment of heavy metals in groundwater of an industrial area in north India. *Expo Health.* (2016) 8:3–18. doi: 10.1007/s12403-015-0178-2
8. Li F, Qiu ZZ, Zhang JD, Liu WC, Liu CY, Zeng GM. Investigation, pollution mapping and simulative leakage health risk assessment for heavy metals and metalloids in groundwater from a typical brownfield, middle China. *Int J Environ Res Public Health.* (2017) 14:768. doi: 10.3390/ijerph14070768
9. Zhang H, He PJ, Shao LM. Fate of heavy metals during municipal solid waste incineration in Shanghai. *J Hazard Mater.* (2007) 2007:365–73. doi: 10.1016/j.jhazmat.2007.12.025
10. Guo YH, Sun XC, Zhang SB, Yu GJ, Tang Z, Liu ZH, et al. Pollution characteristics, source analysis and potential ecological risk assessment of heavy metals in soils surrounding a municipal solid waste incineration plant in Shanghai. *Environ Sci.* (2017) 38:5262–71. doi: 10.13227/j.hjkx.201704113
11. Wang JJ, Zhao HW, Zhong XP, Liu YS, Zeng H. Concentration levels and spatial distribution of heavy metals in soil surrounding a municipal solid waste incineration plant (Shenzhen). *Environ Sci.* (2011) 32:298–304. doi: 10.1631/jzus.A1010009
12. Israel D, David E, Gustav G, Samuel D, Elliot K, David S. Spatial distribution, accumulation and human health risk assessment of heavy metals in soil and groundwater of the Tano Basin, Ghana. *Ecotoxicol Environ Safety.* (2018) 165:540–6. doi: 10.1016/j.ecoenv.2018.09.015
13. Wongsasuluk P, Chotpantarat S, Siriwong W, Robson M. Heavy metal contamination and human health risk assessment in drinking water from shallow groundwater wells in an agricultural area in Ubon Ratchathani province, Thailand. *Environ Geochem Health.* (2014) 36:169–82. doi: 10.1007/s10653-013-9537-8
14. Hofmann J, Watson V, Scharaw B. Groundwater quality under stress: contaminants in the Kharaa River basin (Mongolia). *Environ Earth Sci.* (2015) 73:629–48. doi: 10.1007/s12665-014-3148-2
15. Bhutiani R, Kulkarni DB, Khanna DR, Gautam A. Geochemical distribution and environmental risk assessment of heavy metals in groundwater of an industrial area and its surroundings, Haridwar, India. *Energy Ecol Environ.* (2017) 2:155–67. doi: 10.1007/s40974-016-0019-6
16. Kashyap R, Verma KS, Uniyal SK, Bhardwaj SK. Geospatial distribution of metal(loid)s and human health risk assessment due to intake of contaminated groundwater around an industrial hub of northern India. *Environ Monit Assess.* (2018) 190:136. doi: 10.1007/s10661-018-6525-6
17. Nkpaa KW, Amadi BA, Wegwu MO. Hazardous metals levels in groundwater from Gokana, rivers state, Nigeria: non-cancer and cancer health risk assessment. *Hum Ecol Risk Assess.* (2018) 24:214–24. doi: 10.1080/10807039.2017.1374166
18. Ahmadi SH, Sedghamiz A. Geostatistical analysis of spatial and temporal variations of groundwater level. *Environ Monit Assess.* (2007) 129:277–94. doi: 10.1007/s10661-006-9361-z
19. Lin ML, Gui HR, Peng LH, Sun LH, Chen S, Li ZC. Health risk assessment of heavy metals in deep groundwater from different aquifers of a typical coal mining area: A case study of a coal mining area in northern Anhui Province. *Acta Geosci Sin.* (2014) 35:589–98. doi: 10.3975/cagsb.2014.05.09
20. Li ZH, Zhang S, Bi EP, Yu J, Wang WZ, Ma LS. The health risk assessment of groundwater organic pollution at a certain oil depot. *Acta Geosci Sin.* (2010) 31:258–62. doi: 10.1631/jzus.A1000244

21. Kumar B, Verma VK, Naskar AK, Sharma CS, Mukherjee DP. Bioavailability of metals in soil and health risk assessment for populations near an Indian chromite mine area. *Hum Ecol Risk Assess.* (2014) 20:917–28. doi: 10.1080/10807039.2013.791589
22. Moradi A, Honarjoo N, Najafi P, Fallahzade J. A human health risk assessment of soil and crops contaminated by heavy metals in industrial regions, central Iran. *Hum Ecol Risk Assess.* (2016) 22:153–67. doi: 10.1080/10807039.2015.1056293
23. Obiora SC, Chukwu A, Davies TC. Heavy metals and health risk assessment of arable soils and food crops around Pb-Zn mining localities in Enyigba, southeastern Nigeria. *J Afr Earth Sci.* (2016) 116:182–9. doi: 10.1016/j.jafrearsci.2015.12.025
24. Zhang HJ, Wang XR, Chen CY, Liu X, Wang Q. The health risk assessment and remediation guide limit value of typical chromium slag contaminated sites. *Acta Sci Circum.* (2010) 30:1445–50. doi: 10.13671/j.hjkxxb.2010.07.015
25. Guan Y, Shao CF, Gu QB, Ju MT, Zhang Q. Method for assessing the integrated risk of soil pollution in industrial and mining gathering areas. *Int J Environ Res Public Health.* (2015) 12:14589–609. doi: 10.3390/ijerph121114589
26. Li F, Zhang JD, Yang J, Liu CY, Zeng GM. Site-specific risk assessment and integrated management decision-making: a case study of a typical heavy metal contaminated site, middle china. *Hum Ecol Risk Assess.* (2016) 22:1224–41. doi: 10.1080/10807039.2016.1151348
27. Leeuwen CJV, Vermeire TG. *Risk Assessment of Chemicals: An Introduction. 2nd ed*. Heidelberg: Springer Press (2007).
28. World Bank. *Overview of the Current Situation on Brownfield Remediation and Redevelopment in China*. Danvers, MA (2010).
29. Chen XY, Li F, Zhang JD, Liu SQ, Ou CH, Yan JJ, et al. Status, fuzzy integrated risk assessment, and hierarchical risk management of soil heavy metals across china: a systematic review. *Sci Total Environ.* (2021) 785:147180. doi: 10.1016/j.scitotenv.2021.147180
30. Watson DF, Philip GM. A refinement of inverse distance weighted interpolation. *Geo-Processing.* (1985) 2:315–27.
31. Liu R, Chen Y, Sun C. Uncertainty analysis of total phosphorus spatial-temporal variations in the YangtzeRiver Estuary using different interpolation methods. *Mar Pollut Bull.* (2014) 86:68–75. doi: 10.1016/j.marpolbul.2014.07.041
32. Shepard D. A two-dimensional interpolation function for irregularly-spaced data. *ACM Natl Conf.* (1968) 23:517–24. doi: 10.1145/800186.810616

Conflict of Interest: The authors declare that the research was conducted in the absence of any commercial or financial relationships that could be construed as a potential conflict of interest.

Publisher's Note: All claims expressed in this article are solely those of the authors and do not necessarily represent those of their affiliated organizations, or those of the publisher, the editors and the reviewers. Any product that may be evaluated in this article, or claim that may be made by its manufacturer, is not guaranteed or endorsed by the publisher.

frontiers in Public Health

ORIGINAL RESEARCH
published: 29 October 2021
doi: 10.3389/fpubh.2021.751103

The Status Quo and Attribution of Wildlife Crimes: A Study of Cases in China From the Perspective of Ecological Economic Ethics

Zhongmin Zhang[1], *Yuting Zeng*[2] *and Danqi Xie*[3]*

[1] Law School, Institute of Ecological Civilization, Zhongnan University of Economics and Law, Wuhan, China, [2] Law School, Zhongnan University of Economics and Law, Wuhan, China, [3] School of Philosophy, Institute of Economic Ethics, Zhongnan University of Economics and Law, Wuhan, China

The COVID-19 pandemic, which has ravaged the world, has led to a rethinking of the relationship between humans and nature and the clichés of the economic-centered model. Thus, the ecological economy has been reviewed, especially from an ethical worldview. This paper uses statistical methods to retrieve and categorize 3,646 wildlife crime cases for analysis and quantitative research. It adopts legal and ethical perspectives to analyze the subject and the subjective, incidence, and sentencing factors of wildlife crimes and uses the ecological economic ethical model to measure wildlife crimes. We argue that the existing judicial system fails to answer the difficulties of the economic ethics of wildlife crimes. It is recommended that ecological and economic ethical awareness be internalized. We suggest calling for comprehensive legislation on wildlife crimes from the perspective of ecological economic ethics to effectively prevent and reduce wildlife crime and eventually promote public health.

Keywords: COVID-19 epidemic, wildlife crimes, economic ethics, ecological economic ethics, public health

OPEN ACCESS

Edited by:
Hongtao Yi,
The Ohio State University,
United States

Reviewed by:
Yongping Sun,
Hubei University of Economics, China
Shuai Shao,
East China University of Science and Technology, China

***Correspondence:**
Danqi Xie
danqixie@zuel.edu.cn

Specialty section:
This article was submitted to Environmental health and Exposome, a section of the journal Frontiers in Public Health

Received: *31 July 2021*
Accepted: *20 September 2021*
Published: *29 October 2021*

Citation:
Zhang Z, Zeng Y and Xie D (2021) The Status Quo and Attribution of Wildlife Crimes: A Study of Cases in China From the Perspective of Ecological Economic Ethics. Front. Public Health 9:751103. doi: 10.3389/fpubh.2021.751103

INTRODUCTION

As COVID-19 affects the world, wildlife conservation issues have returned to the limelight. COVID-19 is much more serious than SARS's shock in 2002–2003. Notably, the COVID-19 pandemic brought tragic consequences for public health in both 2020 and 2021. According to the World Health Organization, COVID-19 is the disease caused by a new coronavirus called SARS-CoV-2. Moreover, most coronaviruses originate from animals (1). The World Organization for Animal Health confirms that the virus that triggered the outbreak originated from animals. Research since the COVID-19 pandemic began has shown that a range of animals, including wild and farmed species, are susceptible to infection (2). This ecological alarm and public health crisis are a reminder for all of humanity, and the outbreak of the COVID-19 pandemic has led to a review of the relationship between humans and nature, especially the relationship between human beings and animals. Eventually, this phenomenon has encouraged society to become more introspective about solutions to the ecological crisis.

A crime, as a damaging and destructive act against human society, involves conduct that is incompatible with social expectations. Crime is viewed not only as harm to a community's recognized morals and sentiments but also as a violation of others' rights and the order of the legal system. Crime is contrary to the public interest and harmful to individuals or public safety (3). Engels classically noted that crime is the most extreme manifestation of contempt for the

social system (4). The most typical wildlife crimes are among the top five environmental crimes, including the illegal hunting and killing of rare and endangered wildlife and the illegal purchase, transportation, and sale of rare and endangered wildlife and their manufactured products (5). This is a testimony to offenders' disdain for the wildlife conservation order because the violation and denial of wildlife rights are the most typical misconduct. Therefore, we raise the following questions: what type of regularity does the subject of wildlife crimes present? What is its subjective element? Is it based on certain values, and does it reflect a certain social consciousness? What are the objective patterns of wildlife crimes? What values can we use for judgment? Can justice, as the last safeguarding frontier of wildlife protection, provide a full remedy? This paper focuses on wildlife crimes, conducts an in-depth analysis of their causes and contributes to restoring the order of wildlife protection.

MATERIALS AND METHODS

Focusing on the Integration of Three Disciplines

We used "wildlife crime" as a keyword to search on the website "www.pkulaw.com" (6) and obtained detailed research data. This database collects many repeated cases; thus, we removed repeated cases, such as second trial cases and retrial cases, and chose criminal and first trial cases because they echoed our goals. In the end, we obtained 3,646 cases that met our criteria, namely, the first trial criminal cases with no repeated cases. Then, we used statistical methods to analyze the variables of wildlife crimes, including the subject and the subjective, incidence, and sentencing variables. Next, we classified these data and transformed some of the textual data into numeric data. The data are shown in the form of statistical graphs that characteristically display the variable distributions and reveal the structure, inner relations of the cases, and trends of the variables. From legal and ethical perspectives, our research can help to integrate the three disciplines of statistical analysis and processing, legal logic, and ethical thinking.

A New Study Pattern

A traditional paradigm of crime research is to address the phenomenon of crime, analyze the causes of crime, and then propose solutions; this approach analyzes the crime situation (incidence, type of dispute, means and forms, areas, consequences, and characteristics) and basic situation of the perpetrators (age, educational background, occupation, and criminal history) to summarize the causes of the crime (social and personal causes) and form crime prevention countermeasures (7). For instance, when we analyze a criminal case, we consider the objective factors first such as the answers to who committed the crime? What did he or she do? What were the results? Is there causality between the behaviors and the results? Sequentially, we identify the subjective factors, specifically, intentional crime or negligent crime and the age and capability of the perpetrator. This is how criminologists conduct their research on crimes of various types.

TABLE 1 | Wildlife crimes distribution.

Crimes	Number	Proportion (%)
Illegal hunting and killing of rare and endangered wild animals	1,287	34.52
Illegal purchase, transportation, and sale of rare and endangered wild animals and their manufactured products	1,894	50.80
Illegal hunting	537	14.40
Smuggling of rare animals, illegal transportation, and sale of rare and endangered wild animals	10	0.27
Total	3,728	100

This paper adopts a new research paradigm that aims to derive the inherent rules of cases through empirical research on a large number of cases. This paper concentrates on ethical thinking integrated with legal analysis and develops an innovative pattern that compares and contrasts the subject and the object and the subjective and objective factors of different wildlife crimes to consider social awareness, value judgments, and their ranks. Thus, the width and depth of ethical misconduct can be identified in all aspects. The innovation of this paper is that it moves away from traditional perspectives and uses empirical research through case studies, ethical value judgments, and a jurisprudential normative analysis. An innovative model that crosses over the disciplines of statistics, law, and ethics is designed to study the ethical reasons for wildlife crimes and the absence of public health.

RESULTS

The website "www.pkulaw.com" was used as a search platform to collect "wildlife crime" cases. The trial procedure was limited to "trial at first instance" and "criminal cases" were input as the type of dispute. The final retrieval of 3,646 articles was achieved after eliminating duplicate and unrelated cases. The cases were as follows: "illegal hunting and killing of rare and endangered wild animals;" "illegal purchase, transportation, and sale of rare and endangered wild animals and their manufactured products;" "illegal hunting;" and "smuggling of rare animals, illegal transportation, and sale of rare and endangered wild animals." Among the cases (**Table 1**), there were 1,287 cases of "illegal hunting and killing of rare and endangered wild animals," 1,894 cases of "illegal purchase, transportation, and sale of rare and endangered wild animals and their manufactured products," 537 "illegal hunting" cases, and 10 cases of "smuggling of rare animals, illegal transportation, and sale of rare and endangered wild animals." Notably, in the latest revision of China's Criminal Law in 2020, a new clause was added under Article 341 to criminalize the hunting, purchasing, transporting, and selling of rare and endangered wild animals criminalize hunting, purchasing, transporting, and selling—for the purpose of consumption as food. However, this crime was newly updated,

TABLE 2 | The subjective aspects (negligence crime).

Circumstance	Number	Proportion (%)
First offense	1,295	35.51
Second-time or greater	693	19.00
Surrendering criminal	2,574	70.60
Demonstrate repentance	2,307	63.27

TABLE 3 | The subjective aspects (intentional crime).

Circumstance	Number	Proportion (%)
Intentional crime	908	24.90
Criminal record	1,314	36.04
Gun-toting	502	13.77

TABLE 4 | Punishments and circumstances.

	Consequences	Number	Proportion (%)
Punishments	Detention	2,107	44.63
	Community correction	673	14.26
	Suspended sentence	1,321	27.98
	Sentence of more than 10 years	150	3.18
	Combined sentence of principal and supplementary punishment	3,201	67.80
	Sentence of "not guilty"	6	0.13
Circumstances	Lesser punishment	2,515	53.27
	Commutation	1,789	37.89
	Abatement of criminal punishment	737	15.61
	Heavier punishment	391	8.28

and relative crimes were rare. We did not take this crime into consideration. We can conclude that "illegal hunting and killing of rare and endangered wild animals" and "illegal purchase, transportation and sale of rare and endangered wild animals and their manufactured products" account for the largest number of cases.

Subjective Aspects

The subjects of the crime were mainly natural persons in 3,593 cases, which accounted for 98.57% of the total number of wildlife crimes. In contrast, unit crimes constituted a total of 53 cases, which accounted for only 1.45%. Among the wildlife crimes committed by natural persons, 501 cases were committed by minors (under 18 years old), which accounted for 13.94% of the total.

Of all wildlife crime cases (**Table 2**), 1,295 cases were first offenses, and 693 were second-time or greater offenses, and they constituted 35.51 and 19.00%, respectively. The numbers of cases in which the subject of the crime surrendered and demonstrated repentance were 2,574 and 2,307, respectively, which represented 70.60 and 63.27% of the total, respectively. These numbers suggest a higher degree of first-time offending and a certain degree of repentance on the part of the criminal subjects.

In addition, 908 cases were intentional crimes, and 1,314 offenders had criminal records (**Table 3**), which constituted 24.90 and 36.04%, respectively. There were 502 cases where the perpetrator was armed with a gun, which was 13.77% of the total. The defendants were represented by a lawyer in 1,984 of the 3,646 cases, or 54.42% of the total number. There were 302 cases of attempted crimes or 8.28% of the total. This number is higher than that of first-time and occasional offenders and indicates a lower level of remorse for crimes and a higher likelihood of recidivism.

Sentencing

As shown in **Table 4**, we collected 3,646 wildlife crime cases and identified 4,721 defendants, 1,321 of whom were given suspended sentences, which accounted for 51% of the number of cases with fixed-term imprisonment. The individuals who were sentenced were placed on between a minimum 3-year probation and a maximum of 6 years and 3 months of probation. A total of 58,463,275 RMB in fines and confiscated properties was imposed, which is an average of 12,383.66 RMB per defendant and a minimum value of 500 RMB and a maximum of 1 million RMB. Among the defendants, 2,590 were sentenced to fixed-term imprisonment, which constituted 54.86% of the total number, with a minimum term of 2 months and a maximum term of 18 years. The set-term imprisonment period was mainly

TABLE 5 | The distribution of the sentencing period.

Period	Number	Proportion (%)
0–1 Year	603	23.28
1 Year	404	15.60
1–2 Years	309	11.93
2 Years	299	11.54
2–3 Years	125	4.82
3 Years	223	8.61
3–4 Years	39	1.51
4 Years	34	1.31
4–5 Years	9	0.35
5 Years	155	5.98
5–6 Years	50	1.93
6 Years	70	2.70
6–7 Years	13	0.51
7 Years	48	1.85
7–8 Years	5	0.19
8 Years	26	1.00
8–9 Years	0	0.00
9 Years	16	0.62
9–10 Years	1	0.04
10 Years	78	3.01
Above 10 Years	83	3.20
Total	2,590	100

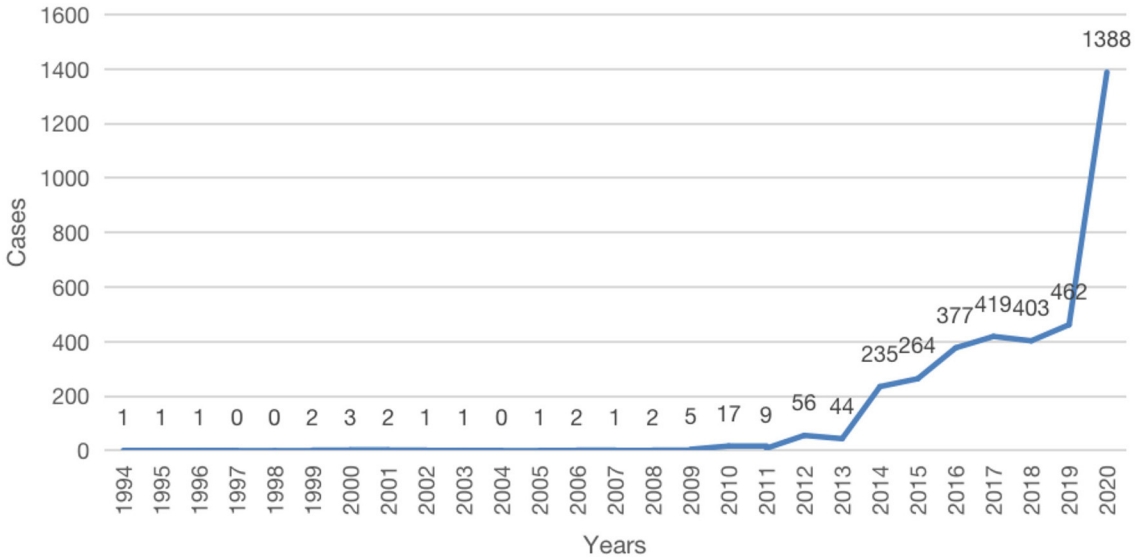

FIGURE 1 | Time heard distribution.

within 3 years. The distribution of the sentencing periods is shown in **Table 5**.

The distributions of the sentencing periods within 1 year were concentrated at 6, 8, 10 months, and 1 year. The sentencing times were concentrated mainly within 3 years. It can be concluded that the sentence (penalty) is lighter than the serious consequences of the offenders' crimes. Judges prefer less punishment, commutation, and the abatement of criminal punishment to heavier punishment. People charged with illegal hunting misconduct were punished only with an additional fine. Therefore, light penalties and suspended sentences are prominent in wildlife crimes. Although the sentencing criteria range from <5 years to more than 10 years of imprisonment, the statutory penalty for wildlife crimes cannot cover different circumstances, and the term limit of a statutory sentence is relatively low compared with other environmental pollution offenses. Thus, the punitive function and deterrent effect of the penalty are limited (8). In practice, scholars and experts also tend to endorse lighter sentences for wildlife crimes and call for reduced punishment, mitigation and acquittal for wildlife crimes. It can be concluded that judges, experts, and scholars are not sufficiently aware of wildlife protection to reach an ecological economic ethical consensus within the domain of the legal community. Therefore, judicial remedies for wildlife are weakened.

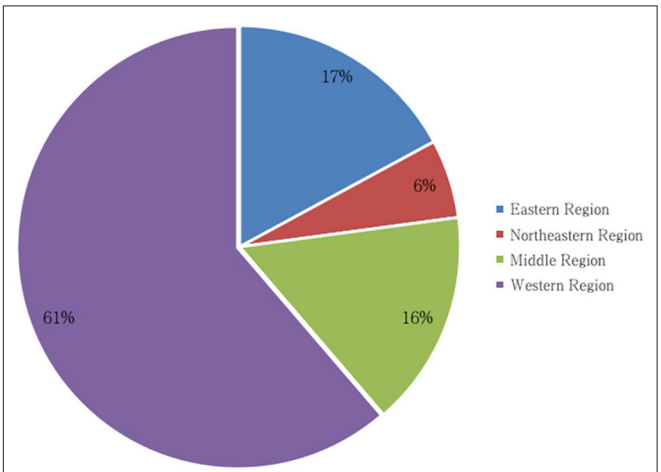

FIGURE 2 | The regional distribution of wildlife crimes.

The Years

Figure 1 shows that wildlife crime cases are concentrated from 2012 to 2020, with the highest number of wildlife crimes at 1,388 in 2020.

In 2000, the Supreme People's Court issued "Opinions on Several Issues Concerning the Concrete Application of Law in the Trial of Criminal Cases Involving Destruction of Wildlife Resources," which reflected the awareness of wildlife protection at the national level. In 2003, China experienced a concentrated outbreak of SARS; thus, the Wild Animal Conservation Law was amended in 2004. The law experienced three amendments in 2009, 2016, and 2018. The three amendments indicate that national awareness of wildlife conservation has improved, but national awareness has not established a foundation for citizens to protect wildlife because wildlife crimes have not decreased. Although the National People's Congress (NPC), the decision-making organ in China, adopted the Interpretation of Articles 341 and 312 of the "Criminal Law of the People's Republic of China," the number of crimes is still rising year-on-year across the country, and it peaked in 2020. The Standing Committee of the 13th NPC swiftly voted to pass a "Decision

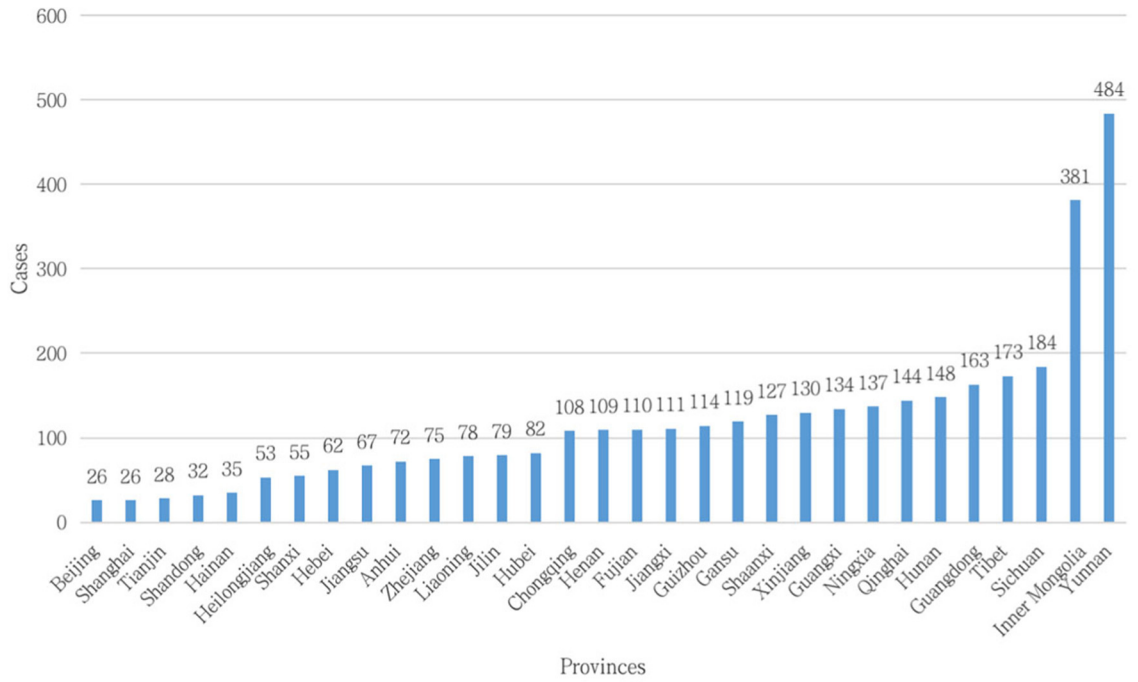

FIGURE 3 | Provincial distribution of wildlife crimes.

of the Standing Committee of the National People's Congress to Comprehensively Prohibit the Illegal Trade of Wild Animals, Break the Bad Habit of Excessive Consumption of Wild Animals, and Effectively Secure the Life and Health of the People." The good news is that with this speedy decision passed by the NPC, the Chinese government launched a drive to fight wildlife crimes across China. Thus, there was a dramatic surge in the number of wildlife crimes in 2020. The coronavirus outbreak in 2020 witnesses that closer attention is given to this issue, and the situation is being alleviated around the country. It also reveals that the issues about wildlife markets and trade were overlooked by the central and local governments. The expanding market demand for wild animals due to China's economic boom, ingrained traditional culture of wildlife consumption and the desire to preserve the health of the people encourage consumer affluence. The increasingly greater law enforcement attention given by forest police and customs to wildlife offenses also made the number in 2020 very different from other years. However, social awareness of wildlife conservation is still relatively low, and the increasing number of wildlife crimes is the evidence for this.

The Regions

The three provinces with the highest number of wildlife crimes (**Figures 2**, **3**) are Yunnan, Inner Mongolia, and Sichuan Provinces. All are located in western China, which had 2,235 wildlife crimes, which constituted 61.30% of the country's total. The northeastern region had the lowest number of wildlife crimes at 210, or 5.76 %, while the middle and eastern regions had 15.82 and 17.11% wildlife crimes, respectively (**Table 6**).

TABLE 6 | The regions of wildlife crimes.

Region	Number	Proportion (%)
Eastern region	624	17.11
Northeastern region	210	5.76
Middle region	577	15.82
Western region	2,235	61.30
Total	3,646	100

TABLE 7 | The distribution of nature reserves in China (8).

Region	Number	Proportion (%)
Eastern region	83	17.51
Northeastern region	92	19.41
Middle region	90	18.99
Western region	209	44.09
Total	474	100

The western region ranks at the top in terms of nature reserves (**Table 7**), which accounts for 44.09% of them nationwide (9). The regions with the most nature reserves and the highest number of wildlife crimes are closely correlated. Rich wildlife resources are bestowed on people living in the western area, which objectively provides a breeding ground for wildlife crimes. Additionally, the western region is not economically developed compared with other regions nationally. Furthermore, the western region has a

lower economic capacity. As a result, stimulated by economic incentives, crimes involving rare and endangered wild animals with high economic value are more rampant in this area. At the same time, the educational level is lower than that of the developed areas in eastern and middle China, and this area has underdeveloped educational resources; therefore, the education level is lower on average. Consequently, the awareness of wildlife protection is generally weaker.

DISCUSSION

The Purpose of the Legislation and Legal Principle: Relationships Between Ecological Economic Ethics and Relative Laws

Human practice is generally self-conscious and purposeful. Marx argued that an end cannot be an end if it is not particular, just as an action is meaningless if it has no purpose (4). Legislation practice also follows this inherent rule. Legislation is a conscious activity that entails a certain purpose. Serving as the law's soul and guidance, the purpose of legislation is reflected in the design of the legal system. The purpose of legislation not only embodies the value of all legal provisions and objectives (10) but also restrains the legislature from acting beyond its authority, balances the social reality and different interests, and lays the foundation for the judiciary to interpret the spirit of the law and to judge cases accordingly. Therefore, the purpose of legislation is an important criterion for evaluating the quality of the legislation, and the realization of the purpose of the legislation must be considered when evaluating the implementation of laws.

The term "legal principle" refers to comprehensive principles and standards that can serve as the foundation or source for legal rules (11). According to Hart, legal principles are considered to involve some purpose, goal, entitlement, or value and are regarded as desirable to maintain or to adhere to. Therefore, legal principles not only provide an explanation or rationale for the rules that exemplify them but also contribute to their justification (12). In countries with written law, including China, principles of law are usually expressed by the legislature in the law, its interpretation or its enactment. Principles of law embody the guiding philosophy and values of the law.

Relations Between the Environmental Protection Law and Wild Animal Conservation Law

The "Environmental Protection Law of the People's Republic of China" (hereinafter referred to as the Environmental Protection Law) is the governing ecological environmental protection law in China. The "Wild Animal Conservation Law of the People's Republic of China" (hereinafter referred to as the Wild Animal Conservation Law) serves as the basic law for wildlife protection. The purpose of the two comprehensive laws can be divided into two levels of legislation. The first level has a general purpose; it potentially shapes people's attitude, choice and estimation of the law and enables members of society in general to participate in legislative activity to showcase their consensus on the law and legal values. Thus, it is possible to select, evaluate, and agree with legislation (13). Regarding this level, the legislative purpose of the Environmental Protection Law is of a higher order and encompasses diversified legislative purposes, such as environmental protection, pollution prevention and control, public health protection, the promotion of ecological civilization, and the development of economic society. The second level is the legislative purpose of specific legal sectors, which is determined by the specific function and role of different sectoral laws in adjusting different social relations. The purpose of legislation evolves as the social background changes and members of society upgrade their legal values. The Wild Animal Conservation Law was enacted in 1988 and was amended in 2004, 2009, 2016, and 2018. Its legislative purpose in 1988, 2004, and 2009 was to protect, rescue, and conserve rare and endangered species, to protect, develop, and rationally use wildlife resources, and to maintain the ecological environment balance. In the 2016 and 2018 versions, the purpose changed to protecting wild animals, rescuing rare and endangered wildlife, maintaining biodiversity and ecological balance, and promoting ecological civilization. The expression "protect, develop, and rationally use wildlife resources" was deleted from the legislative purpose in 2016 and 2018, and "maintain biodiversity" and "promote ecological civilization" were added. The ecological meanings of the purpose of the law were deepened. Accordingly, the legislative principles were revised from "strengthening resource protection, domesticating and breeding wild animals, and rationally developing and utilizing wild resources" to "prioritizing protection, utilization and strictly supervising" wildlife resources, with the additional connotation of protection and supervision.

At the same time, the scope of wild animals referred to in the Wild Animal Conservation Law was changed from "rare and endangered animals with economic and scientific value" to "rare and endangered animals with ecological, scientific and social value." Although the focus changed from "economic value" to "ecological and social value," the scope of protection is still classified by the values of animals' scarcity and availability (14).

The Environmental Protection Law, as the basic law in the field of environmental resource protection, still insists on two goals: environmental protection and economic social development. On the one hand, people relentlessly pursue rapid economic growth and continuously accumulate material wealth. On the other hand, people fear that the economy-centered model will become a burden on ecology and society. This anxiety showcases a contradiction between the excessive speed of development and the pressure of environmental burdens (15) and reflects a reluctant concession to the priority of economic development. It is not essentially ecological. Although the purpose, legislative principles and scope of protection of the Wild Animal Conservation Law have given way to some extent to protect wildlife, the substance and core are still rooted in the utilization and management of wildlife resources. This means that the law betrays its legislative purpose and principles (16). The Wild Animal Conservation Law, which focuses on the economic end, does not fully match its ecological ethical needs. A large part of the Wild Animal Conservation Law is devoted to wildlife utilization. It is still based on economic thinking (14), which

indicates that the wildlife resource value remains unchanged (17). Additionally, the amended versions of the "Wild Animal Conservation Law" do not cover the prevention and control of major public health risks and lack consideration of public health and hygiene.

Therefore, the two basic laws in environmental and wildlife protection both fail to include the value of wildlife protection and the consideration of the value of public health and ecological ethics. Instead, people fall prey to utilitarian economic value.

Relations Between the Criminal Law and Wild Animal Conservation Law

The "Criminal Law of the People's Republic of China" (hereinafter referred to as the Criminal Law) was originally established to combat crimes, protect citizens' lives and property, and maintain social and economic order. Subsequently, current wildlife-related offenses under the Criminal Law have focused on punishing the disruption of the economic order and protecting state property while preventing crimes. Thus, wildlife crime provisions do not embrace the discipline of ecological ethical misconduct and concentrate only on the economic value of wildlife resources. Regarding the provisions for wildlife crimes and adjudication practices, the configurations of the penalties are inconsistent: the types of wildlife crime punishment are relatively homogeneous, and some misconduct is not addressed by the Criminal Law; thus, the cost of committing the offense is low. These findings indicate that the penalties have an insufficient deterrent effect on perpetrators and fail to effectively reflect the punitive effect of this law on wildlife crimes and the role of the law in improving the ethical quality of the ecological economy (18). Regarding the subjective aspects of the crime, wildlife crime offenders have both negligence and intentional considerations, but the common feature is that they view economic interests as the most important incentive; therefore, the concept of ecological morality is not formed subconsciously. Concerning the object aspect of the crime, the wildlife crime provisions in the Criminal Law describe violations of property interests and the national wildlife protection order, but more attention is given to the stability and orderliness of property interests. From an objective viewpoint, the provisions for wildlife crime discuss social harm and consequences. Articles 341 and 151 of the Criminal Law make the "seriousness of circumstances" a condition for aggravating the statutory punishment for wildlife protection. The "Judicial Interpretation of Criminal Cases Involving Wild Animals" provides for "serious circumstances" and "particularly serious circumstances," and it rules that for the serious cases that include excessive wild animals beyond regulations and seriously harmful means, high economic value can be defined. This judicial interpretation provides for "aggravated circumstances" and "particularly aggravated circumstances." However, it is unclear how to understand the criteria in the addenda tables for interpreting the terms of "illegal hunting, killing, purchase, transportation, and sale of rare and endangered wild animals," "serious circumstances," "particularly serious circumstances," and "quantity criteria." Are these criteria interpreted in accordance with ecological science or laws? Is the clause the tool for judges to abuse their discretionary power? These issues are unclear. Therefore, the supporting judicial interpretation for punishing wildlife crimes needs to be discussed further.

Wildlife Crimes and Ecological Economic Ethics

As we discussed before, the purpose of legislation serves the needs of certain guidelines and values. However, it is so abstract that it must be interpreted into specific rules or articles. We discuss the relations between wildlife crimes and ecological economic ethics. In a sense, the article crystallizes the purposes of the legislation.

The Notion: Ecological Economic Ethics

A legal system must exhibit specific conformity with morality or justice or rest on a widely diffused conviction so that there is a moral obligation to obey it. That is, it follows that the criteria of the legal validity of particular laws in a legal system must include, tacitly if not explicitly, a reference to morality or justice (13). As we mentioned before, the Standing Committee of the 13th NPC passed a decision. However, the spokesman also confessed that this move was temporary and that the comprehensive revision of wildlife protection was a long-term goal (19). At the same time, some cities and provinces in China have introduced local regulations to combat the indiscriminate consumption of wild animals; however, supporting legislation is still pending. Although the law is not omnipotent, and legislation is not the sole solution for wildlife crimes, effectively implemented and enforced laws are those consistent with or similar to prevailing customs (20). Thus, without a shift in awareness about wildlife, legislation is still bounded by the superficial level of economic value. Even though wildlife legislation is sophisticated and well-designed, authorities cannot expect it to be automatically accepted by the people and transferred into actions by the public. Therefore, the legal system must combine the law with the conscious acceptance of people's moral sentiments to produce a solid social foundation for the legal system.

It is suggested that given the subjective factors of wildlife crimes, offenders only consider economic interests and have weaker ecological ethical awareness. Regarding the objective consideration of wildlife crimes, the original aim of establishing wildlife crime clauses is to maintain the economic order. The scope of wildlife animals protected by the law is also limited to the animals that are of use or that have economic value; however, animals with little economic value but great ecological value are not on the protected list. Considering the incidence and sentencing of wildlife crimes, although the Wild Animal Conservation Law has been amended several times, its amendments have not produced a positive impact on the deterrence of wildlife crimes as expected. In judicial practice, this can result from a dismissive ecological ethic and lighter punishment or even no punishment since the judges focus excessively on the necessity principle of criminal law. This is demonstrated by the fact that illegal hunting actions are punished by fines but not by harsher sentences; there is a high proportion of suspended sentences, and the average sentence is short. These situations illustrate the limitations of using economics as a standard to judge wildlife crimes. Therefore, it is necessary

to introduce ecological economic ethics to compensate for the shortcomings caused by prioritizing economics.

Given the large number of issues posed by prioritizing economic interests, calls for ecological ethics and ecological morality are snowballing, and ecological economic ethics is in the spotlight. Leopold expands the content of ethics from studying the relationships among people and between people and society to the relationship between people and the land (21). He notes the limitations of traditional ethics (22) and proposes the concept of "land ethics," which is the prototype of ecological ethics. Holmes Rolston develops the doctrine of land ethics and proposes considering a fundamental, natural sense of environmental ethics (23). However, in the current context of anthropocentric ecology, solely emphasizing ecological ethical values may ignore reality because economic activity is the basis of human existence. Living standards will regress if people overlook economic development. This ideology can be echoed by law, which regulates the interrelationships among human beings. Without this consensus, the ideology that protects a pure environment with no human participation cannot be accepted, recognized, or protected by law (24). Again, it is necessary to introduce the economic-centered development model and choose a sustainable ecological economic path.

Ecological economic ethics regulates the economy with ecological ethics and explores the rationality of economic development, which means that in traditional economic practice, ecological elements are included in the indicators of economic evaluation and ethical considerations. The rationality of economic behavior is related to whether it meets the requirements of natural law and ecological environmental protection. With the integration of ethics, ecology, and economics (25), ecological economic ethics refers to people obeying ethical norms, building ethical relationships and performing ethical practices to consciously reconcile and balance economic construction, social development and environmental protection in economic society. Ultimately, people can unite and balance social, economic, and ecological benefits. Ecological economic ethics justifies the promotion of the ecological economy and a sustainable development path from an ethical perspective, which paves the way for a moral order or moral climate (26). According to Leopold, human actions can be explained as the result of an aggregation of individual actions that originate from the inner will. In addition to their hunting and economic value, wild animals have potential significance for all humanity that most people are unaware of (22). One of the most important reasons for the persistence of wildlife crimes is that people lack ecological economic ethics, which entails powerful moral means because laws are incapable of solving the problem. People's obsession with money should be upgraded to ecological economic awareness to thus create an ecological economic atmosphere in society.

Ecological Economic Ethics Model of Wildlife Crimes

Ecological economic ethics plays two roles: to provide the necessary moral defense for the development of the ecological economy and to create the necessary moral order or moral atmosphere. Therefore, the "internalization" of eco-economic ethics can provide a new perspective to seek a more universal and inherent moral mechanism and perspective for the "human-nature-human" behavior model. Ecological economic ethics can be divided into three parts, namely, awareness, rules and practices. To fulfill the mission of eco-economic ethics, it is necessary to go through the three levels of moral awareness, moral rules and moral practice. First, moral awareness is needed to establish the ideology and cognition of ecological ethics and to clarify the boundary between morality and immorality. Second, internalized or externalized rules are used to embody and express ecological ethics. Finally, practice can promote the guidance of economic behavior through the operation of ecological ethics rules to form a benign interaction. Thus, the connection between wildlife crimes and ecological economic ethics must be considered. First, as one of the extreme behaviors of polluting the environment or causing great ecological damage, how can the moral failure of wildlife crimes be reflected? Is it a subjective consciousness or an objective behavior? Is it, and how should it be judged from a value standard? Second, can the penalties of wildlife crimes meet the demand of eco-economic ethics? That is, can the judicial interpretation of wildlife crimes improve the quality of eco-economic ethics?

Specifically, ecological economic ethics can be divided into three parts, specifically, ethical awareness, ethical rules, and ethical practice. A model can bridge the gap between the four constitutive elements of wildlife crimes (this paper adopts the "Four Constitutive Elements Theory," i.e., the subject, the subjective, the object and the objective) and the three levels of ecological economic ethics (awareness, rules and practice) (18). The model is shown in **Table 8**.

From the subject view of wildlife crimes, these crimes are mainly committed by natural persons, which indicates that the parties are less socially conscious. From the subjective viewpoint of wildlife crimes, the social awareness of the people who commit negligent crimes is neither good nor bad but socially conscious. The offenders of intentional wildlife crimes have malice and weak social awareness. From the perspective of the object, wildlife crimes destroy the social relations that operate through private rights; thus, they are difficult to judge. From the perspective of the objective, wildlife crimes center on economic value, which is easy to judge and achieve. The high incidence and excessive practices of wildlife crimes demonstrate that offenders defy ecological economic ethics. This high incidence and these excessive practices show the deep misconduct of ecological and economic ethics. However, at the same time, we should hold a dynamic and dialectical view about the volume of cases. A high number of cases is generally considered to be more serious moral misconduct. However, from the perspective of adjudication, a high number of cases may also mean that certain provisions that correspond to the crime are invoked more than other provisions to thus become "popular" provisions, which increases the frequency of punishment. For example, after the outbreak of the 2020 epidemic, the surge in the number of wildlife cases illustrates the increase in punished wildlife misconduct brought about by the enactment of rules created with a strong awareness to

TABLE 8 | Ecological economic ethics model of wildlife crimes (18).

Constitutive elements	Ecological economic ethics model	Measures	Consequences
The subject	Awareness	Strong or weak social awareness	If the subject is a unit, then its social awareness is strong. If the subject is a natural person, then its social awareness is weak.
The subjective	Awareness	Value judgment of awareness	If the offenders are criminally negligent, then they have strong social awareness with a neutral attitude toward the crime. If the offenders are criminally intentional, then they have weak social awareness with malice.
The object	The static rules	How to protect the ecological ethic relationship	If it relies on the social relations run by public power, then the standard of judgment is high, but it is easy to judge. If it relies on the social relations protected by private law, then the standard of judgment is low, but it is difficult to judge.
The objective	The dynamic rules	Value ranking in measures	If it takes an economic value as the judgment, then it is easy to judge and achieve. If it takes an ecological value as the judgment, then it is difficult to judge and achieve.
The cases	Practices	Width of ethic misconduct	If the misconduct is wide, then the cases are excessive. If not, then the cases are less quantitative.
Sentencing	Practices	Depth of ethical misconduct	If the level of misconduct is deep, then the sentencing is heavy. If not, then the sentencing is light.

TABLE 9 | Ecological economic ethics dimensions of wildlife crimes (18).

Clauses	Crimes	Ecological economic ethics					
		Awareness		The static rules	Practice		The dynamic rules
		The subject	The subjective	The objects	The cases	Sentencing	The objective
Article 341I	Illegal hunting and killing of rare and endangered wild animals	Weak social awareness	Uncertain	It is easy to judge and achieve.	The cases are excessive.	Sentencing is light.	It is difficult to judge and achieve.
Article 341 I	Illegal purchase, transportation, and sale of rare and endangered wild animals and their manufactured products						
Article 341 II	Illegal hunting				The cases are less quantitative.		It is easy to judge and achieve.
Article 151 III	Smuggling of rare animals, illegal transportation, and sale of rare and endangered wild animals						

thus enable more moral misconduct to be deterred or punished by law.

Different dimensions of wildlife crimes echo different ecological economic ethical dimensions. The details are as follows.

As shown in **Table 9**, although all of the crimes are committed by natural persons, the corresponding ecological economic ethics dimensions of different wildlife crimes vary, such as the "illegal hunting and killing of rare and endangered wild animals" and "illegal purchase, transportation, and sale of rare and endangered wild animals and their manufactured products." The two crimes are abundant in real life because of weak social consciousness, such as the ecologically friendly and green-environment awareness of the parties involved. Second, the offense is easy to judge since it focuses on economic values. Conversely, although offenders of the illegal hunting and smuggling of rare animals and the illegal transportation and sale of rare and endangered wild animals have weak social awareness, they destroy administrative licenses such as hunting licenses and chartered hunting licenses. The crime of smuggling rare animals and precious animal products infringes on the national trade management system (27). As a result, it is easy to identify and judge.

Accordingly, eco-economic ethics are rarely seen in wildlife crimes. The reasons are as follows. The interests protected by wildlife crimes are relatively scattered and fragmented, and they fail to cover all aspects of the ecosystem and establish an overall and systematic meaning of eco-economic ethics. Second, most of these interests reflect or emphasize economic value instead of

ecological value. From an internal perspective, although the criminal composition of wildlife crimes and eco-economic ethics are closely related, the corresponding relationships between different variables are not consistent and show a non-linear distribution.

SUGGESTIONS

Dangerous zoonotic diseases are not only highly contagious but also highly lethal. Studies indicate that 70% of new diseases will originate from wild animals (28). The widespread lack of ecological economic ethics has led people to focus on the economic value of wildlife and to ignore its health risks. People should bear in mind the separation of the economic and ecological value of wild animals, whose neglect could eventually lead to a public health crisis across the globe. Therefore, promoting ecological economic ethics as a guide, implementing the notion of public health and improving relevant legislation are the keys to safeguarding human health and preventing public health crises.

The penal sanction in the Criminal Law, as the final defense of the legal system, is the most severe sanction. The Criminal Law is designed to provide final protection (24) for the legal interests that are established and protected by preceding laws in the overall legal order. The improvement of crime prevention mechanisms lies not only in amending criminal laws but also in observing the laws that precede criminal laws to constitute systematic legislation for wildlife protection. Furthermore, although it marks the cornerstone of wildlife protection law, the Wild Animal Conservation Law includes a narrow range of wildlife that should be protected; consequently, the supporting regulation, the List of Key Protected Wild Animals, does not cover the wild animals that are of ecological value to the environment. The scope of "protected wild animals" in this list should be expanded to include more wild animals. As a basic law in environmental protection, the Environmental Protection Law has established the "protection of public health" among its legislative purposes; article 39 provides for an environmental and health monitoring, investigation and risk assessment system, and incentive measures, while article 47 establishes an emergency and warning system for the environment and public health. In contrast, as an indispensable part of the legal framework for environmental protection and natural resources, the Wild Animal Conservation Law does not reflect the values of public health and hygiene and fails to protect public health as it should. For this reason, the legal system should be equipped with content related to public health and should integrate public health content into the different legal sectors and dimensions. To coordinate with different laws, a system to protect public health can be formed with close institutional links and reasonable structural arrangements to maintain public health security.

Five points should be discussed.

1. Support legal obligation mechanism. Under the principle of punishment, the supporting legal obligation mechanism plays a critical role in combating wildlife crimes. Although the severity of the penalty and the intensity of combating crime may not be coincidentally correlated, according to the principle of fitting the punishment to the crime, the severity of the penalty reflects the level of harm and awareness of the crime (29). For wildlife crimes, the average sentencing term is <3 years, and a lesser term is likely less costly for the offender, which makes it difficult to renew the wildlife conservation order. Therefore, it is necessary to impose more obligations by increasing penalties. The punishment standard that solely depends on the economic value of wild animals and their products should be optimized by taking into account ecological economic ethics. The legal obligation for the consumption of wild animals can be explicitly stipulated in article 337 of the Criminal Law. People can form an expectation of the wildlife protection order through the deterrent effect of criminal law, which can effectively deter wildlife crimes.

2. Implement the precautionary principle. The "precautionary principle" was established in the "Rio Declaration on Environment and Development": countries should extensively use precautionary measures to protect the environment according to their capabilities. Where there is a threat of serious or irreversible damage, countries are not allowed to postpone precautionary measures with the excuse that there is a lack of scientific and sufficient evidence (30). Humanity has also learned a lesson from this epidemic. Without risk prevention mechanisms in place, a highly contagious and devastating disease can create a public health and safety crisis whose consequences are difficult to predict. Recently, science has been incapable of studying the uncertainty between viruses in wildlife and zoonotic infectious diseases; therefore, ecological ethics and an understanding of the relationship between human beings and nature are badly needed. It is necessary to eliminate the indiscriminate consumption of wild animals, such as by creating an eating blacklist that restricts wildlife consumption, adding preventive mechanisms for public health, and using risk contingency plans in the Wild Animal Conservation Law to deepen the implementation of the precautionary principle. Additionally, as a supplement to the laws, an article should be included in the Criminal Law to prevent people from consuming wild animals.

3. Improve public participation in legislation. Citizens, or the public, practice democratic decision making, participate in social life, and enjoy environmental rights. These activities play an important role in standing up for the right to make laws, impeach authorities, accuse, and supervise in their interests. Therefore, this principle is an essential element of environmental governance. The implementation of this principle contributes to safeguarding citizens' environmental rights, improving the efficiency of environmental governance, and realizing environmental democracy and justice. We believe that public and social organizations, including environmental and animal protection organizations, should play their full role in environmental protection and wildlife conservation, while the government should improve the participation of citizens and social organizations in the prevention and control of major public health risks and in legislative procedures.

4. Break the bad habit of eating wild animals. First, we should keep in mind the idea that wild animals are an indispensable part of the environment that maintain biodiversity; thus, they

are beneficial to the ecosystem. In a sense, this point has been emphasized numerous times, but people still have narrow-minded perceptions. Second, wild animals may carry diseases that can cause zoonosis, as demonstrated by great epidemics in research and human history. Preserving one's health is currently trendy. Influenced by traditional Chinese medicine and overstated rumors about the benefits of wildlife, unreasonable people rush to the wildlife market and believe that wild animals can cure rare illnesses and even save people's lives. Modern medicine has proven that wild animals' bones or organs fail to perform this function. Finally, wild animals are the best choice for a loss of appetite. Our predecessors have helped us choose tasty food instead.

5. Strengthen the guidance and education function of schools. Contemporary education is centered on economic supremacy. The renowned ecological economist John B. Cobb Jr. reflected on and criticized the role of schools, and he noted that the purpose of schools currently is to serve the economy, which betrays the aim of serving an ecological civilization and the common welfare of human beings and nature (31). Therefore, legislation can encourage schools to take on the guidance and education of ecological economic ethics by cultivating a climate of awareness of ecological economic ethics, strengthening beliefs in ecological economic ethics, and developing environmentally friendly behaviors. Schools should encourage students to break the illicit trend of consuming wild animals due to blind regimens and hunting and should cultivate positive feelings for animals and the environment. In this way, sustainable development and a green economy can be adopted by students, and schools can effectively play a role in guiding and educating students.

CONCLUSION

This paper analyzes the subject and subjective factors, time, areas, sentencing term, and suspended and additional sentences to reveal the lack of ecological economic ethics in the legislative purposes and principles of the Environmental Protection Law, the Wild Animal Conservation Law, and the Criminal Law. By establishing a model of ecological economic ethics, we find that the social awareness of wildlife crime is weak. From the subject view, wildlife crimes are mainly committed by natural persons, which indicates that the parties are less socially conscious and that their social awareness is neither good nor bad. From the perspective of the object, wildlife crimes destroy the social relations that operate according to private rights; therefore, they are difficult to judge. From the perspective of the objective, wildlife crime offenses center on economic value, and they are easy to judge and achieve. The high incidence and excessive practices of wildlife crimes demonstrate that offenders defy ecological economic ethics. The high incidence and practices indicate deep misconduct. The corresponding ecological economic ethics dimensions of different wildlife crimes vary, such as those for the "illegal hunting and killing of rare and endangered wild animals" and the "illegal purchase, transportation, and sale of rare and endangered wild animals and their manufactured products." The culprit of these two crimes is weak social consciousness, such as the ecologically friendliness and green-environment awareness of the parties involved. These factors show that the existing judicial and legal systems fail to fully embody the value of ecological economic ethics and that legislation related to wildlife protection that values ecological economic ethics is not yet in place; the law is still at the level of a tool rather than reflecting the ultimate value of ecological economic ethics. Therefore, this paper advocates for the deepening of ecological economic ethics consciousness and the establishment of a public health system. Ultimately, we will comprehensively establish a legislative system for ecological economic ethical value and public health.

DATA AVAILABILITY STATEMENT

The original contributions presented in the study are included in the article/supplementary material, further inquiries can be directed to the corresponding author.

AUTHOR CONTRIBUTIONS

ZZ contributed to the study design, including the conceptualization and methodology, prepared datasets, and promoted project administration. YZ contributed to the resources, data analysis, and original draft preparation. DX contributed to the study's organization, identified the research methods, and performed the review and editing of the manuscript. All authors read and approved the final manuscript.

FUNDING

This study was financially supported by the Major Program of the National Social Science Foundation of China: Research on the legal innovation of ecological environment supervision system in the new era (18 VSJ039).

REFERENCES

1. World Health Organization. *Are Animals Responsible for COVID-19 in People?* (2020). Available online at: https://www.oie.int/en/scientific-expertise/specific-information-and-recommendations/questions-and-answers-on-2019novel-coronavirus/ (accessed July 26, 2021).
2. WHO. *WHO-Convened Global Study of the Origins of SARS-CoV-2.* (2020). Available online at: https://www.who.int/publications/m/item/who-convened-global-study-of-the-origins-of-sars-cov-2 (accessed September 4, 2021).
3. Gao MX, Ma KC. *Criminal Law, 8th edn*. Beijing: Peking University Press (2017).
4. Karl M, Friedrich E. *The Complete Works of Marx and Engels*, Vol. 2. Beijing: Renmin Press (1957).
5. Zhang ZM. Judicial remedies for ecological damage-analysis based on 5792 environmental jurisprudence instruments. *Law Sci.* (2016) 4:111–24.

6. "www.pkulaw.com" is a professional and advanced intelligent platform for one-stop legal information search in China. It supports multicategory search.
7. Liu WC. *Criminology: Phenomena, Causes, Responses to Crime*. Beijing: Qunzhong Press (2001).
8. Zhang ZM. Clarity of environmental pollution crimes. *Guizhou Soc Sci.* (2019) 4:59–67. doi: 10.13713/j.cnki.cssci.2019.08.009
9. China Wildlife Conservation Association. *National Natural Conservation List*. (2018). Available online at: http://www.cwca.org.cn/resources/protection/overall/ff80808161da671a0163e2dd3a4803cf.html (accessed July 26, 2021).
10. Lv ZM, Liu JQ. How to amend wild animal conservation law after its first adoption. *Environ Econ.* (2016) 4:28–31.
11. Zhang WX. *Jurisprudence*. Beijing: Higher Education Press (2018).
12. Hart HLA. *The Concept of Law, 2nd edn*. Oxford: Clarendon Press (1994).
13. Li JF. On the principles of law. *J Grad School Chin Acad Soc Sci.* (1992) 4:54–61.
14. Liang ZP. *The Half of the Earth. What Kinds of Wild Animal Conservation Law China is Calling For*. (2020). Available online at: https://www.thepaper.cn/newsDetail_forward_5998207 (accessed July 26, 2021).
15. Gao LH, Zhou YF. The spirit of environmental law—additionally, on the legislative purpose of Environmental Protection Law in China. *J Zhengzhou Univ.* (2015) 48:54–7.
16. Wang JB, Wang H. For whom-rediscuss the purpose of wild animal conservation law. Zhejiang Acad J. (2020) 4:4–9. doi: 10.16235/j.cnki.33-1005/c.2020.03.001
17. Lv ZM. *Interview with Lv Zhongmei: Integrating the Concept of Environment and Health into the Rule of Law*. (2020). Available online at: http://www.pcels.cn/archives/2022 (accessed July 26, 2021).
18. Xie DQ, Zhang ZM. Ecological economic ethical dimension of environmental crimes and its judicial regulation. *China Popul Resour Environ*. (2020) 30:113–20. doi: 10.12062/cpre.20200640
19. Hu L, Bai Y. *Complete Prohibit Illegal Wildlife Trade and Eradicate Wild Animal Consumption-the Spokesperson of the Legal Work Committee of the Standing Committee of the National People's Congress Meet the Media*. (2020). Available online at: http://www.xinhuanet.com/2020-02/24/c_1125620750.htm (accessed July 26, 2021).
20. Su L. Reform, the rule of law and local resources. *Peking Univ Law J.* (1995) 4:1–9.
21. Li YF, Yang QSH, Li Y. *The Ecological Ethic*. Harbin: Harbin Institute of Technology Press (2017).
22. Leopold A. *A Sand County Almanac*. Oxford: Oxford University Press (1949).
23. Holmes R. *Philosophy Gone Wild*. Amsterdam: Prometheus Books (1989).
24. Tian HJ. Ideas and approaches of improving wild animal protection through criminal law. *J Guizhou Univ*. (2020) 38:75–84. doi: 10.15958/j.cnki.gdxbshb.2020.03.08
25. Yin JZ, George E. *Developing Business Ethics in China*. Shanghai: Shanghai Academy of Social Sciences Press (2003).
26. Xiang YQ. *The Research for Ecological Economic Study*. Hunan: Normal University Press (2002).
27. Zhao CY. *The Penalty Standard for Illegally Purchasing Rare and Endangered Wildlife Products Urgently Crime Needs to be Revised*. Beijing:Democracy and Legal System Times, Democracy and Legal System Times (2015).
28. World Animal Protection. *Implementing a Global Ban on Wildlife Trade is an Important Way to Prevent the Outbreak of COVID-19-like Outbreaks*. (2020). Available online at: https://www.worldanimalprotection.org.cn/news/wildlife-trade-ban-an-important-way-to-prevent-outbreaks-similar-to-COVID-19 (accessed July 26, 2021).
29. Zhang ZM. The dilemma and breakthrough of environmental and health litigation—take the public judgment document (2009-2011) of Henan High Court as a sample. *Gansu Social Sci*. (2014) 4:140–50. doi: 10.15891/j.cnki.cn62-1093/c.2014.06.034
30. Lv ZM. *Introduction to Environmental Law*. Beijing: Peking University Press (2010).
31. Ke JH, Cobb JB. *The Study of Post Modern Ecological Thought*. Zhejiang: Zhejiang University Press (2018).

Conflict of Interest: The authors declare that the research was conducted in the absence of any commercial or financial relationships that could be construed as a potential conflict of interest.

frontiers in Public Health

ORIGINAL RESEARCH
published: 17 November 2021
doi: 10.3389/fpubh.2021.766984

Trace Metal Lead Exposure in Typical Lip Cosmetics From Electronic Commercial Platform: Investigation, Health Risk Assessment and Blood Lead Level Analysis

Yanan Li[1,2], *Yanyan Fang*[1,3], *Zehua Liu*[1,3], *Yahan Zhang*[1,3], *Kangli Liu*[1], *Luping Jiang*[1,2], *Boyuan Yang*[1,3], *Yongdie Yang*[3], *Yongwei Song*[3] *and Chaoyang Liu*[1,3,4]*

[1] *Research Center for Environment and Health, Zhongnan University of Economics and Law, Wuhan, China,* [2] *School of Business Administration, Zhongnan University of Economics and Law, Wuhan, China,* [3] *Department of Environmental Science and Engineering, Zhongnan University of Economics and Law, Wuhan, China,* [4] *Renmin Hospital of Wuhan University, Wuhan, China*

OPEN ACCESS

Edited by:
Hongtao Yi,
The Ohio State University, United States

Reviewed by:
Liqin Yu,
Huazhong Agricultural University, China
Zhihua Xiao,
Hunan Agricultural University, China

***Correspondence:**
Chaoyang Liu
lcy@zuel.edu.cn

Specialty section:
This article was submitted to Environmental health and Exposome, a section of the journal Frontiers in Public Health

Received: *30 August 2021*
Accepted: *21 October 2021*
Published: *17 November 2021*

Citation:
Li Y, Fang Y, Liu Z, Zhang Y, Liu K, Jiang L, Yang B, Yang Y, Song Y and Liu C (2021) Trace Metal Lead Exposure in Typical Lip Cosmetics From Electronic Commercial Platform: Investigation, Health Risk Assessment and Blood Lead Level Analysis. Front. Public Health 9:766984. doi: 10.3389/fpubh.2021.766984

Lead (Pb) in lipstick products has become an increasing concern, which can cause safety problems to human body directly with diet. To investigate the Pb exposure and potential health risk level of typical popular lip cosmetics in Chinese e-commerce market, Python crawler was introduced to identify and select 34 typical popular lip cosmetics, including 12 lipsticks, 13 lip glosses, and 9 lip balms. And then this study used ICP-MS to determine the content of Pb. Furthermore, the ingestion health risk assessment method issued by United States Environmental Protection Agency (USEPA) and Monte Carlo simulation algorithm were applied to assess the probabilistic health risks of adults exposure. Finally, taking the possible exposure of children contacting with lip products, the health risk assessment of children blood Pb was carried out. The results showed that the concentration of Pb in lip products ranged from 0 to 0.5237 mg/kg, which was far lower than the limit set by various countries. The probabilistic non-carcinogenic risks and carcinogenic risks were $4.93 \times 10^{-7} \sim 2.82 \times 10^{-3}$ and $1.68 \times 10^{-12} \sim 9.59 \times 10^{-9}$, respectively, which were in an acceptable level. The results of blood Pb assessment suggested that the Pb content of lip cosmetics had no obvious influence on blood Pb concentration of children, and background Pb exposure is the main factor affecting children's blood Pb level (BLL). Overall, the samples of lip products are selected by Python crawler in this study, which are more objective and representative. This study focuses on deeper study of Pb, especially for the health risk assessment of blood Pb in children exposed to lip products. These results perhaps could provide useful information for the safety cosmetics usage for people in China and even the global world.

Keywords: lip cosmetics, Pb, health risk, Python crawler, Monte Carlo, Chinese e-commerce market

INTRODUCTION

In recent years, the security of cosmetics is increasingly recognized as a worldwide public health concern (1–3). The Food and Drug Administration (FDA) of the United States, the Food and Drug Safety Administration of the ROK, and the National Drug Administration of China have successively reported that the problem of excessive heavy metals in cosmetics is serious (4–7). To improve product performance, heavy metals are added to cosmetics by manufacturers. For example, the addition of Pb, Hg (mercury), and other metals makes cosmetics have the whitening function of covering or inhibiting pigment formation (8). In addition, with the aggravation of environmental pollution and the influence of some natural factors, some heavy metals widely existing in the surrounding environment will also enter people's lives with the use of cosmetic raw materials (9–11). Studies have shown that low-dose but long-term exposure of heavy metals to the human body can cause chronic poisoning or even canceration, causing irreversible adverse effects on human organs and seriously threatening human health (12–14). As one of the most commonly used cosmetics for modern women, lip cosmetics can not only moisten the lips but also improve personal performance (15). Compared with other cosmetics, lip products are easily exposed to the human body directly with the diet, and result in a higher health risk. Therefore, the assessment of exposure levels and health risks of heavy metals in lip products would be of great value to design manufacturers and relevant supervisory departments to provide scientific reference for health risk control of lip cosmetics consumers.

At present, some studies have focused on heavy metal pollution and health risks in lip products (16–18). Al-Saleh et al. measured the contents of various heavy metals in lipsticks obtained from offline markets in different years, the results indicated that the content of Pb was lower than the standard set by FDA, but special attention should be paid to the effect of Ni (nickel) and Cr (chromium) on allergic dermatitis (19, 20). Pinto et al. investigated the contents of 44 elements in 96 lipsticks from Brazil and Portugal, the results ranged from $<1\,\mu g/g$ to a few tens of $\mu g/g$ (such as Zn, Mn, Pb) (21). Gao et al. simulated the absorption of eight heavy metals in lip cosmetics by hydrochloric acid dilution method, vitro gastrointestinal method and American Pharmacopeia method, and the results suggested that Cu (copper), Pb and Cd (cadmium) were the main components of heavy metal pollution (22). Kilic et al. analyzed the lipsticks collected from the local markets in Turkey, and found the concentrations of all heavy metal were below the allowable limits (18). Although these researches are widely investigated the contents of various heavy metal, few studies focus on the deep study of a specific heavy metal element. Hence, this study attempted to select the element of Pb for deeper study. As a kind of 2B carcinogen, once Pb is absorbed by human body for about 3 months, the concentration of blood Pb will reach balance. Then, the majority of Pb is stored in the liver and the littleness left in the kidney, while the rest Pb is dispersed throughout the body (spinal cord, adrenal gland, brain, heart, etc.) (23). Excessive Pb in the human body can initiate gastrointestinal diseases, even poison the liver, central nervous system, and cause other serious harm to human health (24–27). The experts of WHO have stressed the significance of control on Pb in children, since the disadvantageous effects of Pb on central nervous system (28). Particularly for children under 6 years old, Pb is more harmful because it can damage memory, reduce intelligence, hinder growth and development (29). As mentioned above, Pb is significant among many heavy metals (30, 31), and it is high time to investigate the exposure of Pb to human body in lip products. What's more, some studies have shown that the contents of Pb and Cr in lip cosmetics exceed the standard, and it is strongly recommended to pay concern to the health risks of lip cosmetics (18, 22, 32). The contents of Pb in lip cosmetics from local supermarkets in Malaysia were 0.77–15.44 mg/kg (33). In South Korean, the maximum contents of Pb in lip products from local supermarkets were 12.77 mg/kg (34). A result, from a survey of lipstick from Portuguese and Brazilian markets, showed that the systemic exposure of lipstick was <0.2% of the daily allowable exposure, except for Pb (21). Alnuwaiser detected the content of Pb in the lipstick of Chinese products, there were only three samples above the limit, while the Pb level in other groups between 0.7 and 12.34 ppm (35). Feizi et al. found the concentrations of Pb were higher than those of Cd in lipsticks, only 33% of lipsticks had Pb contents less than the FDA limit (36). In Turkey, Kilic et al. found the concentration of Pb in Lipstick was 1.1 mg/kg (18). Obviously, the contents of Pb and corresponding health risks have been shown to vary in many different lip products and countries, and there have been little deep discussion about the health risk analysis. Therefore, this study attempts to focus on deeper study of the health risk assessment of Pb of typical popular lip cosmetics in Chinese e-commerce market.

Besides, the assessment results are uncertain due to the differences in sample distribution and exposure parameters during the actual risk assessment process (13, 37–39). To deal with the uncertainty of sample distribution, this study introduced Monte Carlo simulation to analyze the distribution of sample contents. As a statistical simulation method, the Monte Carlo simulation can descent the uncertainty of the mean value under complex condition, and get more accurate prediction results (40–42). The essence of Monte Carlo simulation is to simulate the possible random phenomena in the actual system by random numbers which obey a certain distribution. And the basic idea is to input abundant of random numbers satisfying a certain probability distribution into the model as parameters to determine the probability distribution of the concerned variables (43, 44). Combined with the Monte Carlo simulation and the health risk assessment model recommended by USEPA, the corresponding probability risk assessment range is further obtained.

Of particular concern is Pb mainly existing in the form of blood Pb in the human body (45). Kinds of pollution factors in the environment may result in the increase of blood Pb concentration, such as the Pb pollution in soil (46, 47). In recent years, some studies have begun to pay attention to the blood Pb problem of children caused by the use of lip cosmetics (48). Among them, there are mainly two pathways for children to expose. One is that children directly use lip

balm, and the other is that Pb in lip products will also be released into children through maternal transmission (49). At present, several methods currently exist for the measurement of health risks of blood Pb, mainly include Adult Lead Model (ALM) and Integrated Exposure Uptake Biokinetic Model (IEUBK) (48, 50, 51). Among them, the IEUBK mainly involves children aged 0∼7. These two models not only consider the existence and quantity of corresponding harmful substances in the health risk assessment of blood Pb, but also combine the estimated background exposure and the comparison with the basic health standards (52). Through the health risk assessment of adults and blood Pb in children exposed to lip products, this study perhaps could provide useful information for the safety cosmetics usage for people in China and even the global world.

In brief, this study selected 34 typical best-selling lip cosmetics from Chinese e-commerce market based on Python crawler technology, and analyzed the health risk level of adults and children caused by Pb exposure of lip products. The main objectives were (i) to investigate the popular lip cosmetics in Chinese e-commerce market, and determine the content of heavy metal Pb; (ii) to estimate the non-carcinogenic and carcinogenic risks of lipstick users with different frequencies using the health risk assessment model recommended by USEPA; (iii) to evaluate the effects of lip cosmetics on children's blood Pb content by ALM and IEUBK.

MATERIALS AND METHODS

Samples Selection

With the generality of online shopping in Chinese market, this study used Python crawler technology to select the most popular lip products in Chinese typical e-commerce market. JingDong, as one of Chinese top ten e-commerce markets, was selected as the research object of this study. The main Python crawler steps were shown in **Figure 1**. The first step was to establish the initial URL link: www.jingdong.com. Links unrelated to the topic were filtered based on the webpage analysis algorithm, while the useful links were retained and put into the URL pool. The second step was to start the crawler scheduler and initialize the Python crawler. Then, the crawler program simulated the browser to send a request "response" to obtain the HTML file of the corresponding link in the URL pool, and the server sent the "response" file object back to the browser. Python crawler called the BeautifulSoup library to parse HTML in "response." Next, it parsed the Web page according to HTML syntax and accessed valuable data. The third step, Pandas was used to analyze and obtain the value data after the end of the crawler data process, and got the analysis results finally.

As shown in **Figure 2**, the box price distribution of lip cosmetics was obtained on the basis of crawler data. The price distribution of lip cosmetics mainly ranged from 0 to 400 RMB, so the study classified the unified brand of lip cosmetics according to the 33th percentiles and the 66th percentiles, 0∼95 RMB, 96∼266 RMB, and more than 267 RMB, respectively.

Samples Collection and Analysis

Samples Collection

Based on the crawler analysis results above, the top lipstick brands were selected from each section by combining market share and commodity reviews. A total of 34 samples were purchased in this study, including lipsticks (LS, $n = 12$), lip glosses (LG, $n = 13$) and lip balms (LB, $n = 9$). Detailed information involves sample number, brand, origin, color, and price are shown in **Table 1**.

Sample Determination

The sample pretreatment experiment was carried out by wet digestion method according to *Safety specification for cosmetics* (2015 edition) (53). Firstly, 0.5000∼1.0000 g of samples were weighed using EL204 electronic balance (Mettler-Toledo Co., Ltd.) and placed in the crucible. The samples were heated at 100°C using a DK-98-11A electrothermal constant temperature water bath (Tianjin Tester Instrument Co., Ltd.) to make all the samples flow into the bottom of the crucible. 10∼15 ml mixed acid were added, which was mixed with high grade pure nitric acid (Kaifeng Dongda Chemical Co., Ltd.) and high grade pure perchloric acid (Tianjin Zhengcheng Chemical Products Co., Ltd.) at a ratio of 3:1. Heating digestion was carried out on DB-4A stainless steel electric heating plate (Changzhou Boyuan Experimental Analysis Instrument Factory) to produce white smoke in the digestion solution, and the crucible was shaken slowly from time to time to make the digestion solution uniform. When the acid solution is pale yellow or colorless, turn off the power supply of the electric heating plate. The liquid was diluted with ultra-pure deionized water to

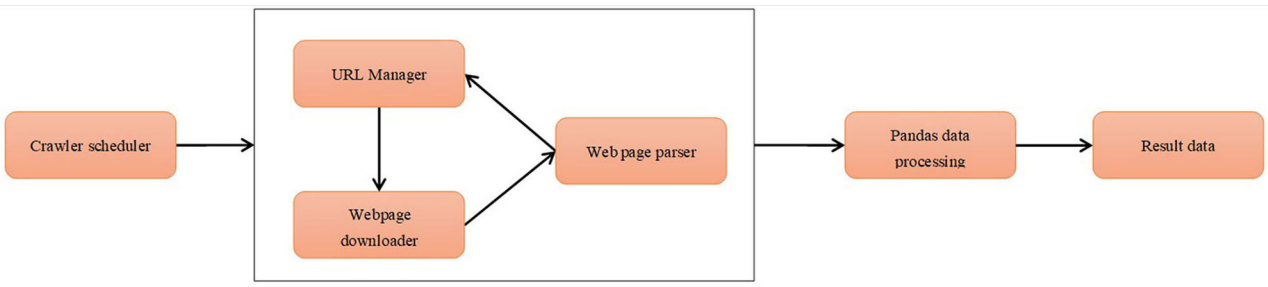

FIGURE 1 | The crawling process by Python.

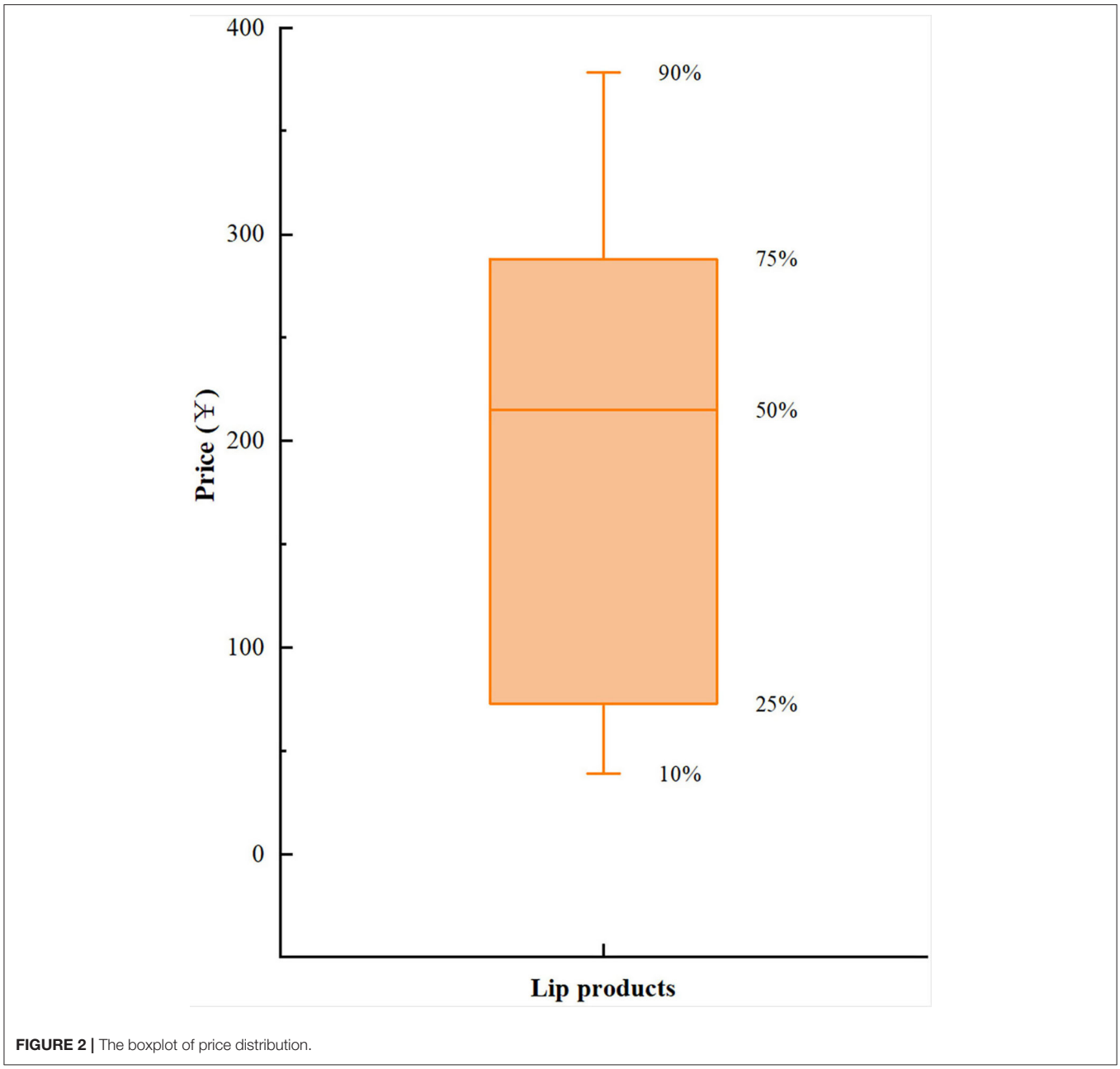

FIGURE 2 | The boxplot of price distribution.

a final volume of 25 ml when the remaining solution was only about 2∼3 ml. In this study, Pb in lip cosmetics was selected for determination. The pretreated samples, parallel samples, and blank samples were put into the preheating inductively coupled plasma mass spectrometer (Nexlon350x, PE, USA) to determine the concentrations of heavy metals. The instrument was calibrated with 187Re in the determination of heavy metals by ICP-MS.

In order to remove the background values of heavy metals in the reagents and containers, the samples were not exposed to metal containers during the experiment, and the required experimental containers were soaked in nitric acid for more than 24 h before drying and using. Besides, parallel samples were more than 20% level and set blank control throughout the experiment. In the determination experiment, Pb standard solution and blank solution were selected to control the metal concentration of the sample. The whole blank test results are less than the detection limit of the method to ensure that the sample is not contaminated during digestion and determination. The standard curve was drawn for each sample test, and the correlation coefficient of the standard curve was $\geq$0.995, and the relative deviation of the parallel sample test results was controlled within 10%.

TABLE 1 | The basic information for all samples ($N = 34$).

Category	Number	Brand	Production Country	Color	Price (RMB)
Lipsticks	LS1	Chanel	France	Orange red	320
($n = 12$)	LS2	YSL	France	True red	320
	LS3	Armani	France	True red	320
	LS4	Dior	France	True red	330
	LS5	Dhc	Japan	Orange	158
	LS6	Mac	Canada	Brick red	185
	LS7	L′ Oreal	China	Orange red	135
	LS8	Maybelline	China	Orange red	120
	LS9	Carslan	China	Cameo brown	139
	LS10	Revlon	America	Orange red	78
	LS11	Kiko	Italy	Cameo brown	90
	LS12	Zeesea	China	Brick red	70
Lip glosses	LG1	YSL	France	Cameo brown	320
($n = 13$)	LG2	Armani	France	Orange red	310
	LG3	Chanel	France	Purplish red	330
	LG4	Dior	France	True red	330
	LG5	Mac	Canada	Pink	170
	LG6	Maybelline	China	True red	122
	LG7	L′ Oreal	China	Cameo brown	145
	LG8	Carslan	China	Orange red	109
	LG9	Revlon	America	Cameo brown	48
	LG10	Chioture	China	Cameo brown	60
	LG11	Zeesea	China	Brick red	80
	LG12	Kiko	Italy	Pink	90
	LG13	Kiko	Italy	Colorless	90
Lip balms	LB1	Dhc	Japan	Colorless	78
($n = 9$)	LB2	Uriage	France	Colorless	78
	LB3	Maybelline	China	Light red	30
	LB4	Mentholatum	China	Colorless	35
	LB5	Vaseline	America	Colorless	25
	LB6	Vaseline	America	Light red	25
	LB7	Herbacin	Germany	Colorless	45
	LB8	Mentholatum	China	Light red	36
	LB9	Burt's bees	America	Colorless	70

Health Risk Assessment of Pb Exposure

Carcinogenic and Non-carcinogenic Health Risk Assessment Models

Considering the particularity of lip products exposed to the human body through diet, this study selected the health risk assessment model recommended by USEPA for oral ingestion (54, 55). The calculation formula was shown in Equations (1-3).

$$\mathrm{ADDing} = \mathrm{C}\times\mathrm{IR}\times\mathrm{EF}\times\mathrm{ED}\times\mathrm{CF}/\mathrm{BW}/\mathrm{AT} \quad (1)$$

$$\mathrm{HQ} = \mathrm{ADD}/\mathrm{RfD} \quad (2)$$

$$\mathrm{LCR} = \mathrm{ADD}\times\mathrm{SF} \quad (3)$$

Where ADD represents the average daily dose of Pb in lip products, mg/(kg·d). C is the concentration of Pb in lip products, mg/kg. All parameters are shown in **Table 2**, IR represents the intake rate of lip products, g/d. The Intake rate of average users and high users was 0.02578 and 0.14902 g/d, respectively (54). EF is the exposure frequency, set as 365 d/a (55). ED represents the exposure duration, 70a (55). CF represents the conversion rate, set to 0.001 (56). AT is the average exposure time, 25,550 d (56). BW is the average body weight of the exposed population, which is 60 kg (57). RfD is the non-carcinogenic reference dose, mg/(kg·d). The general toxicity data of IRIS of USEPA, shown in plenty of researches, can be applied not only for food (58–60), but also for soil (61, 62), dust (63, 64) or other media, such as lip products (22, 33, 65). Therefore, according to the previous studies (22, 66), it is appropriate to cite the general toxicity data of IRIS of USEPA as the reference dose (RfD) of metals in lip products. The RfD was set to 0.0004 in this study (67). SF is carcinogenic slope factor, (kg·d)/mg, set to 0.0085 (67). HQ and LCR are the non-carcinogenic risk value and carcinogenic risk value of oral intake of Pb, respectively. The reference values of non-carcinogenic risk and carcinogenic risk are 1 and 10^{-6}, respectively. If the calculated results are greater than the corresponding value, it is considered that the risk is large, and certain control measures are needed to reduce the risk. Otherwise, it is considered that the risk is at an acceptable level (56, 57, 67).

TABLE 2 | Parameter selection and references of health risk assessment model for oral ingestion.

Parameter type	Parameter value	References
Intake rate of average users IR(g/d)	0.02578	(54)
Intake rate of high users IR(g/d)	0.14902	(54)
Exposed frequency EF(d/a)	365	(55)
Exposure duration ED(a)	70	(55)
Turnover rate CF	0.001	(56)
Average exposure time AT(d)	25550	(56)
Body weight BW(kg)	60	(57)
Non-carcinogenic reference dose RfD (mg/(kg·d))	0.0004	(67)
Cancer slope factors SF ((kg·d)/mg)	0.0085	(67)

Blood Lead Level Model

ALM is mainly composed of three parts: namely soil exposure, lip cosmetics exposure, and reference value. The detailed expression is shown in formula (4).

$$\begin{aligned}\mathrm{PbB} = {} & (\mathrm{Pbs}\times\mathrm{BKSF}\times\mathrm{IR}_{\mathrm{S+D}}\times\mathrm{AF}_{\mathrm{S,D}}\times\mathrm{EFs}/\mathrm{AT}_{\mathrm{S,D}}) \\ & +(\mathrm{Pb}_{\mathrm{L}}\times\mathrm{BKSF}\times\mathrm{IR}_{\mathrm{L}}\times\mathrm{AF}_{\mathrm{L}}\times\mathrm{EF}_{\mathrm{L}}/\mathrm{AT}_{\mathrm{L}}) + \mathrm{PbB}_0 \quad (4)\end{aligned}$$

In the formula, PbB represents adult blood Pb concentration, μg/dl. Pbs and Pb_L are BLL in soil and lip cosmetics, respectively, μg/g. According to the research results of scholars on the soil Pb reference value in China, the value of Pbs was set as 282 μg/g (68). Based on the experimental data in this study, the average concentration of Pb in three kinds of lip cosmetics was set to 0.05791 μg/g. PbB_0 was taken 1.62μg/dl as the reference blood Pb content. BKSF is the biokinetic slope factor, set as 0.4 d/dl. IR represents daily intake, and soil intake IR_{S+D} is 0.05 g/d. For

lip cosmetics intake, average users was 0.0258 g/d and high users was 0.1490 g/d (67). AF represents the absorption rate, $AF_{S,D}$ for soil is 0.12. AF_L for lip cosmetics is conservatively considered to be 1. EF represents the contact frequency. EFs for soil is set to 220 d/year, and EF_L for lip cosmetics is set to 365 d/year (69). AT represents the average contact time, which is 365 d/year (69). When blood Pb in adults is transmitted through the mother, the transmission rate is 0.85 in ALM and 0.9 in IEUBK (48).

The IEUBK model for children exposed to Pb was developed by USEPA to predict the blood Pb concentration of children under 7 years old (0∼84 months) and the possibility of Pb poisoning in children after a certain degree of Pb exposure (70–72). This model can set up integral and external parameters with the consideration of soil, water, food, air and conditions of Pb exposure. The integral parameters can't be changed arbitrarily, while the external parameters can be modified based on local actual data at the input interface to simulate the relationship between Pb absorption efficiency and blood Pb concentration in the human body (68, 73). Taking the actual situation of children's use of lip cosmetics into account, this study defaulted that children were exposed only to lip balms, and Pb exposure in other types of lip cosmetics was transmitted by the mother (48). The reference value of Pb concentration in soil in China is set at 282 mg/kg, and the default absorption rate of Pb in soil and dust by children is 45% (68, 69). In accordance with the national revised limit of Pb concentration in the atmosphere in 2012, the background value of Pb concentration in the air was set as an annual average of 0.5 μg/m^3 (GB3095-2012) (74), and the default absorption rate was 30%. The background value of Pb in drinking water was 0.01 μg/L (GB5749-2006) (75), and the default values of 0∼7 years old were 0.2, 0.5, 0.52, 0.53, 0.55, 0.58, and 0.59 L/day (69). The blood Pb concentration in pregnant women was set based on the results of the ALM model. In accordance with China standard on the limit of pollutant content in food (GB2762–2017) (76), the limit of Pb content in infant formula foods was 0.15 and 0.02 mg/kg with solid and liquid food, respectively. The limit of Pb content in infant auxiliary food was 0.2∼0.3 mg/kg, and the limit of Pb content in food was below 0.5 mg/kg except for seafood. According to the pyramid distribution of children's food intake, the background value of Pb intake in children aged 0∼3 was set to 8 μg/day, and 20 μg/day in children aged 3∼7 (68, 69). The statistical software is IEUBK win1.1_Build 11 (77).

Statistical Analysis

Microsoft Excel 2019 was used for data processing. The correlation analysis was performed in SPSS (20.0), and the significance level was $P < 0.05$. In order to quantify the uncertainty of sample content distribution, Crystal Ball software (16.0) was used for Monte Carlo simulation in this study, and the number of iterations was set to be 10,000. The box diagrams of probability risk were drawn in Origin Pro 8.0.

RESULTS AND DISCUSSION

Pb Content Characteristics in Lip Cosmetics

The Pb content in 34 lip products was determined in this study, as shown in **Figure 3**; **Table 3**. It can be seen from **Figure 3** that the Pb content varies greatly among different lip products. In this study, the Pb element was not detected in about 41.18% lip products. At present, different countries, including China, the United States and Canada, have set limits for Pb in cosmetics, which are 10 mg/kg. The contents of lip products in this study

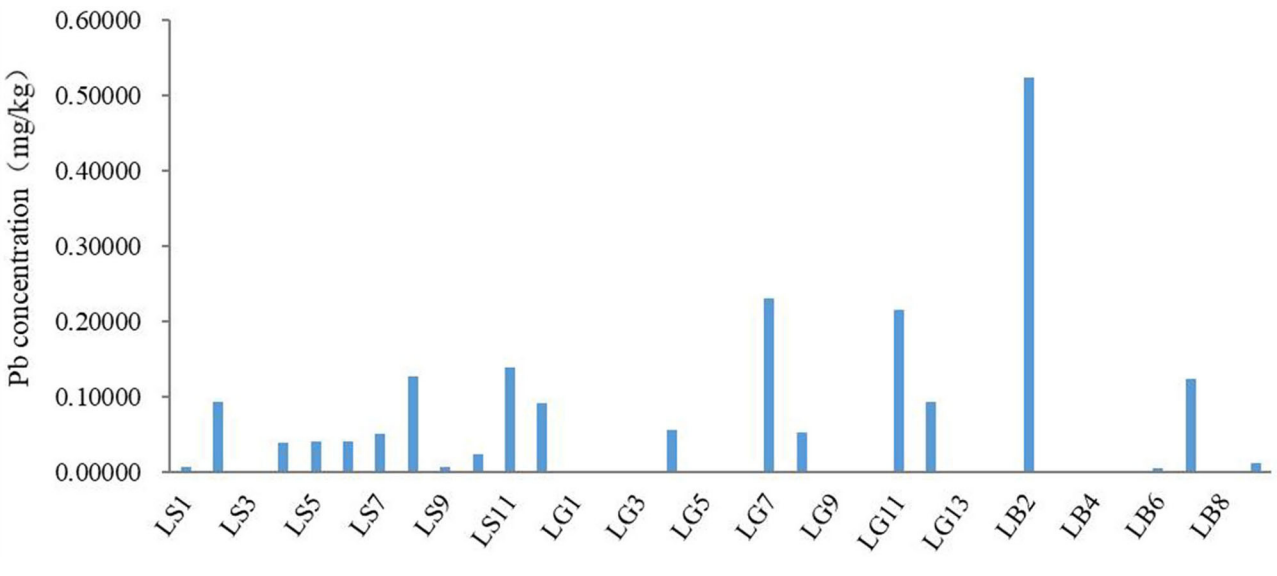

FIGURE 3 | The contents of Pb in typical popular lip cosmetics ($N = 34$).

TABLE 3 | The contents of Pb in various lip products (mg/kg).

Parameter	Lipstick ($n = 12$)	Lip glosses ($n = 13$)	Lip balms ($n = 9$)	Totals ($N = 34$)
Average value	0.05482	0.04976	0.07380	0.05791
Standard deviation	0.04506	0.07922	0.16358	0.10146
Maximum value	0.13849	0.23093	0.52470	0.52370
Minimum value	0.00000	0.00000	0.00000	0.00000

were far below the limit. Therefore, the trace metal Pb element in lip cosmetics is at an acceptable level.

According to **Table 3**, the content of Pb in lip products ($N = 34$) ranged from 0 to 0.5237 mg/kg, which was far lower than that reported in previous studies such as South Korea (34), the United States (78), Iran (65), Saudi Arabia (20) and Turkey (18). This may be related to the batch, color, raw materials, and ratio of lip cosmetics (36, 79, 80). The average Pb content of all kinds of lip products decreased in the following order: lip balms ($n = 12$) > lipsticks ($n = 13$) > lip glosses ($n = 9$), while the result of Iwegbue et al. showed that the content of Pb in lipsticks is more than in lip glosses/lip balms (17). Probably, it reflected differences in the origin, color, brand and batch of lip cosmetics. In addition, in order to investigate the relationship between the content of Pb, the category and the price of lip products, this study carried out correlation analysis in SPSS. The results showed that the correlation coefficient between Pb content and category was 0.067 ($P = 0.707 > 0.05$), and the correlation coefficient between Pb content and price was −0.136 ($P = 0.443 > 0.05$). Therefore, there is no significant correlation among the content of Pb, the category and the price of lip products, which corroborate the findings of little relevance between the cost of cosmetics and the concentration of heavy metals (81). However, these results differ from some published studies which indicated that the concentration of Pb in cheaper brands was higher than the expensive brands (82, 83). This discrepancy could be attributed to the differences in limited sample selection.

Carcinogenic and Non-carcinogenic Health Risk Assessment

To evaluate the uncertainty caused by the difference in sample content, Monte Carlo algorithm was introduced for analysis. The results showed that the Pb content in lip cosmetics in this study was in line with the lognormal distribution. Combined with the health risk assessment model, 10,000 iterations were carried out to predict the final non-carcinogenic and carcinogenic risks, as shown in **Figures 4**, **5**.

The non-carcinogenic risk prediction results of Pb in lip cosmetics showed that the 95th percentiles of high users and average users were 2.82×10^{-3} and 4.88×10^{-4}, respectively, which were far below the threshold 1. Thus, the non-carcinogenic risk of exposure to Pb in lip products is acceptable, this result is consistent with previous research conclusions (33, 34, 84).

From **Figure 5**, it appeared that the carcinogenic risk of Pb in lip cosmetics was between 10^{-12} and 10^{-8}. The 95th percentiles of high users and average users were 9.59×10^{-9} and 1.66×10^{-9}, respectively, which were far lower than the threshold of 10^{-6}. Therefore, it can be considered that the carcinogenic risk of Pb in contact with lip products is at a safe level. Though the carcinogenic risk of Pb in contact with lip products and other cosmetics, in many previous studies, is lower than the threshold of 10^{-6} (34), there will be a requirement for attention if the risk is above 10^{-4}. In this study, the exposure of Pb may be considered safe currently. However, with daily using of the cosmetics, the heavy metals may poison and accumulate in human body. Therefore, the data provided in this study may be important to the managerial organization of cosmetic safety.

In this study, the exposure and health risks of Pb in lip products are the concerned objects. Exposure of hazardous substances in lip products is the result of interaction of various heavy metals and pollutants (22, 78), and this comprehensive exposure may have higher health risks, which need to be further enriched and deepened in the following studies.

Blood Lead Level Analysis of Blood Lead

The use of lip cosmetics may affect the blood Pb content in children, especially through maternal transmission. Hence, based on the calculation results of different data parameters of the ALM model, the influence of adult exposure on blood Pb concentration in infants was obtained, as shown in **Table 4**.

The left half of the table shows the corresponding adult blood Pb concentration of every part with low background value, which the reference value 1.62 μg/dl. And the other half of that displays the blood Pb content affected by high background value, which is 2.03 μg/dl with the combination of soil and reference exposure. And line labeled "Lip cosmetic" presents the blood Pb content affected by lip products exposure, which is 0.0006 and 0.0035 for average and high users, respectively. Subsequently, the adults blood Pb concentration could be summarized, as shown in the next line of the table. Finally, based on the fact that the transmission rate, in general, can be set as 0.85 or 0.9, the blood Pb concentrations from the mother to the fetus can be obtained. The results showed that under the condition of low background value and the transmission rate was 0.85, the blood Pb concentrations from the mother to the fetus of the average user and the high user were 1.3775 and 1.3799 μg/dl, respectively. While the transmission rate under the children's blood Pb pharmacokinetic model was 0.9, the blood Pb concentrations from the mother to the fetus of the average user and the high user were 1.4585 and 1.4611 μg/dl, respectively. Similarly, under the condition of high background value, the blood Pb concentrations from maternal to fetal were 1.7260 and 1.7284 μg/dl for both average and high users at adult blood Pb transmission rate, respectively. Under the condition of IEUBK for children, the blood Pb concentrations from maternal to fetal were 1.8275 and 1.8301 μg/dl for both average users and high users, respectively. No matter the concentration of Pb in lip cosmetics under average or high exposure, there is little difference in blood Pb content from mother to fetus. Hence, the main factor affecting fetal blood Pb concentration is the maternal background environment.

When running the IEUBK program, the maternal body was set to 0, 1.41925, and 1.77800 μg/dl, respectively. Under the background of average exposure, 0.00190 μg/d Pb was ingested from lip cosmetics and 0.07819 μg/d Pb was ingested from lip

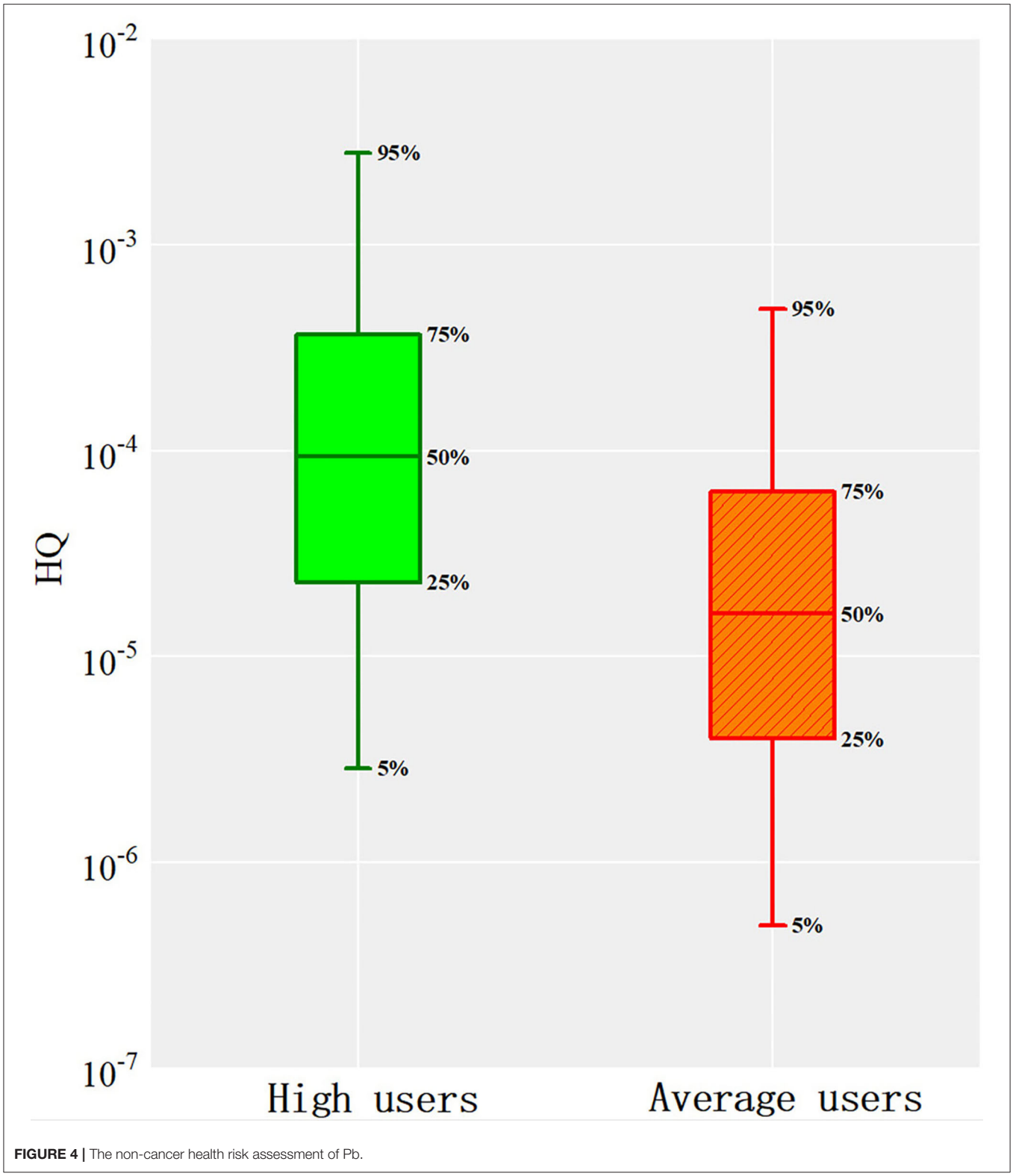

FIGURE 4 | The non-cancer health risk assessment of Pb.

cosmetics under the condition of high exposure. The changes of blood Pb concentration in 0∼7 years old children under the above six conditions were found, as shown in **Table 5**. Even if the total intake of Pb content changed slightly, the operation results of blood Pb concentration under the six conditions were the same.

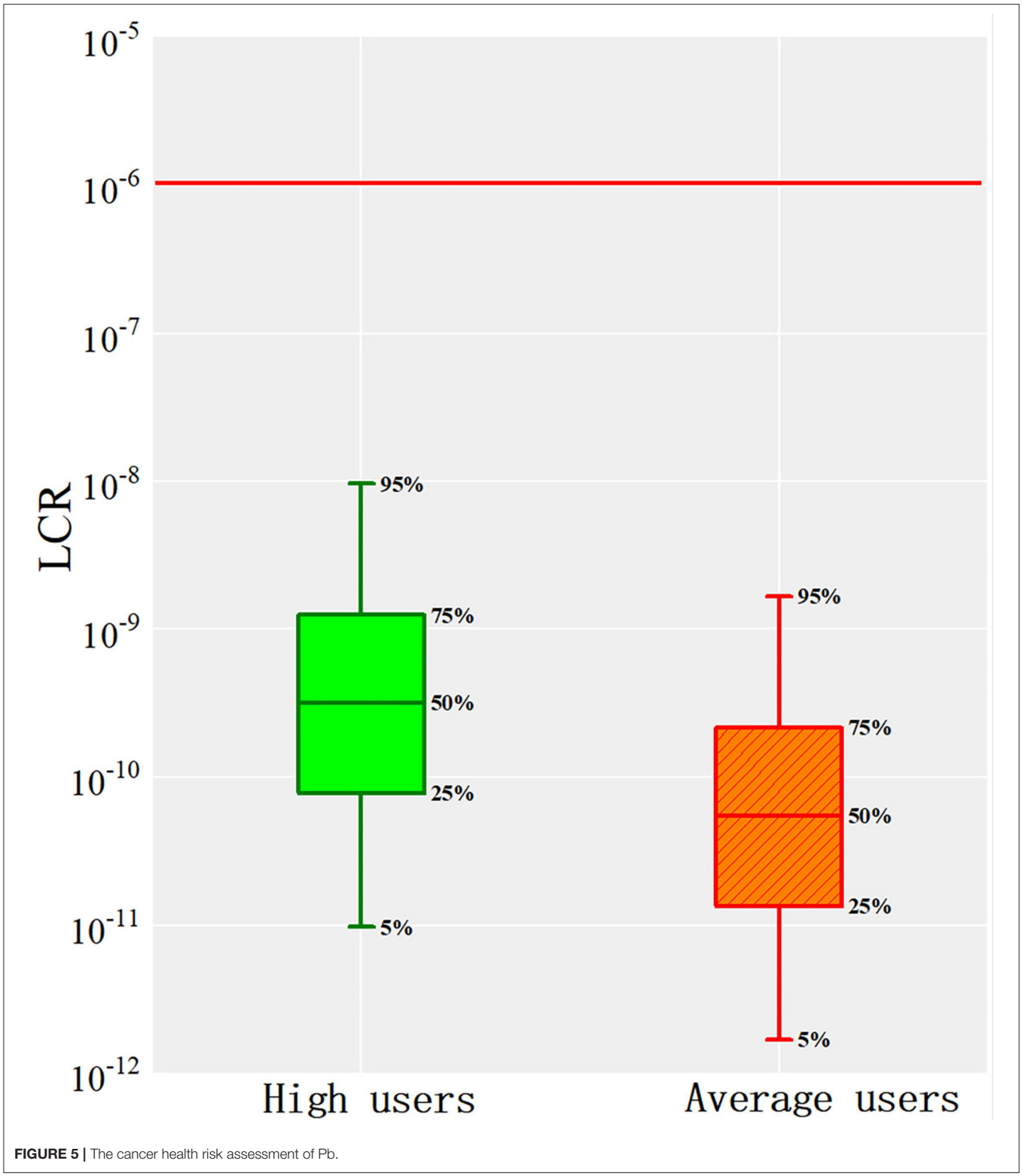

FIGURE 5 | The cancer health risk assessment of Pb.

In developed countries, the BLL of children <6 μg/dl are considered to be relatively safe (85), and the international threshold for children's blood Pb is 10 μg/dl (86). There would exist embryonic development toxicity and the pregnant women are prone to miscarriage when the concentration of blood Pb reach the standard. With the rise of BLL, people gradually experience the impact of heme metabolism, which can lead to renal dysfunction and even death (48, 87). Based on the data

TABLE 4 | The running results for adult blood Pb model.

Exposure scenarios	Blood Pb levels BLL(μg/dl)							
Background	1.62				2.03			
Lip cosmetic	0.0006		0.0035		0.0006		0.0035	
PB_L	1.6206		1.6235		2.0306		2.0335	
From mother to fetus	1.3775	1.4585	1.3799	1.4611	1.7260	1.8275	1.7284	1.8301

TABLE 5 | The running results for the IEUBK model.

Age (years)	Total Pb absorption (μg/d)	Blood Pb levels (μg/dl)
0.5∼1	9.694 ± 0.002	5.2
1∼2	13.224 ± 0.002	5.9
2∼3	13.574 ± 0.002	5.1
3∼4	18.684 ± 0.001	6.0
4∼5	16.679 ± 0.002	5.7
5∼6	16.294 ± 0.002	5.1
6∼7	16.048 ± 0.002	4.6

obtained in this study, although the blood Pb concentration in children did not exceed the international threshold, the blood Pb content of children aged 3∼4 years old had reached the standard value in developed countries. In addition, there was little difference between the blood Pb data from the mother and the lipstick separately and the total of them. The results indicated that whether the average-exposed or the high-exposed population, the background Pb exposure is the main factor affecting the BLL of children. The Pb exposure of lip cosmetics did not significantly increase the blood Pb content of children, this conclusion is consistent with previous studies (48, 88). Compared with previous study, Monnot et al. found that the baseline BLLs of child born to mothers with high BLLs were 0.04 μg/dl higher than the BLLs of children born to mothers with average BLLs, and the lipstick exposure has little contribution to resulting in a higher level of BLLs than the dose of background exposure (48). Hence, more attention should be paid to the Pb content of air and soil around the living environment of children, as well as the safety of food and drinking water for adults and children.

Uncertainty Analysis

A large number of studies have shown that heavy metal content in different lip products varies greatly, which may be related to origin, brand, color, price, raw materials and ratio (55, 63). Therefore, there is great uncertainty in sample selection. The selection of samples plays a fundamental role in the investigation of lip products, to effectively reduce the uncertainty of sample selection, Python crawler technology, is innovatively introduced in this study to select the best-selling brands in typical e-commerce platforms, which is in accord with the reality of market and consumers, making sample selection more objective and representative (89–91). The data of the e-commerce platform are updated in real-time observation. In order to carry out long-term effective risk control, it is necessary to continuously monitor the pollution levels of Pb and other heavy metals in lip cosmetics.

Furthermore, the risk levels appeared to be affected by metal contents. In the process of implementing risk assessment, this study introduces Monte Carlo simulation and predicts the risk assessment results through 10,000 iterations, which can reduce the uncertainty of risk assessment to some extent. Further investigations can obtain reliable data through short-term observation experiments on population exposure parameters, and more accurately measure the health risk of lip cosmetics.

Finally, it should be noted that this study assumes that the smeared lipstick is human intake, the absorption rate is 100%. In fact, due to the limitation of human body absorption, it is difficult to reach 100%. There are few existing studies regarding human body absorption, which brings certain uncertainty to risk assessment. Further work on human body absorption rate is particularly important.

CONCLUSIONS

This study intends to investigate the heavy metal Pb content, assess health risks and analysis blood Pb level in popular lip cosmetics across Chinese e-commerce market. Python crawler technology, particularly, was introduced to identify and select the most popular 34 lip cosmetics. The findings clearly found that the average content of Pb in the tested lip products is 0.05791 mg/kg, far below the limit value. And the contents of Pb in various lip products decreased in the following order: lip balms > lipstick > lip glosses. There is no significant non-carcinogenic and carcinogenic risk caused by adult exposure to lip cosmetics. Furthermore, blood Pb model analysis showed that the exposure of Pb in lip cosmetics had little effect on children's blood Pb health. Compared with the Pb content of lip cosmetics, it is necessary to pay more attention to the safety of children's diet, drinking water and living environment to prevent the heavy metals from causing health damage.

DATA AVAILABILITY STATEMENT

The raw data supporting the conclusions of this article will be made available by the authors, without undue reservation.

AUTHOR CONTRIBUTIONS

YL organized study, prepared datasets, performed the statistical analysis, and drafted the manuscript. CL designed the study, organized study, prepared datasets, and revision of the manuscript. YF contributed to organize study, prepare datasets, and draft the manuscript. ZL contributed to study design and revision of the manuscript. YZ contributed to prepare datasets, perform the statistical analysis, and draft the manuscript. KL, LJ, and YY organized study and revision of the manuscript. BY and YS contributed to datasets prepare and revision of the manuscript. All authors read and approved the final manuscript.

FUNDING

This study was financially supported by National Social Science Foundation of China (19FJYY02), China Postdoctoral Science Foundation (2020M672420), and Special Fund for the Reform of Education and Teaching in Central Universities, Zhongnan University of Economics and Law (YZKC202143).

REFERENCES

1. Choi CM, Hwang YS, Park AS, Jung SJ, Kim HJ, Kim JH. A study on heavy metal concentrations of color cosmetics in Korea market. *J Soc Cosmet Sci Korea.* (2014) 40:269–78. doi: 10.15230/SCSK.2014.40.3.269
2. Borowska S, Brzoska MM. Metals in cosmetics: implications for human health. *J Appl Toxicol.* (2015) 35:551-72. doi: 10.1002/jat.3129
3. Salama AK. Assessment of metals in cosmetics commonly used in Saudi Arabia. *Environ Monitor Assess.* (2015) 188:553. doi: 10.1007/s10661-016-5550-6
4. CCTV Finance. *Heavy Metals in 13 Kinds of Cosmetics Exceeded the Standard.* CCTV Finance (2018). Available online at: http://baijiahao.baidu.com/s?id=1595517502888349927&wfr=spider&for=pc (accessed June 2020).
5. SFDA (State Food and Drug Administration). *Notice of the State Food and Drug Administration on 8 Batches of Unqualified Cosmetics.* SFDA (2020). Available online at: https://www.nmpa.gov.cn/xxgk/ggtg/hzhpchj/hzhpgjgg/20201013172259176.html (accessed December 2020).
6. Matta MK, Zusterzeel R, Pilli NR, Patel V, Volpe DA, Florian J, et al. Effect of sunscreen application under maximal use conditions on plasma concentration of sunscreen active ingredients: a randomized clinical trial. *JAMA.* (2019) 321:2082–91. doi: 10.1001/jama.2019.5586
7. Liu XS, Zhang HL, Zhang HL, Jiang YH, Lv L, Zu J, et al. Assessment of heavy metal content in cosmetics of Chinese market. *Basic Clin Pharmacol Toxicol.* (2021) 128:151.
8. Bocca B, Pino A, Alimonti A, Forte G. Toxic metals contained in cosmetics: a status report. *Regulat Toxicol Pharmacol.* (2014) 68:447–67. doi: 10.1016/j.yrtph.2014.02.003
9. Peng G, Sa L, Zhaohan Z, Ping M, Nan L, Binyu L, et al. Health impact of bioaccessible metal in lip cosmetics to female college students and career women, northeast of China. *Environ Pollut.* (2015) 197:214–20. doi: 10.1016/j.envpol.2014.11.006
10. Zhang J, Jiang L, Liu Z, Li Y, Liu K, Fang R, et al. A bibliometric and visual analysis of indoor occupation environmental health risks: development, hotspots and trend directions. *J Clean Product.* (2021) 300:126824. doi: 10.1016/j.jclepro.2021.126824
11. Chen Y, Wang J, Shi G, Sun X, Chen Z, Xu S. Human health risk assessment of lead pollution in atmospheric deposition in Baoshan District, Shanghai. *Environ Geochem Health.* (2011) 33:515–23. doi: 10.1007/s10653-010-9368-9
12. Zhang J, Li Y, Liu C, Li F, Zhu L, Qiu Z, et al. Concentration levels, biological enrichment capacities and potential health risk assessment of trace elements in eichhornia crassipes from Honghu Lake, China. *Sci Rep.* (2019) 9:2431. doi: 10.1038/s41598-018-36511-z
13. Li F, Lu Y, Zhang J, Wang Y, Chen X, Yan J, et al. Investigation and regional fuzzy health risk management of lead and cadmium in best-selling cigarettes across China. *J Clean Product.* (2020) 261:121005. doi: 10.1016/j.jclepro.2020.121005
14. Zhao J, Jiang JC, Hu JJ, Wang YF, Jian XD, Ge HH. Pollution status and control countermeasures for pharmaceutical and personal care products in China. *Asian J Ecotoxicol.* (2020) 15:21–7. doi: 10.7524/AJE/1673-5897.20191030002
15. Iwegbue CMA, Bassey FI, Tesi GO, Onyeloni SO, Obi G, Martincigh BS. Safety evaluation of metal exposure from commonly used moisturizing and skin-lightening creams in Nigeria. *Regulat Toxicol Pharmacol.* (2015) 71:484–90. doi: 10.1016/j.yrtph.2015.01.015
16. Escher K, Shellock FG. Evaluation of MRI artifacts at 3 Tesla for 38commonly used cosmetics. *Magn Reson Imaging.* (2013) 31:778-82. doilink[10.1016/j.mri.2012.11.002]10.1016/j.mri.2012.11.002
17. Iwegbue CMA, Bassey FI, Obi G, Tesi GO, Martincigh BS. Concentrations and exposure risks of some metals in facial cosmetics Nigeria. *Toxicol Rep.* (2016) 3:464–72. doi: 10.1016/j.toxrep.2016.04.004
18. Kilic S, Kilic M, Soylak M. The determination of toxic metals in some traditional cosmetic products and health risk assessment. *Biol Trace Elem Res.* (2021) 199:2272–7. doi: 10.1007/s12011-020-02357-8
19. Al-Saleh I, Al-Enazi S, Shinwari N. Assessment of lead in cosmetic products. *Regulat Toxicol Pharmacol.* (2009) 54:105–13. doi: 10.1016/j.yrtph.2009.02.005
20. Al-Saleh I, Al-Enazi S. Trace metals in lipsticks. *Toxicol Environ Chem.* (2011) 93:1149–65. doi: 10.1080/02772248.2011.582040
21. Pinto E, Paiva K, Carvalhido A, Almeida A. Elemental impurities in lipsticks: results from a survey of the Portuguese and Brazilian markets. *Regul Toxicol Pharmacol.* (2018) 95:307–13. doi: 10.1016/j.yrtph.2018.04.009
22. Gao P, Lei T, Jia L, Yury B, Zhang Z, Du Y, et al. Bioaccessible trace metals in lip cosmetics and their health risks to female consumers. *Environ Pollut.* (2018) 238:554–61. doi: 10.1016/j.envpol.2018.03.072
23. Sirivarasai J, Kaojarern S, Chanprasertyothin S, Panpunuan P, Petchpoung K, Tatsaneeyapant A, et al. Environmental lead exposure, catalase gene, and markers of antioxidant and oxidative stress relation to hypertension: an analysis based on the EGAT study. *Biomed Res Int.* (2015). 2015:856319. doi: 10.1155/2015/856319
24. Wei YH, Huang QC. The toxicological effect of lead on the human health and its measures of prevention. *Stud Trace Elem Health.* (2008). 25:62–64. doi: 10.3969/j.issn.1005-5320.2008.04.026
25. Yue QL, Huo J, Cao MS, Chen JY, Zhang LS. Research progress in neurobehavioral toxicity of lead. *J Food Saf Qual.* (2018) 9:3567–72. doi: 10.3969/j.issn.2095-0381.2018.14.003
26. Flora SJS. Lead exposure: health effects, prevention and treatment. *J Environ Biol.* (2002) 23:25–41. doi: 10.1016/S0169-7722(01)00143-7
27. Debnath B, Singh WS, Manna K. Sources and toxicological effects of lead on human health. *Indian J Med Special.* (2019) 10:66–71. doi: 10.4103/INJMS.INJMS_30_18
28. WHO (World Health Organization). *WHO Expert Consultation: Available Evidence for the Future Update of the WHO Global Air Quality Guidelines (AQGs).* (2016). Available online at: https://www.euro.who.int/__data/assets/pdf_file/0013/301720/Evidence-future-update-AQGs-mtg-report-Bonn-sept-oct-15.pdf (accessed August 2020).
29. Charkiewicz AE, Backstrand JR. Lead toxicity and pollution in Poland. *Int J Environ Res Public Health.* (2020) 17:4385. doi: 10.3390/ijerph17124385
30. Dong ZM, Wu SM, Hu JY. Health risk assessment for children due to lead exposure in some region of China. *Zhongguo Huanjing Kexue/China Environ Sci.* (2011) 31:1910–6.
31. Wang B, Zhang J, Zhang Y, Pan L, Liu L, Zhao X, et al. Health risk assessment for lead exposure of children in China. *Acta entiae Circumstantiae.* (2013). 33:1771–79. doi: 10.13671/j.hjkxxb.2013.06.007

32. Zhao D, Li J, Li C, Juhasz AL, Scheckel KG, Luo J, et al. Lead relative bioavailability in lip products and their potential health risk to women. *Environ Sci Technol.* (2016) 50:6036-43. doi: 10.1021/acs.est.6b01425
33. Zakaria A, Ho YB. Heavy metals contamination in lipsticks and their associated health risks to lipstick consumers. *Regul Toxicol Pharmacol.* (2015) 73:191–5. doi: 10.1016/j.yrtph.2015.07.005
34. Lim DS, Roh TH, Kim MK, Kwon YC, Choi SM, Kwack SJ, et al. Non-cancer, cancer, and dermal sensitization risk assessment of heavy metals in cosmetics. *J Toxicol Environ Health A.* (2018) 81:432–52. doi: 10.1080/15287394.2018.1451191
35. Alnuwaiser MA. Determination of As, Hg, Pb, Cd and Al in the lipsticks in the kingdom of Saudi Arabia. *Int J Pharm Sci Res.* (2018) 9:4750–58. doi: 10.13040/IJPSR.0975-8232.9(11).4750-58
36. Feizi R, Jaafarzadeh N, Akbari H, Jorfi S. Evaluation of lead and cadmium concentrations in lipstick and eye pencil cosmetics. *Environ Health Eng Manag J.* (2019) 6:277–82. doi: 10.15171/EHEM.2019.31
37. Chen D, Zhang ZJ, Gao FL, Li QQ, Wang BG. Study on health risk assessment of aromatic hydrocarbons from a typical oil refinery in Pearl River Delta, China. *China Environ Science.* (2017) 37:1961–70. doi: 10.3969/j.issn.1000-6923.2017.05.045
38. Yang LH, Zhao-Yue KE, Xie ZY, Qun YU. The heavy metal content of atmospheric-particulates and the risk assessment of exposed people in the surrounding area of a lead-zinc mine in Guangdong. *Environ Monitor China.* (2015). 31:48–53.doi: 10.19316/j.issn.1002-6002.2015.04.008
39. Li F, Wang Y, Zhang J, Lu Y, Zhu X, Chen X, et al. Toxic metals in top selling cigarettes sold in China: pulmonary bioaccessibility using simulated lung fluids and fuzzy health risk assessment. *J Clean Product*. (2020) 275:124131. doi: 10.1016/j.jclepro.2020.124131
40. Chaudhary A, Hantush MM. Bayesian Monte Carlo and maximum likelihood approach for uncertainty estimation and risk management: application to lake oxygen recovery model. *Water Res.* (2017) 108:301–11. doi: 10.1016/j.watres.2016.11.012
41. Seifi A, Dehghani M, Singh VP. Uncertainty analysis of water quality index (WQI) for groundwater quality evaluation: Application of Monte-Carlo method for weight allocation. *Ecol Indicat.* (2020) 117:106653. doi: 10.1016/j.ecolind.2020.106653
42. Zhu H, Liu X, Xu C, Zhang L, Chen H, Shi F, et al. The health risk assessment of Heavy Metals (HMs) in road dust based on Monte Carlo simulation and bio-toxicity: a case study in Zhengzhou, China. *Environ Geochem Health.* (2021). 021:00922. doi: 10.1007/s10653-021-00922-1
43. Guo P, Li H, Zhang G, Tian W. Contaminated site-induced health risk using Monte Carlo simulation: evaluation from the brownfield in Beijing, China. *Environ Sci Pollut Res Int.* (2021) 28:25166–78. doi: 10.1007/s11356-021-12429-4
44. Qiu H, Gui H, Fang P, Li G. Groundwater pollution and human health risk based on Monte Carlo simulation in a typical mining area in Northern Anhui Province, China. *Int J Coal Sci Technol.* (2021) 8:118–29. doi: 10.1007/s40789-021-00446-0
45. Zhang Y, Geng. Review on models for lead exposure on human health risk assessment. *Environ Chem.* (2013) 32:943-51. doi: 10.7524/j.issn.0254-6108.2013.06.004
46. Zhou XY, Lei M, Yang J. Effect of lead on soil quality and human health around a lead smeltery. *China Environ Science*. (2013) 34:3675-8. doi: 10.13227/j.hjkx.2013.09.051
47. Ren HM, Wang JD, Wang GP, Zhang XL, Wang CM. Influence of soil lead upon children blood lead in Shenyang City. *China Environ Science*. (2005) 26:153-8. doi: 10.13227/j.hjkx.2005.06.032
48. Monnot AD, Christian WV, Abramson MM, Follansbee MH. An exposure and health risk assessment of lead (Pb) in lipstick. *Food Chem Toxicol.* (2015) 80:253–60. doi: 10.1016/j.fct.2015.03.022
49. O'Halloran K, Spickett JT. The interaction of lead exposure and pregnancy. *Asia Pac J Public Health.* (1992) 6:35–9. doi: 10.1177/101053959300600206
50. Yang KL, Zhang HZ, Zhang ZG, Yan PS. Localization study of environmental health risk assessment model for lead exposure. *China Popul Resources Environ.* (2016). 26:163–9. doi: 10.3969/j.issn.1002-2104.2016.02.020
51. Yang Y, Li X, Wang Q, Li D, Yu Y. Lead benchmarks for soil based on human health model (IEUBK and ALM) in Wenling region. *Huanjing Kexue Xuebao/Acta entiae Circumstantiae.* (2014) 34:1808–17. doi: 10.13671/j.hjkxxb.2014.0526
52. Delgado-Caballero MR, Valles-Aragon MC, Millan R, Alarcon-Herrera MT. Risk assessment through ieubk model in an inhabited area contaminated with lead. *Environ Prog Sustainable Energy.* (2018) 37:391-8. doi: 10.1002/ep.12692
53. National Medical Products Administration (NMPA). *Safety and Technical Standards for Cosmetics*. NMPA (2015). Available online at: http://mpa.gd.gov.cn/zwgk/zcfg/bmgz/content/post_1841027.html (accessed July 2020).
54. Zhou JM, Jiang ZC, Guang-Li XU, Qin XQ, Huang QB, Zhang LK. Distribution and health risk assessment of metals in groundwater around iron mine. *China Environ Sci.* (2019) 39:1934–44. doi: 10.19674/j.cnki.issn1000-6923.2019.0230
55. Gao RZ, Qin ZY, Zhang S, Jia DB, Wang XX. Health risk assessment of Cr6+, As and Hg in groundwater of Jilantai salt lake basin, China. *Zhongguo Huanjing Kexue/China Environ Sci.* (2018) 38:2353–62. doi: 10.19674/j.cnki.issn1000-6923.20180305.004
56. USEPA (United States Environmental Protection Agency). *Risk Assessment Guidance for Superfund. Volume I: (Part A: Human Health Evaluation Manual; Part E, Supplemental Guidance for Dermal Risk Assessment; Part F, Supplemental Guidance for Inhalation Risk Assessment).* Washington DC, USEPA (2011).
57. USEPA (United States Environmental Protection Agency). *Risk Assessment Guidance for Superfund. Volume? (Part A: Human Health Evaluation Manual; Part E, Supplemental Guidance for Dermal Risk Assessment; Part F, Supplemental Guidance for Inhalation Risk Assessment).* Washington DC, USEPA (1999).
58. Hosseini Koupaie E, Eskicioglu C. Health risk assessment of heavy metals through the consumption of food crops fertilized by biosolids: a probabilistic-based analysis. *J Hazard Mater.* (2015) 300:855–65. doi: 10.1016/j.jhazmat.2015.08.018
59. Peng Q, Nunes LM, Greenfield BK, Dang F, Zhong H. Are Chinese consumers at risk due to exposure to metals in crayfish? A bioaccessibility-adjusted probabilistic risk assessment. *Environ Int.* (2016) 88:261-8. doi: 10.1016/j.envint.2015.12.035
60. Wang J, Shan Q, Liang X, Guan F, Zhang Z, Huang H, et al. Levels and human health risk assessments of heavy metals in fish tissue obtained from the agricultural heritage rice-fish-farming system in China. *J Hazard Mater.* (2020) 386:121627. doi: 10.1016/j.jhazmat.2019.121627
61. Yang S, Zhao J, Chang SX, Collins C, Xu J, Liu X. Status assessment and probabilistic health risk modeling of metals accumulation in agriculture soils across China: a synthesis. *Environ Int.* (2019) 128:165–74. doi: 10.1016/j.envint.2019.04.044
62. Wu J, Li J, Teng Y, Chen H, Wang Y. A partition computing-based positive matrix factorization (PC-PMF) approach for the source apportionment of agricultural soil heavy metal contents and associated health risks. *J Hazard Mater.* (2020) 388:121766. doi: 10.1016/j.jhazmat.2019.121766
63. Kurt-Karakus PB. Determination of heavy metals in indoor dust from Istanbul, Turkey: estimation of the health risk. *Environ Int.* (2012) 50:47-55. doi: 10.1016/j.envint.2012.09.011
64. Sun G, Feng X, Yang C, Zhang L, Yin R, Li Z, et al. Levels, sources, isotope signatures, and health risks of mercury in street dust across China. *J Hazard Mater.* (2020) 392:122276. doi: 10.1016/j.jhazmat.2020.122276
65. Malvandi H, Sancholi F. Assessments of some metals contamination in lipsticks and their associated health risks to lipstick consumers in Iran. *Environ Monit Assess.* (2018) 190:680. doi: 10.1007/s10661-018-7065-9
66. Arshad H, Mehmood MZ, Shah MH, Abbasi AM. Evaluation of heavy metals in cosmetic products and their health risk assessment. *Saudi Pharm J.* (2020) 28:779–90. doi: 10.1016/j.jsps.2020.05.006
67. Sook KJ. Study on the intake amount of lipstick and lip-gloss and content monitoring focusing on butylparaben and tar color. *J Korean Soc Cosmetol.* (2013) 19:54–61. https://www.kci.go.kr/kciportal/ci/sereArticleSearch/ciSereArtiView.kci?sereArticleSearchBean.artiId=ART001744376&locale=en&SID=8EpyLIo1RyrJNORrVms (accessed May 2020).
68. Zhang HZ, Luo YM, Zhang HB, Song J, Xia JQ, Zhao QG. Development of lead benchmarks for soil based on human blood lead level in China. *China Environ Science.* (2009) 30:3036–42. doi: 10.13227/j.hjkx.2009.10.051

69. Can LI, Zeng Y, Liu SY, Wang Q. Lead benchmarks for soils based on blood lead model for children and adult in China. *J Environ Health.* (2017). 34:789–93, doi: 10.16241/j.cnki.1001-5914.2017.09.010
70. USEPA (United States Environmental Protection Agency). *Guidance Manual for the Integrated Exposure Uptake Biokinetic Model for Lead in Children*; *Chapter 1*. Washington DC, USEPA (1994).
71. White PD, Van Leeuwen P, Davis BD, Maddaloni M, Hogan KA, Marcus AH, et al. The conceptual structure of the integrated exposure uptake biokinetic model for lead in children. *Environ Health Pers.* (1998) 106(Suppl 6):1513–30. doi: 10.1289/ehp.98106s61513
72. Li YY, Hu J, Wu W, Liu SY, Li M, Yao N, et al. Application of IEUBK model in lead risk assessment of children aged 61-84 months old in central China. *Sci Total Environ.* (2016) 541:673–82. doi: 10.1016/j.scitotenv.2015.09.103
73. Heusinkveld D, Ramirez-Andreotta MD, Rodriguez-Chavez T, Saez AE, Betterton E, Rine K. Assessing children's lead exposure in an active mining community using the integrated exposure uptake biokinetic model. *Expo Health.* (2021) 13:517–33. doi: 10.1007/s12403-021-00400-0
74. Ministry of Environmental Protection of China. *Ambient Air Quality Standards*. Beijing: Standards Press of China (2012).
75. MOHC (the Minister of Health of the People's Republic of China). *Standards for Drinking Water Quality*. Beijing: Standards Press of China (2006).
76. CFDA (China Food and Drug Administration). *National Standards for Food Safety Limits of Pollutants in Food.* Beijing: Standards Press of China (2017).
77. Gulson B, Taylor A, Stifelman M. Lead exposure in young children over a 5-year period from urban environments using alternative exposure measures with the US EPA IEUBK model – a trial. *Environ Res.* (2018) 161:87–96. doi: 10.1016/j.envres.2017.10.040
78. Liu S, Hammond SK, Rojas-Cheatham A. Concentrations and potential health risks of metals in lip products. *Environ Health Perspect.* (2013) 121:705–10. doi: 10.1289/ehp.1205518
79. Mattioli M, Giordani M, Dogan M, Cangiotti M, Avella G, Giorgi R, et al. Morpho-chemical characterization and surface properties of carcinogenic zeolite fibers. *J Hazard Materials.* (2016) 306:140–8. doi: 10.1016/j.jhazmat.2015.11.015
80. Janetos TM, Akintilo L, Xu S. Overview of high-risk food and drug administration recalls for cosmetics and personal care products from 2002 to 2016. *J Cosmet Dermatol.* (2019) 18:1361–5. doi: 10.1111/jocd.12824
81. Sani A, Gaya MB, Abubakar FA. Determination of some heavy metals in selected cosmetic products sold in kano metropolis, Nigeria. *Toxicol Rep.* (2016) 3:866–9. doi: 10.1016/j.toxrep.2016.11.001
82. Malakootian M, Mazandarany MP, Eskandari M, Pourmahyabady R. Determination of lead concentration in solid and liquid lipsticks available in Iran-Kerman. *Trans Chin Soc Agri Eng.* (2012) 25:21–6. doi: 10.3969/j.issn.1002-6819.2009.09.004
83. Sharafi K, Fatahi N, Yarmohammadi H, Moradi M, Dargahi A. Determination of cadmium and lead concentrations in cosmetics (lipstick and hair color) in Kermanshah Markets. (2017) 8:143–50. http://healthjournal.arums.ac.ir/article-1-1180-en.html (accessed June 2020).
84. Ghaderpoori M, Kamarehie B, Jafari A, Alinejad AA, Hashempour Y, Saghi MH, et al. Health risk assessment of heavy metals in cosmetic products sold in Iran: the Monte Carlo simulation. *Environ Sci Pollut Res Int.* (2020) 27:7588-95. doi: 10.1007/s11356-019-07423-w
85. USEPA (United States Environmental Protection Agency). *Region 6 Human Health Medium-Specific Screening Levels*. Washington DC, USEPA (2009).
86. Jusko TA, Henderson CR, Lanphear BP, Cory-Slechta DA, Parsons PJ, Canfield RL. Blood lead concentrations < 10 microg/dL and child intelligence at 6 years of age. *Environ Health Perspect.* (2008) 116:243–8. doi: 10.1289/ehp.10424
87. Zhu H, Yang ZJ. Effect of lead exposure during pregnancy on mother and infants and the related factors. *Hainan Med J.* (2011) 22:12–5. doi: 10.3969/j.issn.1003-6350.2011.24.005
88. Gonzalez Valdez E, Gonzalez Reyes E, Bedolla Cedeno C, Arrollo Ordaza EL, Manzanares Acuna E. Blood lead levels and risk factors for lead poisoning in mexican children. *Revista Facultad De Ingenieria-Universidad De Antioquia.* (2008) 43:114–9. http://www.scielo.org.co/scielo.php?script=sci_arttext&pid=S0120-62302008000100010 (accessed July 2020).
89. Tao Y, Zhang F, Shi C, Chen Y. Social media data-based sentiment analysis of tourists' air quality perceptions. *Sustainability.* (2019) 11:5070. doi: 10.3390/su11185070
90. Li Y, Liu Z, Zhang Y, Jiang L, Cai Y, Chen X, et al. Investigation and probabilistic health risk assessment of trace elements in good sale lip cosmetics crawled by Python from Chinese e-commerce market. *J Hazard Materials.* (2021) 405:124279. doi: 10.1016/j.jhazmat.2020.124279
91. Wu Z, Wang X, Pan R, Huang X, Li Y. Study of the relationship between ICU patient recovery and TCM treatment in acute phase: a retrospective study based on python data mining technology. *Evid Based Complement Alternat Med.* (2021) 2021:5548157. doi: 10.1155/2021/5548157

Conflict of Interest: The authors declare that the research was conducted in the absence of any commercial or financial relationships that could be construed as a potential conflict of interest.

Publisher's Note: All claims expressed in this article are solely those of the authors and do not necessarily represent those of their affiliated organizations, or those of the publisher, the editors and the reviewers. Any product that may be evaluated in this article, or claim that may be made by its manufacturer, is not guaranteed or endorsed by the publisher.

frontiers in Public Health

ORIGINAL RESEARCH
published: 31 December 2021
doi: 10.3389/fpubh.2021.792590

Spatio-Temporal Variation of Health Production Efficiency Considering Environmental Pollution in China Based on Modified EBM and Spatial Econometric Model

Fan Liu[1], *Gen Li*[2]*, *Ying Zhou*[2], *Yinghui Ma*[2] *and Tao Wang*[2]

[1] School of Business Administration, Zhongnan University of Economics and Law, Wuhan, China, [2] School of Economics and Management, Jiangsu University of Science and Technology, Zhenjiang, China

OPEN ACCESS

Edited by:
Hongtao Yi,
The Ohio State University,
United States

Reviewed by:
Kang Zheng,
Harbin Medical University, China
Antonino Maniaci,
University of Catania, Italy

***Correspondence:**
Gen Li
ligen@just.edu.cn

Specialty section:
This article was submitted to Environmental health and Exposome, a section of the journal Frontiers in Public Health

Received: *10 October 2021*
Accepted: *10 December 2021*
Published: *31 December 2021*

Citation:
Liu F, Li G, Zhou Y, Ma Y and Wang T (2021) Spatio-Temporal Variation of Health Production Efficiency Considering Environmental Pollution in China Based on Modified EBM and Spatial Econometric Model. Front. Public Health 9:792590. doi: 10.3389/fpubh.2021.792590

In order to strengthen the construction of China's health industry and improve the health of the people, based on the data of 31 provinces and cities in China from 2009 to 2019, the improved EBM model is used to measure the health production efficiency of each region, and Moran index is used to study the Spatio-temporal variation of health production efficiency of each province. Finally, the spatial econometric model is applied to study the influencing factors of the Spatio-temporal variation of health production efficiency. The results show that generally speaking, the average efficiency of 31 provinces and cities is above 0.7, and the average efficiency of some regions is above 1. From the perspective of time variation, the average efficiency value in the eastern region and the middle region increases from 0.816 to 0.882 and from 0.851 to 0.861, respectively. However, the average efficiency value in the western region and northeast region decreases from 0.861 to 0.83 and from 0.864 to 0.805, respectively. From the perspective of spatial distribution, HH agglomeration and LL agglomeration exist in most regions. By comparing Moran scatter plots in 2009 and 2019, it is found that the quadrants of most regions remain unchanged, and LL agglomeration is the main agglomeration type in local space. There is a significant spatial dependence among different regions. From the perspective of spatial empirical results, *Pgdp*, *Med,* and *Pd* have a positive effect on health production efficiency. The direct effect and indirect effect of *Pgdp*, *Med*, and *Gov* all pass the significance test of 1%, indicating that there are spatial spillover effects of the three indicators. Each region should reasonably deal with the spillover effect of surrounding regions, vigorously develop economic activities, carry out cooperation with surrounding regions and apply demonstration effect to accelerate the development of overall health production.

Keywords: health production efficiency, Spatio-temporal variation, improved EBM model, spatial econometric model, Moran's I

INTRODUCTION

The economy of China is developing rapidly, and the economic level is rising day by day. Under the current high-speed development, we also need to pay attention to the high-quality development of the economy. The rapid economic development has had a great impact on the residents' life, and the modern social civilization has changed the residents' life in many ways. The concept of healthy production has been more mentioned. The report of the 19th National Congress of the Communist Party of China put forward "the implementation of Healthy China Strategy." Promoting high-quality development of health care is an integral part of the implementation of the Healthy China Strategy and the only way to meet people's growing health needs. According to the data, the national economy in the first quarter of 2021 is generally stable and the development quality is steadily improving. According to the preliminary calculation, the GDP of the first quarter is 24,931 billion yuan, up 18.3% year on year. Meanwhile, the scale of China's health service industry reaches 8 trillion yuan in 2020, accounting for 6.5% of GDP. Market forecast analysis of ChinaIRN has announced that the big health industry will usher in a real outbreak period from 2021 to 2025. In order to respond positively to the Healthy China Strategy, the healthy production level in China on the premise of considering environmental pollution is calculated and the strategies conducive to the development of healthy production are put forward by this paper.

According to the existing research literature on healthy production, scholars mostly use DEA and SFA to measure health production efficiency. For example, Yu Jiali et al. (1) used the DEA-Malmquist model, the decomposable Theil index, and the spatial (traditional) econometric model to study the dynamic evolution of Chinese residents' health production efficiency and its influencing factors from 2002 to 2017. The model was used to calculate the comprehensive efficiency, scale efficiency, and pure technical efficiency of Chinese residents' healthy production. Shi Zhen et al. (2) combined water consumption with wastewater discharge, pollutant concentration in sewage, local medical expenditure, and other factors, and incorporated them into the water resources, energy, and health measurement model, using DEA model to calculate the total efficiency, production efficiency, and health efficiency of 30 provinces from 2014 to 2017. The results show that the key impact indicators were different in each province, and each province should formulate different policies according to its own specific situation, deepen the energy, economic and medical reform in each province, and promote sustainable economic development while improving health efficiency. Shen Shuguang et al. (3) applied SFA to investigate the health production efficiency of various provinces and cities in China from 2010 to 2014 and analyzed the influencing factors of health production efficiency. The study found that since 2010, the health production efficiency in China had improved and regional disparities had narrowed. Based on the data of 30 provinces in China from 2011 to 2017, Shi Zhen et al. (4) adopted the improved undesirable dynamic network SBM model to investigate the economic production stage efficiency and sewage treatment stage efficiency of each province. The results showed that the stage efficiency of sewage treatment was the main factor affecting the overall efficiency. Provinces should therefore follow key indicators to improve efficiency according to local conditions. Ye Li et al. (5) combined the fixed Malmquist-Luenberger (ML) index with the SBM model considering unexpected output, A new slack based measure-Malmquist-Luenberger model was proposed to measure the level of green development in the Pearl River Delta region from 2005 to 2018. The changes of the green development level were analyzed from time and space dimensions. Li Xiangqian et al. (6), Zhang Ning et al. (7), Ma Yuan et al. (8), and Laurie J. Bates et al. (9) all used DEA to study health production efficiency. The above scholars improve and innovate DEA and SFA to make them more consistent with the problems studied, and their conclusions also lay a solid foundation for the research of this paper. In order to study radial ratio and non-radial relaxation improvement simultaneously, the EBM model is used to measure health production efficiency.

At present, there are few studies on the Spatio-temporal variation of health production efficiency, and some scholars have conducted studies on the Spatio-temporal variation of carbon emissions, innovation efficiency, and ecological efficiency. In order to explore the relationship between urban innovation efficiency and high-quality economic development from the perspective of total factors, Yang Weili et al. (10) took Shaanxi province as an example to analyze the static and dynamic characteristics of urban innovation efficiency from 2008 to 2018 and conducted a Spatio-temporal analysis of the coupling relationship between urban innovation efficiency and high-quality economic development: The urban innovation efficiency was effective in most cities, and the growth rate of urban innovation efficiency presented a fluctuating upward trend. The coupling coordination degree between urban innovation efficiency and high-quality economic development increased steadily on the whole. Based on the coupling coordination degree model and factor analysis model, Liu Zhihua et al. (11) took the data of 30 provinces and cities in China from 2001 to 2017 as an example to build a comprehensive evaluation index system for the coupling coordination of carbon emission reduction, economic growth and environmental protection at the provincial level and analyzed the Spatio-temporal variation and driving mechanism of the coupling coordination degree. From the perspective of time, the coupling coordination level of the three systems at the provincial level gradually improved, but it was still in a low state. From the perspective of space, the overall trend was "higher in the Southeast region and lower in the Middle and Western regions," and the agglomeration was poor. Guo Fuyou et al. (12) comprehensively constructed the evaluation index system of green development in the Yellow River Basin and studied the Spatio-temporal variation characteristics and driving factors of green development in the eco-economic corridor of the Yellow River Basin from 2005 to 2017 by using a variety of measurement methods such as entropy method, spatial autocorrelation analysis, and geographic detector model. The results showed that the green development of the Yellow River Basin mainly came from

the external driving effect of large-scale expansion and total growth, and it was inevitable that the endogenous driving effect would be insufficient and unsustainable if the green development of the Yellow River Basin focused on the development speed and ignored the convolution improvement of quality and efficiency. At present, the research on the Spatio-temporal variation of green economy and sustainable development in the academic circle has gradually matured, which provides valuable experience for the research on the Spatio-temporal variation of health production efficiency from the perspective of spatial correlation and spatial heterogeneity in this paper.

According to the current works of literature, most scholars choose to influence factor variables from the aspects of government support, technological level, medical and health care, population density, and so on. He Guanjie et al. (13) adopted the sub-grade index of hospital visitors as a proxy variable of residents' health status and selected regional ecological efficiency and six other control variables as explanatory variables to construct a support vector sensitivity measurement method (SMM-SVM). Li Xiangqian et al. (14) showed that government input capacity and urbanization level had a negative effect on national health production efficiency, and service accessibility had a positive effect on national health production efficiency. Ding Jingmei et al. (15) used DEA to measure the efficiency of the medical and health system in 31 administrative regions of China except for Hong Kong, Macao, and Taiwan and discussed its influencing factors by general linear regression. The results suggest that policymakers should take into account the socio-economic development level and population composition and make targeted changes to the amount of input. Gao Qiuming et al. (16) studied the impact of hospital efficiency on medical service equity based on a proprietary hospital characteristic data set and 630,000 inpatient records from 149 public hospitals in a representative city in China. The results showed that efficiency-oriented health care policies may lead to the loss of social benefits. Wu Haitao et al. (17) found that environmental pollution inhibited the development of comprehensive urbanization, population urbanization, economic urbanization, and urbanization of living conditions in China, but promoted the development of urbanization of the living environment. However, with the increase of residents' health costs, the inhibition effect of environmental pollution on China's comprehensive urbanization, population urbanization, economic urbanization, and housing urbanization was gradually strengthened, while the inhibition effect on housing environment urbanization was weakened. Based on considering the impact of environmental pollution on human health, Zhao Kai et al. (18) extended and constructed the endogenous economic growth model of production, research and development, human capital cultivation, and resource development, and reinterpreted the driving force of China's economy from the perspective of human health by using the public panel model and the space panel model. The study found that China's economic growth relied on physical capital investment and energy consumption. It can be seen from the research conclusions of the above scholars that among the influencing factors, the level of economic development has a positive effect on health production efficiency, and the increase of population density can provide residents with more medical and health services under a moderate financial budget (19). Policy support and health care level can promote the health of the domestic floating population (20). The above research results are numerous, and the selected influencing factors are representative, which is conducive to the construction of the influencing factor index system in this paper. However, the spillover effect is not analyzed and the transmission effect between regions is also worth pondering. This paper will explore the regional transmission mechanism of influencing factors of health production efficiency from the perspective of spatial spillover effect.

After summarizing the above literature, this paper puts forward the following improvements: (1) Environmental pollution is considered in the construction of the input-output index system, and the amount of medical waste produced and the mortality rate are selected as the unexpected output variables. (2) In order to make up for the limitations of the DEA model, this paper decides to use the EBM hybrid model including radial and non-radial distance functions to analyze regional differences in health production efficiency of various provinces and cities. (3) The spatial econometric model is used to analyze the spatial spillover effects of the influencing factors of health production efficiency.

RESEARCH DESIGN

Measurement Model of Health Production Efficiency in China

In this paper, the super-efficiency EBM model is used to measure the health production efficiency of Chinese residents considering environmental pollution. Existing studies on the measurement of health production efficiency are mainly based on radial or non-radial CCR, BCC, and SBM models in traditional DEA models, but all of them have certain deficiencies: Radial model requires all input-output factors to be reduced or expanded in the same proportion, which is not in line with reality. Although the non-radial model considers the problem of relaxation, the loss rate is the proportion of information between the target input-output value and the actual value (21). In 2010, Tone and Tsutsui put forward the EBM model, which considered both radial ratio and non-radial relaxation improvement quantity, eliminated the coarse and extract the essence of the radial model and non-radial model, kept the radial ratio of the projection value and the original value of the elements and took into account the relaxation variable of the difference of each element. Therefore, in this paper, the EBM model considering the unexpected output will be adopted. Due to the efficiency value of most decision-making units may exceed 1, Andersen et al. (22) established the super-efficiency DEA model to further compare and analyze all decision-making units and realize the calculation of effective decision-making units. In this paper, based on the research of Han Jieping et al. (23), the programming formula of the super-efficiency EBM model which is improved based on non-guidance

and considering non-expected output is constructed:

$$\begin{aligned}\gamma^* = \min \frac{\theta - \varepsilon^- \sum_{i=1}^{m} \frac{w_i^- s_i^-}{x_{ik}}}{\varphi + \varepsilon^+ \left(\sum_{r=1}^{s} \frac{w_r^+ s_r^+}{y_{rk}} + \sum_{p=1}^{q} \frac{w_p^{u-} s_p^{u-}}{u_{pk}} \right)} \\ i = 1, 2, ..., m; \ r = 1, 2, ..., s; \ p = 1, 2, ..., q \\ s.t \sum_{j=1, j\neq k}^{n} \lambda_j x_{ij} + s_i^- \leq \theta x_{ik} \\ \sum_{j=1, j\neq k}^{n} \lambda_j y_{ij} - s_r^+ \geq \varphi y_{rk} \\ \sum_{j=1, j\neq k}^{n} \lambda_j u_{pj} + s_p^+ \leq \varphi u_{pk} \\ \lambda_j \geq 0, s_i^-, s_r^+, s_p^+ \geq 0 \end{aligned} \quad (1)$$

Where, γ^* represents the health production efficiency of the province. k represents the number of decision units, and x_{ik}, y_{rk}, u_{pk} represents the input, expected output, and unexpected output of the k decision unit, respectively. s_i^-, s_r^+, s_p^{u-} represent the relaxation variables of input, expected output, and unexpected output, respectively; w_i^-, w_r^+, w_p^{u-} represent the weight of each input indicator, expected output and non-expected output indicator; θ and φ are radial components of γ^*; ε is a key parameter with a value range of [0∼1], indicating the importance of the non-radial part. When $\varepsilon = 0$, the ultra-efficient EBM model is equivalent to the radial model; when $\theta = \varepsilon = 1$, the ultra-efficient EBM model is equivalent to the non-radial SBM model.

Spatial Correlation Analysis Method of Health Production Efficiency in China

In order to explore the spatial correlation of health production efficiency in China, this paper applies the spatial analysis method (24) to study its regional impact. Firstly, the global Moran's I (25) is selected to reveal the spatial distribution pattern of health production efficiency (26). The calculation formula is as follows:

$$I = \frac{n \sum_{i=1}^{n} \sum_{j=1}^{n} W_{ij} |\gamma_i^* - \overline{\gamma^*}| |\gamma_i^* - \overline{\gamma^*}|}{\sum_{i=1}^{n} \sum_{j=1}^{n} W_{ij} \sum_{i=1}^{n} |\gamma_j^* - \overline{\gamma^*}|^2} \quad (2)$$

In Formula (2), γ_i^*, γ_j^* is the efficiency value of each spatial unit, $\overline{\gamma^*}$ is the average efficiency value of each spatial unit, and W_{ij} is the spatial weight matrix of each spatial unit. Finally, the spatial correlation between various regions can be judged according to the positivity and negativity of Moran's I.

The global Moran's I can measure the global spatial correlation of observed variables. Considering the instability of local variables, the *Getis-Ord* G_i^* index is introduced to analyze the spatial aggregation phenomenon between local variables. The calculation formula is as follows:

$$G_i^* = \sum_{j=1}^{n} (W_{ij} \gamma_j^*) / \sum_{j=1}^{n} \gamma_j^* \quad (3)$$

According to the value of the *Getis-Ord* G_i^* index, the aggregation of each local space is judged.

Spatial Econometric Model of Health Production Efficiency in China

Currently, the spatial econometric models are commonly used in academic circles to study health production efficiency, including two modes, one is the spatial panel lag model (SLM) and the other is spatial panel error model (SEM) (27).

The spatial lag model mainly discusses whether a certain region has spillover and diffusion effects on its surrounding regions. The following expression of the SLM model is established in this paper according to the influencing factors:

$$\gamma_{it}^* = \rho W y + X\theta_{it} + \varepsilon_{it} \quad (4)$$

Where, γ_{it}^* represents the health production efficiency of the i province in the year t, and ρ is the spatial regression estimation coefficient, which reflects the spatial dependence between the observed values of samples, namely, the observed values of adjacent regions. W is the $n \times n$-order spatial weight matrix, which generally selects the proximity matrix or distance matrix. Wy is the spatial lag explanatory variable, representing the observed value of the dependent variable in the surrounding area, reflecting the effect of spatial distance on each space unit. ε is the random error term vector, and X is the $n \times k$-order explanatory variable matrix.

The spatial error model is different from the spatial lag model. The spatial dependence in the spatial error model mainly exists in the error term. The spatial error model is mainly used to reflect the different relative positions between regions. The mathematical expression is:

$$\begin{aligned}\gamma_{it}^* &= X\theta_{it} + \mu_{it} \\ \mu_{it} &= \lambda W_z + \varepsilon_{it}\end{aligned} \quad (5)$$

Where γ_{it}^* represents the health production efficiency of the i province in the year t, X is the exogenous explanatory variable matrix of $n \times k$, W is the spatial weight matrix of $n \times n$, ε is the random error vector, μ is the random error vector of normal distribution, and λ is the spatial error coefficient of the dependent variable vector.

VARIABLE DESIGN

Input-Output Variables

In reference to the relevant works of literature on healthy production, this article selects the total health expenses, per capita expenditure of medical insurance, per capita medical capital stock, and health technical personnel as the input variables, through the analysis of health input indicators, health input index system covers the health, labor, and capital in the field of production elements, the total health expenses and per capita medical capital stock covers the medical equipment investment, the cost such as the construction of medical institutions, so used to measure the health capital investment, health technical personnel to reflect the connotation of human capital investment,

per capita expenditure of medical insurance reflect medical spending, it has also been identified as one of the indicators of health investment.

At present, health outcomes are mostly measured using vital statistics. However, there are many gaps in current data on life expectancy that do not reflect continuous levels of healthy production. Perinatal survival rate and mortality rate are highly available indicators and reflect healthy levels of production in the region, the perinatal survival rate as expected output variables. Medical waste production and mortality rate are selected as the unexpected output variables. The relevant variables are explained as follows.

(1) Input variables. ① Total health expenses. Total health cost includes the government, society, and individuals' investment in health and medical services, which is used to describe the health situation of a region. This paper selects total health costs to represent the medical capital investment of each region. ② Per capita expenditure of medical insurance. According to the expenditure scope and expenditure standard stipulated by the national policy, the medical insurance treatment expenses are paid from the social overall planning fund to the employees and retirees participating in the basic medical insurance, and the medical expenses are paid from the personal account fund to the employees and retirees participating in the basic medical insurance, as well as other expenses. Per capita medical insurance is used in this paper. ③ Per capita medical capital stock. In order to measure the input of medical and health materials in each region, this paper selects the index of medical capital stock, which is measured by the number of beds in medical and health institutions per thousand population. ④ Health technical personnel. In this paper, the index of the number of health technical personnel needs to use the relative quantity index, and the index of the number of health technical personnel per thousand population is used. The index can reflect the investment of human capital in health organizations and measure the level of technology in each region.

(2) Expected output variables. In many previous studies, average life expectancy is selected as the output index, but due to the lack of data, the perinatal survival rate is used as the expected output index in this paper. The perinatal mortality rate is often expressed in permillage. Between the 28th week of gestation and the 7th day after birth (or birth weight above 1,000 g), the perinatal mortality rate is the ratio of stillbirths, dead-birth and neonatal deaths caused by fatal diseases or maternal diseases affecting the fetus to survival number of newborns (2). After obtaining the perinatal mortality, the perinatal survival rate (1-perinatal mortality rate) can be converted.

(3) Unexpected output variables. ① Medical waste production. This paper considers the impact of environmental pollution on healthy production. In order to reflect environmental pollution factors in health efficiency, this paper selects medical waste production. In consideration of the availability of data, this paper chooses hazardous waste production data as a substitute. ② Mortality rate. The output variables of health production are mainly related variables such as mortality. In this paper, the perinatal survival rate is selected above, and the population mortality variable is selected to measure the unexpected output.

Influencing Factor Variables

Based on previous studies, variables of economic development level, the service level of medical institutions, government support system, and population density degree are often selected as influencing factors. Besides, this paper chooses medical non-marketization degree as an explanatory variable by referring to Shen Shuguang et al. (3).

(1) Economic development level

The economic development level of each province is most directly reflected by the GDP index. In this paper, the per capita GDP index is selected. Ochalek Jessica et al. used per capita GDP as an empirical control variable (28). Generally speaking, areas with high economic development levels will have higher social production efficiency, higher social construction level, and higher living standard of people. Therefore, areas with higher levels of health production efficiency will also have higher levels of health production efficiency. It is predicted that per capita GDP will have a positive effect on health production efficiency.

Urbanization level represents the degree of agglomeration of urban residents, which can reflect the urbanization process and the economic development level of each province. It is an important indicator of regional economic development degree. It is also a condition to measure the level of regional social development. It is assumed that the level of urbanization will have a positive effect on health production efficiency.

(2) Service level of medical institutions

The service level of medical institutions determines the length of hospitalization and recovery time of residents, so this paper adopts the average length of hospitalization to measure the service level of medical institutions. Liu Weilin et al. used an average length of hospitalization to represent health resource output utilization (29). The average length of stay in a hospital refers to the average length of stay of each patient in a certain period, which can reflect the management ability and medical technology level of medical service institutions. The larger the average length of stay, the lower the service level of the medical institution, and the smaller the average length of stay, the higher the service level of the medical institution. At the same time, it can save the medical resources of each institution and improve the healthy production level of residents. Therefore, the average length of stay is assumed to have a negative effect on health production efficiency.

(3) Medical non-marketization

Since there are too many public hospitals in the medical market, the market competition is relatively calm, which will reduce the reform and innovation motivation of each hospital. This paper chooses the ratio of public hospitals to private hospitals as a quantitative index of the degree of medical non-marketization. Private hospitals can play a role in causing benign competition in the market, which is conducive to intensifying competition in the medical market and causing public hospitals to carry out reform and innovation, so as to promote the development of the medical market and improve the medical level of each region. This paper assumes that the degree of medical non-marketization has a negative effect on health production efficiency.

(4) Government support system

Government policies in each region determine the development direction of the region. Government support for healthy production can be measured by government financial health expenditure, and the relative quantity is selected as the index. In this paper, the proportion of government financial health expenditure in GDP is chosen as the expression. Cheng Zhaohui et al. used government financial health expenditure as environment variables for empirical research (30). Government financial expenditure specifically refers to the financial allocation of health undertakings by local governments, which is generally used for public health service funds and free medical funds. Government financial health expenditure has an important influence on regional public health construction levels. The more government financial health expenditure, the higher the level of medical and health facilities construction is. It is assumed that government expenditure on health has a positive effect on health production efficiency.

(5) Population density

Population density refers to the population per unit of land, which is one of the important indices for regional population distribution. It influences the output level of regional healthy production. On one hand, high population density would have a burden on the local medical and health institutions, but at the same time, the higher the population density, regional production efficiency will be higher. Maniaci Antonino et al. (31) and Chandra Bharatendu et al. (32) showed that long-term use of N95 protective masks in the work of medical staff would reduce the work level of medical staff, and larger public hospitals would make more complete rules in this regard. Combining previous research on the index, it assumes that population density has a positive effect on health production efficiency. To sum up, the selected variables are summarized, as shown in **Table 1**.

TABLE 1 | Variable description.

Variable	Symbol	Definition
Expected output	y	Perinatal survival rate (‰)
Capital investment	K_e	Total expenditure on health (million yuan, Ln, based on 2009)
	K_i	Per capita medical insurance (ten thousand yuan, based on 2009)
	K_b	Number of beds in medical and Health institutions per thousand population (sheets)
Human input	I	Number of health technicians per thousand population (persons, Ln)
Unexpected output	B_w	Medical waste production amount (ten thousand tons)
	B_m	Mortality rate (%)
Per capita GDP	*Pgdp*	GDP/Population by region (ten thousand Yuan/person, based on 2009)
Urbanization level	*Urb*	Urbanization level (%)
Service level of medical institutions	*Med*	Average length of stay in hospital (days)
Medical non-marketization	*Mnm*	Number of public/Private hospital establishments (%)
Government support system	*Gov*	Fiscal health expenditure /GDP (%)
Population density	*Pd*	Area population/Area (People/km^2)

Sample Selection and Data Sources

In this paper, the data of 31 provinces and cities in China from 2009 to 2019 are selected for the analysis of health production efficiency. Due to the lack of some data in Tibet and Hong Kong, Macao, and Taiwan, the study is not included. The data of all indicators come from the China Statistical Yearbook, China Health Statistical Yearbook, China Urban Statistical Yearbook, and relevant statistical yearbook data of all provinces and cities. For some missing data, interpolation and weighted average are used to complete the data. Descriptive statistics of relevant variables are shown in **Table 2**. **Table 2** shows that there are large inter-provincial differences in the amount of medical waste produced and population density.

SPATIO-TEMPORAL VARIATION OF HEALTH PRODUCTION EFFICIENCY IN CHINA

Health Production Efficiency in China

In this paper, MAXDEA (Professional edition) software (Beijing Rewomaidi Software Co., LTD, Beijing, China) was used to calculate the health production efficiency of 31 provinces in China. The results are shown in **Table 3**. According to the National Bureau of Statistics' economic regional division of China, 31 provinces are divided into four regions: Eastern region, Middle region, Western region, and Northeastern region. **Table 3** describes the health production efficiency of 31 provinces and cities from 2009 to 2019. The health production efficiency of 31 provinces and cities each year can be seen intuitively.

(1) From the Eastern region, the average efficiency of Hainan is the highest at 1.090. The efficiency value of Hainan from 2009 to 2019 is >1, and the comprehensive efficiency value of Guangdong province is also >1 each year, slightly lower than Hainan province. Hainan takes the tertiary industry as the main target of development and implements high-quality and high-standard green development on every project. Therefore, only in this way can the health production efficiency of Hainan be maintained above 1 and the quality of healthy development can be maintained. Hainan and Shandong belong to the eastern region, but there is a big gap in healthy production efficiency, because the annual hazardous waste discharge in Hainan is much lower than that in Shandong, so the efficiency value in Hainan is higher than that in Shandong.

Among other provinces and cities, Jiangsu province's health production efficiency has been on the rise, and Jiangsu province has achieved initial results in the development of healthy output. On the contrary, the health production efficiency of Beijing decreased from 1.005 to 0.752 in 2018. In terms of efficiency decomposition, the scale efficiency of Beijing is 0.748. Therefore, Beijing should pay attention to the rational allocation of medical resources and strengthen the management level of medical and

TABLE 2 | Descriptive statistics of variables.

Variable	Minimum	Maximum	Standard deviation	Mean
Perinatal survival rate (‰)	0.760	0.982	0.034	0.936
Total expenditure on health (million yuan, Ln, based on 2009)	3.519	8.662	0.903	6.789
Per capita medical insurance (ten thousand yuan, based on 2009)	0.044	0.598	0.101	0.225
Number of beds in medical and Health institutions per 1,000 population (sheets)	2.390	7.550	1.192	4.871
Number of health technicians per thousand population (persons, Ln)	2.370	15.460	2.027	5.794
Medical waste production amount (ten thousand tons)	0.050	1046.04	173.690	140.849
Mortality rate (%)	0.042	0.076	0.008	0.060
per capita GDP (ten thousand Yuan/person, based on 2009)	1.1062	16.1642	2.561	4.832
Urbanization level (%)	0.223	0.896	0.136	0.555
Service level of medical institutions (days)	8.1	16.2	2.401	9.923
Degree of medical non-marketization (%)	0.1976	32.000	2.7254	1.4347
Government support system (%)	0.0074	0.0753	0.0119	0.0213
Population density(People/km^2)	2.4104	3853.9683	683.6284	450.4962

TABLE 3 | Health production efficiency in China 2009-2019.

CRS	2009	2010	2011	2012	2013	2014	2015	2016	2017	2018	2019	Max	Min	Mean	Region
BeiJing	1.017	1.027	1.026	1.012	1.009	1.008	1.000	1.012	1.005	0.752	0.728	1.027	0.728	0.963	Eastern
TianJin	0.696	0.707	0.695	0.758	0.750	0.787	1.004	1.003	1.014	1.010	1.022	1.022	0.695	0.859	Eastern
HeBei	0.744	0.763	0.779	0.846	0.831	0.899	1.000	0.889	0.849	0.835	0.838	1.000	0.744	0.843	Eastern
GuangDong	1.019	1.030	1.034	1.024	1.027	1.027	1.037	1.037	1.036	1.032	1.031	1.037	1.019	1.030	Eastern
HaiNan	1.074	1.114	1.107	1.092	1.066	1.081	1.080	1.099	1.097	1.093	1.090	1.114	1.066	1.090	Eastern
ShangHai	0.655	0.816	0.747	0.787	0.758	0.820	0.872	1.004	0.904	0.830	0.765	1.004	0.655	0.814	Eastern
JiangSu	0.687	0.708	0.708	0.743	0.730	0.780	0.789	0.778	0.773	0.804	0.845	0.845	0.687	0.758	Eastern
ZheJiang	0.748	0.768	0.781	0.803	0.790	0.804	0.812	0.807	0.804	0.804	0.797	0.812	0.748	0.793	Eastern
FuJian	0.822	1.012	1.006	0.943	0.807	0.833	0.903	0.876	0.893	0.893	0.978	1.012	0.807	0.906	Eastern
ShanDong	0.706	0.717	0.705	0.710	0.734	0.724	0.738	0.727	0.715	0.725	0.723	0.738	0.705	0.720	Eastern
ShanXi	0.735	0.846	0.780	0.789	0.801	0.788	0.887	0.868	0.879	0.892	0.819	0.892	0.735	0.826	Middle
AnHui	1.002	1.008	1.008	0.975	1.008	1.004	1.002	1.002	1.003	1.008	1.013	1.013	0.975	1.003	Middle
JiangXi	1.073	1.032	1.044	1.028	1.024	1.025	1.020	1.023	1.011	1.008	1.004	1.073	1.004	1.027	Middle
HeNan	0.808	0.853	0.846	0.845	0.876	0.832	0.862	0.878	1.003	1.007	0.807	1.007	0.807	0.874	Middle
HuBei	0.761	0.824	0.830	0.805	0.804	0.758	0.798	0.760	0.753	0.763	0.783	0.830	0.753	0.785	Middle
HuNan	0.730	0.751	0.747	0.758	0.761	0.755	0.768	0.752	0.757	0.765	0.743	0.768	0.730	0.753	Middle
GuangXi	0.866	1.001	0.891	0.798	0.804	0.784	0.810	0.809	0.806	0.820	0.810	1.001	0.784	0.836	Western
ChongQing	1.005	0.822	0.838	0.825	0.872	0.812	0.830	0.790	0.780	0.760	0.751	1.005	0.751	0.826	Western
SiChuan	0.745	0.740	0.741	0.741	0.815	0.740	0.776	0.754	0.761	0.766	0.763	0.815	0.740	0.758	Western
GuiZhou	1.028	1.029	1.025	1.007	1.010	0.865	0.875	0.838	0.788	0.771	0.761	1.029	0.761	0.909	Western
YunNan	0.758	0.758	0.748	1.002	0.770	0.777	0.784	0.768	0.773	0.785	0.764	1.002	0.748	0.790	Western
XiZang	1.132	1.120	1.143	1.161	1.185	1.189	1.193	1.193	1.190	1.170	1.160	1.193	1.120	1.167	Western
ShaanXi	0.752	0.767	0.786	0.791	0.779	0.765	0.773	0.762	0.757	0.748	0.761	0.791	0.748	0.767	Western
GanSu	0.775	0.786	0.857	0.857	0.877	0.838	0.888	0.855	0.845	0.827	0.787	0.888	0.775	0.836	Western
QingHai	0.821	1.002	0.797	1.001	0.752	0.772	0.782	0.793	0.777	0.780	0.785	1.002	0.752	0.824	Western
NingXia	1.021	1.007	1.016	1.022	1.028	1.027	1.023	1.016	1.012	0.806	0.821	1.028	0.806	0.982	Western
XinJiang	0.697	0.676	0.731	0.741	0.713	0.722	0.749	0.812	0.833	0.860	1.001	1.001	0.676	0.776	Western
NeiMengGu	0.742	0.785	0.790	0.785	0.771	0.770	0.812	0.802	0.789	0.771	0.799	0.812	0.742	0.783	Western
LiaoNing	0.782	0.693	0.715	0.735	0.742	0.752	0.780	0.753	0.755	0.744	0.762	0.782	0.693	0.747	Northeastern
JiLin	1.007	0.749	0.808	0.892	0.959	0.794	0.910	0.838	0.815	0.796	0.798	1.007	0.749	0.852	Northeastern
HeiLongJiang	0.802	1.008	0.801	0.786	0.771	0.778	0.832	0.825	0.816	0.851	0.855	1.008	0.771	0.830	Northeastern

health institutions. From 2009 to 2019, the value of health production efficiency in Shanghai also increases from 0.655 to 0.765. As an important member of the Yangtze River Delta Economic Zone, Shanghai vigorously promotes the policy of healthy development. In 2019, Shanghai Health Promotion Committee issued the "Healthy Shanghai Action (2019-2030)." However, as the health service industry in Shanghai is in the initial stage of development, there is still a huge space for the development of health production in Shanghai.

(2) In the Middle region, the average efficiency values of Anhui and Jiangxi are both >1, indicating a good trend of healthy development. The health production efficiency values of Shanxi and Henan remain near 0.8, with little regional difference. In the Middle region, the fluctuation of health production efficiency of all provinces and cities is not large, and the regional development is relatively stable. The level of economic development in middle China is relatively balanced. The efficiency value of Jiangxi province is the highest and that of Hunan province is the lowest, which is not only related to the medical level of the two provinces but also related to the difference of waste discharge between Jiangxi province and Hunan province. At the same time, the population density of Hunan province is too large, resulting in a huge burden on local medical treatment and a lower efficiency level among the middle region.

(3) The development level of the Western region is relatively low in all regions. The implementation of the "Western Development" policy has driven the economic recovery of the Western region. As the development of the Western region focuses on the primary and secondary industries, the economic recovery has also brought negative impacts on the environment and residents' health. The health production efficiencies of Guangxi, Chongqing, Guizhou, Qinghai, Ningxia are dropping. The elevation and bad natural environment of Tibet and Xinjiang are not conducive to the development of the second industry. At the same time, due to the special natural scenery and tourism service industry, health production efficiency is rising slowly.

(4) In the Northeast region, with the support of the central party committee, the old industrial base has been established since 2004. Health production efficiency values of Liaoning, Jilin, and Heilongjiang in 2019 do not reach 0.9. It stands for the low level of healthy development. The Northeast region needs to draw lessons from foreign areas of heavy industry and explore a characteristic road of healthy development. The average efficiency of Liaoning in Northeast China is the lowest and that of Jilin is the highest. This is related to the level of medical technology in Jilin province, which has more medical technicians than the other two provinces. The excessive discharge of medical waste and heavy environmental pollution in Liaoning led to the decline of efficiency value.

Time Variation of Health Production Efficiency

Regional Analysis of Health Production Efficiency

After exploring the health production efficiency values of 31 provinces from 2009 to 2019, the efficiency values will be divided into four regions, namely the Eastern region, the Middle region, the Western region, and the Northeast region, to explore the inter-regional differences in the development of healthy production.

As shown in **Figure 1**, the Eastern region has the highest efficiency value in 2019, while the Northeastern region has the lowest efficiency value. The health production efficiency in the Eastern region fluctuates from 0.816 to 0.882. There is a slight downward trend in health production efficiency in both the Western and Northeast regions, and the health production efficiency in the Western region decreases from 0.861 to 0.83. In the Northeast region, it drops from 0.864 to 0.805. The Middle region shows a slow growth trend from 2009 to 2018 but suddenly decreases in 2019. However, there is a slight increase from 0.851 to 0.861 in general. There has been a slow decline in the Western region. The efficiency value in the Northeast region fluctuates greatly. The ups and downs of the efficiency values in the four regions are different, but the dispersion degree of the health production efficiency in each region is not large, and there is little difference in the health production efficiency values in each region.

Decomposition Analysis of Health Production Efficiency

The comprehensive efficiency of healthy production is decomposed to explore the role of pure technical efficiency and scale efficiency in the process of healthy production.

As shown in **Figure 2**, the fluctuation range of the overall efficiency at the national level is relatively small, and there is a similarity in the fluctuation trend of TE and PTE, indicating that the health production efficiency of provinces and cities is greatly affected by technical factors. Before 2009, China's economy was hit by the financial crisis caused by the US subprime mortgage risk, but at the same time, the 2008 Beijing Olympic Games was successfully held, the economy began to recover. China's health production efficiency began to show positive growth. Since 2015, China's health production efficiency had shown a trend of slow decline. In 2015, the haze had increasingly appeared, which had a huge impact on the respiratory health of Chinese residents. With an increase in respiratory diseases, it resulted in a decrease in health production efficiency. Since 2016, the CPC Central Committee and the State Council had issued the outline of the "Healthy China 2030" plan, calling on the whole society to strengthen their sense of responsibility and mission. It encouraged every effort to promote the building of a healthy China. Subsequently, the decline rate of China's health production efficiency began to slow down, and the health production efficiency would definitely return to the upward trend after the reform in the future. From the decomposition results, SE and TE had the same fluctuation trend from 2009 to 2014, indicating that the allocation and utilization of medical resources before 2014 led to the fluctuation of TE, and after 2014, PTE had a major impact on the fluctuation of TE. The future reform should focus on the development of technical level and the improvement of medical resource management level.

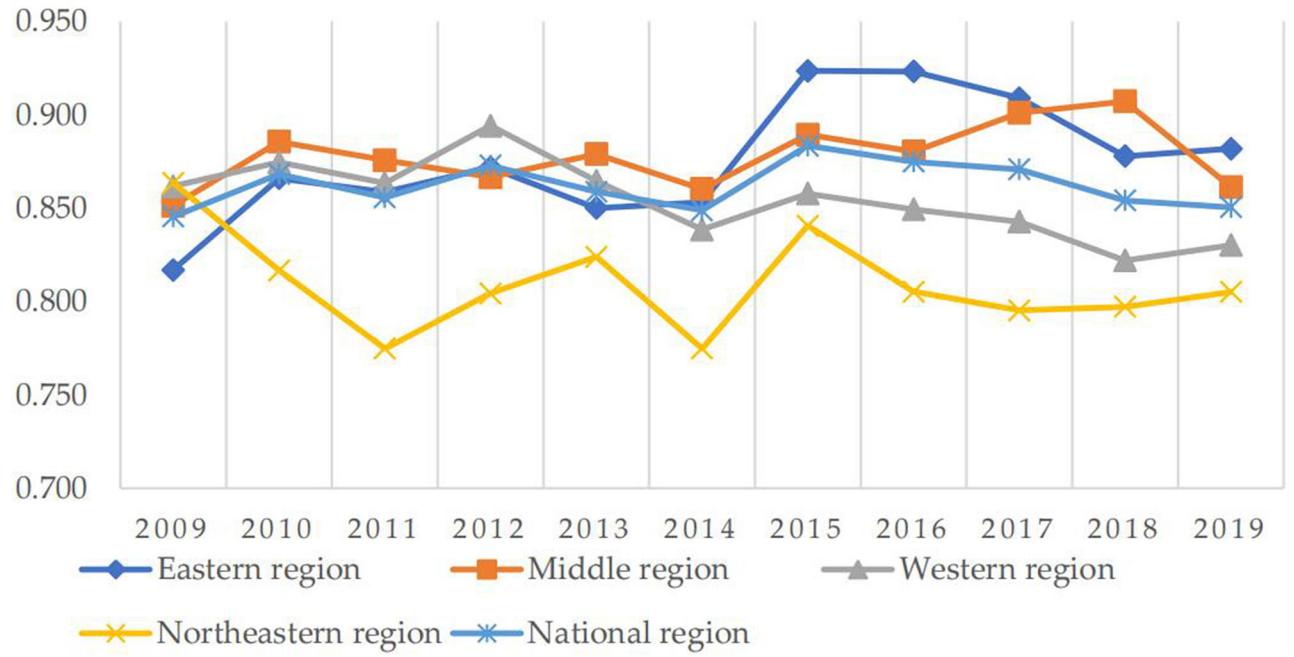

FIGURE 1 | Health production efficiencies of National and four regions from 2009 to 2019.

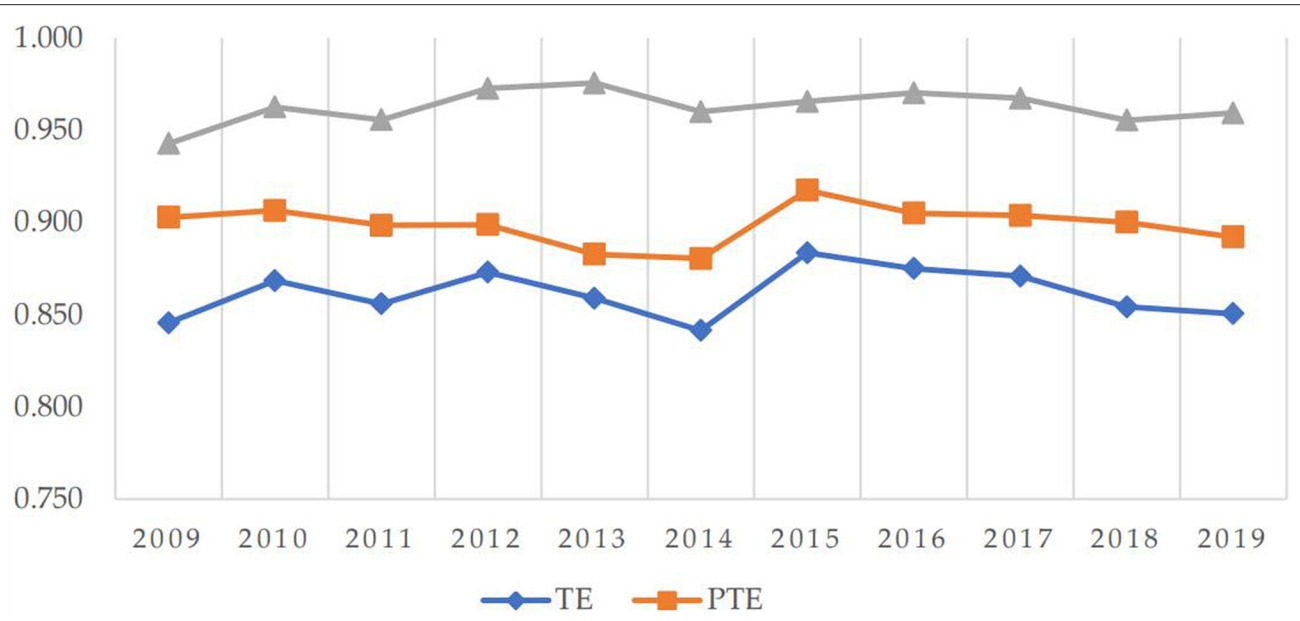

FIGURE 2 | Breakdown of health production efficiency from 2009 to 2019.

Spatial Variation of Health Production Efficiency

In order to conveniently analyze the Spatio-temporal evolution of health production efficiency values in each region, the efficiency values are divided into eight grades, which is shown in **Figure 3**. (0, 0.8] is low efficiency, (0.8, 1] is medium efficiency and higher than 1 is high efficiency. Meanwhile, in order to evenly reflect the spatial distribution of efficiency values in each time period, 4 years of 2010, 2013, 2016, and 2019 are selected to draw the map of health production efficiency of 31 Provinces and cities. It can be seen from the map above: (1) Health production efficiencies in Tianjin, Hebei, Shanxi, Shanghai, and Xinjiang are on the rise; Health production efficiencies in Beijing, Jilin, Chongqing, and Ningxia are on the decline. (2) The efficiency value in the Western

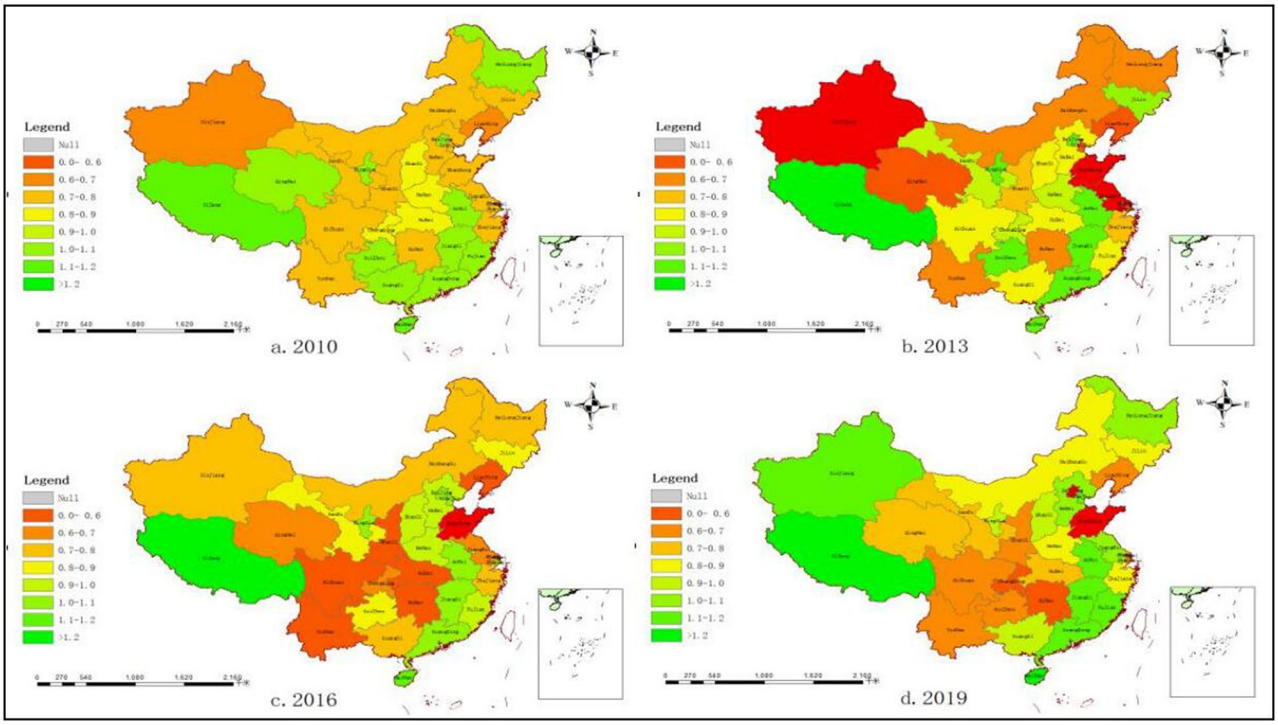

FIGURE 3 | Distribution of health production efficiencies in 31 provinces and cities in China. **(A)** Distribution of health production efficiencies in 2010. **(B)** Distribution of health production efficiencies in 2013. **(C)** Distribution of health production efficiencies in 2016. **(D)** Distribution of health production efficiencies in 2019.

region has been significantly improved. Tourism in Xinjiang and other regions has developed rapidly and residents' living standards have improved. The distribution of efficiency values in the Middle region shows LL agglomeration. The distribution chart in 2019 shows that most of the Middle region is at a low level. In order to improve the economic level, Anhui, Jiangxi, Hunan, and other regions vigorously develop modern equipment manufacturing and high-tech industries, which have an impact on the environment and lead to the decline of efficiency values. The efficiency value in the Northeast region rises first and then falls. The establishment of the industrial base in the Northeast region improves people's salary level and produces a large amount of waste pollution, which leads to the fluctuation of efficiency value. There is a slight decrease in efficiency in the Eastern region, which is related to the development trend of the Eastern region. While developing the service industry, the maturity of the primary and secondary industries has a double effect on efficiency. The map above visually reflects the spatial change process of health production efficiency in different regions. (3) The distribution of health production efficiency in China changes from low in the Western region, medium in the Middle region, high in the Eastern region, and medium in the Northeast region to high in the Western region, medium in the Middle region, high in the Eastern region, and high in the Northeast region. From the perspective of spatial distribution, there are more efficient regions in China, especially in the Western and Northeast regions. In recent years, the government's policy for the Northeast region has achieved initial results, and the healthy production difference among regions is gradually narrowing.

TABLE 4 | Global Moran index of health production efficiency from 2009 to 2019.

Year	Moran index	*Z*	*P*-value
2009	0.152	1.370	0.037
2010	0.106	1.169	0.041
2011	0.091	1.460	0.035
2012	0.108	1.630	0.029
2013	0.161	1.007	0.016
2014	0.147	1.099	0.049
2015	0.119	1.096	0.045
2016	0.145	1.591	0.025
2017	0.117	1.153	0.013
2018	0.183	1.702	0.062
2019	0.186	1.878	0.040

Spatial Pattern Texture Features

This paper uses Geoda software (Dr. Luc Anselin and his team, Chicago, IL, USA) to calculate the global Moran index of China's health production efficiency from 2009 to 2019, which is shown in **Table 4**. The Moran index values are all above 0.1 at the significant level of 10%, indicating that there is a positive spatial autocorrelation. This paper is suitable to use a spatial econometric model to empirically analyze the influencing factors.

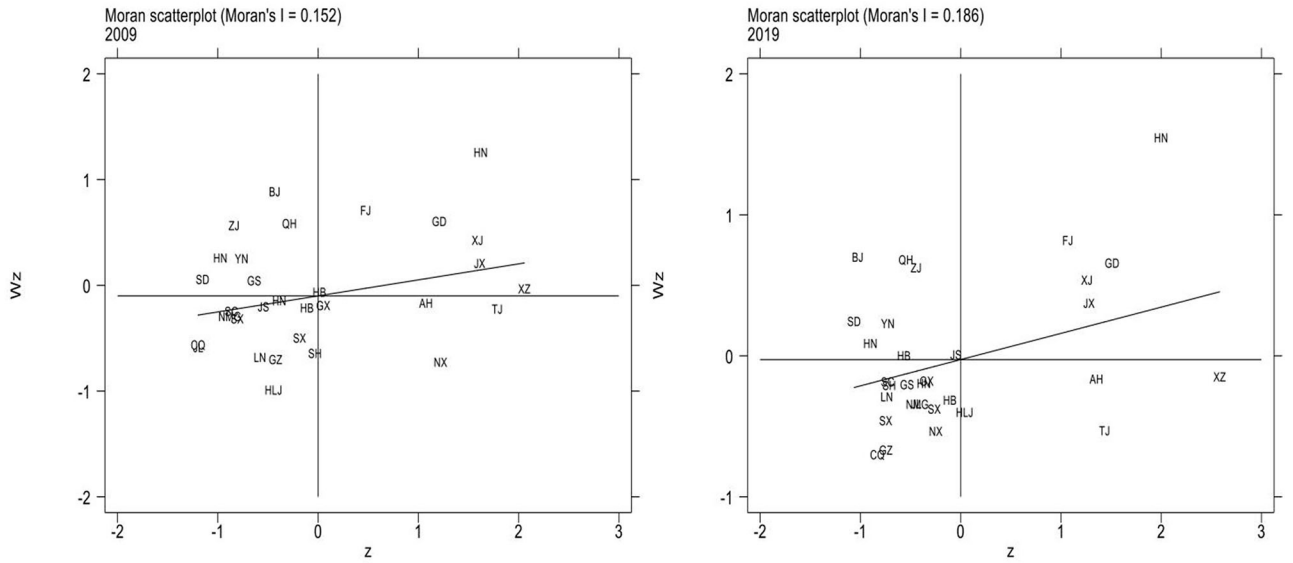

FIGURE 4 | Local Moran scatter plots in 2009 and 2019.

Figure 4 shows local Moran scatter plots of China's health production efficiency in 2009 and 2019. The first quadrant (HH) is the high-level region surrounded by the high-level regions. The second quadrant (LH) is the low-level region surrounded by the high-level regions. The third quadrant (LL) is the low-level region surrounded by low-level regions. Quadrant 4 (HL) is the high-level region surrounded by low-level regions. For brevity, the names of the provinces in **Figure 4** are abbreviated. The abbreviations of provinces should be in accordance with the provisions of the Announcement on the Adjustment of China Internet Domain Name System issued by the Ministry of Information Industry.

In the 2009 Moran scatter chart, Hunan, Guangdong, and Xinjiang are high cluster regions, while Shanxi, Liaoning, and Heilongjiang are low cluster regions. According to the 2019 Moran scatter chart, most regions are clustered in the first and third quadrants. Hainan, Fujian, and Jiangxi are high cluster regions in 2019, while Chongqing, Ningxia, and Shanxi are low cluster regions. It can be seen that the quadrants of most regions have not changed. Ningxia has changed from HL to LL, and Tibet from HH to HL. In general, LL agglomeration is the main agglomeration type in local space. Therefore, the spatial distribution of health production efficiency in China is correlated. There is a significant spatial dependence among different regions and the effect between regions is worth further study.

INFLUENCING FACTORS OF SPATIO-TEMPORAL VARIATION OF HEALTH PRODUCTION EFFICIENCY IN CHINA

Applicability Analysis of the Model

Before conducting a spatial empirical study on data, a unit root test should be carried out on data to measure the stability of data and ensure that no false regression will occur. Since T < N in this paper belongs to the short panel, the HT test method is used (26). In this paper, the stationarity test of six influencing factor variables is carried out by using Stata software (StataCorp, College Station, TX, USA), and the results are shown in **Table 5**. It can be seen that the test results of the six influencing factor variables reject the original hypothesis and they are significant at the level of 1%, which means that the six influencing factor variables have passed the stationarity test.

TABLE 5 | Panel unit root inspection results.

Variables	Statistic	*Z*	*P*-value
Pgdp	0.8762	−4.6248	0.0000
Urb	0.4892	−19.0797	0.0000
Med	−0.0078	−37.6424	0.0000
Mnmt	0.6321	−13.7406	0.0000
Gov	0.4001	−22.4070	0.0000
Pd	0.5160	−18.0766	0.0000

TABLE 6 | Test values of LM test statistics.

Test statistics	LM-error	LM-lag	Robust LM-error	Robust LM-lag
p-value	123.585***	119.061***	8.216**	3.693*
	0.000	0.000	0.004	0.055

**Means significant at the 10% level.*
***Means significant at the 5% level.*
****Means significant at the 1% level.*

According to the Moran index analysis results above, the regions have spatial correlations. Then the spatial panel model is selected, which needs to carry out an LM test on the data. Stata/mp16.0 space measurement software (StataCorp, College Station, TX, USA) was used to complete the following space

TABLE 7 | LR test and Wald test results.

Model	SEM_a	SAR_a
LR	83.41***	91.47***
	0.000	0.000
Wald	49.97***	38.85***
	0.000	0.000

****Represents significant at 1% level.*

measurement operations. According to **Table 6**, LM error and LM lag are significant at the level of 1%. Therefore, the OLS regression is rejected and the spatial econometric model is selected, the value of the spatial error model is greater than that of the spatial lag model. Therefore, the spatial error model is more in line with the empirical analysis of health production efficiency in this paper.

Then it is necessary to choose to use a random effect model or fixed-effect model. It is determined according to the results of the Hausman test. The results of the Hausman test are 45.9 and significant at the level of 1%. Therefore, the original hypothesis is rejected and the fixed effect model is selected.

According to the above regression results, we can know that the data in this paper have both spatial error effect and spatial lag effect. Therefore, the spatial Durbin model (SDM) is preliminarily selected for empirical analysis. At the same time, it is necessary to test the robustness of the model by running the LR test and Wald test to observe whether the SDM model will degenerate into SEM and SAR. The results are shown in **Table 7**. The LR test results are significant at the level of 1%, and SDM will not degenerate into SEM and SAM. The Wald test results also show that the SDM model is the most consistent with the empirical model of health production efficiency.

Then the SDM model is selected for regression, and the time fixed-effect model, individual fixed-effect model, and double fixed effect model are used for regression, respectively. Finally, the R coefficient values of the three regression models are compared. The test results show that the R coefficients of the time fixed-effect model, individual fixed-effect model, and double fixed effect model are 0.2230, 0.1105, and 0.1188, respectively, so the time fixed effect model is selected for regression.

Regression Analysis of Time Fixed Effect SDM

After the regression model is selected, the data are empirically analyzed by using Stata16.1 software (StataCorp, College Station, TX, USA). The regression results of the SDM are shown in **Table 8**, and the regression coefficients and significance levels of six influencing factors are obtained.

The test result of per capita GDP is significant at the level of 1%, and the coefficient value is 0.021, indicating that per capita GDP has a positive effect on regional health production efficiency. Per capita GDP can measure the level of economic construction in a region. Similar to the conclusion of other scholars, the higher the Per capita GDP, the higher the health production efficiency of the region is. Per capita GDP not only reflects the living standard and consumption capacity of residents but also reflects the economic operation of a region from the macro level. Under a good socio-economic management system, environmental pollution is contained, medical facilities are improved, and people's health is improved, which leads to an increase in health production efficiency value.

TABLE 8 | Regression results of SDM.

Variables	Main	Wx	Spatial	Variance
Pgdp	0.021***	0.046***		
	(0.00)	(0.00)		
Urb	−0.694***	−0.605**		
	(0.00)	(0.05)		
Med	−0.028***	−0.037**		
	(0.00)	(0.01)		
Mnm	−0.001**	−0.006*		
	(0.05)	(0.08)		
Gov	3.339***	7.787***		
	(0.00)	(0.00)		
Pd	0.890***	−0.718*		
	(0.00)	(0.06)		
rho			0.074	
			(0.32)	
sigma^2_*e*				0.003***
				(0.00)
R-squared	0.111	0.111	0.111	0.111

**Represents significant at 10% level.*
***Represents significant at 5% level.*
****Represents significant at 1% level.*

The regression coefficient of urbanization level is −0.694, which is significant at a 1% level. The result shows that the higher the urbanization level is, the lower the health production efficiency is, which is contrary to the expected result. The urbanization level reflects the progress of urbanization in a region and stands for the advanced degree of local social organization and management level. It is an important indicator of the process of urban development. The improvement of urbanization level can provide residents with better urbanization services, a perfect medical system, and a mature social supervision system. It is helpful to improve people's lives and health production efficiency. Yet, on the other hand, considering its own special national condition, the improvement of urbanization level also means that the dramatic increase in urban population will make enormous pressure on the health service and community building. The government should deal with the increasing pressure on the development of population and find the right speed of urbanization development to let people really enjoy the benefits of urbanization.

The service level of medical institutions is expressed by the average length of stay, and the result shows that the coefficient of service level of medical institutions is −0.028, which is significant at the level of 1%, meaning that the lower the average length of stay, the higher the health production efficiency level is. It is the same as the expected result. The average length of stay in

a hospital not only represents the technical level of the medical and health institutions but also highlights the comprehensive management ability of the medical institutions in the region. The shorter the length of stay, the less the consumption of medical resources is. Reducing the average length of stay in a hospital can not only minimize the cost of medical resources but also save the cost of medical treatment for patients. Medical institutions should be strongly supported to improve service levels in order to increase health production efficiency.

The test result shows that the regression coefficient of the degree of medical non-marketization is −0.001 at the significant level of 5%. The degree of medical non-marketization would have a negative impact on the health production efficiency, which is the same as the expected result. The higher the degree of medical non-marketization, the fewer private hospitals in the medical market are. Too many public hospitals and insufficient market competition are not conducive to the reform and innovation of the medical market, thus reducing the regional health production efficiency. According to the analysis results, the medical marketization degree should be properly improved and the competitiveness of regional medical service institutions should be enhanced.

The regression coefficient of the government support system is 3.339, which is significant at the level of 1%. It is the same as the predicted result. The proportion of government financial health expenditure in GDP can reflect the resources used for health and medical service construction in a certain period of time. The higher the proportion of government financial health expenditure in GDP is, the higher the local government attaches importance to medical and health construction, and the health production efficiency of local residents will increase accordingly.

Population density has dual influences on economic development in each region. If it is too high, it can cause residents living costs to increase, such problems as shortage of resource allocation and commuter crowd. While if population density is too low, it will cause a shortage of labor supply, a declining birth rate, and lower production efficiency. According to the test results of this paper, the regression coefficient of population density is 0.89 at the significant level of 1%, indicating that the population density of China's 31 provinces is in a state of equilibrium, and the uniform distribution of population plays a role in promoting health production efficiency, so it is necessary to balance the population growth rate and economic development rate in the future development.

Spatial Spillover Effects of Influencing Factors of Health Production Efficiency

In order to further study the spatial spillover effects of the six influencing factors, effect decomposition of the SDM is carried out, and it is found that the direction of the coefficient of total utility is the same as the direction of the spatial Durbin empirical results, as shown in **Table 9**.

Population density (*Pd*) does not pass the significance test of direct effect, *Urb, Mnm*, and *Pd* do not pass the significance test of indirect effect. However, *Pgdp, Med*, and *Gov* all pass the significance test of 1%, indicating that the three indicators all have spatial spillover effects. The direct effect of *Pgdp* is negative, and the indirect effect is positive, indicating that the higher the level of *Pgdp* in a certain region has a promotion effect on the health production efficiency of the surrounding regions. The indirect effect of *Med* is negative, that is the higher service level of the medical institutions will cause the loss of health production efficiency in surrounding regions. The higher regional medical service organization level will attract surrounding residents to see a doctor, resulting in medical institutions in surrounding regions is difficult to improve the service level. As a result, it has an inhibiting effect on the health production efficiency of surrounding regions. The indirect effect of *Gov* is negative, indicating that the higher the local government support system is, the lower the health production efficiency of surrounding regions. The direct effect of *Gov* is 6.9213, indicating that government support has a great promoting effect on local health production efficiency, and there is a demonstration effect on surrounding regions.

TABLE 9 | Effect decomposition results of SDM.

Variable	Direct effect	Indirect effect	Total effect
Pgdp	−0.0148***	0.0255***	0.0107***
Urb	−0.7887***	0.1863	−0.6024***
Med	−0.0289***	−0.0715***	−0.1004***
Mnm	−0.0010*	−0.0016	−0.0026***
Gov	6.9213***	−3.2741***	3.6472***
Pd	0.0020	0.0057	0.0077***

*Represents significant at 10% level.
***Represents significant at 1% level.

CONCLUSIONS AND RECOMMENDATIONS

Based on the EBM model, Moran index, and SDM, this paper measures and studies the Spatio-temporal variation of health production efficiency in China. The results show that:(1) In general, the average efficiency of 31 provinces and cities is above 0.7, and the average efficiency of some regions is above 1, such as Guangdong, Hainan, Anhui, and Jiangxi. From the results of the Eastern region, there is no clear causal relationship between the value of health production efficiency and the amount of health investment. (2) The spatial correlation of health production efficiency is analyzed. The results show that there are "high" and "low" clustering phenomena of health production efficiency in most regions, and there is a spatial correlation between regions. (3) The data of influencing factors of health production efficiency in 31 provinces of China pass the panel unit root test, indicating the smoothness of the data. From the perspective of spatial empirical results, *Pgdp*, *Gov*, and *Pd* have a positive effect on health production efficiency. The direct effect and indirect effect of *Pgdp*, *Med*, and *Gov* all pass the significance test of 1% and the three indicators have spatial spillover effects. At the same time, *Pgdp* can promote the health production efficiency of surrounding regions.

Based on the above research results, this paper puts forward the following countermeasures and suggestions to improve the health production efficiency of provinces and cities in China:

First, the government should strengthen the urbanization of provinces and cities to provide better modern services for residents. Economic and social development is bound to bring urbanization, and in the process of promoting urbanization, it is bound to bring the problem of over-density of the urban population. In order to explore the development path suitable for China's urbanization layout and form, all provinces and cities should actively respond to the implementation of new urbanization policy, and promote the coordinated development of large, small, and medium-sized cities.

Second, the government should promote medical marketization and increase healthy competition in the medical market. From the point of the current status of the medical market, public hospitals occupy most of the medical resources in the market. Public hospitals also have far more credibility in the health care market than private hospitals. It not only can lead to narrow roads in the development of private hospitals but also lead to too much pressure on the public hospital market. The problem of seeing a doctor is difficult to solve. A partial marketization can increase the competitiveness of the medical market, promote reform and innovation in public hospitals and improve the development environment for private hospitals.

Third, the government's financial investment structure in health should be optimized. The decomposition result of the health expenditure effect of government finance shows that government support can promote regional health production efficiency. There is no doubt that public health expenditure has a positive impact on people's health, but more consideration should be given to the coverage of rural areas, and the medical condition gap between rural and urban should be narrowed to achieve comprehensive health coverage for people.

Fourth, in order to improve China's health production efficiency, reduce regional differences, improve China's overall health production efficiency level, the government should also increase government financial investment in health, expand the scale of the health industry, improve the green level of various industries, reduce environmental pollution and improve the health of residents in each region. Each region should make reasonable use of the spillover effect of surrounding regions, vigorously develop economic activities, carry out cooperation with surrounding regions and use the demonstration effect to accelerate the development of overall health production efficiency.

DATA AVAILABILITY STATEMENT

Publicly available datasets were analyzed in this study. This data can be found here: China Statistical Yearbook, China Health Statistical Yearbook, China Urban Statistical Yearbook and relevant statistical yearbook data of all provinces and cities. For some missing data, interpolation and weighted average are used to complete the data.

AUTHOR CONTRIBUTIONS

FL: conceptualization, methodology, and software. GL: data curation, visualization, and investigation. YZ: software, validation, and writing-original draft preparation. YM and TW: reviewing and editing. All authors contributed to the article and approved the submitted version.

FUNDING

This paper was funded by the National Natural Science Foundation of China (No. 71503106 and No. 71803197), Jiangsu Social Science Fund (19EYB016), Jiangsu College Philosophy Social Science Outstanding Innovation Team Construction Project, Ministry of Education Humanities and Social Sciences Foundation (No. 18YJC630094), Fundamental Research Funds for the Central Universities (No. 31511910801).

REFERENCES

1. Yu JL, Yang SG, Liu JS. Dynamic evolution of healthy production efficiency of Chinese residents and its influencing factors. *Chin J Popul Sci.* (2020) 05:66–78+127.
2. Shi Z, Wu F, Huang H, Sun X, Zhang L. Comparing economics, environmental pollution and health efficiency in China. *Int J Environ Res Public Health*. (2019) 16:4827. doi: 10.3390/ijerph16234827
3. Shen SG, Zheng QY. Healthy production efficiency and its influencing factors in China. *J Sun Yat Sen Univ*. (2017) 57:153–66. doi: 10.13471/j.cnki.jsysusse.2017.06.016
4. Shi Z, She Z, Chiu YH, Qin S, Zhang L. Assessment and improvement analysis of economic production, water pollution, and sewage treatment efficiency in China. *Socio Econ Plann Sci*. (2020) 74:100956. doi: 10.1016/j.seps.2020.100956
5. Li Y, Chen Y. Development of an SBM-ML model for the measurement of green total factor productivity: the case of pearl river delta urban agglomeration. *Renew Sust Energy Rev*. (2021) 145:111131. doi: 10.1016/j.rser.2021.111131
6. Li XQ, Li D, Huang L. Regional healthy production efficiency and its changes in China: a comparative analysis based on DEA, SFA and Malmquist indices. *J Appl Stat Manag*. (2014) 33:878–91. doi: 10.13860/j.cnki.sltj-20130510-001
7. Zhang N, Hu AG, Zheng JH. Application of DEA method to evaluate healthy production efficiency in different regions of China. *Econ Res J*. (2006) 7:92–105.
8. Ma Y, Yang L, Duan ZQ, Sun Q, Xiong KJ, Zhong ZG, et al. Study on health efficiency of provincial total health expenditure based on chain model. *Chin Health Econ*. (2019) 38:55–9.
9. Bates LJ, Mukherjee K, Santerre RE. Medical insurance coverage and health production efficiency. *J Risk Insurance*. (2010) 77:211–29. doi: 10.1111/j.1539-6975.2009.01336.x
10. Yang WL, Tan JB, Liu DH, Tang F. The coupling relationship between urban innovation efficiency and high-quality economic development and its spatio-temporal differentiation characteristics. *J Stat Inform*. (2021) 36:104–19.
11. Liu ZH, Xu JW, Zhang CH. Spatio-temporal differentiation and driving mechanism of coordinated development of carbon abatement, economic growth and environmental protection at provincial level. *Human Soc Sci J Hainan Univ*. (2021) 9:1–10. doi: 10.15886/j.cnki.hnus.20210416.001

12. Guo FY, Tong LJ, Qiu FD, Li YM. Spatial and temporal differentiation characteristics and identification of influencing factors of green development in eco-economic corridor of Yellow River Basin. *Acta Geogr Sin*. (2021) 76:726–39. doi: 10.11821/dlxb202103016
13. He G, Ma Z, Wang X, Xiao Z, Dong J. Does the improvement of regional eco-efficiency improve the residents' health conditions: empirical analysis from China's provincial data. *Ecol Indicat*. (2021) 124:107387. doi: 10.1016/j.ecolind.2021.107387
14. Li XQ, Li D, Huang L. Healthy production efficiency differences and influencing factors in China. *J Stat Inform*. (2013) 28:52–8. doi: 10.3969/j.issn.1007-3116.2013.08.009
15. Ding JM, Zhang XZ, Zhang JQ, Lu Z, Yang L, Yu M. Analysis of health system efficiency and its influencing factors in 31 provinces and cities in China in 2014. *ChinHealth Serv Manag*. (2017) 34:432–5+471.
16. Gao Q, Wang D. Hospital efficiency and equity in health care delivery: a study based in China. *Socio Econ Plann Sci*. (2020) 76:100964. doi: 10.1016/j.seps.2020.100964
17. Wu, H, Gai, Z, Guo, Y, Li, Y, Hao, Y, Lu, ZN. Does environmental pollution inhibit urbanization in China? A new perspective through residents' medical and health costs. *Environ Res*. (2020) 182:109128. doi: 10.1016/j.envres.2020.109128
18. Zhao J, Zhou N. Impact of human health on economic growth under the constraint of environment pollution. *Technol Forecast Soc Change*. (2021) 169:120828. doi: 10.1016/j.techfore.2021.120828
19. Cochrane AL, St Leger AS, Moore F. Health service "Input" and Mortality "Output" in developed countries. *J Epidemiol Commun Health*. (1978) 32:200–5. doi: 10.1136/jech.32.3.200
20. Fu M, Liu C, Yang M. Effects of public health policies on the health status and medical service utilization of Chinese internal migrants. *China Econ Rev*. (2020) 62:101464. doi: 10.1016/j.chieco.2020.101464
21. Long LJ. Performance evaluation and international comparison of China's ecological civilization construction from the perspective of comprehensive welfare. *J Nat Resour*. (2019) 34: 1259–72. doi: 10.31497/zrzyxb.20190611
22. Andersen P, Petersen NC. A procedure for ranking efficient units in data envelopment analysis. *Manag Sci*. (1993) 39:1261–4. doi: 10.1287/mnsc.39.10.1261
23. Han JP, Cheng C, Yan J, Yang XL. Measurement of urban industrial ecological green development based on network super-efficiency EBM model: a case study of 47 key cities in 10 groups of three districts. *Sci Technol Manag Res*. (2019) 39:228–36.
24. Lv YF, Chen L. Discussion on unit root test method and stability of panel. *Math Pract Theory*. (2010) 40:49–61.
25. Wang XH, Feng YC, Hu SL. FDI, OFDI and Green total factor productivity in China: An analysis based on spatial econometric model. *Chinese J Manag Sci*. (2021) 29:1–12. doi: 10.16381/j.cnki.issn1003-207x.2018.0346
26. Wang CY, Jiang SM, Xiong WJ, Dai TL. Research on regional innovation output of Zhejiang Province based on spatial econometric analysis. *J Central China Norm Univ*. (2021) 55:1–18. doi: 10.19603/j.cnki.1000-1190.2021.05.014
27. Han J, Wang Y, Chen CF. Regional differences and influencing factors of Industrial carbon emission performance in China: a spatial econometric analysis based on provincial data. *Compar Econ Soc Syst*. (2015) 1:113–24.
28. Ochalek J, Wang H, Gu Y, Lomas J, Cutler H, Jin C. Informing a cost-effectiveness threshold for health technology assessment in China: a marginal productivity approach. *Pharmacoeconomics*. (2020) 38: 1319–31. doi: 10.1007/s40273-020-00954-y
29. Liu WL, Xia Y, Hou JL. Health expenditure efficiency in rural China using the super-SBM model and the Malmquist productivity index. *Int J Equity Health*. (2019) 18:1–13. doi: 10.1186/s12939-019-1003-5
30. Cheng Z, Tao H, Cai M, Lin H, Lin X, Shu Q, et al. Technical efficiency and productivity of Chinese county hospitals: an exploratory study in Henan province, China. *BMJ Open*. (2015) 5:e007267. doi: 10.1136/bmjopen-2014-007267
31. Maniaci A, Ferlito S, Bubbico L, Ledda C, Rapisarda V, Iannella G, et al. Comfort rules for face masks among healthcare workers during COVID-19 spread. *Annal Ig* . (2021) 33:615–27. doi: 10.7416/ai.2021.2439
32. Bharatendu C, Ong JJY, Goh Y, Yan BYQ, Chan ACY, Tang JZY, et al. Powered Air Purifying Respirator (PAPR) restores the N95 face mask induced cerebral hemodynamic alterations among Healthcare Workers during COVID-19 Outbreak. *J Neurol Sci*. (2020) 417:117078. doi: 10.1016/j.jns.2020.117078

Conflict of Interest: The authors declare that the research was conducted in the absence of any commercial or financial relationships that could be construed as a potential conflict of interest.

frontiers in Public Health

ORIGINAL RESEARCH
published: 16 February 2022
doi: 10.3389/fpubh.2022.839204

Estimation of Relative Risk of Mortality and Economic Burden Attributable to High Temperature in Wuhan, China

Si Chen[1], *Junrui Zhao*[1], *Soo-Beom Lee*[2] *and Seong Wook Kim*[3]*

[1] School of Resources and Environmental Science, Hubei University, Wuhan, China, [2] Department of Transportation Engineering, University of Seoul, Seoul, South Korea, [3] Department of Applied Mathematics, Hanyang University, Ansan, South Korea

In the context of climate change, most of the global regions are facing the threat of high temperature. Influenced by tropical cyclones in the western North Pacific Ocean, high temperatures are more likely to occur in central China, and the economic losses caused by heat are in urgent need of quantification to form the basis for health decisions. In order to study the economic burden of high temperature on the health of Wuhan residents between 2013 and 2019, we employed meta-analysis and the value of statistical life (VSL) approach to calculate the relative risk of high temperature health endpoints, the number of premature deaths, and the corresponding economic losses in Wuhan City, China. The results suggested that the pooled estimates of relative risk of death from high temperature health endpoints was 1.26 [95% confidence interval (CI): 1.15, 1.39]. The average number of premature deaths caused by high temperature was estimated to be 77,369 (95% CI: 48,906–105,198) during 2013–2019, and the induced economic losses were 156.1 billion RMB (95% CI: 92.28–211.40 billion RMB), accounting for 1.81% (95% CI: 1.14–2.45%) of Wuhan's annual GDP in the seven-year period. It can be seen that high temperature drives an increase in the premature deaths, and the influence of high temperature on human health results in an economic burden on the health system and population in Wuhan City. It is necessary for the decision-makers to take measures to reduce the risk of premature death and the proportion of economic loss of residents under the impacts of climate change.

Keywords: high temperature, mortality relative risk, economic burden, meta-analysis, value of statistical life (VSL)

OPEN ACCESS

Edited by:
Hongtao Yi,
The Ohio State University,
United States

Reviewed by:
Weijing Ma,
Lanzhou University, China
Gui Jin,
China University of Geosciences Wuhan, China

***Correspondence:**
Seong Wook Kim
seong@hanyang.ac.kr

Specialty section:
This article was submitted to Environmental health and Exposome, a section of the journal Frontiers in Public Health

Received: *19 December 2021*
Accepted: *24 January 2022*
Published: *16 February 2022*

Citation:
Chen S, Zhao J, Lee S-B and Kim SW (2022) Estimation of Relative Risk of Mortality and Economic Burden Attributable to High Temperature in Wuhan, China. Front. Public Health 10:839204. doi: 10.3389/fpubh.2022.839204

INTRODUCTION

Climate change poses a threat to human health, which through direct effects including increased frequency of high temperatures, floods, droughts and severe storms, and indirectly through impacts on ecosystems (1). The first part of Sixth Assessment Report of the Intergovernmental Panel on Climate Change (IPCC) finished by Working Group I has reported that the current global average surface temperature is about 1°C above pre-industrial levels, and the global surface temperature will continue to rise until at least the middle of this century. If greenhouse gas emissions are not reduced in the future, global temperature will be likely to exceed 1.5 and 2°C by the end of twenty-first century (2). As the global temperature rises, the intensity and frequency of extreme heat events are rapidly increasing.

Most regions are already suffering from extreme heat, which has had significant impacts on human health. Some epidemiological studies have illustrated that exposure to high temperatures results in cardiovascular disease, respiratory disease and cerebrovascular disease (3). Extreme heat not only leads to a range of diseases but also results in mortality. In California during 2006 and Wisconsin from July 16 to July 18 in 2012, there were 655 premature deaths and 27 deaths, respectively (4, 5) due to heat. A report published by The Oregonlive on July 1, 2021, announced that at least 63 people had died in Oregon from the heat, and Multnomah County, where the largest number of deaths occurred, had received 491 emergency medical calls in 1 day (6). Moreover, the death toll in Oregon had risen to 107 in the next week (7). Global News also reported on July 29, 2021 that 570 people died from heat-related deaths in British Columbia (8). From 2000 to 2019, Asia, Africa, and the global excess deaths due to high temperatures were 224,022, 25,549 and 489,075, respectively (9). Exposure to high temperature in addition to the health risks, which can lead to premature death, also places a burden on the economy. Several economically developed countries have quantified the economic costs of health hazards from high temperatures, and according to data regarding Michigan from 1971 to 2000 and California in 2006, the economic losses due to heat-related deaths were about $4.2 million and $5.1 billion, respectively (4, 10). Moreover, a study on heat-related deaths in Zaragoza, Spain showed that the hospitalization costs for these deaths amounted to €426,087 in 2002–2006 (11). From 2013 to 2014, Australia experienced a further economic burden of $6.2 billion per year due to reduced labor productivity as a result of heat stress (12).

Heat-related deaths have also increased along with global temperatures. Among the five continents in addition to Antarctica, Asia, specifically Southern and Eastern Asia ranked first and third in the number of excess deaths due to high temperature, respectively (9). Because of their higher vulnerability and limited capacity to adapt to high temperatures, developing countries are more likely to be exposed to heat-related health threats than developed countries (13) and therefore are desperately in need of a quantitative health outcomes analysis. In contrast, China, one of the developing countries, is very limited on articles regarding quantitative analysis of high-temperature health outcomes. The frequent activities of tropical cyclones formed over the western North Pacific Ocean affect the climate in East and Southeast Asia, while indirectly leading to an increase in the number of high-temperature days in the middle and lower reaches of the Yangtze River region in the east-central region (14). In the 60 years from 1955 to 2014, central China was the most severely threatened by heatwaves (a type of hot weather) and had the highest frequency and number of annual heatwaves (15). Information on the economic burden of heat is also in urgent need in the central region, which is most affected by high temperature. Therefore, it is most fitting to consider Wuhan, the largest city in central China, in a case study to assess the economic losses of premature death caused by high temperature in 2013–2019.

The purpose of this paper is to: (1) calculate the overall estimate value by pooling the relative risk (RR) effect values of heat-related disease deaths from previous studies in Wuhan; (2) assess the burden of heat-related disease deaths on the GDP of Wuhan using the value of statistical life (VSL) method; (3) propose management countermeasures to assist policymakers in establishing a heat warning system that reduces heat exposure mortality among the population, especially vulnerable populations, and improving the quality and level of public health management.

METHODS

Study Area

Wuhan City is the capital of Hubei Province (29°58′N to 31°22′N,113°41′E to 115°05′E) and a total area of 8,494 km^2. Located in the subtropical high-pressure belt, Wuhan has the famous title of a "furnace" city. From 1951 to 2018, there were 386 days when the daily maximum temperature in Wuhan exceeded 35°C, and the days with a maximum temperature of 38°C accounted for about 2.8% of the warm season (May to September). As the largest city in central China, Wuhan ranked fourth and third among 15 sub-provincial cities in China in terms of total GDP in 2013 and 2015, respectively. Its GDP topped central China in 2014, and it was selected as a new first-tier city in 2019. The study of heat-related diseases and deaths, as well as their economic burden in Wuhan, can alert policymakers to mitigate the health and economic losses caused by high temperatures, which is significant for the city to accelerate its development as a national economic center. The geographical location of Wuhan within China and the map of the city are shown in **Figure 1**.

Overall Study Description

High-temperature weather is a health threat and leads to premature death in the population. In this paper, with the context of health risk assessment being widely applied to provide a quantitative evaluation of the potential negative impact of hazards on human health (16), a two-stage analysis combined with meta-analysis were applied to calculate the relative risk of exposure to high temperature and the number of premature deaths successively. Further discussed are five monetization methods to estimate the economic losses caused by premature death, with the most optimal one selected and combined with health impacts to derive health economic losses. The research flowchart is shown in **Figure 2**.

Estimation of Health Impacts

In this part, a two-stage analysis was used to estimate the health effects and premature deaths from exposure to high temperatures. In the first stage, due to unavailability of epidemiological data, we extracted and pooled the estimates of relative risks (RRs) from searched and screened literature. A study of collecting heavy metal and metalloid from surface soils in central China during 2007–2017 also collected data from various literature for the same reason (17). The number of premature heat deaths from the overall RRs was calculated in the second stage.

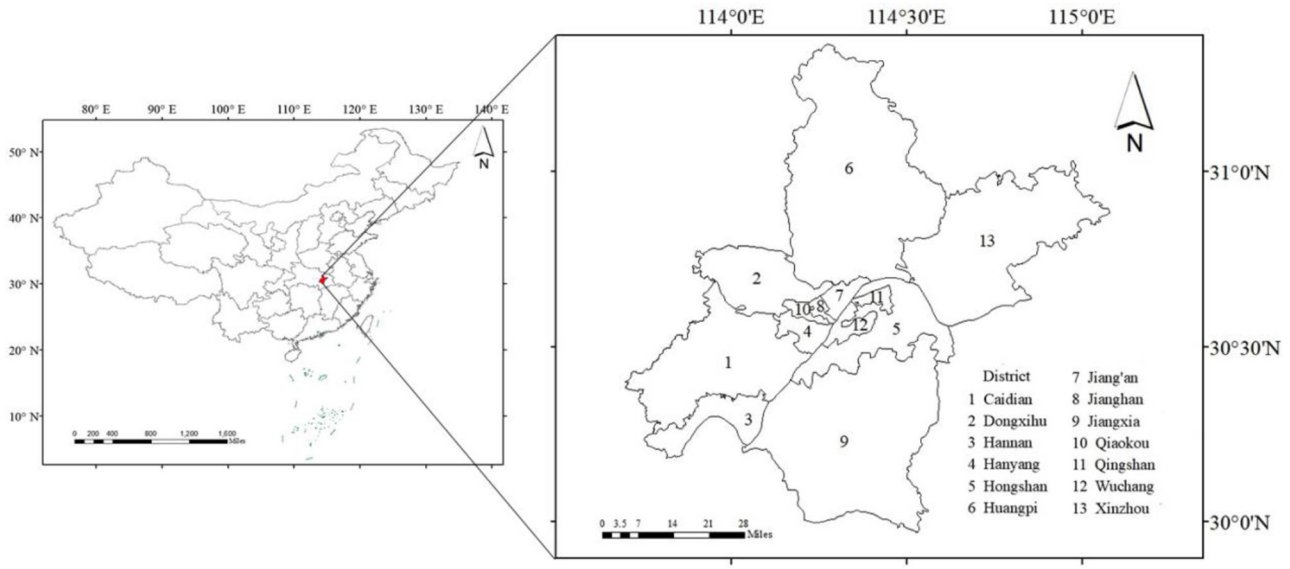

FIGURE 1 | Geographical location of Wuhan.

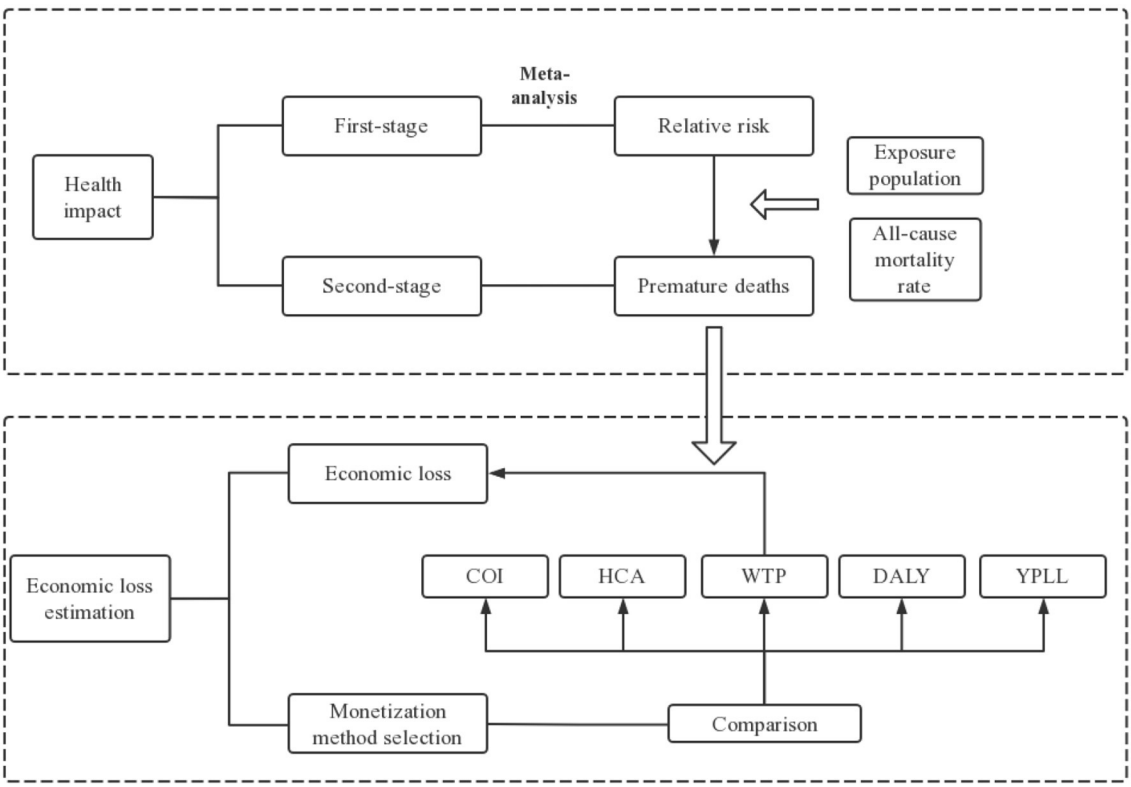

FIGURE 2 | Research route flowchart.

First-Stage Analysis

Since most current studies on heat-related deaths have focused on cardiovascular disease, cerebrovascular disease, respiratory disease, ischemic heart disease, and non-accidental death (3), we used these five major causes of heat-related death in the first stage as health endpoints.

Then the literature was searched on CNKI, PubMed, Web of science and Wanfang Data. The search key words combined "China/Chinese/Hubei/Wuhan", "High temperature/Heat/Heat wave/Hot temperature/Extreme temperature" with "death/mortality" and "relative risk/RR (relative risk)/increase risk." To ensure a more complete coverage of the literature, we also consider the references of the searched literature. The searched literature were screened according to the following inclusion and exclusion criteria.

Inclusion criteria are (1) studies on the relationship between high temperature and death in five health endpoints and (2) effect estimates and corresponding 95% confidence interval for the risk of death from the high temperature on health endpoints such as Odds Ratio (OR), Relative Risk, and percent change which can be converted into RR.

Exclusion criteria are (1) overview literature pieces, (2) No Wuhan City as a study area, and (3) duplicate literature.

The final literature was determined by viewing the titles and abstracts of the literature as well as the entire literature from start to finish. Then data from the included literature was extracted to make a characteristics summary table. The extracted data include title, author, study period, type of death, and effect estimates. Moreover, when the effect estimate is shown as percentage change, it is converted to RR using Equation (1), or, if it is shown as OR, using Equation (2):

$$RR = \frac{percent\ change}{100} + 1 \tag{1}$$

$$RR = \frac{OR}{(1 - P_0) + (P_0 \times OR)} \tag{2}$$

where RR is relative risk, *OR* is Odds Ratio, P_0 is the incidence of disease in non-exposed populations.

Finally, we calculated the heterogeneity (I^2) and pooled RRs with either a random effect model if $I^2 > 50\%$, or a fixed effect model if otherwise. When pooling RR, we chose the largest estimates of RR (18). The process of pooling RRs was performed using Stata SE version 15.

Second-Stage Analysis

With the above RR estimates, Equation (3) was used to assess the number of premature deaths due to high temperature (19).

$$\begin{aligned} P &= y_0 \times Pop \times \left(\frac{RR - 1}{RR}\right) \\ &= y_0 \times Pop \times AF \end{aligned} \tag{3}$$

where P (person) is premature deaths, y_0 (‰) is the baseline rate of all-cause death, Pop (person) is the exposed population, RR is the relative risk of health endpoints mortality due to high temperature, and AF is the attributable fraction of high temperature to death. The values of y_0 (‰) and Pop (person) were obtained from Wuhan statistical yearbook (20) (details in **Table 1**), and the RR is derived from the overall RR estimated by the first-stage analysis.

Economic Loss Estimation

Current studies on the monetization of health hazards caused by environmental issues consist of the cost of illness (COI) approach (21), the human capital approach (HCA) (22), the modified human capital approach [Years of Potential Life Lost (YPLL)] (23), disable adjusted life years (DALY) (22), and the willingness to pay approach (WTP) [i.e., value of statistical life (VSL)] (21). COI is a calculation of the costs incurred by the disease; however, it is deficient in assessing health loss from premature death. First, it targets people as research subjects and has a large amount of data, which can easily lead to incomplete data during the survey and thus affect the accuracy of the final results. Second, it considers only all costs caused by diseases without taking into account the health preferences of affected individuals (23). HCA refers to capital embodied in workers, while non-labor force populations such as the out-of-work and elderly populations are considered less valuable because they have no income at the time of death. There are ethical and moral flaws in this approach (23). The modified human capital approach considers per capita GDP as a statistical life year contribution to society, which differs from the human capital approach in that it considers the contribution of the labor force to the socio-economy from the perspective of society as a whole, but it may have a significant regional variation due to the difference of per capita GDP (24). DALY measures the difference in quality of life between a disabling health condition and a normal health condition. This method lost uniformity in the choice of weights corresponding to different levels of incapacity when the weighting method of health-related quality differences was introduced into the calculation, and it has limitations in age and gender weights (25). WTP is the amount people are willing to pay to reduce a certain level of health hazard, and VSL is the quotient of the amount paid and the risk of hazard reduction. Willingness-to-pay based on the contingent valuation method (CVM) allows flexible assessment of environmental health losses of the population (26).

Based on the characteristics of the above methods, this study adopted the willingness-to-pay (i.e., value of statistical life) method to calculate the economic loss of the health endpoints of heat-related death. Due to the lack of VSL value related to high temperature, Adélaïde et al. analyzed health-related economic impacts in 96 French metropolitan areas during heat waves from 2015 to 2019 and proposed that some values such as VSL in the context of air pollution could be relied upon health-related economic losses estimation (27). Although the VSL of air pollution is available from various research, there is little information of a ready estimate for Wuhan City found from published works up to now. In this paper, a total of three different paths to obtain VSL estimate are proposed as follows:

(1) Employing meta-analysis to obtain VSL;
(2) Based on the WTP method calculated according to the following formula:

$$VSL = \frac{WTP}{\Delta P} \tag{4}$$

TABLE 1 | Exposed population and all-cause mortality rate in Wuhan between 2013 and 2019.

Year	2013	2014	2015	2016	2017	2018	2019
Exposed population (person)	8,220,493	8,273,117	8,292,666	8,338,450	8,536,517	8,837,299	9,063,973
All-cause death rate (‰)	4.98	4.97	5.75	5.44	11.62	5.52	5.72

where WTP is the amount of money residents are willing to pay to reduce the risk of death; ΔP is a certain risk of death reduction;

(3) Converting VSL data of known cities into VSL of study cities by benefit transfer (BT) approach (28):

$$VSL_{WH,k} = VSL_{city,i} \times \left(\frac{I_{WH,k}}{I_{city,i}}\right)^{\beta} \quad (5)$$

where $VSL_{WH,k}$ (million RMB/person) is the VSL of Wuhan in year k; $VSL_{city,i}$ (million RMB/person) is the VSL of city in year i; $I_{WH,k}$ (RMB/person) and $I_{city,i}$ (RMB/person) are the per capita disposable income of Wuhan and city in year k and i respectively; and β is the income elasticity of VSL (the income elasticity of 0.8 was recommended by the Organization for Economic Co-operation and Development (29).

Once the VSL estimate could be obtained from the selected method, the economic value of environmental hazards, such as air pollution, to mortality mitigation is the product of estimates of "statistical lives saved" and "statistical value per life" (30). Thus, the economic value of high-temperature loss is the product of the "number of premature deaths" and "statistical value per life." The health economic loss can then be calculated using Equation (6) (19):

$$EC_{al} = P \times VSL \quad (6)$$

where P (person) is premature deaths; VSL (million RMB/person) is statistical value per life, and EC_{al} is high temperature all-cause premature death economic loss.

RESULTS

Literature Selection and Summary

A total of 1,841 publications were identified initially from Web of science (963), Pubmed (297), CNKI (424) and Wanfang (157) databases search. After removing duplicate publications, a total of 1,653 articles have remained. Of those, 17 publications fit the exclusion and inclusion criteria based on the study titles and abstracts. Among them, 6 papers were determined to have sufficient information and therefore finally included in meta-analysis, with 5 papers in English and 1 in Chinese (**Figure 3**). The summary of the included literature on the risk of death from high temperature on health endpoints in Wuhan are listed in **Table 2**.

Relative Risk of High Temperature Exposure and Premature Deaths

The estimates of RR of each study and overall pooled RR are shown in **Figure 4**, and the results showed statistical significance ($p < 0.05$). Since the significant heterogeneity ($I^2 = 91.4\%$) was detected, we chose the random effect model to pool the RR. The pooled estimate of RR (95% CI) was 1.26 (95% CI: 1.15, 1.39), which suggests that the risk of mortality from residents' health endpoints will increase by 26% when exposed to high temperatures.

The number of premature deaths due to high temperatures in Wuhan based on the calculation of Equation (3) is presented in **Table 3**. From 2013 to 2019, this number had noticeable fluctuations, rising as high as 77,369. It trended downward from 2013 to 2014 and from 2015 to 2016 but rose sharply after 2016. It peaked in 2017 and fell again in 2018, yet it remained larger than that in 2013.

It should be noted that the number of exposed populations as well as mortality rates in Wuhan varied from 2013 to 2019, and the number of premature deaths determined by these two variables also differed annually. The abnormal number of premature deaths in 2017 was attributed to an abnormal all-cause mortality rate for that year, which was more than twice as high as the rate for the other years over the seven years. In the same year, the mortality rate in Changsha City was similarly abnormal. According to the 2017 Changsha City National Economic and Social Development Statistical Bulletin, the Municipal Public Security Bureau verified the information of people who died but did not cancel their household registration and cumulatively canceled the household registration of these people, causing the mortality rate that year to be higher than usual (37). In this regard, we reasonably assumed that Wuhan City also carried out the same cancellation action in 2017, resulting in an abnormal mortality rate and further causing a high number of premature deaths from high temperature as well.

Value of Statistical Life Obtainment

In this study, three methods were considered to estimate VSL: meta-analysis, willingness-to pay (WTP) and benefit transfer (BT) methods. As for the meta-analysis method, with the wide application of meta-analysis in the field of environmental economics, Xu et al. (38) assessed four publications relevant to the air pollution CVM with meta-regression model to estimate the value of air pollution statistics life in China to be about 86 million RMB. More evidence suggests that income level is positively associated with VSL and is the main factor influencing VSL (39, 40). The time series study in this paper is comprised of time variation of VSL with per capita income. Thus, fixed meta-analysis value cannot be generalized for use in a time series analysis.

It is feasible to obtain VSL based on Equation (4) by using the WTP method. Gao et al. surveyed the willingness to pay for air pollution health risk reduction in three of the six main

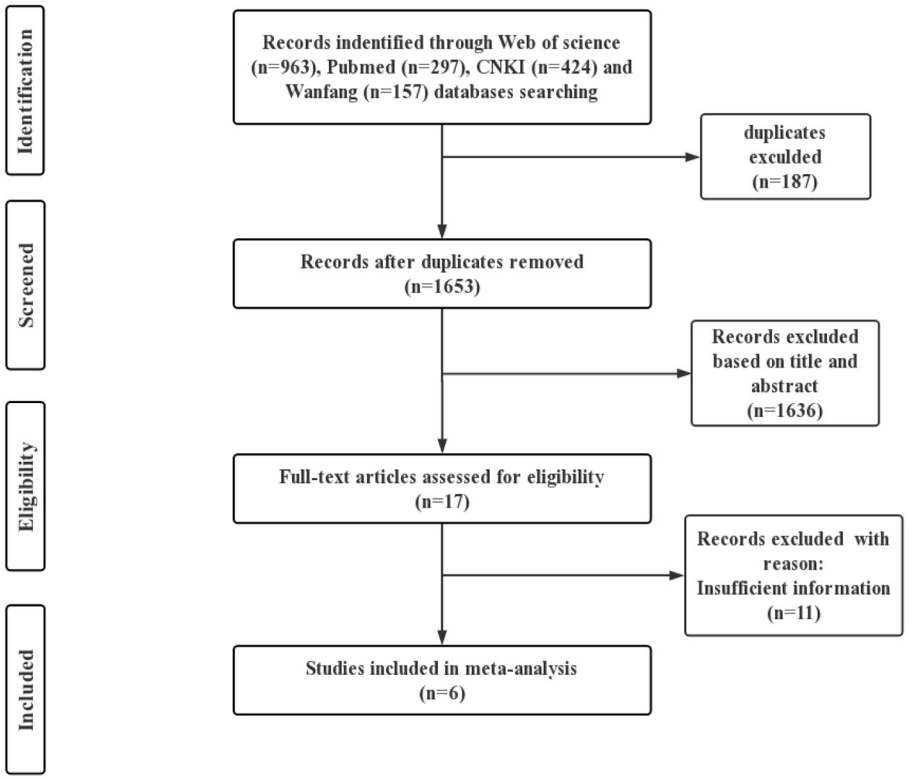

FIGURE 3 | Flow chart of literature selection.

TABLE 2 | Summary of the characteristics of included studies.

References	Study period	Mortality event	RR (95% CI)
Ma (31)	2003–2005	Cardiovascular disease	1.14 (1.04,1.24)
Ma (31)	2003–2005	Respiratory disease	1.11 (0.88,1.39)
Guo et al. (32)	2004–2008	Ischemic heart disease	1.59 (1.16,2.18)
Zhang et al. (33)	2003–2010	Cardiovascular disease	1.34 (1.26,1.43)
Zhang et al. (33)	2003–2010	Respiratory disease	1.57 (1.24,1.98)
Zhang et al. (33)	2003–2010	Cerebrovascular disease	1.69 (1.41,1.95)
Zhang et al. (33)	2003–2010	Ischemic heart disease	1.17 (1.08,1.27)
Zhang et al. (33)	2003–2010	Non-accidental	1.25 (1.19,1.32)
Wu et al. (34)	2003–2010	Ischemic heart disease	1.15 (1.01,1.30)
Bao et al. (35)	2008–2011	Non-accidental	1.35 (1.18,1.55)
Zhang et al. (36)	2004–2008	Cerebrovascular disease	1.01 (0.98,1.05)

urban areas of Beijing measured by contingent valuation method, with VSL values ranging from 0.667 to 1.1 million RMB (41). Similarly, Xu estimated the VSL value for Hangzhou residents in 2004 to be 2.218 million RMB (40). A More recent study by Peng et al. estimated the value of statistical life in Chongqing and Sichuan to be 3.928 million and 4.02 million RMB, respectively, with the single-boundary dichotomous function model of the CVM (42). Unfortunately, we failed to find any willingness-to-pay surveys on air pollution mortality risk reduction carried out in Wuhan city.

The BT method is meant to convert from a specific VSL study that has been estimated for a particular city, based on an exponential linear relationship of the proportion of income levels per capita. Compared to the previous methods, the BT method reduces the consumption of human, material, and financial resources (40) as well as takes the temporary differences in income earnings levels into account, therefore considered the most appropriate method for this study.

When selecting the VSL values of domestic and foreign regions, some scholars discovered that the value of domestic VSL

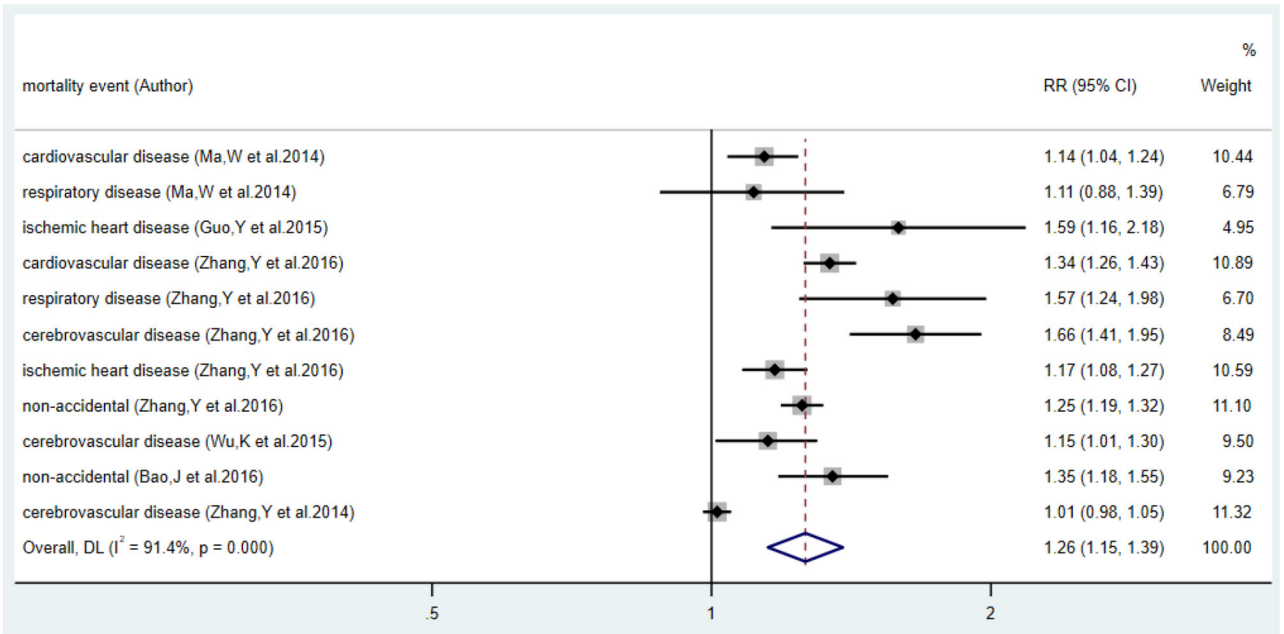

FIGURE 4 | Forest plot of relative risk and 95% CI for relationship between the high temperature and health endpoints.

TABLE 3 | Premature deaths (95%CI) due to high temperature in Wuhan, 2013–2019.

Year	Premature death (person)	Year	Premature death (person)
2013	8,848 (5,340–11,487)	2017	20,469 (12,939–27,832)
2014	8,485 (5,364–11,537)	2018	10,067 (6,363–13,688)
2015	9,840 (6,220–13,379)	2019	10,699 (6,763–14,547)
2016	9,361 (5,917–12,728)	2013–2019	77,369 (48,906–105,198)

TABLE 4 | Value of statistical life in Wuhan between 2013 and 2019.

Year	Per capital disposable income (RMB)	VSL (million/person)	GDP (billion RMB)
2013	26,909	1.57	905.13
2014	29,627	1.70	1,006.95
2015	32,478	1.83	1,090.56
2016	35,383	1.96	1,191.26
2017	38,642	2.10	1,341.04
2018	42,133	2.25	1,484.73
2019	46,010	2.42	1,622.32
2013–2019	–	–	8,641.98

was generally lower than latter (38, 39). We speculate that it is caused by the difference in economic development in China and foreign countries. Therefore, in this paper, VSL of domestic cities was selected, specifically the VSL of Beijing in 2010 (1.68 million RMB) based on Xie (43).

Health Economic Loss Attributed to High Temperature

The corresponding values of the statistical life in Wuhan over the seven-year period were calculated using Equation (5), as presented in the third column of **Table 4**. The VSL values related to high temperature varied from 1.57 million RMB in 2013 to 2.24 million RMB in 2019, revealing a generally increasing trend. The progressive increase in VSL indicates the annual improvement in the per capita disposable income level of Wuhan residents. Meanwhile, it also shows the growing willingness-to-pay of residents of Wuhan city to reduce the risk of heat-related deaths. Based on Equation (6), the annual VSL is combined with the corresponding number of premature deaths attributed to high temperature. The outcomes of economic loss from high temperatures and the corresponding proportion in GDP are displayed in **Figure 5**. The total economic losses between 2013 and 2019 amounted to 156.1 billion RMB (95% CI: 92.28–211.40 billion RMB), accounting for approximately 1.81% (95% CI: 1.14–2.45%) of the GDP of Wuhan in the 7-year period, which turns out to be 8,461.98 billion RMB.

Figure 5A displayed that the health economic losses have increased annually between 2013 and 2019, and the economic losses in 2017–2019 have all exceeded the annual average loss (RMB 22.3 billion), contributing to 58.61% of total economic losses. Meanwhile, the largest three values of economic loss were also observed in these 3 years, i.e., 42.99 billion RMB (95% CI: 27.18–58.46 billion RMB), 22.66 billion RMB (95% CI: 14.32–30.81 billion RMB), and 25.84 billion RMB (95% CI: 16.33–35.13 billion RMB). The escalation in health economic losses is

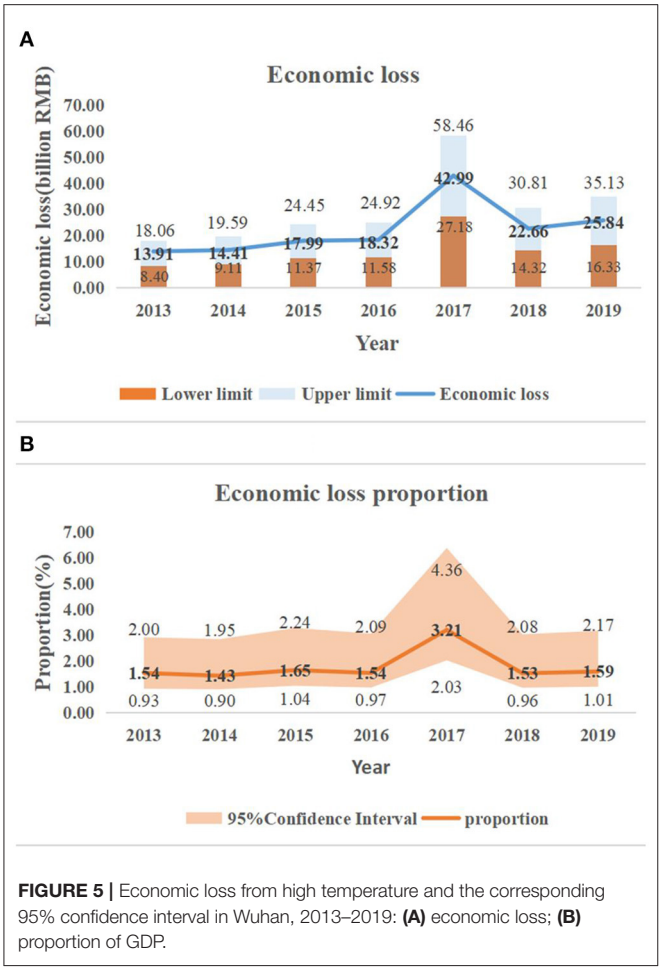

FIGURE 5 | Economic loss from high temperature and the corresponding 95% confidence interval in Wuhan, 2013–2019: **(A)** economic loss; **(B)** proportion of GDP.

associated with a larger frequency and intensity of extremely high temperatures and is further responsible for more premature high temperature-related deaths and a gentle increasing trend in the value of statistical life over time.

Figure 5B reflected the similar trend as **Figure 5A**. Economic losses were more than 1.5% of the GDP in all year except year 2014. The lower fraction of GDP in 2014 were supposed due to the milder temperatures and less premature deaths from heat exposure as well as the higher increment in GDP in that year compared to other years. The annual average heat economic loss was 1.81% (95% CI: 1.14–2.45%) of GDP from year 2013 to 2019. The Lancet Countdown to China report showed that the economic loss of China from the reduction of labor time due to high temperature was 1.4% of its GDP in 2020 (44), which was 22.7% lower than our estimated economic loss. Thus, Wuhan must develop high-temperature warning measures to reduce its economic losses.

DISCUSSION

Influence by climate change, high temperatures have been occurring more frequently and with greater intensity. A large number of scholars have developed various models and methods to investigate the health effects of high temperature in Wuhan (31–36). We not only employed meta-analysis to obtain the total impacts but also monetized and quantified the economic burden generated by these mortality impacts. We estimate the economic burden of premature death for selected health endpoints due to exposure to high temperatures to be 156.10 billion RMB (95% CI: 98.28–211.40 billion RMB), accounting for 1.81% (95% CI: 1.14–2.45%) of Wuhan's 2013–2019 GDP, which is higher than the national heat economic losses as a percentage of national GDP published in The Lancet Countdown to China report. To the best of our knowledge, this is the first study to link meta-analysis calculations of relative risk and value of statistical life to quantify high temperature health-related economic losses. It is also an exemplary study in regions seriously threatened by high temperatures such as central China. Other studies of economic losses from high temperatures have adopted method to obtain relative risk directly from urban studies with similar types of conditions to those of the study city or country (45, 46). In this study, epidemiological studies on Wuhan were obtained from four major databases, and relative risks were not employed from epidemiological studies in other cities.

There are some limitations and uncertainties to this study in assessing the economic loss of premature death at high-temperature health endpoints. First, the number of the exposed population selected for the calculation of premature deaths in this study is the registered population of Wuhan, not the permanent population, since Wuhan's all-cause mortality is calculated based on the number of deaths in the registered population (47). Because the registered population is not the only ones exposed to high temperatures, the economic loss from premature death will be underestimated. Second, only five types of causes of death with the most significant effect of high temperature were selected as health endpoints. A study conducted in Seoul, South Korea, indicated a significant correlation between high temperatures and the risk of preterm birth in pregnant women (48). Several studies also illustrated the burden of heat on death from nervous diseases (49), diabetes (50) and mental health (51). Since the relative risks of Wuhan City for the above-mentioned related diseases are not available, a comprehensive assessment of the economic loss from heat exposure is hard to conduct. Once epidemiological data are provided, further studies can be easily performed with more comprehensive and accurate results. Third, we considered only one aspect of the economic impact of heat: premature death. As a result, outpatient costs, medical costs, and lost wages incurred by residents entering emergency care or hospitalization due to sudden illnesses caused by high temperatures are not considered in this paper (5). To ensure the safety of workers under high temperatures, outdoor workers will adopt a work system that reduces the intensity of work or increases the number of breaks, resulting in a reduction in working hours (52); indoor workers will also be less efficient due to the high temperature (52). Average heat-related work productivity loss is about 6.6 days in developing countries in 2016 (53). Seven percent of Australian respondents missed an average of 4.4 days of work during the heat of 2013–2014, and seventy percent were less productive, working for 27.1 h less (12). In such cases, economic loss will also be generated. Therefore,

once the hospital admission or emergency data are available, they can be considered in further studies of economic loss of heat.

We believe that the results of such studies serve as a cautionary tale for policymakers. A series of resident mortality risk reduction measures in response to the occurrence of heat events are necessary. An electronic study conducted in Victoria, Australia in 2003 revealed a lack of knowledge among the population regarding thermoregulation, heat risk factors, heat-related illnesses and fan use (54), raising awareness that heat-related knowledge should be strengthened.

It is important to disseminate heat warnings in a timely manner. Issuing heat warning announcements through the media is considered feasible for residents, especially for the elderly population, with radio and television being the two best ways to deliver them (54, 55). Since the elderly and children are more obviously affected by the heat (56), society should give extra attention to these more vulnerable groups (57). In addition, the process of urban construction and development is supposed to accelerate the construction of summer space and cool centers in the city to increase the area for residents to escape from the heat. For example, in 2013, the severest year for high temperatures in Wuhan, the citizens of the city spontaneously went to cooled subway stations to escape the heat, and the subway company stated that they would not refuse such escaping without affecting normal subway operations. In 2019, ∼1,400 cool spots in Wuhan city were open to meet the needs of the residents, especially for those of poor households, in accordance with the requirements of civil affairs department of Wuhan. As high temperature momentum is not reducing the trend, Wuhan should consider designating more space throughout the city to escape from the heat.

Different government departments, such as the meteorological department and the health department collaborate to build the emergency response system, complete the simulation implementation and feedback of the system based on big data, and improve the flexibility of the emergency response plan (58). From the perspective of urban construction, ventilation corridors are established according to the prevailing wind direction by relying on the Yangtze River and other lakes, as well as urban roads, parks, and low-density areas in response to the wind brought from the suburbs into the city (59). At the same time, the government accelerated the greening construction focusing on the four banks of the two rivers and the ecological restoration of mountains such as Tortoise Hill and Snake Hill to improve the local microclimate. Since the ecological function protection zones in Wuhan are mainly located in the central part of Huangpi District and the eastern and southwestern parts of Xinzhou District, they have a high resistance valueand these areas can exert ecological benefits, which should be highly valued and protected (60). In addition, greening works in urban parks, roads and scenic areas, as well as forest parks should be renovated to facilitate the mitigation of high temperatures.

CONCLUSION

A meta-analysis revealed a relative risk of 1.26 (95% CI: 1.15, 1.39) for the health endpoints. The number of premature deaths due to high-temperature exposures for the five health endpoints in Wuhan was 77,369 (95% CI: 48,906–105,198), and resulted in a loss of 156.10 billion RMB (95% CI: 98.28–211.40 billion RMB), approximately 1.81% (95% CI: 1.14–2.45%) of Wuhan's 2013–2019 GDP. In the context of high global heat events, premature death from heat and the corresponding economic burden deserves close attention. It is suggested that policymakers should also establish appropriate measures to reduce the number of premature heat-related deaths among residents and reduce the economic loss from premature heat-related deaths proportionate to the GDP of the city. Furthermore, this study is a cautionary warning to policy decision-makers for cities and regions facing similar heat threats as Wuhan in the future and is expected to provide valuable management advice in heat-related policymaking.

DATA AVAILABILITY STATEMENT

The original contributions presented in the study are included in the article/supplementary material, further inquiries can be directed to the corresponding author.

AUTHOR CONTRIBUTIONS

SC and JZ: conceptualization, methodology, and writing—original draft preparation. JZ: software, formal analysis, resources, and data curation. JZ and SK: investigation. S-BL and SK: writing—review and editing. S-BL: visualization. SK: supervision. SC: project administration and validation. SC and SK: funding acquisition. All authors contributed to the article and approved the submitted version.

FUNDING

This study was supported by the Humanities and Social Science Research Program funded by the Ministry of Education of China (21C10512050). SK research was partially supported by Science Research Program through the National Research Foundation of Korea (NRF) funded by the Ministry of Education (NRF-2021R1A2C1005271).

REFERENCES

1. Watts N, Adger WN, Agnolucci P, Blackstock J, Byass P, Cai WJ, et al. Health and climate change: policy responses to protect public health. *Lancet.* (2015) 386:1861–914. doi: 10.1016/S0140-6736(15)60854-6
2. Masson-Delmotte V, Zhai P, Pirani A, Connors SL, Péan C, Berger S, editors. *IPCC, 2021: Climate Change 2021: The Physical Science Basis. Contribution of Working Group I to the Sixth Assessment Report of the Intergovernmental Panel on Climate Change*. (2021). Cambridge University Press.
3. Zhang YQ, Yu CH, Bao JZ, Li XD. Impact of temperature variation on mortality: An observational study from 12 counties

across Hubei Province in China. *Sci Total Environ.* (2017) 587–588:196–203. doi: 10.1016/j.scitotenv.2017.02.117
4. Knowlton K, Rotkin-Ellman M, Geballe L, Max W, Solomon GM. Six climate change-related events in the united states accounted for about $14 billion in lost lives and health costs. *Health Affair.* (2011) 30:2167–76. doi: 10.1377/hlthaff.2011.0229
5. Limaye VS, Max W, Constible J, Knowlton K. Estimating the health-related costs of 10 climate-sensitive U.S. events during 2012. *Geohealth.* (2019) 3:245–65. doi: 10.1029/2019GH000202
6. OregonLive. *Pacific Northwest*. (2021). Available at: https://www.oregonlive.com/pacific-northwest-news/2021/07/at-least-63-people-died-in-oregon-heat-wave-heres-what-we-know.html (accessed July 1, 2021).
7. OregonLive. (2021). *Weather*. Available at: https://www.oregonlive.com/weather/2021/07/death-toll-from-historic-heat-waves-rises-to-107.html (accessed July 6, 2021).
8. Global News. *Health*. (2021). Available at: https://globalnews.ca/news/8071632/bc-heat-wave-deaths-2021/ (accessed July 29, 2021).
9. Zhao Q, Guo YM, Ye TT, Gasparrini A, Tong S, Overcenco A, et al. Global, regional, and national burden of mortality associated with non-optimal ambient temperatures from 2000 to 2019: a three-stage modelling study. *Lancet Planet Health.* (2021) 5:e415–25. doi: 10.1016/S2542-5196(21)00081-4
10. Gronlund CJ, Cameron L, Shea C, O'Neill MS. Assessing the magnitude and uncertainties of the burden of selected diseases attributable to extreme heat and extreme precipitation under a climate change scenario in Michigan for the period 2041-2070. *Environ Health-Glob.* (2019) 18:17–40. doi: 10.1186/s12940-019-0483-5
11. Roldán E, Gómez M, Pino MR, Díaz J. The impact of extremely high temperatures on mortality and mortality cost. *Int J Environ Heal R.* (2015) 25:277–87. doi: 10.1080/09603123.2014.938028
12. Zander KK, Botzen WJW, Oppermann E, Kjellstrom T, Garnett ST. Heat stress causes substantial labour productivity loss in Australia. *Nat Clim Change.* (2015) 5:647–51. doi: 10.1038/nclimate2623
13. Costello A, Abbas M, Allen A, Ball S, Bell S, Bellamy R, et al. Managing the health effects of climate change. *Lancet.* (2009) 373:1693–733. doi: 10.1016/S0140-6736(09)60935-1
14. Zhong Z, Chen X, Yang XQ, Han Y, Sun Y. The relationship of frequent tropical cyclone activities over the western North Pacific and hot summer days in central-eastern China. *Theor Appl Climatol* 138:1395–404. doi: 10.1007/s00704-019-02908-7
15. Li K, Amatus G. Spatiotemporal changes of heat waves and extreme temperatures in the main cities of China from 1955 to 2014. *Nat Hazard Earth Sys.* (2020) 20:1889–901. doi: 10.5194/nhess-20-1889-2020
16. Li F, Cai Y, Zhang JD. Spatial Characteristics, health risk assessment and sustainable management of heavy metals and metalloids in soils from Central China. *Sustainability (Basel, Switzerland).* (2018) 10:91. doi: 10.3390/su10010091
17. Li F, Lu YC, Zhang JD, Wang YL, Chen XY, Yan JJ, et al. Investigation and regional fuzzy health risk management of lead and cadmium in best-selling cigarettes across China. *J Clean Prod*. (2020) 261:121005. doi: 10.1016/j.jclepro.2020.121005
18. Lian H, Ruan YP, Liang RJ, Liu XL, Fan ZJ. Short-Term Effect of Ambient Temperature and the Risk of Stroke: a Systematic Review and Meta-Analysis. *Int J Env Res Pub He.* (2015) 12:9068–88. doi: 10.3390/ijerph120809068
19. Ma GX, Zhou Y, Wu CS, Peng F. Cost-Benefit Assessment of Impacts of China's National Air Pollution Action Plan in Cheng-Yu Region. *Environ Conform Assess.* (2019) 11:38–43. doi: 10.16868/j.cnki.1674-6252.2019.06.038
20. Statistics Bureau of Wuhan Municipality. *Wuhan Statistical Yearbook* (2014–2020). China Statistics Press: Beijing, China.
21. Lei Y, Xue WB, Zhang YS, Xu YL. Health Benefit Evaluation for Air Pollution Prevention and Control Action Plan in China. *Environ Conform Assess.* (2015) 7:50–3. doi: 10.13227/j.hjkx.201811110
22. Yu F, Guo XM, Zhang YS, Pan XC, Zhao Y, Wang JN. Assessment of health economic losses due to air pollution in China in 2004. *J Environ Health.* (2007) 24:999–1003. doi: 10.16241/j.cnki.1001-5914.2007.12.034
23. Zhao XL, Fan CY, Wang YX. Evaluation of Health Losses by Air Pollution in Beijing: a Study Based on Corrected Human Capital Method. *China Popul Resour Environ.* (2014) 24:169–76. doi: 10.3969/j.issn.1002-2104.2014.03.024
24. Li HJ, Zhou DQ, Wei YJ. Review on health economic loss assessment of air pollution. *Res Environ Sci.* (2020) 33:2421–9. doi: 10.13198/j.issn.1001-6929.2020.04.25
25. Zhou F. Comparison of three health level indicators: quality-adjusted life year, disability-adjusted life year and healthy life expectancy. *J Environ Occup Med.* (2010) 27:119–22, 24. doi: 10.13213/j.cnki.jeom.2010.02.001
26. Cai CG, Chen G, Qiao XC, Zheng XY. Application of contingent valuation method to estimate health economic loss caused by environmental pollution. *J Environ Health.* (2007) 265–7. doi: 10.3969/j.issn.1001-5914.2007.04.041
27. Adélaïde L, Chanel O, Pascal M. Health effects from heat waves in France: an economic evaluation. *Eur J Health Econ.* (2021) 1–13. doi: 10.1007/s10198-021-01357-2
28. Zhou MJ, Hu WQ, Yang SY, Zhu X, Zhao CC, Bai ZY. Spatial-temporal analysis of PM2.5-related health impact and economic losses in China from 2000 to 2017. *J HuaZhong Normal Univ (Natural Sciences).* (2021) 55:110–20. doi: 10.19603/j.cnki.1000-1190.2021.01.016
29. OECD. The cost of air pollution health impacts of road transport. In: *Cost Air Pollution*. Leipzig: OECD Publishing (2014). doi: 10.1787/9789264210448-en
30. Hammitt JK, Morfeld P, Tuomisto JT, Erren TC. Premature deaths, statistical lives, and years of life lost: identification, quantification, and valuation of mortality risks. *Risk Anal.* (2020) 40:674–95. doi: 10.1111/risa.13427
31. Ma WJ. *A study on temperature-related mortality in 16 Chinese cities*. Ph. D. thesis, Fudan University, Shanghai (2014).
32. Guo YM, Li SS, Zhang YS, Armstrong B, Jaakkola JJK, Tong S, et al. Extremely cold and hot temperatures increase the risk of ischaemic heart disease mortality: epidemiological evidence from China. *Heart.* (2013) 99:195–203. doi: 10.1136/heartjnl-2012-302518
33. Zhang YQ, Li CL, Feng RJ, Zhu YH, Wu K, Tan XD, et al. The short-term effect of ambient temperature on mortality in Wuhan, China: a time-series study using a distributed lag non-linear model. *Int J Env Res Pub He.* (2016) 13:722. doi: 10.3390/ijerph13070722
34. Wu K, Zhang YQ, Zhu CH, Ma L, Tan XD. Association between heat wave and stroke mortality in Jiang'an District of Wuhan, China during 2003 to 2010: a time-series analysis. *Chin J Cardiol.* (2015) 43:1092–6. doi: 10.16462/j.cnki.zhjbkz.2021.10.005
35. Bao JZ, Wang ZK, Yu CH, Li XD. The influence of temperature on mortality and its Lag effect: a study in four Chinese cities with different latitudes. *Bmc Public Health*. (2016) 16:375. doi: 10.1186/s12889-016-3031-z
36. Zhang YS, Li SS, Pan XC, Tong SL, Jaakkola JJ, Gasparrini A, et al. The effects of ambient temperature on cerebrovascular mortality: an epidemiologic study in four climatic zones in China. *Environ Health.* (2014) 13:24. doi: 10.1186/1476-069X-13-24
37. Statistics Bureau of Changsha Municipality. *Changsha City Economic and Social Development Bulletin*. (2018). China Statistics Press: Beijing, China.
38. Xu XC, Chen RJ, Kan HD, Ying XH. Meta-analysis of contingent valuation studies on air pollution-related value of statistical life in China. *Chin Health Res.* (2013) 16:64–7. doi: 10.3969/j.issn.1007-953X.2013.01.024
39. Zeng XG, Jiang Y. Evaluation of value of statistical life in health costs attributable to air pollution. *China Environ Sci.* (2010) 30:284–8.
40. Xu JF. *Estimation of Environmental Damage Costs for Air Pollution Death Endpoints in Hangzhou. MSEE thesis*. (2008). Zhejiang: Zhejiang University.
41. Gao T, Li GX., Xu MM. Health economic loss evaluation of ambient PM2.5 pollution based on willingness to pay. *J Environ Health*. (2015) 32:697–700. doi: 10.16241/j.cnki.1001-5914.2015.08.011
42. Peng F, Li X, Ma GX, Zhou Y, Yu F, Zhang YS, et al. Assessing the value of a statistical life of air pollution in Chengdu-Chongqing area by contingent value method with single bounded dichotomy. *Environ Conform Assess.* (2021) 13:136–41. doi: 10.16868/j.cnki.1674-6252.2021.01.136
43. Xie XX. *The Value of Health: Applications of Choice Experiment Approach and urban air pollution control strategy. Ph. D. thesis*. (2011). Beijing: Peking University.
44. Cai WJ, Zhang C, Zhang SH Ai SQ, Bai YQ, Bao JZ, et al. The 2021 China report of the Lancet Countdown on health and climate change: seizing the window of opportunity. *Lancet Public Health.* (2021) 6:e932–47. doi: 10.1016/S2468-2667(21)00209-7
45. Yoon SJ, Oh IH, Seo HY, Kim EJ. Measuring the burden of disease due to climate change and developing a forecast model in South Korea. *Public Health.* (2014) 128:725–33. doi: 10.1016/j.puhe.2014.06.008

46. Xia Y, Li Y, Guan DB, Tinoco DM, Xia JJ, Yan ZW, et al. Assessment of the economic impacts of heat waves: a case study of Nanjing, China. *J Clean Prod.* (2018) 171:811–9. doi: 10.1016/j.jclepro.2017.10.069
47. Qu ZG, Wang XY, Li F, Li YN, Chen XY, Chen M. $PM_{2.5}$-related health economic benefits evaluation based on air improvement action plan in Wuhan City, Middle China. *Int J Environ Res Public Health.* (2020) 17:620. doi: 10.3390/ijerph17020620
48. Son JY, Lee JT, Lane KJ, Bell ML. Impacts of high temperature on adverse birth outcomes in Seoul, Korea: Disparities by individual- and community-level characteristics. *Environ Res.* (2019) 168:460–6. doi: 10.1016/j.envres.2018.10.032
49. Su XM, Song HJ, Cheng YB, Yao XY Li YH. The mortality burden of nervous system diseases attributed to ambient temperature: a multi-city study in China. *Sci Total Environ.* (2021) 800:149548. doi: 10.1016/j.scitotenv.2021.149548
50. Yang J, Yin P, Zhou MG, Ou CQ Li MM, Liu Y, et al. The effect of ambient temperature on diabetes mortality in China: a multi-city time series study. *Sci Total Environ.* (2016) 543:75–82. doi: 10.1016/j.scitotenv.2015.11.014
51. Thompson R, Hornigold R, Page L, Waite T. Associations between high ambient temperatures and heat waves with mental health outcomes: a systematic review. *Public Health.* (2018) 161:171–91. doi: 10.1016/j.puhe.2018.06.008
52. Wang YF, Bian JY, Li GQ. The impact of hot weather on regional labor productivity over Xiong'an New District under future climate scenario. *China Popul Res Environ.* (2020) 30:73–83. doi: 10.12062/cpre.20200407
53. Yu S, Xia JJ, Yan ZW, Zhang AZ, Xia Y, Guan DB. Loss of work productivity in a warming world: Differences between developed and developing countries. *J Clean Prod* 208:1219–25. doi: 10.1016/j.jclepro.2018.10.067
54. Ibrahim JE, McInnes JA, Andrianopoulos N, Evans S. Minimising harm from heatwaves: a survey of awareness, knowledge, and practices of health professionals and care providers in Victoria, Australia. *Int J Public Health.* (2012) 57:297–304. doi: 10.1007/s00038-011-0243-y
55. Nitschke M, Hansen A, Bi P, Pisaniello D, Newbury J, Kitson A, et al. Risk factors, health effects and behaviour in older people during extreme heat: a survey in South Australia. *Int J Env Res Pub He.* (2013) 10:6721–33. doi: 10.3390/ijerph10126721
56. Feng L, Li XD. Effects of heat waves on human health:a review of recent study. *J Environ Health.* (2016) 33:182–8. doi: 10.16241/j.cnki.1001-5914.2016.02.025
57. Lowe D, Ebi KL, Forsberg B. Heatwave early warning systems and adaptation advice to reduce human health consequences of heatwaves. *Int J Environ Res Public Health.* (2011) 8:4623–48. doi: 10.3390/ijerph8124623.
58. Cheng SQ,Wei LL, Lu Z, Liao WJ, Liao ZQ, Qi XH. A Study on the Contingency Plan for High Temperature Heat Waves Based on Collaborative Linkage. *J Catastrophol.* (2019) 34:192–8. doi: 10.3969/j.issn.1000-811X.2019.02.035
59. Wuhan Natural Resources and Planning Bureau. *Wuhan City Territorial Spatial Master Plan (2021-2035).* Available at: http://zrzyhgh.wuhan.gov.cn/bsfw_18/ghpqgs/ghcags/202107/t20210713_1737015.shtml (accessed July 14, 2021).
60. Jin G, Shi X, He DW, Guo BS Li ZH, Shi XB. Designing a spatial pattern to rebalance the orientation of development and protection in Wuhan. *J Geogr Sci.* (2020) 30:569–82. doi: 10.1007/s11442-020-1743-6

Conflict of Interest: The authors declare that the research was conducted in the absence of any commercial or financial relationships that could be construed as a potential conflict of interest.

frontiers in Public Health

ORIGINAL RESEARCH
published: 08 March 2022
doi: 10.3389/fpubh.2022.844593

Policy Effects of Ecological Red Lines on Industrial Upgrading and Health Promotion: Evidence From China Based on DID Model

*Penghao Ye**

School of Economics, Hainan Open Economy Research Institute, Hainan University, Haikou, China

The implementation of the Ecological Red Lines (ERL) policy in China is under the background that natural resources have been immoderately exploited for serving rapid economic growth in the last 40 years, where the ecosystem's degradation happened and people's health could be affected. As the secondary industry is the contribution source of rapid growth as well as the threat source that threatens the natural environment and public health, the delimitation of ERL can act as a legal restriction that forces the industries to control the emissions and to upgrade the industrial composition. This paper conducts an ex-post policy evaluation on the improvement effects of industrial structure and residents' health and through ERL's pilot scheme in four provinces of China. By using the difference-in-differences (DID) method, the estimation results show that: (1) The industrial upgrading effect exists but to a small extent, as the ERL policy has generally elevated the tertiary industry's output by only 0.033% and hardly shown any promotion effects on the ratio of the tertiary industry to secondary industry; (2) The residents' health has been significantly improved by 1.029% after ERL policy on the whole, and enhanced over time mostly; (3) The health promotion effects are similar among three out of the four pilot provinces, whereas the industrial upgrading effects performed large heterogeneities among the four. These empirical results may provide references for the wider extension of ERL policy with more practical execution solutions in developing economies.

Keywords: Ecological Red Lines, industrial upgrading, health promotion, policy evaluation, difference-in-differences, event study

OPEN ACCESS

Edited by:
Hongtao Yi,
The Ohio State University, United States

Reviewed by:
Zhen Liu,
University of Surrey, United Kingdom
Weiguo Xiao,
Wuhan University, China

***Correspondence:**
Penghao Ye
paulyph@hainanu.edu.cn

Specialty section:
This article was submitted to Environmental health and Exposome, a section of the journal Frontiers in Public Health

Received: *28 December 2021*
Accepted: *09 February 2022*
Published: *08 March 2022*

Citation:
Ye P (2022) Policy Effects of Ecological Red Lines on Industrial Upgrading and Health Promotion: Evidence From China Based on DID Model. Front. Public Health 10:844593. doi: 10.3389/fpubh.2022.844593

INTRODUCTION

A typical developing region is composed of cities, villages and towns normally distributed with secondary industries. The secondary industries normally produce the manufactured or intermediate goods for domestic and global supply chains. By transaction and usage of the goods, the residents' welfare and economic growth can be promoted. However, while commercial manufacturing can provide intuitive sizable economic statistics, the consumed natural resources, including land, clean water, forest, mines, non-renewable energy sources, and biodiversity, have been neglected or regarded as slight "negative externality" for a long period (1, 2), even though they served as indispensable elements for secondary industry (3). As a result, people's health could be negatively affected by the diminishing resources and contaminated environments. Because of the manufacturing-dominated industrial structure and the production-oriented growing demand,

this situation appears to be more widespread in developing countries compared with developed economies which finished the industrial transformation in the main (4–6). As a consequence, the residents' health degree could come down and the industrial structure remains pollution-intensive and energy-intensive, causing a greater loss for both the individuals and the whole society. According to the Food and Agriculture Organization of the United Nations (FAO), the global resources of soil, land and water is "reaching the limit," as the land area per capita declined by 20% from 2000 to 2017, the groundwater consumption rose from 688 km^3/year in 2010 to 820 km^3/year in 2018 and let to a 250 km^3/year of water loss for the soil aquifer, the globe will suffer from a higher risk of environmental disasters and prevalence of disease if the current consumption trends have not ceased (7).

This circumstance began to change since the environmental and illness events continually occurred in multiple developing regions, as the adverse effects of heavy-polluting industries became more noticeable and received broader concerns in the societies. To contain the frequent ecological hazards, some developing countries have begun to take environmental protection measures. In order to protect the biological diversity, South Africa has built 422 ecological preservation zones with a total area of 67,000 square kilometers, where much stricter environmental laws and higher farm chemical standards are executed (8); In Brazil, a construction project of the potential world's third-largest hydropower station with a capacity of 11.3 gigawatts on a tributary of the Amazon River in Belo Monte came to a halt in 2012, for the reason that the submerged rainforest upstream of the dam may infringe the local biodiversity, especially for the species of fish and bird (9, 10). These actions indicated that the emerging economies are attaching more importance to ecological protection, despite economic growth still being the primary goal.

China is the second-largest economic entity as well as the biggest developing country around the world currently, experiencing a spectacular increase of production capacity in the last two decades, but also accompanied by an enormous depletion of natural resources and environment due to the rapid expansion of secondary industries. During the booming period of foreign trade (2001–2009) and infrastructure construction (2005–2014), environmental pollution and climate change events became more frequent and extensive than before. For the storm-flood event, few Chinese cities had encountered it before 2001, but the waterflood came out many more times since then, where 60% of the cities in China have witnessed the happening of storm-flood in 2015 (11). For the air quality issues, the annual haze pollution event in northern China increased from 30–50 days in 2000 to 80–90 days in 2006, and maintained at a level of 70–90 days until 2014 (12); some parts of southern China have also been intruded by winter haze caused by El Niño events since 2,000 (13). As for the water quality, every 1% transfer of the state-owned land transfer could bring 0.08–0.113% agriculture wastewater discharge at the prefecture-level (14), and the water pollution in rural areas was even much worse (15). All these environmental pollution events can threaten the residents' health to varying degrees by environmentally related diseases or declining food quality, then the wellbeing of most families would be deprived as a consequence.

Apart from the environmental issues, the resource depletion in manufacturing-based China is also tremendous. Taking energy consumption as an example, China consumed an average of around 4,000 megaton coal in 2011–2015, accounting for half of the world's consumption, and was five times as much as the consumption in the US. The electricity consumption per GDP in China was 0.508 kilowatt/USD in 2015, which was 2.28 times as Japan's and 4.65 times as UK's in the same year (source: World Bank); In terms of thermal unit, China's energy intensity was about 7.60–9.19 kBtu/USD in 2011–2015, which was 50.2–67.5% higher than the world average level (source: International Energy Agency). One reason accounting for this high consumption is the "world factory" status of China, as China has become the world's biggest exporter for trade in goods since 2009, accompanied by high production demands for both the domestic and the foreign market. Another reason is the coal-based energy structure and energy-intensive industries: China can produce 7,128.2–8,306.3 billion megajoule of raw coal annually, but the annual yield of the crude oil and natural gas are 834.7–896.8 billion and 373.6–533.8 megajoule; the secondary industry shared more than 40% of gross output before 2015 (source: National Bureau of Statistics of China), which was doubled compared to the developed countries averagely.

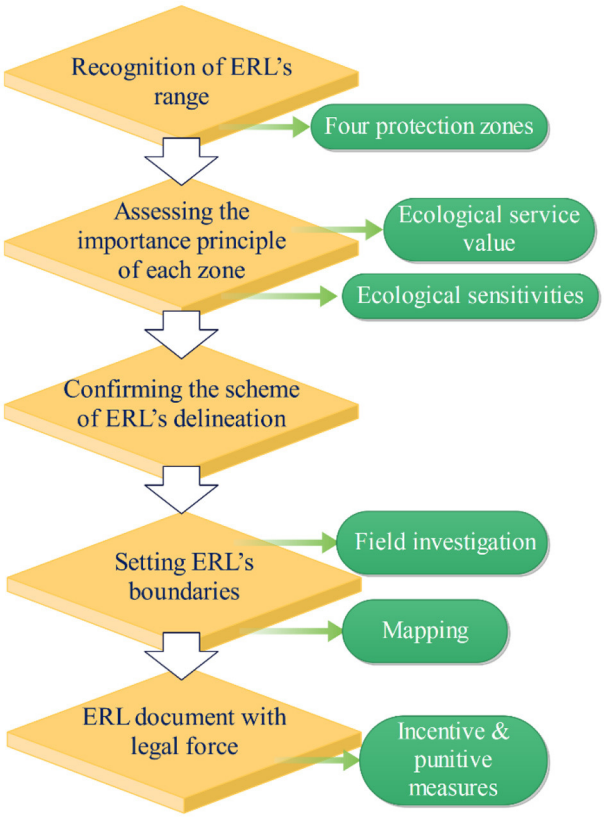

FIGURE 1 | Formulation process of ERL policy.

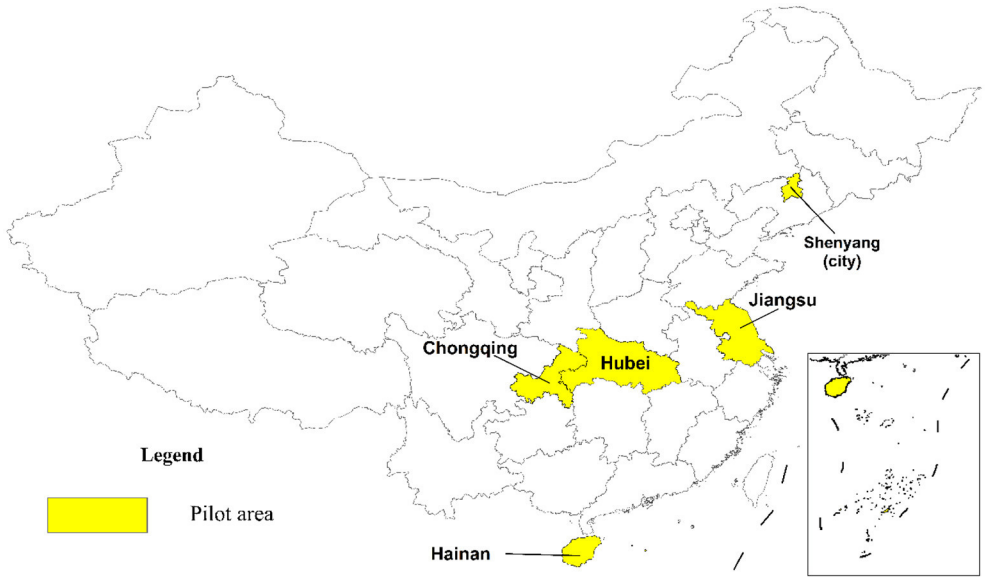

FIGURE 2 | The pilot regions for ERL implementation in 2015.

These intermittent environmental and climate events, along with continuous high resource consumption, aroused great concern from the Chinese government and residents, a plentiful of anti-pollution measures and environmental regulations have been carried out hard upon. Being different from other countermeasures that are directed at one or several specific pollutants or greenhouse gas, the Ecological Red Lines (ERL) policy is an all-around ecological and environmental action that limits the misuse of resources and immoderate emissions. The Ministry of Ecology and Environment (MEE) of China introduced this policy in 2015, and it can also be called the Ecological Conservation Red Lines.

According to **Figure 1**, the delimiting of the ERL can is carried through with five main steps. The initial step is the recognition of the ERL's range, in which four protection zones are divided (see **Figure 3**). The subsequent step is assessing the importance principle of each zone in terms of service value and sensitivities of the ecosystems. Based on the assessment results, the scheme of ERL's delineation and its boundaries will then be confirmed and set. Finally, the formal ERL document with legal force will come into force, preventing the ecological protection areas from improper exploitations.

The concept of ERL was officially proposed in 2012 when the MEE launched the formulation of ERL. Subsequently, from 2012 to 2014, more refined concepts and more detailed management practices of ERL have deepened, as some city-level pilot programs were attempted and offered valuable experiences useful for the follow-up policies enactment making of ERL for MEE (16). Based on the above efforts and investigations, a policy mix was released in 2015 (17), that is, the official document *Technical Guide for Delimiting Ecological Protection Red Lines* (18) issued by MEE, then four provincial-level regions and one city-level region were formally selected as the pilot areas for the implementation of ERL (shown in **Figure 2**), where the ecological preservation areas were defined with strict supervisory policies.

As **Figure 2** indicates, four provinces, Jiangsu, Hubei, Hainan and Chongqing, with Shenyang city, are the pilot regions for the ERL's trial implementation. Each administrative unit has a representative feature in China: Jiangsu is a typical advanced eastern coastal province, Hubei is a medium-developed inland province in central China, Hainan is a tropical island at an economic take-off stage and fit for wide-range reforms, Chongqing is a provincial-level mountainous municipality shouldered with poverty alleviation tasks, Shenyang is a northeastern provincial capital city with central heating in winter. Within the ERL zones of these pilot areas, environmental entry, ecological performance assessment, ecological compensation, emission control and other rigid protection measures were strictly put into practice.

According to the technical guide of the ERL pilot policy (18), four ecology protection zones constitute the ERL zones in **Figure 3**: key eco-function zone, ecological sensitive/fragile zone, forbidden development zone, and other zones (e.g., Ecological public-welfare forests, key wetlands). Each zone was treated differently in management details, but they may have intersections of coverage, as they have common features including the limitation of land development, resource exploitation, and emission dumping. In these zones, four control requirements are strictly executed: the land usage must not be transformed, the ecological function must not be lowered, the area of the zone must not be reduced, and the protection responsibilities of the forest, grassland, wetland and wilderness must not be changed. Also, ecological restoration is another important target in the red line areas, as they may have been damaged by industry and agriculture expansion in the past two decades before 2015.

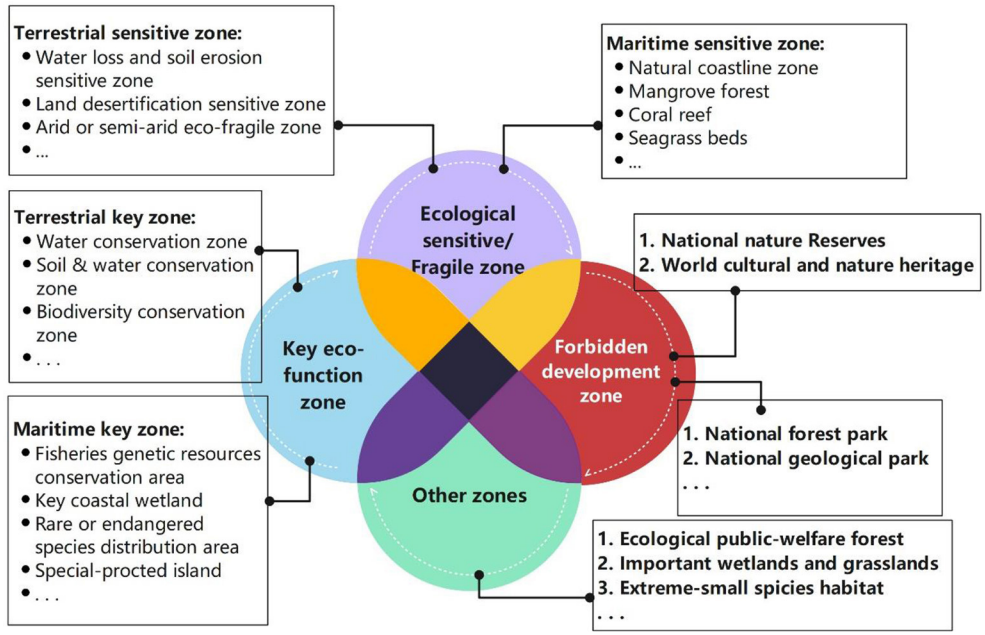

FIGURE 3 | Diagram of the ERL's delineation.

Based on these actions, it is noteworthy to evaluate what has ERL achieved in multiple aspects. Focused on four pilot provinces shown in **Figure 2**[1] and by using the policy evaluation econometric models, this paper chooses the industrial upgrading as the direction index for assessing the direct effect of the ERL policy, and the health promotion as the indicator for investigating the indirect effect, aiming at finding out the effect significance, the effect degree, and the possible regional heterogeneities of the ERL. Moreover, an event study applied to discovering the year-by-year effect will be carried out if the result shows high significance and extensiveness among the four pilot provinces both as a whole or individually.

LITERATURE REVIEW AND HYPOTHESIS PROPOSING

Existing Studies on ERL

Although the notion of ecological protection came a long time ago and relevant policies and actions had been taken in many countries or regions, the concept of the Ecological Red Line was first proposed in China in 2005 but remained at the discussion stage for over a decade (19). During the period of discussion, the academic expectation emerged before the ERL came to trial implementation. Si et al. pointed out that systematic delimitation, scientificity and maneuverability were the main principles for formulating the marine regional ERL (20). Based on the potentialities of ERL's functions, Lu et al. made a comparison study on the traditional Marine functional zoning (MFZ) and more recent Marine ERL, discovering that the Marine ERL can strengthen the MFZ by more specified regulations on administrations (21). As the basic execution unit of ERL is a province, Wang et al. assigned different indices with different weightiness in China's Liaoning Province, emphasizing the fundamental role of ecological inventory for the dynamical protection of the ERL.

Because the ERL is a dynamic policy that needs continuous improvement, several scholars have put forward their understandings and suggestions on how to effectively delimit its scope and strengthen its protection measures. Xu et al. conducted a case study on the Yangtze River Economic Belt which covers 11 provinces or municipalities, identifying that the key indicators, the evaluation methods, and the synergetic protection with other protection zones are the three knowledge gaps of the understanding of ERL; therefore, standardization, independent professional agencies, third-party evaluation systems, and cross-provincial ecological compensation strategies are four appropriate countermeasures for the implementing of ERL (16). He et al. unscrambled the ERL pilot policy in 2015 by classifying four types of ERL zones into more sub-zones with different functions and distinguishing the implementation points of land ERLs and maritime ERLs, then proposed that the financial support is a long-term guarantee of ERL's maintenance (22). The literature above has interpreted the ERL policy or provided the evaluation criteria of the ERL, but hardly examined the implementation effects of the ERL pilot policy. Hence, this paper chooses the industrial upgrading and residents' health as the main indicators, attempting to find out whether the

[1]Shenyang is not included in our analysis because of its city-level size and feature, hence it is improper to share the same comparable provincial-level groups with other four provinces, future work may carry through a city-level evaluation on Shenyang.

ERL policy can markedly reduce the sickness rate in the pilot provinces from 2015 to 2019.

Policy Evaluation Method

Policy evaluation, or policy assessment, is a prevalent research method in empirical econometric studies, these methods include the instrumental variable (IV) method, regression discontinuity design (RDD), synthetic control method (SCM), and difference-in-difference (DID) method. The IV method can effectively solve the endogenous problem in causal analysis (23), but the appropriate selection of IVs and the excluding of the study objects' heterogeneities are not easy to overcome (24). The RDD became widespread since Hahn et al. provided a comprehensive theoretical framework (25), but its high requirement of geographical homogeneities could restrict the evaluation of multiple observation subjects scattered in different regions (26). The SCM can give an intuitive graphical result displaying the trend variation before and after the policy implementation (27), but lacks quantitative outcomes and has difficulties in constructing complicated models (28). Among the methods for policy evaluation, the DID approach can provide the quantified results while overcoming the disturbance from the unobserved confounders (29). Ashenfelter came up with the earliest concept of DID (30), and Heckman et al. firstly put the DID method into policy assessment (31, 32). The DID model has served as an extensive tool in various kinds of research fields since then and was developed into multiple derivative models by scholars. In the field of environment and climate change, Greenstone and Hanna adopted DID estimator to find the distinctive results of the air pollution control acts and the water pollution control act in India (33). Lin et al. (34) used this approach to calculate out that greenhouse gas in China can be reduced by 1.75% annually due to the opening of high-speed railways. Nunn and Qian (35) extended their functions to estimate more than a single impact through multiple-period difference-in-differences (35).

DID method has also been widely used in the research field of public health for inspecting the achievements of a health policy or evaluating the impact of a pandemic. Dimick and Ryan summarized the use of DID in the assessments of health policies, believing that it is a better approach to solve the unpredictable background changes than the observational studies (36). Agüero and Beleche used DID to explore the health shocks and the long-lasting influences brought by the 2009 H1N1 influenza pandemic in Mexico, finding that although the H1N1 had caused health losses, the people's health was improved in the long run, owing to the awareness of personal hygiene has been promoted in a wider range (37). Li et al. adopted DID method to estimate the effect of lock-down during the prevention and treatment period of COVID-19, indicating that the citizen's short-term health can be improved due to the temporary improvement of the air quality (38).

Hypothesis

As mentioned before, the observation of two important indicators, industrial upgrading and health promotion, may reflect the effectiveness of the ERL pilot policy. To verify these effects, this paper presents a mechanism that the ERL may act on, as **Figure 4** displays:

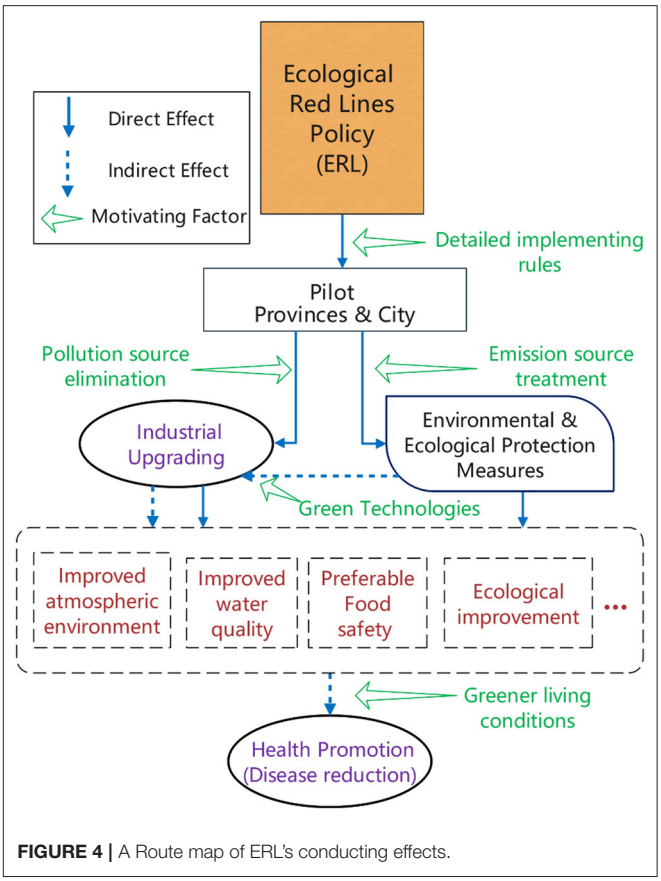

FIGURE 4 | A Route map of ERL's conducting effects.

Figure 4 depicted the ERL's possible influence paths on the two indictors (in ovals), in which the industrial upgrading is directly affected. Considering this direct path, the industrial upgrading which turns the secondary industries into tertiary industries can be seen as a direct reaction to the environmental policy for the pilot provinces. Hence, a hypothesis (H_1) that reflects the direct feedback of the ERL can be proposed as:

> **H_1**: *The ERL policy can significantly urge the pilot provinces to carry through industrial transformation by promoting the service industry's scale and its ratio to secondary industry.*

Compared to those observable or measurable indices such as forestry area, PM2.5, chemical oxygen demand (COD), or the three industrial wastes (wastewater, waste gases, and residues), the positive indirect effects of ERL policy are worth evaluating as well. This is why empirical studies based on panel data and econometric models are of use for discovering the indirect effects.

Figure 4 also describes a potential route that changes the health conditions. The ERL policy changed the industrial distribution where fewer eco-spaces were occupied; the environmental and ecological protection measures, which is another direct action that paralleled to industrial upgrading, would be taken to reduce the emission of hazardous substances.

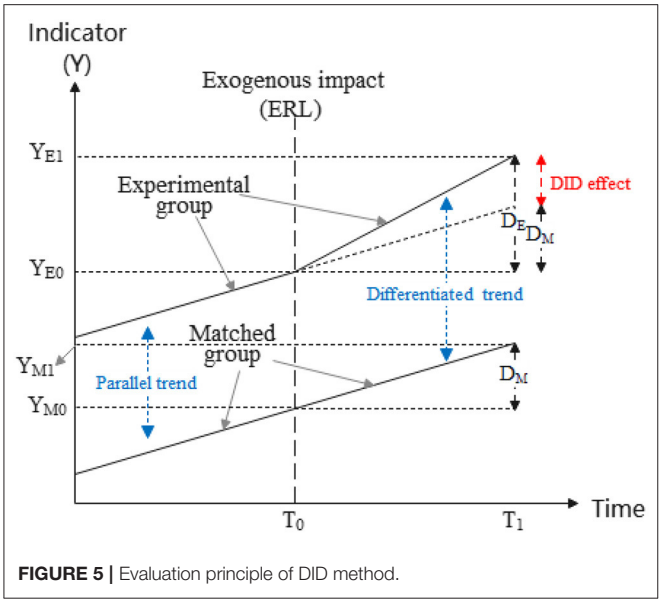

FIGURE 5 | Evaluation principle of DID method.

During these two direct reactions of the ERL, atmospheric environment and water quality would be improved as a result, food safety could be ensured, and more green technologies may contribute to the cleaner industrial production since then. Finally, the residents' health conditions could be promoted as a consequence of a cleaner ecological environment physically and psychologically, which can be seen as an indirect effect from the ERL as a whole. Hence, hypothesis 2 (H_2) is put forward as follows:

H_2: *The ERL policy can significantly improve the residents' health in the pilot provinces by reducing the number of disease-infected people.*

METHOD

Model Principle

The DID method is suitable for evaluating the trend differentiation of an object affected by an exogenous impact (e.g., A pilot policy), where the object can be a single entity or a group of individuals. Similar to a scientific experiment, the affected object can be identified as the experimental group or the treated group, whereas the other unaffected individuals can be regarded as the matched group or the controlled group, as shown in **Figure 5**.

The most critical concern is the trend differentiation of the indicators between the experimental group and the matched group after the exogenous impact. **Figure 5** labeled the indicator's variation of the experimental group as D_E, and that of the matched group as D_M, thus D_E and D_M can be calculated by a first-time difference as:

$$D_E = Y_{E1} - Y_{E0} = E(Y_{E1}|t = T_1) - E(Y_{E0}|t = T_0) \quad (1)$$

$$D_M = Y_{M1} - Y_{M0} = E(Y_{M1}|t = T_1) - E(Y_{M0}|t = T_0) \quad (2)$$

Where the T_0 and T_1 in (1) and (2) are the start time and the cut-off time for observation of the exogenous impact. Therefore, the DID effect that indicates the differentiated trend at the observation period (T_0-T_1) can be figured out by a second-time difference as:

$$DID\ effect = D_E - D_M \quad (3)$$

Besides, the prerequisite of a feasible DID estimation is that the experimental group and the matched group are sharing a common trend before the exogenous impact (39), that is, they have a parallel trend before T_0. Hence, the parallel trend test will be carried through after the empirical tests.

Empirical Model Specification

In this study, the implementation of the ERL pilot policy is treated as the exogenous impact, the experimental group consisted of the four pilot provincial units in China, which are Jiangsu, Hubei, Hainan, and Chongqing, whereas the matched group is composed of other provinces without ERL policy (even in city-level) before the cut-off time and have the regional homogeneities with the former. The implementation time T_0 is 2015 when the ERL pilot policy was put into effect, and the cut-off time T_1 of ERL is 2019 due to the dataset availability.

To estimate the industrial upgrading effect of the ERL pilot policy (verifying H_1), the DID models are set as:

$$ln\left(Tertiary_{it}\right) = \alpha + \beta \cdot (ELR_i \times Post_t) + \sum_{j=1}^{n} \left(\gamma_j \cdot Control_{it}\right) + \delta_i + \mu_t + \varepsilon_{it} \quad (4)$$

$$Update_{it} = \alpha + \beta \cdot (ELR_i \times Post_t) + \sum_{j=1}^{n} \left(\gamma_j \cdot Control_{it}\right) + \delta_i + \mu_t + \varepsilon_{it} \quad (5)$$

Where in model (4), the explained variable (dependent variable) $ln\left(Tertiary_{it}\right)$ indicates the logarithmic value of tertiary industry's output (production value of service sector) at province i in year t. The explained variable $Update_{it}$ in model (5) refers to the ratio of the tertiary industry's output to the secondary industry's output at province i in year t. Considering the industrial upgrading indexes are multitudinous but the tertiary industry is the core factor among all of them (40), its direct output value and its ratio value to the traditional secondary industry are both adopted to reflect the comprehensiveness of the empirical study. β is the estimated coefficient of this study's concern, as its significance will prove the effectiveness of the ERL policy, and its value will reflect its effect degree. The policy dummy variable ELR_i is a binary variable denote to whether the ERL policy had been executed in province i, where it takes the value 1 if the province i had executed ERL and takes zero otherwise. The time dummy variable $Post_t$ is also bivariate with 1 or 0, where it takes 1 when the pilot year of ERL begins (that is, $t \geq 2015$) and equals zero before that ($t < 2015$). The $Control_{jt}$ in the sum term are controlled variables that may have a relationship with the dependent variable but are unaffected

by the policy (41), consisting of the real estate investment [in logarithmic form as $\ln\left(Estate_{jt}\right)$] and the energy consumption [in logarithmic form as $\ln\left(Energy_{jt}\right)$] in model (4) and (5), as they serve as the normal contributions to industrial development in immense amounts (42).

The indirect effect is also worth estimating, that is, the health promotion of the residents in the pilot provinces. To estimate this indirect effect of ERL pilot policy, the DID model is set accordingly as:

$$ln\left(Disease_{it}\right) = \alpha+\beta\cdot\left(ELR_i\times Post_t\right)+\sum_{j=1}^{n}\left(\gamma_j\cdot Control_{it}\right) + \delta_i+\mu_t+\varepsilon_{it} \quad (6)$$

Where the dependent variable $ln(Disease_{it})$ in model (6) represents the logarithmic value of disease-infected people with their premarital examination at province i in year t, which is an indicator that delegates the residents' health. The controlled variables here are the number of health personnel [in logarithmic form as $ln\left(H.Personnel_{it}\right)$], and the total assets of medical and health organization [in logarithmic form as $ln\left(M.H.Asset_{jt}\right)$], considering that these two components can affect the dependent variable but has no relationship with the policy implemented (41, 43). The other coefficients and terms have the same meaning as those in model (4) or (5).

In consideration of the health data availability, the choice of the explained variable in model (6) can keep off the chronic disease primarily infected by the elders, which may bring the lagged elements or even deviations of the estimation results. As the newly-married people in China are mainly under 35, their health conditions can reflect the effects of the ecological environment much more explicitly. Moreover, the controlled group in model (4), (5) and (6) are all provincial units in China, but Liaoning Province is excluded as its capital city Shenyang is also the ERL pilot region. Finally, considering the inherent regional difference in four pilot provinces, each model will be estimated 5 times, including one merging effect and four individual effects on each of them.

Data Source and Descriptive Statistics of Variables

In this empirical study, the data in the model (4), (5) and (6) are all collected from the EPS China database website (44), where the statistics are all legally collected from the National Bureau of Statistics of China, National Health Commission of P.R.China, and National Energy Administration of China. **Table 1** presents the descriptive statistics of all the datasets to be analyzed.

All statistics above are panel data that are suitable for the econometrics regression analysis for model (4), (5) and (6), where 26.7% of them belong to the experimental group and the rest 73.3% are from the matched group.

RESULTS AND DISCUSSION

Estimation of Industrial Upgrading

Setting tertiary industry's output as the explained variable in model (4) and the ratio of tertiary industry's output to secondary industry's output in model (5), the DID estimation results of the ERL policy on industrial upgrading are shown in **Table 2**, where the overall effect among the four pilot provinces, and the individual effect on every single province, are all included[2].

In the mass, the results from **Table 2** indicate that the industrial upgrading effect brought by the ERL is effective but insufficient, as the output value of tertiary (*Tertiary*) industry has increased 0.033% by the reason of the EPR policy [in column (1-a)]. Moreover, the insignificant estimated coefficient in column (1-b) indicates that the ratio of tertiary industry's output to secondary industry's output (*Update*) has not been proved in connection with the ERL policy.

Moreover, the provincial-level results of industrial upgrading reveal the regional heterogeneity to a great extent, because the significances and values of their DID coefficients $\hat{\beta}$ have been varied by and large. The ERL policy has no significant effect in Jiangsu Province completely [see the $\hat{\beta}$ in column (2-a) and (2-b)], has a positive effect on *Tertiary* but negative on *Update* in Hubei [in (3-a), (3-b)]; for Hainan and Chongqing, both their *Update* terms are significantly related to the ERL but in the opposite direction [see (4-b) and (5-b)] and other indicators are insignificant [(4-a) and (5-a)], where Hainan's industrial upgrading ratio *Update* is positive and that of Chongqing is negative [(4-b) and (5-b)]. These differentiated results may reflect the different actions in each pilot province due to their own situations, which will be discussed further in 4.3.

In summary, the industrial upgrading effect of the ERL exists but with limitations, therefore hypothesis H_1 is only partially true.

Estimation of Health Promotion

In order to estimate the health promotion effect from the ERL policy, the number of disease-infected people with their premarital examination in model (6) is treated as the explained variable. The DID estimation results are listed in **Table 3** as follows.

In **Table 3**, each study object has been estimated twice, the results in columns (x-1) (x = 1, 2, 3, 4, 5) are the estimation results without the controlled variables in model (6), and in the columns (x-2) are with them. From the columns (1–1) and (1–2), we are able to find that the coefficient of the DID term ($\hat{\beta}$) is statistically significant, and the significance level is improved to 5% level when the controlled variables have been reckoned in. If the controlled variables are unconsidered, the ERL policy can bring the reduction of −0.793% on the number of sick people in four pilot provinces on the whole; if considered, it can markedly reduce 1.029% of the people detected sickness generally. Compared with the industrial upgrading effect, the health promotion effect of the ERL is much higher both in significance and magnitude.

Besides the overall ERL effect, its effects on each pilot province are listed in the rest of the columns in **Table 3**.

[2]Considering the table space and secondary status, the estimation results without the controlled variables for model (4) and (5) are moved into the **Supplementary Material**.

TABLE 1 | Descriptive statistics of variables.

Variable	Obs	Mean	Std	Min	Median	Max	Unit
DID = ERL × post	150	0.133	0.341	0.000	0.000	1.000	–
Tertiary	150	930.868	866.150	56.740	725.190	5,085.210	Billion CNY
Update	150	1.157	0.393	0.527	1.098	2.923	–
Estate	150	3.88×10^6	1.08×10^7	108.19	3,057.38	5.67×10^7	100 million CNY
Energy	150	1.35×10^4	7,540.005	1,358.507	1.26×10^4	3.25×10^4	Million ton of standard coal
Disease	150	21,463.520	26,644.912	9.000	7,050.500	1.09×10^5	Person-time
H.Personnel	150	342.351	212.536	35.224	291.936	887.78	Thousand people
M.H.Asset	150	10,740.763	7,686.491	727.686	9,030.770	35,246.375	Billion CNY

TABLE 2 | Policy estimation results of industrial upgrading.

Explained variable	Overall *ln (Tertiary)* (1-a)	Overall *Update* (1-b)	Jiangsu *ln (Tertiary)* (2-a)	Jiangsu *Update* (2-b)	Hubei *ln(Tertiary)* (3-a)
$DID = ERL_i \times post_t$ ($\hat{\beta}$ =)	0.033* (1.95)	0.027 (0.67)	0.003 (0.10)	−0.048 (−0.93)	0.066** (2.06)
ln(Estate) ($\hat{\gamma}_1$ =)	0.104** (6.03)	−0.014 (−0.33)	0.102*** (5.43)	−0.015 (−0.631)	0.108*** (2.90)
ln(Energy) ($\hat{\gamma}_2$ =)	−0.174 (−3.31)	−0.281** (−2.17)	−0.164** (−2.62)	−0.734*** (−6.92)	−0.189*** (−3.00)
Constant ($\hat{\alpha}$ =)	9.217*** (15.39)	4.293*** (2.92)	9.210*** (12.78)	9.515*** (7.80)	9.373*** (13.01)
Time fixed effects	Yes	Yes	Yes	Yes	Yes
Region fixed effects	Yes	Yes	Yes	Yes	Yes
Observations	150	150	120	120	120
R^2	0.987	0.762	0.985	0.855	0.986
Explained variable	**Hubei *Update* (3-b)**	**Hainan *ln (Tertiary)* (4-a)**	**Hainan *Update* (4-b)**	**Chongqing *ln (Tertiary)* (5-a)**	**Chongqing *Update* (5-b)**
$DID = ERL_i \times post_t$ ($\hat{\beta}$ =)	−0.112** (−2.08)	0.032 (0.99)	0.424*** (6.47)	0.026 (0.81)	−0.215*** (−3.85)
Ln (Estate) ($\hat{\gamma}_1$ =)	−0.015 (−0.48)	0.104*** (5.51)	−0.020 (−0.52)	0.105*** (5.54)	−0.017** (−0.53)
Ln (Energy) ($\hat{\gamma}_2$ =)	−0.724*** (−6.87)	−0.162* (−2.54)	−0.664*** (−5.18)	−0.171*** (−2.75)	−0.693*** (−6.39)
Constant ($\hat{\alpha}$ =)	9.365*** (7.76)	8.834*** (12.37)	8.683*** (6.02)	9.141*** (12.89)	9.008*** (7.29)
Time fixed effects	Yes	Yes	Yes	Yes	Yes
Region fixed effects	Yes	Yes	Yes	Yes	Yes
Observations	120	120	120	120	120
R^2	0.856	0.985	0.837	0.986	0.843

****, **, and * means the statistical significance is at the 1, 5, and 10% accuracy level. The values in the brackets are the t statistics for each regression.*

The results show that the ERL policy is thoroughly effective in Jiangsu Province and Hainan Province (as their DID coefficients $\hat{\beta}$ are significant in both two regressions), and is even larger in degree for them (their absolute values of $\hat{\beta}$ are larger than the overall's). However, in Chongqing Municipality, the ERL is effective to a limited degree because only column (5-1) appears significant. Hubei Province is thoroughly uninfluenced by the ERL as its insignificant results with or without the controlled variables [(3-1) and (3-2)]. Upon the results above, hypothesis H_2 is basically true except for the Hubei province.

Discussion on the Estimation Results

From the results of the health promotion effect in 4.2, the ERL policy shows a homogeneous favorable effect among the

TABLE 3 | Policy estimation results of health promotion.

Explained variable	Overall (1-1)	Overall (1-2)	Jiangsu (2-1)	Jiangsu (2-2)	Hubei (3-1)
$DID = ERL_i \times post_t$ ($\hat{\beta}$ =)	−0.793* (−2.07)	−1.029** (−2.72)	−1.063* (−4.40)	−1.319** (−2.37)	−0.061 (−0.25)
Ln (H.Personnel) ($\hat{\gamma}_1$ =)	–	4.391*** (3.47)	–	4.474** (2.89)	–
Ln (M.H.Asset) ($\hat{\gamma}_2$ =)	–	−0.191 (−0.11)	–	0.065 (0.03)	–
Constant ($\hat{\alpha}$ =)	7.830*** (51.68)	−43.970** (16.952)	7.636*** (27.09)	−48.367** (−2.53)	7.449*** (26.90)
Time fixed effects	Yes	Yes	Yes	Yes	Yes
Region fixed effects	Yes	Yes	Yes	Yes	Yes
Observations	150	150	120	120	120
R^2	0.414	0.469	0.456	0.517	0.482
Explained variable	**Hubei (3-2)**	**Hainan (4-1)**	**Hainan (4-2)**	**Chongqing (5-1)**	**Chongqing (5-2)**
$DID = ERR_i \times post_t$ ($\hat{\beta}$ =)	−0.189 (−0.89)	−1.544*** (−6.39)	−1.671*** (−0.88)	−0.503* (−2.08)	−0.946 (−4.34)
ln(H.Personnel) ($\hat{\gamma}_1$ =)	5.094** (2.90)	–	4.968** (3.08)	–	4.830** (2.92)
ln(M.H.Asset) ($\hat{\gamma}_2$ =)	−0.360 (−0.17)	–	−0.369 (−0.17)	–	−0.338 (−0.15)
Constant ($\hat{\alpha}$ =)	−51.540** (−2.54)	7.474*** (26.66)	0.275*** (17.09)	7.385*** (26.70)	−48.285** (−2.54)
Time fixed effects	Yes	Yes	Yes	Yes	Yes
Region fixed effects	Yes	Yes	Yes	Yes	Yes
Observations	120	120	120	120	120
R^2	0.553	0.449	0.515	0.473	0.537

****, **, and * means the statistical significance is at the 1, 5, and 10% accuracy level. The values in the brackets are the t statistics for each regression.*

three out of four pilot provinces, which means the residents' health conditions can largely benefit from this ecological conservation policy. However, Hubei is the only unaffected province on health promotion, this is perhaps because the scale of its secondary industry was still ramping up rapidly rather than being controlled steadily, as its output value showed an average of 8.4% annual growth rate in 2016–2019, higher than that of 6.9, 5.3, and 6.9% in Jiangsu, Hainan and Chongqing (data source: National Bureau of Statistics of China). In fact, Hubei province has indeed introduced considerable chemical industries in the recent 10 years (45, 46), which may serve as a "pollution haven" for the eastern coastal areas which are seeking the relocation of the pollution-intensive industries.

Considering the lower development level in the Midwest, the urgency and the execution strength of the ecological protection there might give way to the economic growth and employment rate, where the manufacturing industry can bring them straightaway. In view of the bigger environmental capacity in terms of freshwater resources and land space, the Midwest has larger intake carrier space for the industry expansion. This implies that the ERL policy may play a role in industrial relocation from East to Midwest, and the results in 4.1 reinforce this view, where the industrial upgrading for Hubei and Chongqing are negatively affected by the ERL policy [see column (3-b) and (5-b) in **Table 2**], manifesting the ERL have enlarged their proportion of secondary industry.

Hainan province has benefited most from the ERL policy, as its health promotion degree and industrial upgrading degree are both the highest compared to the other three provinces. Two factors may explain this: one is that Hainan is an island province where the existing scale of the secondary industry is fairly less, its output value was equivalent to 2.6% of the Jiangsu and 6.5% of Hubei in 2015, bringing about much smaller inertia in industrial transformation; another is the stricter environmental rules in Hainan compared with mainland provinces, as Hainan has long been famous of the tourism, incurring more prohibitions on resource exploitation.

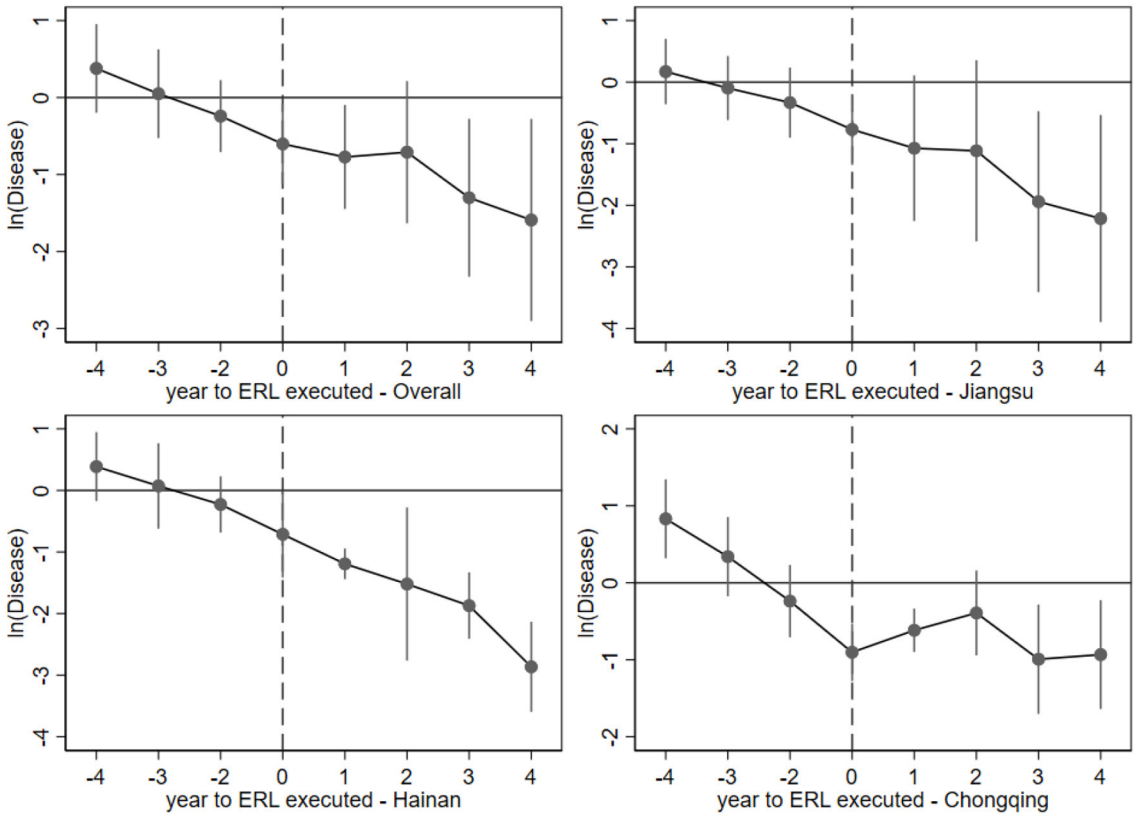

FIGURE 6 | Parallel trend test results.

ROBUSTNESS TEST AND DYNAMIC EFFECT

Parallel Trend Test

As mentioned in 3.1, a critical precondition of a practicable DID estimation is that the experimental group and the matched groups are sharing a similar parallel trend before 2015, the year of the policy implementation. Model (6) has shown effective results whose robustness is worth verifying. To verify the parallel trend before the year of ERL's implementation, I select 2014 (one year before 2015) as the base period, then generate the interaction terms of the time dummy variable and the experimental group. If the coefficients of these interactions are not significantly negative before the time of the exogenous impact, then the DID estimation passes the parallel trend test (33, 47, 48).

By referring to the existing studies (34, 37, 49, 50), an event study model to conduct the parallel trend test of ERL policy can be set as follows:

$$ln\left(Disease_{it}\right) = \alpha + \sum_{k\geq -4, k\neq -1}^{4} \beta_k \cdot D_{it}^{k} + \sum_{j}^{n} \gamma_j \cdot Control_{it} + \delta_i + \mu_t + \varepsilon_{it} \quad (7)$$

Compared with single a DID term $\beta \cdot (ELR_i \times Post_t)$ in model (6), the second term in model (7) is changed into a sum term where a binary variable D_{it}^{k} is set to signify the ERL policy, where k $(-4 \leq k \leq 4)$ delegates the year distance to 2015 at year t. D_{it}^{k} equals 1 only if the individual i is the ERL pilot province and $k = t - 2015$, otherwise $D_{it}^{k} = 0$ (D_{it}^{-1} is not exist because 2014 is set as the base year). The other variables and coefficients are set the same as with that in the model (6).

Using the same dataset in model (6), the result of the parallel trends test is plotted in **Figure 6**, where the year 2014 has been dropped because of the inexistence of D_{it}^{-1}, and Hubei province is untested because of its insignificant results in 4.2.

Knowing from **Figure 6**, the coefficients of the DID term in the event study are around zero before the ERL implementation year, and their 95% confidence interval (the vertical solid lines) covers value zero, which means they cannot reject the null hypothesis and can be zero. Hence, the pre-policy coefficients are basically statically insignificantly, while the coefficients after the ERL execution year are mainly negative and free from the null hypothesis. Based on the outcome of the event study, the DID model (6) conforms to the parallel trend, and it effectively proved that the ERL policy has reduced the number of diseases tested after 2015.

Dynamic Effect Estimation

Although 4.1 has proved the fundamental effectiveness of the ERL policy in general and in three of the four

TABLE 4 | ERL's dynamic effect on health promotion.

Explained variable	Overall (1)	Jiangsu (2)	Hainan (3)	Chongqing (4)
$ERL_i \times Post_{2015}$	−0.603**	−0.769**	−0.713**	−0.903***
$(\hat{\beta}_0 =)$	(−2.49)	(−2.94)	(−2.24)	(−5.32)
$ERL_i \times Post_{2016}$	−0.773**	−1.073*	−1.192***	−0.617***
$(\hat{\beta}_1 =)$	(−2.45)	(−2.00)	(−10.57)	(−4.82)
$ERL_i \times Post_{2017}$	−0.710	−1.114	−1.520**	−0.392
$(\hat{\beta}_2 =)$	(−1.65)	(−1.67)	(−2.69)	(−1.56)
$ERL_i \times Post_{2018}$	−1.302**	−1.941**	−1.871***	−0.993**
$(\hat{\beta}_3 =)$	(−2.72)	(−2.91)	(−7.63)	(−3.08)
$ERL_i \times Post_{2019}$	−1.591**	−2.215**	−2.864***	−0.933**
$(\hat{\beta}_4 =)$	(−2.60)	(−0.29)	(−8.61)	(−2.91)
Ln (H.Personnel)	4.496***	4.812**	4.899**	4.918**
$(\hat{\gamma}_1 =)$	(3.19)	(2.76)	(2.76)	(2.75)
ln(M.H.Asset)	−0.253	−0.162	−0.297	−0.347
$(\hat{\gamma}_2 =)$	(−0.14)	(−0.07)	(−0.13)	(−0.15)
Constant	−44.591**	−50.088**	−49.051**	−49.273**
$(\hat{\alpha} =)$	(−2.50)	(−2.46)	(−2.45)	(−2.46)
Time fixed effects	Yes	Yes	Yes	Yes
Region fixed effects	Yes	Yes	Yes	Yes
Observations	150	120	120	120
R^2	0.498	0.535	0.544	0.546

****, **, and * means the statistical significance is at the 1%, 5%, and 10% accuracy level. The values in the brackets are the t statistics for each regression.*

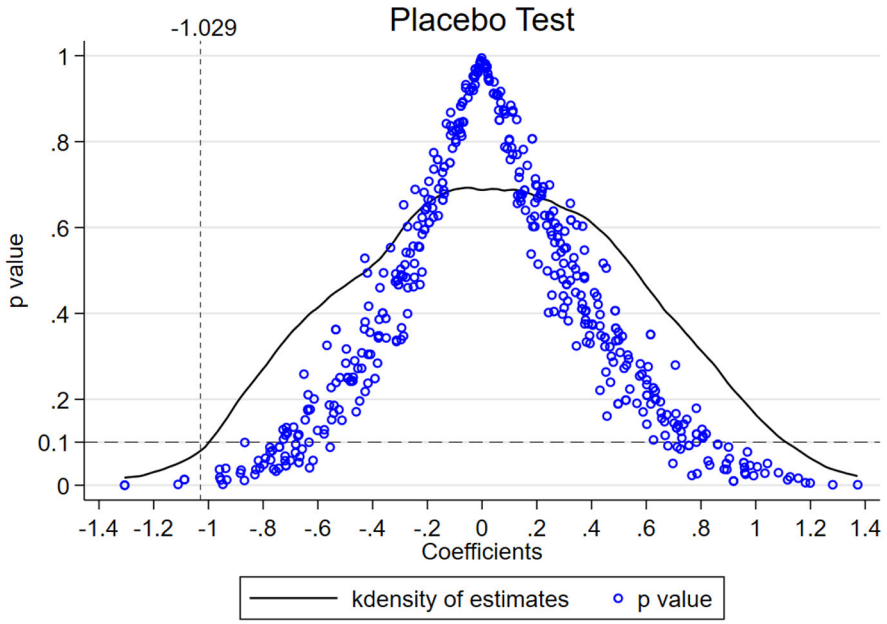

FIGURE 7 | Placebo test result of DID model.

pilot provinces, a time heterogeneity may exist among differently treated individuals. In other words, in the observation period 2015–2019, the significance and the magnitude of the health promotion effect may be varied among them. For a better understanding of the policy dynamic effect, the event study model (7) with its graphical results **Figure 6** can provide a table of ERL's yearly impact below.

From the yearly DID estimation result displayed in **Table 4**, the overall and individual dynamic effects brought by the ERL policy are quantified. As the outcome of the overall test [column (1)], two coastal provinces, Jiangsu and Hainan [column (2)

and (3)], present a similar dynamic effect of strengthening year by year. In contrast, the yearly coefficients for the inland Chongqing municipality show a slight inverted-V tendency after the ERL's execution year, indicating the health promotion effect may come into steady there. Moreover, the absolute values of the Chongqing's coefficients [column (4)] are all less than one, indicating that the magnitude of the ERL's health effect in Chongqing is also smaller.

Placebo Test

Another indispensable precondition of the DID model's effectiveness is the irreplaceability of the exogenous policy, which means the policy cannot affect the non-experimental individuals significantly and the explained variables are not affected by other unobserved variables (51, 52). This irreplaceability can be verified by a placebo test, the multiple assumptive tests where the individuals from the experimental group are substituted randomly by other non-experimental individuals (29). If the assumptive DID coefficients are distributed around zero (fail to reject the null-hypothesis) and most of their *p*-values are larger than 0.1 (fail to show the significance), then the placebo test is passed. To verify the irreplaceability of the ERL policy in model (6), a placebo test where the random process has been repeated 500 times is given, receiving the result in **Figure 7**.

Figure 7 plots the outcome of the placebo test, where the solid curve is the kernel density of the assumptive DID coefficients and the small circles are their *p*-values. Besides, −1.029 is the real DID coefficient estimated in **Table 3**, the *p*-value 0.1 denotes 10% of the significance level. Obviously, the coefficients in the placebo test are approximately in normal distribution around zero, and their *p*-values are basically larger than the 0.1, which means most of the assumptive estimations are insignificant and cannot reject the null hypnosis. Hence, the placebo test of the DID model (6) proves the robustness of the ERL's effects on health promotion.

CONCLUSIONS

Although the policy of Ecological Red Lines (ERL) has reached some achievements, China would step up to utilize and expand the measures from it, including finalizing the regulations of environmental protections, perfecting the bottom lines for the ecological protections, and setting the ceilings of the resource exploitations. The industrial structure could also be upgraded by the innovation of green technologies or reasonable industrial policies, such as reinforcing the market negative list approach or setting the market-entry lists. The ERL policy is only one of China's policy mix in confronting environmental pollution, limiting harmful emissions, and achieving climate change targets. However, as a pilot policy, the ERL has indeed provided foundations for further climatic environment actions, such as Environmental protection tax law[3], or Carbon Peak in 2030 and Carbon Neutrality in 2060[4], which inherits and enlarges the concept of the eco-environmental protection.

This paper is devoted to evaluating a direct and an indirect effect brought by the Ecological Red Lines (ERL) policy implemented in four pilot provinces of China in 2015. By applying DID method, the direct effect indicated by the industrial upgrading is small (0.033% of the tertiary's output value) and even showed a negative effect on the inland Midwest provinces. The indirect effect which is indicated by the residents' health is generally at a much larger degree, as 1.029% of the residents' health conditions have been significantly improved. Moreover, the event study reveals that the ERL policy's effect on health promotion is increasing year by year as a whole, indicating its sustainability and cumulative achievements.

When decomposing the DID estimation into every single pilot province, the result of the industrial upgrading effect manifests a great heterogeneity among them, while the result of the health promotion effect turns out to be a favorable homogeneity. These differentiated outcomes indicate that most of the pilot provinces can reduce the adverse impact on people's health during the industrial restructuring, regardless of the change direction of tertiary industry's ratio. However, as the secondary industry has been expanded in the inland Midwest pilot provinces, the ERL policy may tend to be a cause of industrial relocation rather than reconstitution. Some negative signs have occurred in the Midwest regions: Hubei has not benefited from the health promotion effect significantly, Chongqing has benefited but has a fluctuant lasting effect compared to the two coastal pilot provinces which have shown incremental effects. The transference of the secondary industries from Eastern China to the Midwest may explain this, but more incisive provincial-level research on interregional industry relocations is needed in the future.

For the deficiencies of this study, the missed analysis of Shenyang City is first, which needs to be evaluated in the future city-level studies of the ERL in the future works. The possible incomplete selections of the explained variables may be another, as the environmental indicators are extensive and need more elaborate studies, which requires more comprehensive studies in further studies on the ERL. Moreover, the combined effects of the ERL policy and other environmental policies such as "Action Plan of Air Pollution Prevention and control" have not been embodied in this paper, which can be verified with derivative measurement models in future works, such as triple difference (DDD) models. In addition to this, the ERL may have a spillover effect on the adjacent regions out of the pilot places, future research may detect this effect with spatial econometrics.

Based on the above conclusions, some constructive suggestions can be given as: (1) For the economically developed and densely populated eastern coastal regions, the cover range of the ERL policy can be extended; (2) For the inland Midwest regions with the lagging stage of economic development, some eco-compensation measures should be taken if the ecological protection policies are strict; (3) To maintain an eco-friendly sustainable development without ignoring the development

[3] *Environmental Protection Tax Law of P.R. China*. Available online at: http://www.gov.cn/zhengce/content/2017-12/30/content_5251797.htm (accessed December 30, 2017).

[4] *The Guidelines on Full Implementation Works on the Idea of Development for Peaking Carbon and Carbon Neutrality*. Available online at: http://www.gov.cn/zhengce/content/2017-12/30/content_5251797.htm (accessed October 24, 2021).

demands, some flexible methods are recommended, such as improving green productivity for manufacturing, building ecological protection facilities for waste treatment, and planning reasonable residence zones for the people's health; (4) In view of the heterogeneous effects between coastal and inland regions of the ERL' trial implementation, some distinct protective or restrictive measures are essential, which may be better for the development needs of the less advanced regions. (5) Balancing ecological protection and economic growth is still a dilemma for developing regions, and a "one-size-fits-all" solution is inexistent, therefore, moderate and continuable strategical steps are of the essence, such as the long-term investments of green technologies, reasonable fiscal subsidies on industrial transformations, and the capitalization of the natural resources. Finally, the modifiability and the transparency of the long-run development of the ERL policy is the basic guarantee of sustainable development in all aspects of society.

DATA AVAILABILITY STATEMENT

The original contributions presented in the study are included in the article/**Supplementary Material**, further inquiries can be directed to the corresponding author/s.

AUTHOR CONTRIBUTIONS

PY: conceptualization, project administration, data acquisition, methodology, formal analysis, writing—original draft, and writing—review and editing.

FUNDING

This research is funded by Hainan University Research Start-up Fund.

SUPPLEMENTARY MATERIAL

The Supplementary Material for this article can be found online at: https://www.frontiersin.org/articles/10.3389/fpubh.2022.844593/full#supplementary-material

REFERENCES

1. Capozzi V, Fragasso M, Bimbo F. Microbial resources, fermentation and reduction of negative externalities in food systems: patterns toward sustainability and resilience. *Ferment Basel.* (2021) 7:54. doi: 10.3390/fermentation7020054
2. Öztürk A, Turker M, Pak M. Economic valuation of externalities linked to Turkish forests. *Afric J Agric Res.* (2009) 4:1251–9.
3. Li J, Yu L. Double externalities, market structure and performance: an empirical study of Chinese unrenewable resource industries. *J Clean Prod.* (2016) 126:299–307. doi: 10.1016/j.jclepro.2016.03.048
4. Selden TM, Song D. Environmental quality and development: is there a kuznets curve for air pollution emissions? *J Environ Econ Manag.* (1994) 27:147–62. doi: 10.1006/jeem.1994.1031
5. Grossman GB, Krueger A. Economic growth and the environment. *Quart J Econ.* (1995) 110:353–77. doi: 10.2307/2118443
6. Gill AR, Viswanathan KK, Hassan S. The environmental kuznets curve (EKC) and the environmental problem of the day. *Renew Sust Energ Rev.* (2018) 81:1636–42. doi: 10.1016/j.rser.2017.05.247
7. *The State of the World's Land and Water Resources for Food and Agriculture: Systems at Breaking Point. Synthesis Report*. Food and Agriculture Organization of the United Nations (FAO), Rome (2021).
8. *South Africa Sets up a Sound Ecological Environmental Protection Mechanism. China Policy Research Network*. Available online at: http://www.zgzcinfo.cn/government/show-1770.html (accessed August 22, 2018).
9. Souza-Cruz-Buenaga FVA, Espig SA, Castro TLC, Santos MA. Environmental impacts of a reduced flow stretch on hydropower plants. *Brazil J Biol.* (2019) 79:470–87. doi: 10.1590/1519-6984.183883
10. Kirkman SP, Mann BQ, Sink KJ, Adams R, Livingstone TC, Mann-Lang JB, et al. Evaluating the evidence for ecological effectiveness of South Africa's marine protected areas. *Afric J Marine Sci.* (2021) 43:389–412. doi: 10.2989/1814232X.2021.1962975
11. Jia S, Li Y, Lü A, Liu W, Zhu W, Yan J, et al. City storm-flood events in China, 1984–2015. *Int J Water Res Dev.* (2019) 35:605–18. doi: 10.1080/07900627.2018.1513830
12. Tao M, Chen L, Wang Z, Wang J, Tao J, Wang X. Did the widespread haze pollution over China increase during the last decade? A satellite view from space. *Environ Res Lett.* (2016) 11:054019. doi: 10.1088/1748-9326/11/5/054019
13. Yu X, Wang Z, Zhang H, Zhao S. Impacts of different types and intensities of El Niño events on winter aerosols over China. *Sci Total Environ.* (2019) 655:766–80. doi: 10.1016/j.scitotenv.2018.11.090
14. Chou L, Dai J, Qian X, Karimipour A, Zheng X. Achieving sustainable soil and water protection: the perspective of agricultural water price regulation on environmental protection. *Agric Water Manag.* (2021) 245:106583. doi: 10.1016/j.agwat.2020.106583
15. Wang M, Webber M, Finlayson B, Barnett J. Rural industries and water pollution in China. *J Environ Manag.* (2008) 86:648–59. doi: 10.1016/j.jenvman.2006.12.019
16. Xu X, Tan Y, Yang G, Barnett J. China's ambitious ecological red lines. *Land Use Policy.* (2018) 79:447–51. doi: 10.1016/j.landusepol.2018.08.037
17. *China's Ecological Red Lines Experience is Recommended, What Are the Advantages? Detailed Explanation by Experts From the Ministry of Ecology and Environment*. Available online at: https://www.bjnews.com.cn/detail/163118288214699.html (accessed September 09, 2021).
18. *Technical Guide for Delimiting Ecological Protection Red Lines*. (2015). Available online at: https://www.mee.gov.cn/gkml/hbb/bwj/201505/t20150518_301834.htm (accessed May 08, 2015).
19. Jin W, Lin W. Ecological red lines: the national policy high-tension lines and the ecological security baselines in China. (2016) 25:3587–94.
20. Si Q, Li MC, Zhang GY, Liang SX, Sun ZC. Pilot study on delimited method of marine regional ecological red line. *Adv Mat Res.* (2013) 807-809:728–31. doi: 10.4028/www.scientific.net/AMR.807-809.728
21. Lu W-H, Liu J, Xiang X-Q, Song W-L, McIlgorm A. A comparison of marine spatial planning approaches in China: marine functional zoning and the marine ecological red line. *Marine Policy.* (2015) 62:94–101. doi: 10.1016/j.marpol.2015.09.004
22. He P, Gao J, Zhang W, Rao S, Zou C, Du J, et al. China integrating conservation areas into red lines for stricter and unified management. *Land Use Policy.* (2018) 71:245–8. doi: 10.1016/j.landusepol.2017.11.057
23. Angrist JD, Imbens GW, Rubin DB. Identification of causal effects using instrumental variables. *J Am Stat Assoc.* (1996) 91:444–55. doi: 10.1080/01621459.1996.10476902
24. Heckman JJ, Ichimura H, Todd PE. Matching as an econometric evaluation estimator: evidence from evaluating a job training programme. *Rev Eco Studies.* (1997) 64:605–54. doi: 10.2307/2971733
25. Hahn J, Todd P, van der Klaauw W. *Evaluating the Effect of an Antidiscrimination Law Using a Regression-Discontinuity*

Design. Cambridge: National Bureau of Economic Research, Inc. (1999).
26. Choi JY, Lee MJ. Regression discontinuity: review with extensions. *Stat Papers*. (2017) 58:1217–46. doi: 10.1007/s00362-016-0745-z
27. Abadie A, Gardeazabal J. The economic costs of conflict: a case study of the Basque Country. *Am Eco Rev*. (2003) 93:113–32. doi: 10.1257/000282803321455188
28. Doudchenko NG. Balancing, regression, difference-in-differences and synthetic control methods: a synthesis. National Bureau of Economic Research (2017) 22791:1–35. doi: 10.3386/w22791
29. Abadie A, Cattaneo MD. Econometric methods for program evaluation. *Ann Rev Eco*. (2018) 10:465–503. doi: 10.1146/annurev-economics-080217-053402
30. Ashenfelter O. Estimating the effect of training programs on earnings. *Rev Eco Stat*. (1978) 60:47–57. doi: 10.2307/1924332
31. Heckman JJ, Robb R. Alternative methods for evaluating the impact of interventions: an overview. *J Eco*. (1985) 30:239–7. doi: 10.1016/0304-4076(85)90139-3
32. Heckman JJ, Robb R. Alternative methods for solving the problem of selection bias in evaluating the impact of treatments on outcomes. In: Wainer H, editor. *Drawing Inferences From Self-Selected Samples*. New York, NY: Springer New York (1986). p. 63–107.
33. Greenstone M, Hanna R. Environmental regulations, air and water pollution, and infant mortality in india [Article]. *Am Eco Rev*. (2014) 104:3038–72. doi: 10.1257/aer.104.10.3038
34. Lin Y, Qin Y, Wu J, Xu M. Impact of high-speed rail on road traffic and greenhouse gas emissions. *Nat Climate Change*. (2021) 11:952–957. doi: 10.1038/s41558-021-01253-w
35. Nunn N, Qian N. The potato's contribution to population and urbanization: Evidence from a historical experiment. *Q J Econ*. (2011) 126:593–650. doi: 10.1093/qje/qjr009
36. Dimick JB, Ryan AM. Methods for evaluating changes in health care policy: the difference-in-differences approach. *JAMA*. (2014) 312:2401–2. doi: 10.1001/jama.2014.16153
37. Agüero JM, Beleche T. Health shocks and their long-lasting impact on health behaviors: evidence from the 2009 H1N1 pandemic in Mexico. *J Health Eco*. (2017) 54:40–55. doi: 10.1016/j.jhealeco.2017.03.008
38. Yumin L, Shiyuan L, Ling H, Ziyi L, Yonghui Z, Li L, et al. The casual effects of COVID-19 lockdown on air quality and short-term health impacts in China. *Environ Poll*. (2021) 290:117988. doi: 10.1016/j.envpol.2021.117988
39. Meyer BD. Natural and quasi-experiments in economics. *J Busin Eco Stat*. (1995) 13:151–61. doi: 10.1080/07350015.1995.10524589
40. Li K, Lin B. Economic growth model, structural transformation, and green productivity in China. *Appl Energy*. (2017) 187:489–500. doi: 10.1016/j.apenergy.2016.11.075
41. Pippel G, Seefeld V. R&D cooperation with scientific institutions: a difference-in-difference approach. *Econ Innov N Technol*. (2016) 25:455–69. doi: 10.1080/10438599.2015.1073480
42. He P, Liang J, Qiu Y, Li Q, Xing B. Increase in domestic electricity consumption from particulate air pollution. *Nat Energy*. (2020) 5:985–95. doi: 10.1038/s41560-020-00699-0
43. Ye P, Xia S, Xiong Y, Liu C, Li F, Liang J, et al. Did an ultra-low emissions policy on coal-fueled thermal power reduce the harmful emissions? Evidence from three typical air pollutants abatement in China. *Int J Environ Res Public Health*. (2020) 17:8555. doi: 10.3390/ijerph17228555
44. *EPS China Data*. Available online at: http://www.epschinadata.com/ (accessed date November 28, 2021).
45. *Environmental Inspectors Paint Damning Picture of Provincial Failings*. Available online at: https://www.caixinglobal.com/2019-05-13/environmental-inspectors-paint-damning-picture-of-provincial-failings-101415270.html (accessed May 13, 2019).
46. *Central Environmental Inspector: Yangtze River Protection in Hubei Still Has Shortcomings, the Layout Adjustment of Chemical Industries Are Not in Place*. Available online at: https://science.caixin.com/2021-12-14/101817655.html (accessed December 14, 2021).
47. Abadie A. Semiparametric difference-in-differences estimators. *Rev Eco Studies*. (2005) 72:1–19. doi: 10.1111/0034-6527.00321
48. Houngbedji K. Abadie's semiparametric difference-in-differences estimator. *Stata J*. (2016) 16:482–90. doi: 10.1177/1536867X1601600213
49. Goodman-Bacon A. Difference-in-differences with variation in treatment timing. *J Eco*. (2021) 225:254–77. doi: 10.1016/j.jeconom.2021.03.014
50. Liu X, Ji Q, Yu J. Sustainable development goals and firm carbon emissions: evidence from a quasi-natural experiment in China. *Energy Eco*. (2021) 103:105627. doi: 10.1016/j.eneco.2021.105627
51. Lee M-J, Kang C. Identification for difference in differences with cross-section and panel data. *Eco Lett*. (2006) 92:270–6. doi: 10.1016/j.econlet.2006.03.007
52. Heckman JJ, Sedlacek G. Heterogeneity, aggregation, and market wage functions: an empirical model of self-selection in the labor market. *J Polit Eco*. (1985) 93:1077–125. doi: 10.1086/261352

Conflict of Interest: The author declares that the research was conducted in the absence of any commercial or financial relationships that could be construed as a potential conflict of interest.

Publisher's Note: All claims expressed in this article are solely those of the authors and do not necessarily represent those of their affiliated organizations, or those of the publisher, the editors and the reviewers. Any product that may be evaluated in this article, or claim that may be made by its manufacturer, is not guaranteed or endorsed by the publisher.

frontiers in Public Health

ORIGINAL RESEARCH
published: 09 March 2022
doi: 10.3389/fpubh.2022.843862

Exploring the Spatiotemporal Evolution and Socioeconomic Determinants of PM2.5 Distribution and Its Hierarchical Management Policies in 366 Chinese Cities

Minli Zhu[1], *Jinyuan Guo*[2], *Yuanyuan Zhou*[2] *and Xiangyu Cheng*[3]*

[1] School of Criminal Justice, Zhongnan University of Economics and Law, Wuhan, China, [2] School of Information and Safety Engineering, Zhongnan University of Economics and Law, Wuhan, China, [3] The Co-innovation Center for Social Governance of Urban and Rural Communities in Hubei Province, Zhongnan University of Economics and Law, Wuhan, China

From 2013 to 2017, progress has been made by implementing the *Air Pollution Prevention and Control Action Plan*. Under the background of the *3 Year Action Plan to Fight Air Pollution* (2018–2020), the pollution status of PM2.5, a typical air pollutant, has been the focus of continuous attention. The spatiotemporal specificity of PM2.5 pollution in the Chinese urban atmospheric environment from 2018 to 2020 can be summarized to help conclude and evaluate the phased results of the battle against air pollution, and further, contemplate the governance measures during the period of the 14th Five-Year Plan (2021–2025). Based on PM2.5 data from 2018 to 2020 and taking 366 cities across China as research objects, this study found that PM2.5 pollution has improved year by year from 2018 to 2020, and that the heavily polluted areas were southwest Xinjiang and North China. The number of cities with a PM2.5 concentration in the range of 25–35 $\mu g/m^3$ increased from 34 in 2018 to 86 in 2019 and 99 in 2020. Moreover, the spatial variation of the PM2.5 gravity center was not significant. Concretely, PM2.5 pollution in 2018 was more serious in the first and fourth quarters, and the shift of the pollution's gravity center from the first quarter to the fourth quarter was small. Global autocorrelation indicated that the space was positively correlated and had strong spatial aggregation. Local Moran's I and Local Geti's G were applied to identify hotspots with a high degree of aggregation. Integrating national population density, hotspots were classified into four areas: the Beijing–Tianjin–Hebei region, the Fenwei Plain, the Yangtze River Delta, and the surrounding areas were selected as the key hotspots for further geographic weighted regression analysis in 2018. The influence degree of each factor on the average annual PM2.5 concentration declined in the following order: (1) the proportion of secondary industry in the GDP, (2) the ownership of civilian vehicles, (3) the annual grain planting area, (4) the annual average population, (5) the urban construction land area, (6) the green space area, and (7) the per capita GDP. Finally, combined with the spatiotemporal distribution of PM2.5, specific suggestions were provided for the classified key hotspots (Areas A, B, and C), to provide preliminary ideas and countermeasures for PM2.5 control in deep-water areas in the 14th Five-Year Plan.

Keywords: air pollution, city, spatiotemporal specificity, driving factors, environmental policy

OPEN ACCESS

Edited by:
Hongtao Yi,
The Ohio State University, United States

Reviewed by:
Zaiyang Ma,
Nanjing Normal University, China
Tanvir Ahmed,
Bangladesh University of Engineering and Technology, Bangladesh

***Correspondence:**
Xiangyu Cheng
xiangyucheng@zuel.edu.cn

Specialty section:
This article was submitted to Environmental health and Exposome, a section of the journal Frontiers in Public Health

Received: *27 December 2021*
Accepted: *02 February 2022*
Published: *09 March 2022*

Citation:
Zhu M, Guo J, Zhou Y and Cheng X (2022) Exploring the Spatiotemporal Evolution and Socioeconomic Determinants of PM2.5 Distribution and Its Hierarchical Management Policies in 366 Chinese Cities. Front. Public Health 10:843862. doi: 10.3389/fpubh.2022.843862

INTRODUCTION

Atmospheric particulate matter <2.5 μm in diameter (PM2.5) pollution has become a worldwide challenge, especially for some developing countries (1, 2). Chinese urban areas have also experienced relatively high air pollution (3). PM2.5 is considered to be one of the most harmful pollutants (4), often coming from coal combustion, industrial activities, vehicle emissions, and so on (5), and it absorbs toxins, such as organic toxic components and heavy metals (6, 7). PM2.5 can increase mortality because it can cause a variety of diseases (8–11) and result in economic losses (12).

Air quality has sparked widespread social debate and China is gradually strengthening its monitoring of PM2.5, which was included in the Chinese conventional key monitoring indicators in 2012. In 2013, there were 612 PM2.5 monitoring stations in China. Since 2015, China has founded a monitoring network covering big cities (13), which has increased the number of monitoring stations to 1,602 as of February 2018. Based on abundant site monitoring data and experiments, some researchers have studied the source, chemical composition, and spatiotemporal characteristics of PM2.5 pollution and its impact on human health (14–16). For example, the spatiotemporal correlation of particulate matter in the Beijing–Tianjin–Hebei region (17) and the sequence pattern of PM2.5 pollution in some regions of China (18) have been studied. In response to the short-term and long-term challenges of PM2.5, the Chinese government has taken several measures, including the *Air Pollution Prevention and Control Action Plan* (2013–2017) and the *3-year Action Plan to Fight Air Pollution* (2018–2020). Since 2013, China has launched a series of initiatives aimed at PM2.5 pollution control, with remarkable achievements in the areas of coal-fired pollution and mobile source pollution control, and the air quality has advanced considerably. Compared with PM2.5 pollution in 2013, the annual average of PM2.5 in the Beijing–Tianjin–Hebei region, the Yangtze River Delta, and the Pearl River Delta declined by 40, 34, and 28%, respectively, in 2017 (19). However, many regions and cities in China are still facing the urgent need to solve PM2.5 pollution, so the work toward improving Chinese air quality still faces great challenges. Therefore, in the face of the goal of a 10% decrease in PM2.5 pollution during the period of the 14th Five-Year Plan (2021–2025), the spatiotemporal specificity of urban PM2.5 pollution in China from 2018 to 2020 can be summarized to help conclude the phased results of the battle against air pollution, and then identify the further challenges and corresponding targeted policies, to promote China's active response to the continuous enhancement of air quality.

In the formulation of different management measures related to PM2.5, it is necessary to discuss the characteristics of different sources, to achieve an accurate and effective control effect. The research trend in recent years shows that scholars are more and more interested in using a spatial econometric analysis method to track the geographical changes of PM2.5 and its socioeconomic driving factors. Taking China as an example, it was found that the spatial distribution of PM2.5 concentration showed an increasing trend from the east to the west (20, 21), and the spatial autocorrelation and clustering characteristics of 338 cities in China were remarkable (22). The urban PM2.5 in the Bohai region of China showed high spatial variation and agglomeration characteristics (23), and the haze pollution in China showed time path dependence and a spatial spillover effect (24). A large amount of literature has studied the socioeconomic driving factors of PM2.5 in a broader sense, indicating that population agglomeration (25, 26), economic growth (27), industrial structure (28), energy structure and efficiency, land-use type (29), and other factors may be the main driving factors of PM2.5 concentration. The spatial scales of urban air quality control were macro (national level), medium (urban level), and micro (specific location) (30). Compared with the medium and micro scales, few researchers have attempted to conduct hierarchical multi-scale studies from a systematic country–region–city perspective for policymaking in the period of China's 14th Five-Year Plan (31). Furthermore, local governments should not adopt a one-size-fits-all policy, but rather establish hierarchical policies according to different social and economic development conditions and needs of Chinese cities (32, 33). In addition, effective communication and cooperation among relevant cities were also important (34). Urban air pollution has the complexity of multi-source, multi-scale, and cross-regional distribution. These problems cannot be solved only by pollution control in one city, and cooperation is needed to reduce transboundary pollutants, such as PM2.5 (35). Therefore, from a country–region–city perspective, identifying the regional pattern of thermal pollution driven by a variety of socio-economic forces and formulating targeted joint management strategies for each regional pattern are of great significance for efficient and fair PM2.5 pollution control in the future (36). Undertaking the *3-Year Action Plan to Fight Air Pollution* and standing at the starting point of the 14th Five-Year Plan, this study analyzed the spatiotemporal distribution and socioeconomic driving factors of PM2.5 pollution from 2018 to 2020, to provide in-depth, hierarchical, and collaborative management countermeasures for the period of the 14th Five-Year Plan.

The objectives of this study are as follows: (1) to characterize the geographical center of PM2.5 pollution and use Global Moran's I method for global autocorrelation analysis, to investigate the spatiotemporal distribution characteristics of PM2.5 from 2018 to 2020; (2) to identify the socioeconomic driving factors in the identified key hotspots by geographic weighted regression (GWR) analysis; (3) to classify the key hotspots by integrating the local autocorrelation analysis of pollution hotspots and the population density features, and to comprehensively provide feasible and targeted control measures, to provide evidence for the air pollution control of Chinese cities.

MATERIALS AND METHODS

Data Collection

PM2.5 data came from the ground monitoring data of 366 cities in China from 2018 to 2020 (excluding Hong Kong, Macao, and Taiwan due to the lack of available data; http://106.37.208.233:20035/). Most of the 366 cities have established

national air quality monitoring stations, and most of the stations are in urban areas. Each monitoring station has a monitoring system according to *Technical Specifications for Installation and Acceptance of Ambient Air Quality Continuous Automated Monitoring System for PM10 and PM2.5* (HJ655-2013) to measure the concentration of fine particles per hour and per day. According to the ground monitoring data provided by the air quality monitoring station, first, some outliers (such as some hourly PM2.5 concentrations that were <0 and missing values) were removed. Second, the daily average of PM2.5 is calculated only when the effective hourly data of the day is more than or equal to 20 h (37). When calculating the monthly average, the effective PM2.5 days per month must be more than or equal to 27 [at least 25 in February; (38)]. Finally, the daily, monthly, seasonal, and annual mean (AM) of the PM2.5 concentrations of the monitoring points were obtained according to the arithmetic average method.

As for economic factor data, based on the Delphi method and available studies (39), a total of 18 indicators were chosen, which were the annual average population (10,000 people), urban construction land area (square kilometers), GDP (the current price; 10,000 Chinese yuan), per capita GDP (Chinese yuan), GDP growth rate (%), the proportion of the primary industry in the GDP, the proportion of the secondary industry in the GDP, the proportion of the tertiary industry in the GDP, the employees (people) of the primary industry (agriculture, forestry, animal husbandry, and fishery), the employees (people) of the secondary industry, the employees (people) of the tertiary industry, the proportion of the employees of the primary industry, the proportion of the employees of the secondary industry, the proportion of the employees of the tertiary industry, the green space area (hectare), the ownership of civilian vehicles (10,000 vehicles), and the annual grain planting area (10,000 mu). The data were from the *China City Statistical Yearbook* (http://www.stats.gov.cn/tjsj/tjcbw/), provincial statistical yearbooks (http://www.stats.gov.cn/tjgz/wzlj/dftjwz/), and some urban statistical bulletins.

Data Analysis

Gravity Model

This study revealed the spatial migration process of PM2.5 by the concept and calculation method of the gravity center in physics. Moreover, the study also characterized the geographical center of PM2.5 pollution by the gravity model. The X and Y coordinates of the PM2.5 pollution center in China are defined as:

$$\overline{X} = \sum_{i=1}^{n} X_i \times S_i \times \frac{W_i}{\sum_{i=1}^{n} S_i} \times W_i \quad (1)$$

$$\overline{Y} = \sum_{i=1}^{n} Y_i \times S_i \times \frac{W_i}{\sum_{i=1}^{n} S_i} \times W_i \quad (2)$$

where $\overline{X}$ is the longitude of the gravity of the PM2.5 pollution center; the latitude of the gravity of the PM2.5 pollution center is expressed by $\overline{Y}$; the number of grids in the research scope is represented by n; the grid number is represented by i; X_i and Y_i represent the longitude and latitude of the geometric center of the grid whose number is i, respectively; S_i represents the area of the grid i; and W_i represents the AM of the PM2.5 of the grid i ($\mu g/m^3$).

Spatial Autocorrelation Analysis Method

Spatial correlation refers to the correlation of the same variable at different locations (40). A variable in a certain position increases or decreases simultaneously with the same variable in its adjacent position, which is called spatial positive correlation. When one increases and one decreases, it is a spatial negative correlation. Spatial autocorrelation analysis describes the potential interdependence of some variables in adjacent spatial units and explores the spatial aggregation mode of factors, which can reveal the potential trend of environmental pollution in recent years (41, 42). According to the size of the analysis space, spatial autocorrelation can be divided into global spatial autocorrelation and local spatial autocorrelation (43), which are listed in the Supporting Information.

Geographic Weighted Regression Model and the Variance Inflation Factor

The change in PM2.5 may be related to industrial activities and human life. Considering the potential multicollinearity between these socio-economic factors, the variance inflation factor (VIF) is usually used for screening. Independent variables with VIF values of more than 10 should be removed before using GWR. The p-value is considered an indicator to determine the reliability of Moran's I. When the p-value of Moran's I is lower than 0.05, spatial econometrics and GWR can be applied. Otherwise, the application of spatial econometrics or GWR is unreasonable. Therefore, the GWR model is used to calculate the coefficients (R) and local regression coefficients for each city in the study area, and these coefficients are then mapped to show spatial variability.

The GWR model is shown as follows:

$$y_i = \beta_0(u_i, v_i) + \sum_k \beta_k(u_i, v_i) x_{ik} + \varepsilon_i \quad (3)$$

where y_i represents the concentration of air pollutants in city i, $\mu g/m^3$; (u_i, v_i) represents the geographical location of city i; $\beta_0(u_i, v_i)$ represents the concept of city i; $\beta_k(u_i, v_i)$ represents the local regression coefficient of meteorological factor k; x_{ik} represents the value of the corresponding meteorological factor in city i; and ε_i represents the residual of city i. The local regression coefficient is calculated as follows:

$$\beta(u_i, v_i) = (X^T W(u_i, v_i) X)^{-1} X^T W(u_i, v_i) Y \quad (4)$$

$$X = \begin{bmatrix} 1, x_{11}, \ldots, x_{ik} \\ 1, x_{21}, \ldots, x_{2k} \\ \ldots \\ 1, x_{n1}, \ldots, x_{nk} \end{bmatrix} \quad (5)$$

$$W(u_i, v_i) = \begin{bmatrix} w_1(u_i, v_i), 0, \ldots, 0 \\ 0, w_2(u_i, v_i), \ldots, 0 \\ \ldots \\ 0, 0, \ldots, w_n(u_i, v_i) \end{bmatrix} \quad (6)$$

where $\beta(u_i, v_i)$ represents the local regression coefficients in cities; x represents the meteorological factor matrix; x^T is the transposition matrix of X; $w(u_i, v_i)$ is the spatial weight matrix; y means the matrix of air pollutants; k means the number of meteorological factors; and n represents the number of samples.

RESULTS AND DISCUSSION

Spatiotemporal Distribution Characteristics of PM2.5 From 2018 to 2020

Temporal Distribution Characteristics From 2018 to 2020

According to the provisions of GB3095-2012 (**Supplementary Table 1**), limiting values for the daily average of PM2.5 concentrations are 15 for Level I and 35 for Level II, and limiting values for the hourly average are 35 for Level I and 75 for Level II. To analyze the pollution level clearly, the PM2.5 content was further divided into five intervals: 15–25, 25–35, 35–55, 55–75, and >75 $\mu g/m^3$. The number of Chinese cities in different PM2.5 content intervals was counted, as shown in **Supplementary Figure 1** and **Supplementary Table 2**. In 2018, the number of cities with an annual PM2.5 concentration in the range of 15–25 $\mu g/m^3$ was the smallest, which was zero. As the years progressed, the number of cities in the range of the annual PM2.5 concentration gradually increased. The number of cities with a PM2.5 concentration in the range of 25–35 $\mu g/m^3$ increased from 34 in 2018 to 86 in 2019 and 99 in 2020. The number of cities with a PM2.5 concentration in the range of 35–55 $\mu g/m^3$ also showed an increasing trend. The average annual concentration of PM2.5 in the range of 55–75 $\mu g/m^3$ showed a significant decreasing trend, from 103 in 2018 to 61 in 2019 and 14 in 2020. This indicated that the air quality was getting better year by year. In the range of the annual PM2.5 concentration above 75 $\mu g/m^3$, the number of cities was seven in 2018, one in 2019, and two in 2020, indicating that the overall trend of pollution was decreasing. Through the above analysis, PM2.5 pollution has improved year by year from 2018 to 2020, thanks to policy support; policies have effectively promoted the improvement of air quality.

Spatial Distribution Characteristics

Gravity Model Analysis

According to the statistical analysis of the geographical locations of the national PM2.5 pollution centers in 2018–2020 (**Supplementary Figure 2**), the pollution center was located in Anqing in 2018, moved northwestward to Huanggang in 2019, and moved southwestward in 2020, but it was still located in Huanggang (Hubei province). A detailed analysis is listed in the Supporting Information.

Macro Analysis

The AM distribution map of PM2.5 from 2018 to 2020 (**Figure 1**) shows that the heavily polluted areas were southwest Xinjiang and North China. The pollution situation in southern China and the Qinghai–Tibet Plateau was relatively light. The factors that caused the above phenomenon may be different industrial structures, a high proportion of the heavy industry, and a different population. The serious pollution in western Xinjiang was mainly caused by an arid climate and low rainfall-related meteorological conditions on the western edge of the Taklamakan Desert; thus, it was less affected by human activities.

Spatiotemporal Distribution Characteristics of PM2.5 in 2018

According to the annual evolution trend, PM2.5 pollution in 2018–2020 was improving year by year. On the whole, there were few areas with serious pollution, and the spatial distribution also showed certain regularity. However, due to the impact of the pandemic from 2019 to 2020, there were some uncertain factors. Therefore, this study selected the PM2.5 pollution status of Chinese cities in 2018 as the main research object for further specific analysis.

Quarterly Characteristics

Figures 2A–D shows that PM2.5 pollution was more serious in the first and fourth quarters of 2018, followed by the second and third quarters. Areas with a PM2.5 concentration of more than 75 $\mu g/m^3$ in the first quarter were mainly distributed in Xinjiang, such as Kashgar, Hotan, Turpan, and Urumqi, as well as Baoding, Weifang, Suihua, Shijiazhuang, and Zaozhuang. There are two main sources of PM2.5. In terms of climate, the rainfall in the first quarter was less than in other quarters. Thanks to warmer weather and increased rain, fine particles can be washed away, and the PM2.5 concentration then goes down in the second quarter. In the third quarter, only the PM2.5 concentration near Hotan in Xinjiang was >75 $\mu g/m^3$, and the pollution in the Beijing–Tianjin–Hebei region was serious. In the fourth quarter, the weather turned cold, the northern region began to heat up, and the pollution in northern China was serious.

The geographical location of the PM2.5 pollution center in the four quarters of 2018 was statistically analyzed. It can be seen from **Figure 2E** that the pollution center in the first quarter was located at the boundary between Huanggang and Anqing. In the second quarter, it moved to the northeast and was located in Anqing. In the third quarter, it moved westward and was located in Huanggang. In the fourth quarter, it moved southeastward at a large distance and was located at the boundary between Jiujiang and Shangrao. From a macro point of view, the shift of the pollution gravity center from the first quarter to the fourth quarter was small, so it can be seen that the PM2.5 pollution in different quarters across the country did not show significant regional differences in terms of increases and decreases.

Spatial Autocorrelation Analysis

Global Autocorrelation

According to the analysis results (**Supplementary Table 3**), Global Moran's I was 2.304041, which was positive, and it indicated that the space was positively correlated and had strong spatial aggregation. The P-value was <0.05, so the data had analytical significance. The Z-value was 73.941729, much more than 1.96, which proved that Global Moran's I meets the test conditions. There was a significant spatial agglomeration

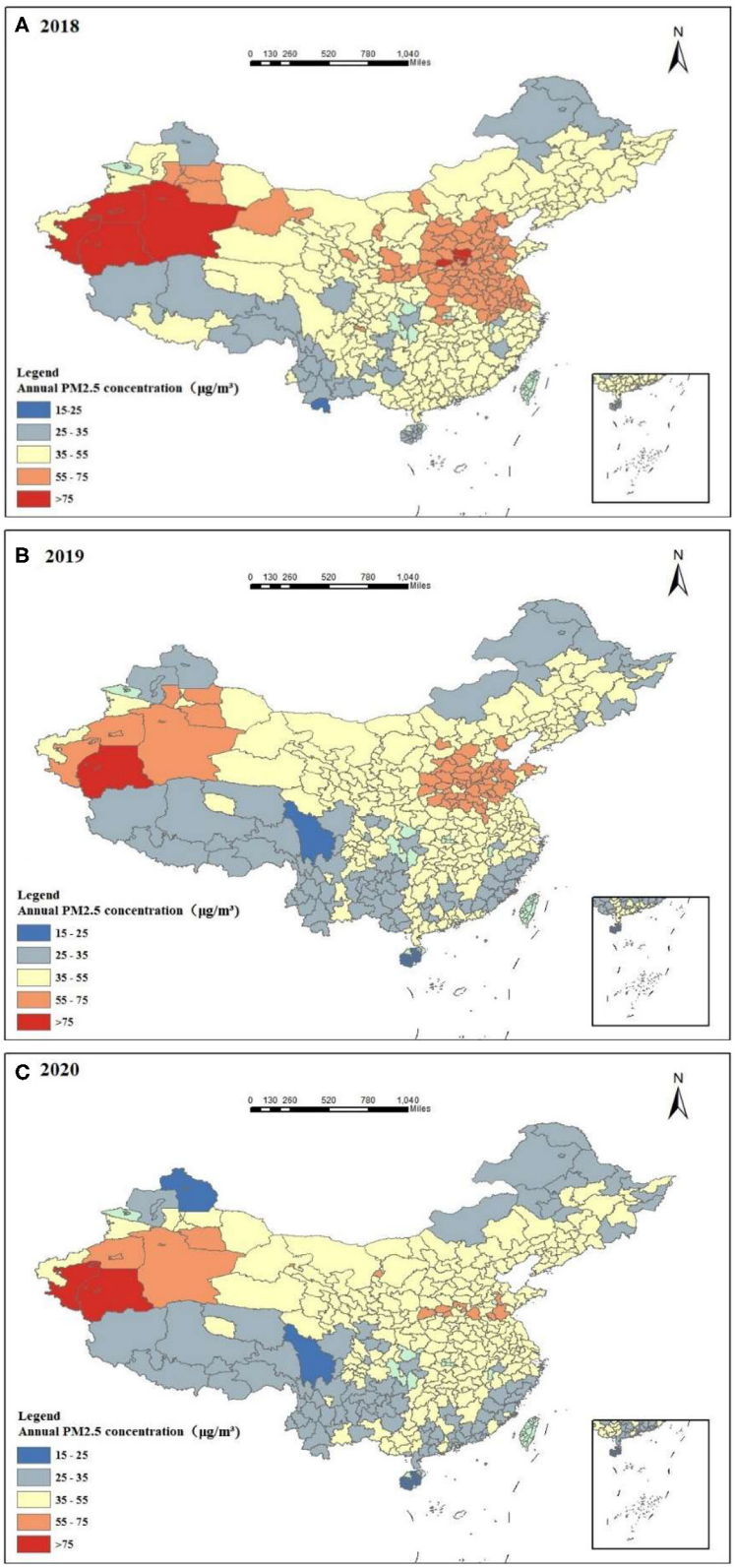

FIGURE 1 | Annual PM2.5 concentration distribution in 2018 **(A)**, 2019 **(B)**, and 2020 **(C)**.

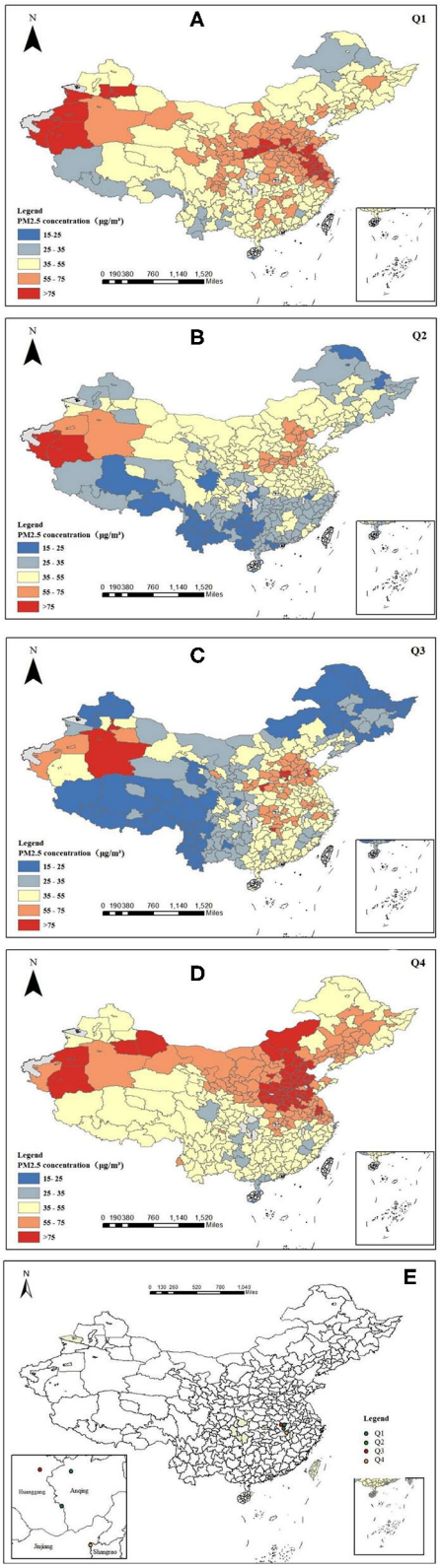

FIGURE 2 | Quarterly distribution map of PM2.5 in 2018 **(A–D)** and the distribution map of the pollution gravity center in 2018 **(E)**.

phenomenon in the AM distribution of PM2.5 in Chinese cities in 2018.

Local Autocorrelation

Local autocorrelation analysis was used to study the distribution of PM2.5 in local areas. Local Moran's I (GeoDa mapping) and Local Geti's G (ArcGIS mapping) were used, and the clustering maps of the local indicators of spatial association were obtained. Zhang and Zhang (44) compared the differences between Moran's I and Geti's G in detecting spatial aggregation by designing a large number of simulation calculations and concluded that Geti's G was better at showing the local autocorrelation. These methods were compared and a more suitable local autocorrelation analysis method for further analysis was selected.

According to **Figure 3** and **Supplementary Figure 3**, the results obtained by Local Moran's I and Local Geti's G were roughly similar, but there were still differences. The comparison showed that Local Geti's G could accurately detect the aggregation area, whereas Local Moran's I could roughly detect the center of the aggregation area, but the recognition deviation of the aggregation range was large, and the detection range was less than the actual range (**Figures 1**, **2**). Therefore, Local Geti's G was selected to reflect the local autocorrelation. **Figure 3** shows that hotspots with a high degree of aggregation were mainly distributed in Kashgar, Hotan, Turpan, and other regions of Xinjiang, the Fenwei Plain, the Yangtze River Delta, the Beijing–Tianjin–Hebei region, and others. Cold spots were mainly distributed in coastal cities in southern China, such as Wenzhou, Longyan, and Lishui. The local aggregation degree of hotspots was high, and most of them were located in inland areas, which was not conducive to the diffusion of pollutants, such as Shaanxi and Shanxi. Due to factors, such as wind and sand in Xinjiang, the pollution situation was grim. Shandong, Hebei, and other regions had a high degree of aggregation. A joint prevention and control mechanism can be adopted in hotspots to achieve an optimal control effect.

Population Density

Human activity is one of the important factors affecting PM2.5 (45). Frequent human activities will increase the concentration of PM2.5 in the atmospheric environment. Population density refers to the number of people living in a unit area, which can accurately represent the population density of a region. Based on the data of the 2010 national population census, the distribution of national population density is shown in **Figure 4A**. From **Figure 4A**, it can be seen that the population density in China showed the law of "high in the east and low in the west." The population density was taken as one of the influencing factors in this study. Compared with the hotspots in **Figure 4B**, different levels of regions were divided more scientifically.

The population density level could be divided into gathering area, transition area, less sparse area, and severely sparse area, and the corresponding population density of each area is 400, 200–400, 50–200, and <50 people/km^2. The hotspots with a

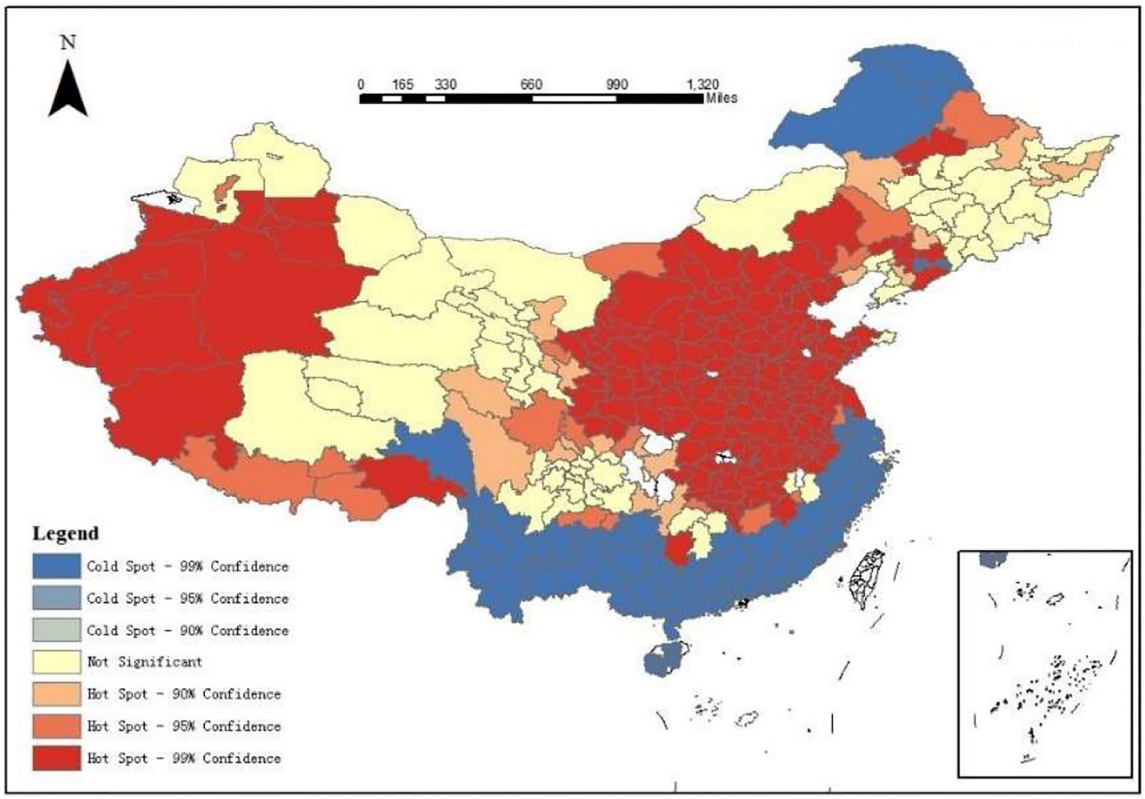

FIGURE 3 | Local Geti's G.

population density of more than 400 people/km^2 were considered Area A, 200–400 people/km^2 were considered Area B, 50–200 people/km^2 were considered Area C, and the hotspots with a population density of fewer than 50 people/km^2 were considered Area D. The results are shown in **Figure 4B**. According to the distribution of monitoring sites, there were few monitoring sites in the western regions of China, and it is particularly necessary to set the classification of areas A, B, C, and D. Due to the small number of sites and the low density of the potentially exposed population in Area D, no further analysis was carried out. Due to the natural environmental conditions, such as wind and sand in Area D, the air conditions were poor. More afforestation should be carried out to increase the coverage of green plants and improve the state of pollution. For Areas A, B, and C, further driving factor analyses were carried out to develop targeted policies.

Analysis of the Socioeconomic Driving Factors

Combined with the population density map and the distribution of hotspots, through local autocorrelation analysis, the Beijing–Tianjin–Hebei region, the Fenwei Plain, the Yangtze River Delta, and the surrounding areas were selected as the key hotspots for GWR analysis.

Factor Selection and the VIF Test

A total of 18 indicators were chosen as independent variables in this study. The average annual concentration of PM2.5 ($\mu g/m^3$) was analyzed as a dependent variable. Before the GWR analysis, the VIF test should be preprocessed first to remove the indicators with VIF values of more than 10 to avoid collinearity affecting the experimental results. Then, the remaining usable indicators were the annual average population (10,000 people), urban construction land area (square kilometers), per capita GDP (Chinese yuan), GDP growth rate (%), the proportion of the primary industry in the GDP, the proportion of the secondary industry in the GDP, the employees (people) of the primary industry (agriculture, forestry, animal husbandry, and fishery), the employees (people) of the secondary industry, the employees (people) of the tertiary industry, the proportion of the employees of the primary industry, the proportion of the employees of the secondary industry, the proportion of the employees of the tertiary industry, the green space area (hectare), the ownership of civilian vehicles (10,000 vehicles), and the annual grain planting area (10,000 mu).

GWR Analysis

After excluding the local and global collinearity, the remaining seven factors were effective, which were the following: the annual average population (10,000 people), urban construction land area

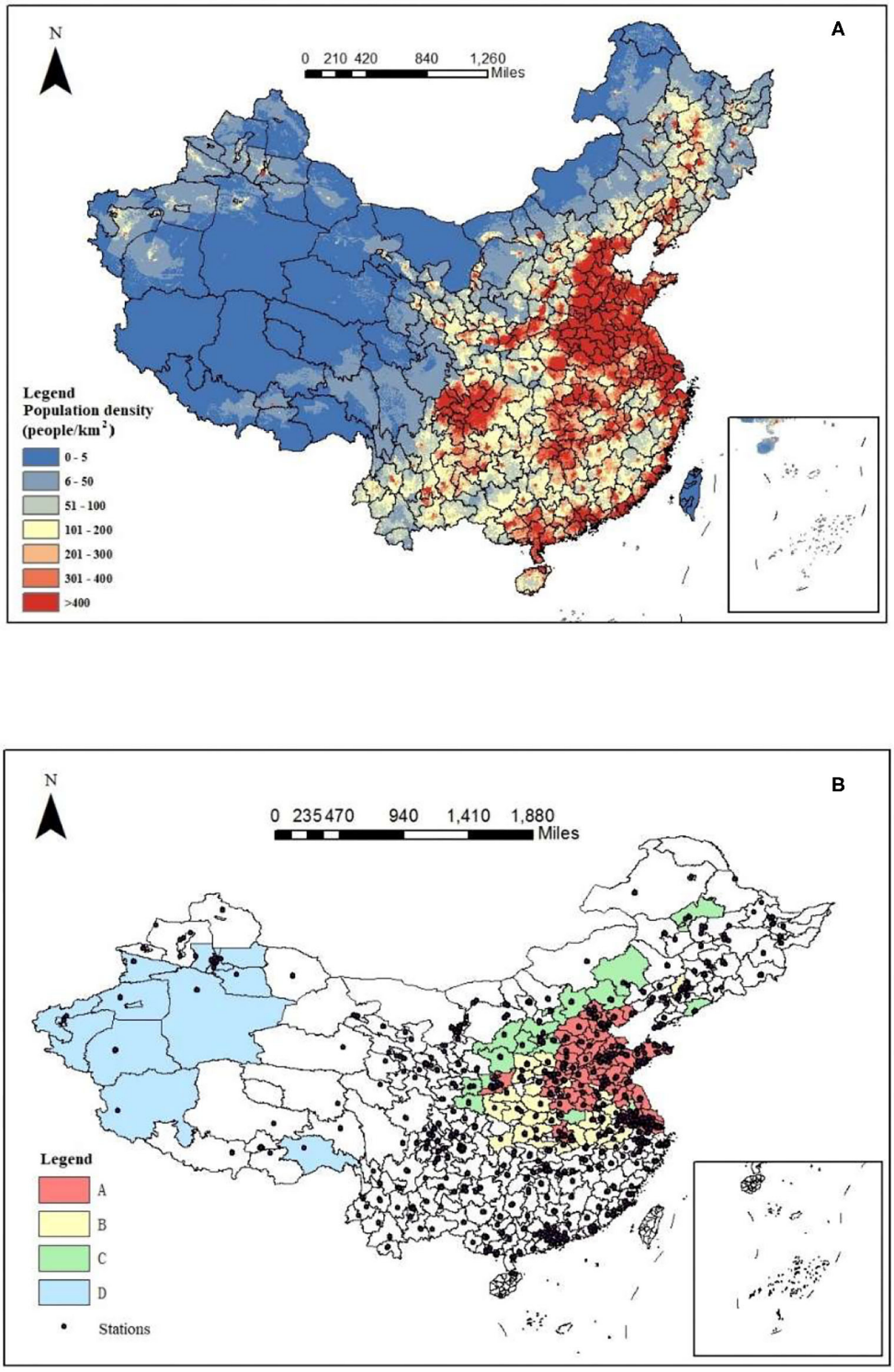

FIGURE 4 | Population density map **(A)** and the distribution of hotspots and monitoring sites **(B)**.

(square kilometers), the per capita GDP (Chinese yuan), the proportion of the secondary industry in the GDP, the green space area (hectares), the ownership of civilian vehicles (10,000 vehicles), and the annual grain planting area (10,000 mu). The spatial distribution of the regression coefficients of these factors is shown in **Figure 5**.

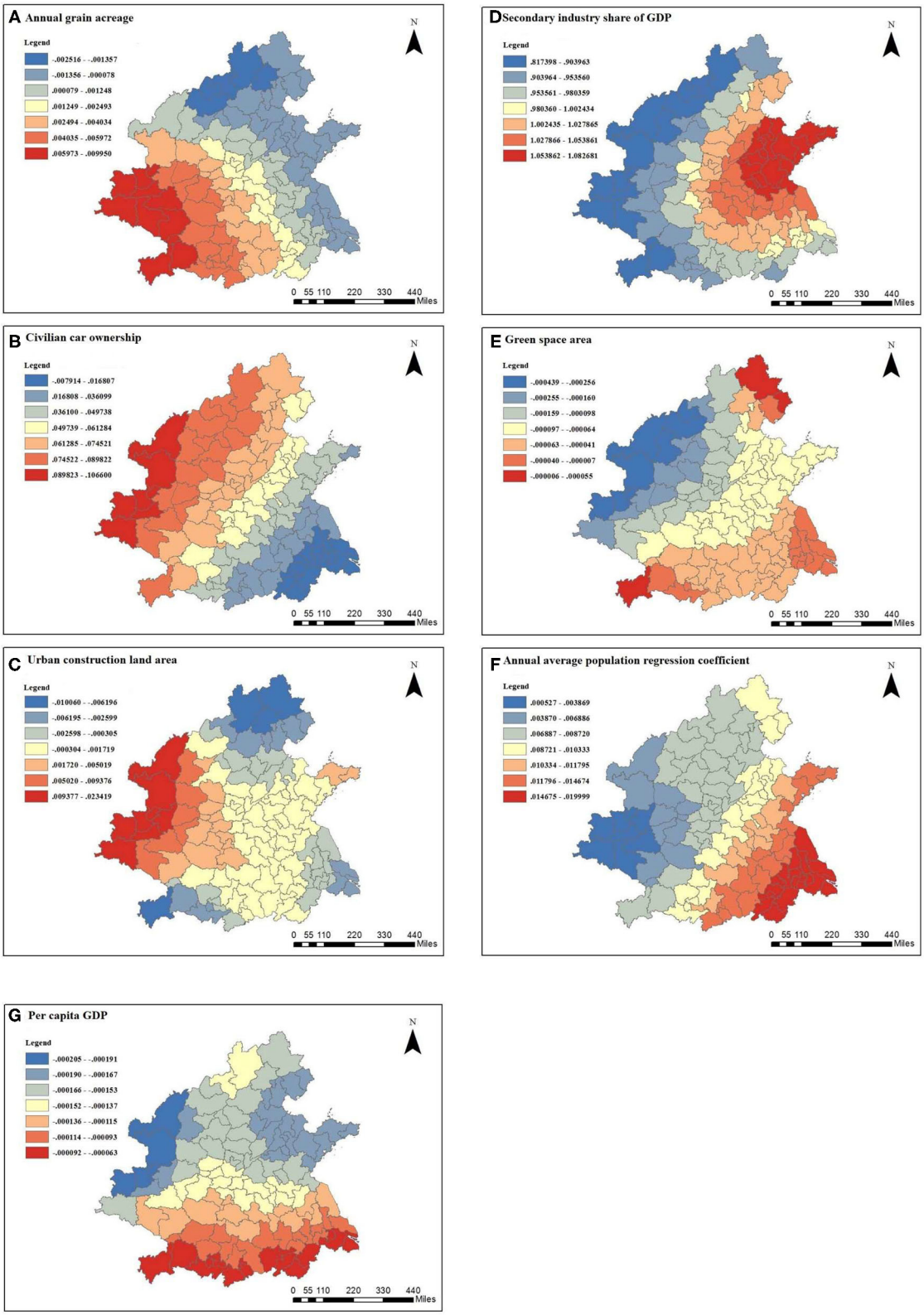

FIGURE 5 | Spatial distribution of the regression coefficients of the parameters in the GWR model: **(A)** annual grain acreage, **(B)** civilian car ownership, **(C)** urban construction land area, **(D)** secondary industry share of GDP, **(E)** green space area, **(F)** annual average population regression coefficient, and **(G)** per capita GDP.

From **Figure 5A**, it can be seen that the annual grain planting area was negatively correlated with the PM2.5 concentration in northern Shanxi, the northern Beijing–Tianjin–Hebei region, eastern Shandong, and most of Jiangsu and Shanghai, and the rest was positively correlated. The correlation coefficients in northern Shanxi, Zhangjiakou, and Beijing were the smallest, and the correlation coefficients in southern Shaanxi and western Hubei were higher, showing an overall increase from the east to the west. The grain planting area in economically developed regions is relatively small. For example, as the political and economic center of the country, Beijing has developed rapidly. The planting area reserved for grain is relatively small, and the correlation coefficient was relatively small. The annual grain planting area was negatively correlated with the PM2.5 concentration, and the air pollution situation was still severe. In southern Shaanxi, for example, the annual grain planting area in Hanzhong in 2018 was 3.8097 million mu, and the grain planting area was relatively large. Straw burning occurred from time to time, which would cause serious air pollution. The annual grain planting area was positively correlated with PM2.5 concentration.

Figure 5B shows that in cities except for Jiangsu, southeast Anhui, and Shanghai, the number of civilian vehicles was positively correlated with PM2.5 concentration, and increased from the southeast to the northwest. Traffic is one of the major factors affecting air pollution. The larger the number of civilian vehicles, the more serious the pollution is. There was a relatively strong correlation between the ownership of civilian vehicles and PM2.5 concentration in most areas of Shaanxi Province. For example, Xi'an has carried out special rectification actions for motor vehicle exhaust pollution in recent years. Since 2016, the concentration of PM2.5 in Xi'an has decreased significantly in winter, and the effect of pollution control and haze reduction was obvious. However, heavy haze weather still occurs. The contribution rate of heavy trucks to PM2.5 pollution in Xi'an was 47.0%, and that of diesel vehicles was 80.2% (46). Therefore, Xi'an should focus on controlling heavy trucks and diesel vehicles to form a targeted management pattern.

As can be seen from **Figure 5C**, the urban construction land area was positively correlated in the west of the hotspot area and was negatively correlated in the rest of the area. Shaanxi and western Shanxi had the strongest positive correlation, indicating that the larger the urban construction land area, the higher the annual average PM2.5 concentration was. For example, Yulin is located in the Loess Plateau and is carrying out urban construction in a large area. The dust generated by a large number of construction projects will cause serious air pollution. The soil of the Loess Plateau is thick and loose, which aggravates the increase in PM2.5 concentration.

According to **Figure 5D**, the proportion of the secondary industry in the GDP was significantly positively correlated with PM2.5 concentration; it decreased from the west to the east, and the correlation coefficient was the highest in eastern Shandong. The second industry is a major force in environmental pollution. The higher the proportion of the second industry in the GDP, the more serious the air pollution is. Yantai is a traditional, strong industrial city, and its industrial output value ranks first in Shandong Province. Yantai vigorously develops the secondary industry, so that the pollution emissions are serious. Yantai should change its urban economic structure, reduce the proportion of the secondary industry, avoid the excessive agglomeration of the same type of secondary industry in the region, and improve the current situation of environmental pollution.

It can be seen from **Figure 5E** that the green area was negatively correlated with PM2.5 pollution. The high-value area was located in Shanxi and northwestern Shaanxi, and the low-value area was located in Enshi, Chengde, and Qinhuangdao. The larger the green area was, the more conducive it was to reducing PM2.5 pollution. Yan'an belongs to northern Shaanxi, and the green space area had a relatively obvious negative correlation with PM2.5 concentration. Green space helps to improve air pollution; therefore, green space can be further expanded in cities.

It can be seen from **Figure 5F** that the annual average population was positively correlated with PM2.5 concentration. The high-value area was located in Anhui, southeast Jiangsu, and Shanghai, and the low-value area was located in southern Shaanxi. The larger the annual population is, the more frequent human activities are, and this leads to more serious pollution and higher PM2.5 concentrations. In Shanghai, with a large population, the annual average population was positively correlated with PM2.5 concentration. It is necessary to promote a green low-carbon lifestyle and advocate for the participation of all people in haze prevention and control. In Shandong, Henan, and other populous provinces, the population should be reasonably controlled, and the population structure should be optimized.

It can be seen from **Figure 5G** that per capita GDP was negatively correlated with PM2.5 concentration. A region with a high per capita GDP has a higher level of economic development, a reasonable industrial structure, and advanced technology. Therefore, the region is more environmentally friendly and produces less pollution. The high-value area was located in the north-central Shaanxi, and the low-value area was located to the south of the hotspot. The per capita GDP of Suzhou was 173,765 Chinese yuan, and the level of economic development was relatively high. The average annual PM2.5 concentration in 2018 was 42 $\mu g/m^3$. The per capita GDP was negatively correlated with PM2.5 concentration. With the rapid economic development of the city, the government should pay attention to the sustainable development of the environment and reduce air pollution.

It can be seen from the above analysis that the seven factors selected in this study had different effects on the average annual PM2.5 concentration. Comparing the average absolute value of the correlation coefficient, the influence degree of each factor on the average annual PM2.5 concentration decreased in the following order: the proportion of the secondary industry in the GDP, the ownership of civilian vehicles, the annual grain planting area, the annual average population, the urban construction land area, the green space area, and the per capita GDP. The proportion of the secondary industry in the GDP has a great influence on PM2.5 concentration. In some areas, the proportion of the secondary industry in the GDP is high, so pollution emissions are serious. It is necessary to

accelerate the transformation of the urban economic structure and increase the proportion of the tertiary industry in the economic structure. At the same time, it is necessary to change the urban economic structure, reduce the proportion of the secondary industry, avoid the excessive aggregation of the same type of secondary industry in the region, and improve the current situation of environmental pollution. In Shaanxi Province, attention should be paid to air pollution in urban construction; strict regulations should be made on the air standards for construction, and a supervision system should be implemented to ensure that air pollution caused by construction is controlled within a reasonable range. At the same time, attention should be paid to air pollution caused by automobile exhaust emission pollution and crop planting. The number of cars should be further controlled, green travel should be promoted, penalties should be strengthened for vehicles with unqualified emissions, supervision should be strengthened in agriculture, and straw burning should be strictly prevented. Good economic conditions are the basis for effective environmental protection, so it is urgent to accelerate the high-quality growth of regional GDP. At the same time, expanding the green space in various regions helps reduce air pollution. Because of the differences in atmospheric resource endowments and the functional positioning of each region and its cities, it is recommended to establish a regional classification management system and ecological compensation strategy.

Hierarchical Management Policies

As mentioned above, PM2.5 pollution has improved year by year from 2018 to 2020 and there was a significant spatial agglomeration phenomenon in the AM distribution of PM2.5 in Chinese cities. According to the local autocorrelation analysis of pollution hotspots, integrated with the population density map (**Figure 4A**), the key hotspots were divided into three areas: Area A, Area B, and Area C. The classification of key hotspots is shown in **Figure 6**. According to the analysis of socioeconomic driving factors, we should pay more attention to sustainable development for Area A (63 cities), and the green industry is one of the solutions. For example, Xi'an, Tongchuan, and Weinan are typical cities in Area A, and they are surrounded by the cities in Area B and Area C. To achieve the regional coordinated management of fine particulate pollution and joint economic development, the idle environmental capacity of the surrounding cities can be used to update the joint industrial layout, to optimize the economic and energy structure and further promote the growth of per capita GDP. At the same time, the air standards for urban construction should be strictly stipulated, and the supervision system should be implemented to ensure that the air pollution generated by construction is controlled within a reasonable range. Attention should be paid to the emission pollution of automobile exhaust, green travel should be advocated, and penalties should be strengthened for vehicles that do not meet the emission standards. In the above three cities and Xiaogan, Wuhan, Ezhou, Jiaozuo, Zhengzhou, Zhumadian, Zhoukou, and Xuchang, the government should strictly prevent and control the open-air burning of straw and implement a global full-time comprehensive prohibition of such burning. In Shijiazhuang and Baoding, it is proposed to form a targeted management pattern for heavy trucks and diesel vehicles. In Xuzhou, Lianyungang, Zibo, Linyi, Weihai, Rizhao, Yantai, Weifang, Qingdao, Jining, Dongying, Zaozhuang, Binzhou, and Jinan, governors should pay attention to the air pollution caused by the secondary industry, change the urban economic structure, reduce the proportion of the secondary industry, prevent the same type of secondary industry from becoming too concentrated in the region, and improve the status of environmental pollution. In Shanghai, Taizhou, Nanjing, Changzhou, Yancheng, Zhenjiang, Suzhou, Wuxi, and Nantong, a green and low-carbon lifestyle should be promoted among citizens, and all people should participate in the prevention and control of haze. The cities in Area B were mainly concentrated in southeastern Shaanxi, southwestern Shanxi, western Henan, Anhui, and most parts of Hubei. For the cities in Area B (a total of 30 cities), it is crucial to develop low-emission industries and short-distance tourism to promote economic integration. For example, decision-makers in Shangluo, Ankang, Shiyan, and Enshi should pay attention to air pollution caused by crop planting, strengthen supervision in agriculture, and strictly prevent straw burning. Decision-makers in Linfen, Changzhi, Yuncheng, Shangluo, Ankang, and Enshi should pay attention to automobile exhaust pollution, promote green travel, and focus on the control of heavy trucks and diesel vehicles. In Hefei, Bengbu, Huainan, Chuzhou, Suzhou, Lu'an, and Kaifeng, it is necessary to accelerate the transformation of the urban economic structure, reduce the proportion of the secondary industry and develop low-emission industries. Area C (16 cities in total) was located in Shaanxi, Shanxi, and northern Hebei. To accelerate the growth of the per capita GDP, good economic conditions are the basis for effective environmental protection and contribute to sustainable development. It is necessary to promote the further improvement of the regional cooperation mechanism in key hotspots, establish a comprehensive regional ecological environment management platform and traffic information platform, promote information sharing, implement joint law enforcement and mutual supervision, learn long-term mechanisms, and improve the emergency linkage mechanism to deal with heavy pollution weather, as well as improve the air quality prediction mechanism (47).

At the same time, the seasonal characteristics of PM2.5 pollution were also worthy of attention. Considering that different cities have different roles and different sensitivities to different socioeconomic driving factors, it is urgent to establish clear transfer compensation policies for haze control cooperation between cities in the first and fourth quarters. In addition, the analysis of pollution centers in the four quarters of 2018 showed that the pollution centers were located in the Huanggang, Anqing, Jiujiang, and Shangrao areas, and the government should focus on the coordinated planning and management of the environmental economy in the above areas. Moreover, the air pollution in the heating period in the north was serious. To build a coal-free area and achieve the goal of clean heating, it is necessary to eliminate the high emission of boilers, reform the gas

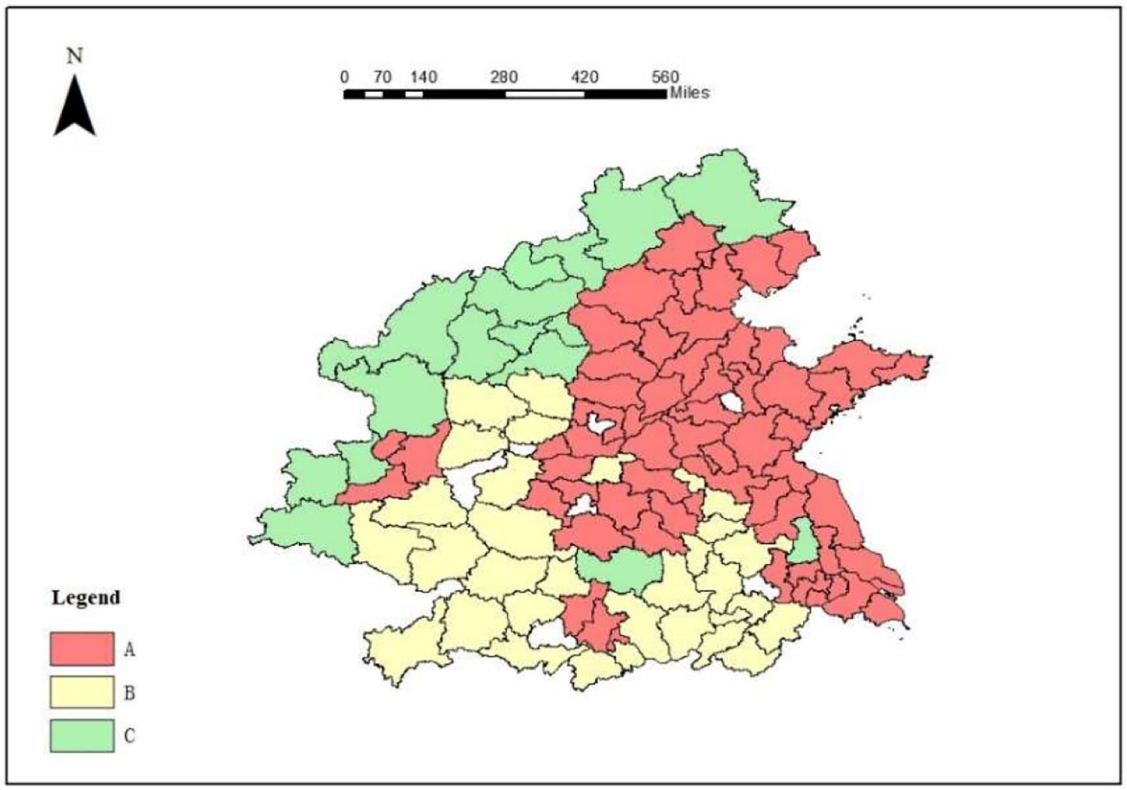

FIGURE 6 | Zoning diagram of the key hotspots.

boilers, strengthen the source management, and strictly control the amount of coal used.

CONCLUSION

PM2.5 pollution has improved year by year from 2018 to 2020. There was a significant spatial agglomeration phenomenon in the AM distribution of PM2.5 in Chinese cities. Based on the local autocorrelation analysis of pollution hotspots and population density features, the Beijing–Tianjin–Hebei region, the Fenwei Plain, the Yangtze River Delta, and surrounding areas were selected as the key hotspots for GWR analysis. The influence degree of each socioeconomic determinant on the average annual PM2.5 concentration decreased in the following order: the proportion of the secondary industry in the GDP, the ownership of civilian vehicles, the annual grain planting area, the annual average population, the urban construction land area, the green space area, and the per capita GDP. Based on the local autocorrelation analysis of pollution hotspots, when integrated with the population density map, the key hotspots were divided into three areas: Area A (63 cities), Area B (30 cities), and Area C (16 cities). Finally, the targeted management policies of each hierarchical area were proposed according to the characteristics of the driving forces of sensitive pollution in each city as well as the roles of each city, combined with the seasonal characteristics of pollution. The cities in Area A should update the joint industrial layout with the surrounding cities to optimize their economic and energy structure. Cities in Area B should consider transitioning to eco-tourism, eco-agriculture, and other green industries to maintain people's livelihoods. Cities in Area C should accelerate the growth of the per capita regional GDP. Cities in Area D should implement more afforestation to increase the coverage of green plants, which would improve pollution. Moreover, the quarterly pollution focus should be on the coordinated planning and management of the environment and economy in the above-mentioned areas. At the same time, air pollution was serious during the heating season in the north, so the government should strengthen source management and strictly control the amount of coal used.

DATA AVAILABILITY STATEMENT

The raw data supporting the conclusions of this article will be made available by the authors, without undue reservation.

AUTHOR CONTRIBUTIONS

MZ: writing—original draft preparation and data analysis. JG and YZ: data analysis. XC: methodology, reviewing, and

revision. All authors contributed to the article and approved the submitted version.

FUNDING

This study was supported by the Humanities and Social Science Research Youth Project funded by the Ministry of Education of China (18YJCZH021), Fundamental Research Funds for the Central Universities from Zhongnan University of Economics and Law (202211412 and 202211413).

SUPPLEMENTARY MATERIAL

The Supplementary Material for this article can be found online at: https://www.frontiersin.org/articles/10.3389/fpubh.2022.843862/full#supplementary-material

REFERENCES

1. Maji KJ, Arora M, Dikshit AK. Premature mortality attributable to PM25 exposure and future policy roadmap for "airpocalypse" affected Asian mega-cities. *Process Saf Environ Protect.* (2018) 118:371–83. doi: 10.1016/j.psep.2018.07.009
2. Zhou Z, Tan ZB, Yu XH, Zhang RT, Wei YM, Zhang MJ, et al. The health benefits and economic effects of cooperative PM25 control: a cost-effectiveness game model. *J Clean Product.* (2019) 228:1572–85. doi: 10.1016/j.jclepro.2019.04.381
3. Fontes T, Li P, Barros N, Zhao P. Trends of PM25 concentrations in China: a long-term approach. *J Environ Manag.* (2017) 196:719–32. doi: 10.1016/j.jenvman.2017.03.074
4. Zhang Y, Chen X, Mao YY, Shuai CY, Jiao LD, Wu Y. Analysis of resource allocation and PM25 pollution control efficiency: evidence from 112 Chinese cities. *Ecol Indicat.* (2021) 127:107705. doi: 10.1016/j.ecolind.2021.107705
5. Zhou JB, Xing ZY, Deng JJ, Du K. Characterizing and sourcing ambient PM25 over key emission regions in China I: water-soluble ions and carbonaceous fractions/ *Atmos Environ.* (2016) 135:20–30. doi: 10.1016/j.atmosenv.2016.03.054
6. Li F, Yan JJ, Wei YC, Zeng JJ, Wang XY, Chen XY, et al. PM25-bound heavy metals from major cities in China: Spatio-temporal distribution, fuzzy exposure assessment and health risk management. *J Clean Product.* (2020) 286:124967. doi: 10.1016/j.jclepro.2020.124967
7. Pui DYH, Chen SC, Zuo Z. PM25 in China: measurements, sources, visibility and health effects, and mitigation. *Particuology.* (2014) 13:1–26. doi: 10.1016/j.partic.2013.11.001
8. Ding L, Zhu D, Peng D, Zhao Y. Air pollution and asthma attacks in children: a case-crossover analysis in the city of Chongqing, China. *Environ Poll.* (2017) 220:348–53. doi: 10.1016/j.envpol.2016.09.070
9. Close J, Cao C, Yang J, Li R, Chen B, Chen D, et al. Association between long-term exposure to outdoor air pollution and mortality in China: a cohort study. *J Hazard Mater.* (2011) 186:1594–600. doi: 10.1016/j.jhazmat.2010.12.036
10. Duan Z, Han X, Bai Z, Yuan Y. Fine particulate air pollution and hospitalization for pneumonia: a case-crossover study in Shijiazhuang, China. *Air Qual Atmos Health.* (2015) 9:723–33. doi: 10.1007/s11869-015-0383-y
11. Guo Y, Jia Y, Pan X, Liu L, Wichmann HE. The association between fine particulate air pollution and hospital emergency room visits for cardiovascular diseases in Beijing, China. *Sci Tot Environ.* (2009) 407:4826–30. doi: 10.1016/j.scitotenv.2009.05.022
12. Zhang Y, Shuai C, Bian J, Chen X, Wu Y, Shen L. Socioeconomic factors of PM25 concentrations in 152 Chinese cities: decomposition analysis using LMDI. *J Clean Product.* (2019) 218:96–107. doi: 10.1016/j.jclepro.2019.01.322
13. Song C, Wu L, Xie Y, He J, Chen X, Wang T, et al. Air pollution in China: status and spatiotemporal variations. *Environ Poll.* (2017) 227:334–47. doi: 10.1016/j.envpol.2017.04.075
14. Jin Q, Fang X, Wen B, Shan A. Spatio-temporal variations of PM2.5 emission in China from 2005 to 2014. *Chemosphere.* (2017) 183:429–36. doi: 10.1016/j.chemosphere.2017.05.133
15. Yan D, Lei Y, Shi Y, Zhu Q, Li L, Zhang Z. Evolution of the spatiotemporal pattern of PM25 concentrations in China–a case study from the Beijing-Tianjin-Hebei region. *Atmos Environ.* (2018) 183:225–33. doi: 10.1016/j.atmosenv.2018.03.041
16. Zhang NN, Ma F, Qin CB, Li YF. Spatiotemporal trends in PM2.5 levels from 2013 to 2017 and regional demarcations for joint prevention and control of atmospheric pollution in China. *Chemosphere.* (2018) 210:1176–84. doi: 10.1016/j.chemosphere.2018.07.142
17. Qin S, Liu F, Wang C, Song Y, Qu J. Spatial-temporal analysis and projection of extreme particulate matter (PM10 and PM25) levels using association rules: a case study of the Jing-Jin-Ji region, China. *Atmos Environ.* (2015) 120:339–50. doi: 10.1016/j.atmosenv.2015.09.006
18. Yang G, Huang J, Li X. Mining sequential patterns of PM25 pollution in three zones in China. *J Clean Product.* (2018) 170:388–98. doi: 10.1016/j.jclepro.2017.09.162
19. Wang YJ, Zhang SJ, Hao JM. Air pollution control in China: progress, challenges and future pathways. *Res Environ Sci.* (2019) 32:1755–62. doi: 10.13198/j.issn.1001-6929.2019.08.22
20. He Q, Geng F, Li C, Yang S, Wang Y, Mu H, et al. Long-term characteristics of satellite-based PM25 over East China. *Sci Tot Environ.* (2018) 612:1417–23. doi: 10.1016/j.scitotenv.2017.09.027
21. Yang Y, Christakos G. Spatiotemporal characterization of ambient PM25 concentrations in Shandong province (China). *Environ Sci Technol.* (2015) 49:13431–8. doi: 10.1021/acs.est.5b03614
22. Ye WF, Ma ZY, Ha XZ. Spatial-temporal patterns of PM2.5 concentrations for 338 Chinese cities. *Sci Tot Environ.* (2018) 631–2:524–33. doi: 10.1016/j.scitotenv.2018.03.057
23. Wang ZB, Fang CL. Spatial-temporal characteristics and determinants of PM25 in the Bohai Rim urban agglomeration. *Chemosphere.* (2016) 148:148–62. doi: 10.1016/j.chemosphere.2015.12.118
24. Cheng Z, Li L, Liu J. Identifying the spatial effects and driving factors of urban PM25 pollution in China. *Ecol Indicat.* (2017) 82:61–75. doi: 10.1016/j.ecolind.2017.06.043
25. Lu X, Lin C, Li W, Chen Y, Huang Y, Fung JC, et al. Analysis of the adverse health effects of PM2.5 from 2001 to 2017 in China and the role of urbanization in aggravating the health burden. *Sci Tot Environ.* (2019) 652:683–95. doi: 10.1016/j.scitotenv.2018.10.140
26. Li W, Sun S. Air pollution driving factors analysis: evidence from economically developed area in China. *Environ Progr Sustain Energy.* (2016) 35:1231–9. doi: 10.1002/ep.12316
27. Xie R, Zhao G, Zhu BZ, Chevallier J. Examining the factors affecting air pollution emission growth in China. *Environ Model Assess.* (2018) 23:389–400. doi: 10.1007/s10666-018-9593-7
28. Li G, Fang C, Wang S, Sun S. The effect of economic growth, urbanization, and industrialization on fine particulate matter (PM25) concentrations in China. *Environ Sci Technol.* (2016) 50:11452–9. doi: 10.1021/acs.est.6b02562
29. Choe SA, Kauderer S, Eliot MN, Glazer KB, Kingsley SL, Carlson L, et al. Air pollution, land use, and complications of pregnancy. *Sci Tot Environ.* (2018) 645:1057–64. doi: 10.1016/j.scitotenv.2018.07.237
30. Gulia S, Nagendra SMS, Khare M, Khanna I. Urban air quality management-a review. *Atmos Poll Res.* (2015) 6:286–304. doi: 10.5094/APR.2015.033
31. Chen ZY, Xu B, Cai J, Gao BB. Understanding temporal patterns and characteristics of air quality in Beijing a local and regional perspective. *Atmos Environ.* (2016) 127:303–15. doi: 10.1016/j.atmosenv.2015.12.011
32. Chen J, Zhou CS, Wang SJ, Hu JC. Identifying the socioeconomic determinants of population exposure to particulate matter (PM25) in China using geographically weighted regression modeling. *Environ Poll.* (2018) 241:494–503. doi: 10.1016/j.envpol.2018.05.083
33. Wang JY, Wang SJ, Li SJ. Examining the spatially varying effects of factors on PM25 concentrations in Chinese cities using geographically

weighted regression modeling. *Environ Poll.* (2019) 248:792–803. doi: 10.1016/j.envpol.2019.02.081
34. Fang CL. Important progress and future direction of studies on China's urban agglomerations. *J Geograph Sci.* (2015) 25:1003–24. doi: 10.1007/s11442-015-1216-5
35. Zhang L, Yang G, Li X. Mining sequential patterns of PM2.5 pollution between 338 cities in China. *J Environ Manag.* (2020) 262:110341.1–8. doi: 10.1016/j.jenvman.2020.110341
36. Chen X, Li F, Zhang J, Zhou W, Wang X, Fu H. Spatiotemporal mapping and multiple driving forces identifying of PM2.5 variation and its joint management strategies across China. *J Clean Product.* (2020) 250:119534.1–11. doi: 10.1016/j.jclepro.2019.119534
37. Li JM, Han XL, Li X, Yang JP, Li XJ. Spatiotemporal patterns of ground monitored PM25 concentrations in China in recent years. *Int J Environ Res Public Health.* (2018) 15:114. doi: 10.3390/ijerph15010114
38. Ambient air quality standards. Ministry of Ecology and Environment, Beijing, China (2012). Available online at: https://english.mee.gov.cn/Resources/standards/Air_Environment/quality_standard1/201605/W020160511506615956495.pdf
39. Zhou L, Zhou CH, Yang F, Che L, Wang B, Sun DQ. Spatio-temporal evolution and the influencing factors of PM2.5 in China between 2000 and 2015. *J Geograph Sci.* (2019) 29:253–70. doi: 10.1007/s11442-019-1595-0
40. Geng L, Bi R, Wang S, Li F, Guo G. The use of spatial autocorrelation analysis to identify PAHs pollution hotspots at an industrially contaminated site. *Environ Monit Assess.* (2013) 185:9549–58. doi: 10.1007/s10661-013-3272-6
41. Wang J, Wang S, Voorhees AS, Zhao B, Jang C, Jiang J, et al. Assessment of short-term PM2.5-related mortality due to different emission sources in the Yangtze River Delta, China. *Atmos Environ.* (2015) 123:440–8. doi: 10.1016/j.atmosenv.2015.05.060
42. Wang Y, Qi Y, Hu J, Zhang H. Spatial and temporal variations of six criteria air pollutants in 31 provincial capital cities in China during 2013–2014. *Environ Int.* (2014) 73:413–22. doi: 10.1016/j.envint.2014.08.016
43. Deng Q, Yang K, Luo Y. Spatiotemporal patterns of PM2.5 in the Beijing–Tianjin–Hebei region during 2013–2016. *Geology. Ecol Landscap.* (2017) 1:95–103. doi: 10.1080/24749508.2017.1332851
44. Zhang SL, Zhang K. Contrast study on the local indices of spatial autocorrelation. *Statist Res.* (2007) 24:65–7. doi: 10.19343/j.cnki.11-1302/c.2007.07.013
45. Liang CY, Liu XY, Li SL. Urban spatial development mode and smog pollution—based on the perspective of population density distribution. *Econ Trends.* (2021) 02:80–94. Available online at: http://www.jjxdt.org/Admin/UploadFile/Issue/NaN/4//20210413083625WU_FILE_0.pdf
46. Wang JF, Song H, Ba LM, Li GH, Sun ZG. Study on the vehicle emission inventory and spatial distribution characteristics in Xi'an. *Environ Poll Prev.* (2020) 42:666–77. doi: 10.15985/j.cnki.1001-3865.2020.06.003
47. Li F, Liu JA, Chen ZP, Huang JH, Liu CY, Qu ZG. Navigating to urban environmental health: professionalized and personalized healthy living assistant based on intelligent health risk management. *Urban Climate.* (2021) 40:101020. doi: 10.1016/j.uclim.2021.101020

Conflict of Interest: The authors declare that the research was conducted in the absence of any commercial or financial relationships that could be construed as a potential conflict of interest.

Publisher's Note: All claims expressed in this article are solely those of the authors and do not necessarily represent those of their affiliated organizations, or those of the publisher, the editors and the reviewers. Any product that may be evaluated in this article, or claim that may be made by its manufacturer, is not guaranteed or endorsed by the publisher.

frontiers | Frontiers in Public Health

ORIGINAL RESEARCH
published: 08 April 2022
doi: 10.3389/fpubh.2022.849766

Prediction for Origin-Destination Distribution of Dockless Shared Bicycles: A Case Study in Nanjing City

Min Cao [1,2,3], *Ying Liang* [1,2,3], *Yanhui Zhu* [1,2,3], *Guonian Lü* [1,2,3] *and Zaiyang Ma* [1,2,3]*

[1] *Key Laboratory of Virtual Geographic Environment (Ministry of Education of PRC), Nanjing Normal University, Nanjing, China,* [2] *State Key Laboratory Cultivation Base of Geographical Environment Evolution (Jiangsu Province), Nanjing Normal University, Nanjing, China,* [3] *Jiangsu Center for Collaborative Innovation in Geographical Information Resource Development and Application, Nanjing Normal University, Nanjing, China*

OPEN ACCESS

Edited by:
Hongtao Yi,
The Ohio State University,
United States

Reviewed by:
Li He,
Xi'an Jiaotong University, China
Xintao Liu,
Hong Kong Polytechnic University,
Hong Kong SAR, China

***Correspondence:**
Zaiyang Ma
zy_ma327@126.com

Specialty section:
This article was submitted to Environmental health and Exposome, a section of the journal Frontiers in Public Health

Received: *06 January 2022*
Accepted: *28 February 2022*
Published: *08 April 2022*

Citation:
Cao M, Liang Y, Zhu Y, Lü G and Ma Z (2022) Prediction for Origin-Destination Distribution of Dockless Shared Bicycles: A Case Study in Nanjing City. Front. Public Health 10:849766. doi: 10.3389/fpubh.2022.849766

Shared bicycles are currently widely welcomed by the public due to their flexibility and convenience; they also help reduce chemical emissions and improve public health by encouraging people to engage in physical activities. However, during their development process, the imbalance between the supply and demand of shared bicycles has restricted the public's willingness to use them. Thus, it is necessary to forecast the demand for shared bicycles in different urban regions. This article presents a prediction model called QPSO-LSTM for the origin and destination (OD) distribution of shared bicycles by combining long short-term memory (LSTM) and quantum particle swarm optimization (QPSO). LSTM is a special type of recurrent neural network (RNN) that solves the long-term dependence problem existing in the general RNN, and is suitable for processing and predicting important events with very long intervals and delays in time series. QPSO is an important swarm intelligence algorithm that solves the optimization problem by simulating the process of birds searching for food. In the QPSO-LSTM model, LSTM is applied to predict the OD numbers. QPSO is used to optimize the LSTM for a problem involving a large number of hyperparameters, and the optimal combination of hyperparameters is quickly determined. Taking Nanjing as an example, the prediction model is applied to two typical areas, and the number of bicycles needed per hour in a future day is predicted. QPSO-LSTM can effectively learn the cycle regularity of the change in bicycle OD quantity. Finally, the QPSO-LSTM model is compared with the autoregressive integrated moving average model (ARIMA), back propagation (BP), and recurrent neural networks (RNNs). This shows that the QPSO-LSTM prediction result is more accurate.

Keywords: dockless shared bicycles, origin and destination (OD), OD distribution, QPSO, LSTM

INTRODUCTION

Shared bicycle systems have been widely adopted in cities as a promising solution to the last mile issues in public transportation (1–3). Apart from the immediate advantage for city commuters, it can also provide benefits to the environment and public health (4–8). In particular, due to its advantages of reducing resource consumption and chemical emissions, the use of shared bicycles is more environmentally friendly than motorized transportation (9). There is little doubt that using shared bicycles rather than automobiles benefits the environment. Meanwhile, the application of shared bicycles has the potential to promote public health. Physical inactivity has been linked to increased morbidity and mortality in numerous studies (10). Shared bicycles can provide means for people to exercise and improve their overall health (5, 11, 12).

At present, there are two types of shared bicycles in Nanjing city, docked shared bicycles and dockless shared bicycles. The docked shared bicycles require unified management with hardware devices, such as parking piles and paying devices. However, the docked shared bicycle user experience is not good due to the cumbersome certification and registration process (13). Moreover, the high capital and space costs of its supporting equipment also limit its development to a certain extent. Based on the mobile internet technology, dockless shared bicycles have rapidly developed in China and have become the main means of shared bicycles in the market due to their better user experience, simple registration and certification process, and convenience afforded when borrowing and returning bikes (14, 15). Dockless shared bicycles provide residents with more convenient services due to their stop-on-ride, flexibility, ease of use and low price. However, there are also many factors that are not conducive to the development of urban transportation, such as disorderly parking and the imbalance between supply and demand (16–18). These problems might decrease the opportunity and willingness of the public to use shared bicycles, but they have occurred in almost every city where shared bicycles are deployed in Asia, Europe and the Americas, including Beijing, Shanghai and Nanjing in China (17, 19, 20).

Short-term forecasts for the origin and destination (OD) number of shared bicycles in different areas can help in the discovery of behavioral patterns and help to solve the above possible future problems in advance (21). With better prediction results, users can be informed of the distribution of bikes in an area sometime in the future to better plan their itinerary. Operators can plan to place and reallocate bikes to improve the customer experience according to short-term demand forecasts. This will further promote the travel efficiency of urban residents and accelerate the improvement of the city's green travel layout. Therefore, it is beneficial not only for users and operators but also for the environment and public health. Geographic modeling is a useful way to discover geographic patterns and predict geographic processes (22, 23). Many scholars have utilized different models for shared bicycle prediction, including linear models based on mathematical statistics, intelligent theoretical models represented by neural networks, and combined models, which combine more than two types of models. The more representative linear model is the autoregressive integrated moving average (ARIMA) model. The ARIMA model was applied to predict the flow number and trip duration of bicycles (24). Although ARIMA is the most common statistical model for time series prediction, it has extremely high data requirements and requires time series data to be stable. It only captures the linear relationship of the data. The intelligent theoretical models used for bike-sharing prediction mainly include back propagation (BP), recurrent neural networks (RNNs), and long short-term memory (LSTM). BP has been used to predict shared bicycle demand and the number of public bicycle rented (25, 26). However, its learning speed is very slow, and network training is more likely to fail. RNNs are particularly good at capturing the temporal and spatial evolution of traffic flow, quantity and speed, so they are often used to predict short-term traffic volumes (27, 28). Although traditional RNNs perform well in non-linear time series data modeling, there are still several issues to be addressed, such as the inability to train time series with long time lags and the difficulty of automatically finding the optimal time window size (29, 30). LSTM makes up for the gradient disappearance and gradient explosion of RNNs and the lack of long-term memory ability so that the recurrent neural network can make full use of the long-term sequence information (31). Thus, LSTM can be applied to predict traffic flow and the demand of dockless shared bicycles (32). Due to the complexity of the traffic system and the shortcomings of various models, scholars have combined multiple models in recent studies to make full use of the advantages of different models for shared bicycle prediction. Combined models usually combine several different intelligent theoretical models and are based on mathematical statistics and intelligent theoretical models. For example, convolutional neural networks (CNNs) and LSTM were combined to predict the short-term distribution of dockless shared bicycles (33); a combination of CNNs and LSTM in a deep learning model was applied to predict the travel distance and OD distribution of shared bicycles (34).

The smart prediction of shared bicycles in this article is based on a deep learning algorithm. The first condition for accurate analysis using machine learning is to determine the appropriate model structure, including the number of stacked layers, the number of layer nodes, the activation function, the batch size and other hyperparameters. Determining the optimal hyperparameter combination in a high-dimensional space is a complicated problem. The traditional method for determining hyperparameters is the manual parameter adjustment method, which mainly relies on the experience of researchers, has strong subjectivity, and requires a long time for conducting experiments. In addition, other hyperparameter optimization methods, such as grid search, random search and Bayesian optimization, have high time complexity. There have been many studies on optimizing hyperparameters by using swarm intelligence algorithms due to their excellent parameter optimization performance. Commonly used swarm intelligence algorithms include ant colony optimization (ACO), particle swarm optimization (PSO), and quantum particle swarm optimization (QPSO) (35, 36). They can be applied to various types of deep learning hyperparameter optimization, but they

were mainly applied to optimize common models such as support vector machines (SVMs) and BP (37–42).

Most short-term demand predictions were based on regular grids. Few studies use swarm intelligence algorithms to optimize models with more parameters, such as LSTM, and even fewer use them for shared bicycle prediction. This article aims to build a comprehensive model, called QPSO-LSTM, for predicting the OD quantity of dockless shared bicycles by combining QPSO and LSTM models. By taking AOI (area of interest) as the basic analysis unit, the model attempts to consider the influence of different urban function types on bicycle distribution. In addition, QPSO is applied to optimize LSTM to obtain better predictions. By taking the main urban areas of Nanjing city as an example, the QPSO-LSTM model is applied to predict the OD number of dockless shared bicycles in different types of AOIs. It can help determine possible problems in advance, such as bike aggregation or an insufficient number of bikes in the future period, to help with the bike scheduling and promote bike distribution rebalancing. Finally, the model is compared with other commonly used models, including BP, ARIMA and RNN, to verify its accuracy.

STUDY AREA AND DATA PROCESSING

Study Area and Data Acquisition

Nanjing is an important gateway city for the development of the Yangtze River Delta. According to the 7th census, it has a permanent population of ∼9 million (2021). Since 2015, shared bicycles have experienced rapid development in Nanjing and have become a new travel choice for residents. Dockless shared bicycles were born as a new form of the sharing economy at the end of 2016, including bike share systems such as Ofo, Mobike and Hello Bike. Dockless shared bicycles quickly swept across the country due to their higher flexibility. As reported by Jiangsu Sina (2019), in 2018 the number of shared bicycles in Nanjing reached a record high of ∼600,000–700,000. Then the total number of shared bicycles was limited to ∼317,000 to regulate the bike-sharing market under the control of the government. According to the Hello Bike use report, in Nanjing (2017), 40,000 shared bicycles have been used 31 million times in 3 months, covering a distance of 54.81 million km, equivalent to cycling 1,367 laps around the equator. In this article, the study area is the downtown area of Nanjing, including

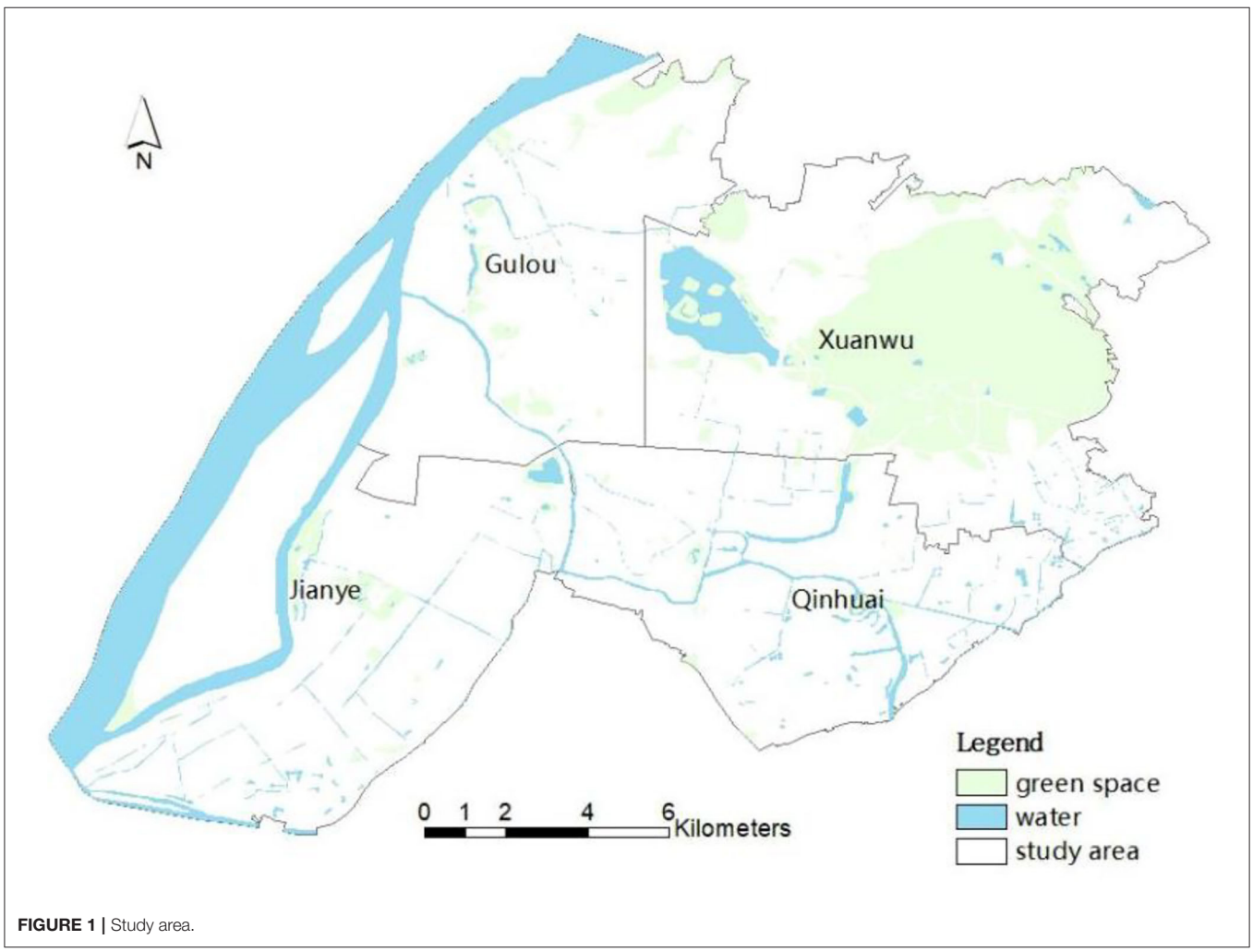

FIGURE 1 | Study area.

Xuanwu, Gulou, Jianye and Qinhuai Districts, as shown in **Figure 1**.

Bicycle share ridership is affected by different weather variables, socio-demographic attributes, land use and built environment, among which the impact of several weather variables on bicycle trips has been investigated in many studies (43–49). This article obtains the datasets of dockless shared bicycles, road networks, traffic facility points, AOI data and administrative zoning data for Nanjing, as shown in **Table 1**. The dockless shared bicycle dataset includes the bike location data, including the date, bike ID, longitude and latitude of each bike from March 9 to April 8, 2018. The location data of 105,901 shared bicycles in the study area over 32 days include ∼100 million records. The meteorological data, including temperature, wind speed, and precipitation from March 8 to April 2, 2018, with an interval of 1 h, were added as factors affecting bicycle trips. AOI is the area data used to represent each geographical entity, such as separate residential areas, independent commercial areas, and scenic zones. It is a carrier of all the social and economic activities of residents and reflects different types of urban functions. The attributes of each AOI include the name, address, category and latitude and longitude. The AOI is taken as the basic analysis unit in the study.

TABLE 1 | Data acquisition in the study area.

Types of data	Data description
Dockless shared bicycle dataset	Bike location data obtained from the mobile clients of Ofo and Mobike every 15 min
AOI data	Gaode map AOI data (data source: https://lbs.amap.com/)
Urban administrative zoning data	Shapefile of urban administrative zoning (data source: http://www.tianditu.gov.cn/)
Meteorological data	NCDC (National Climatic Data Center, China)

Periodicity of Shared Bicycle Trips

Time Interval of Periodic Series

The time interval for shared bicycle location data is 15 min. The number of bicycles in different time intervals was analyzed to determine the appropriate time interval for our study. **Figure 2** shows the curves of bicycle numbers at 15, 30, 60, and 120 min intervals at the original points of residential areas of the study area on March 14. **Figure 2** shows that the curve of the 1-h time interval can express the regularity of bicycle changes, and the

TABLE 2 | Trend similarity in different types of AOIs.

Cosine similarity	Residential area	Commercial building	Scenic area
Residential area	0.762	0.529	0.584
Commercial buildings		0.737	0.517
Scenic area			0.687

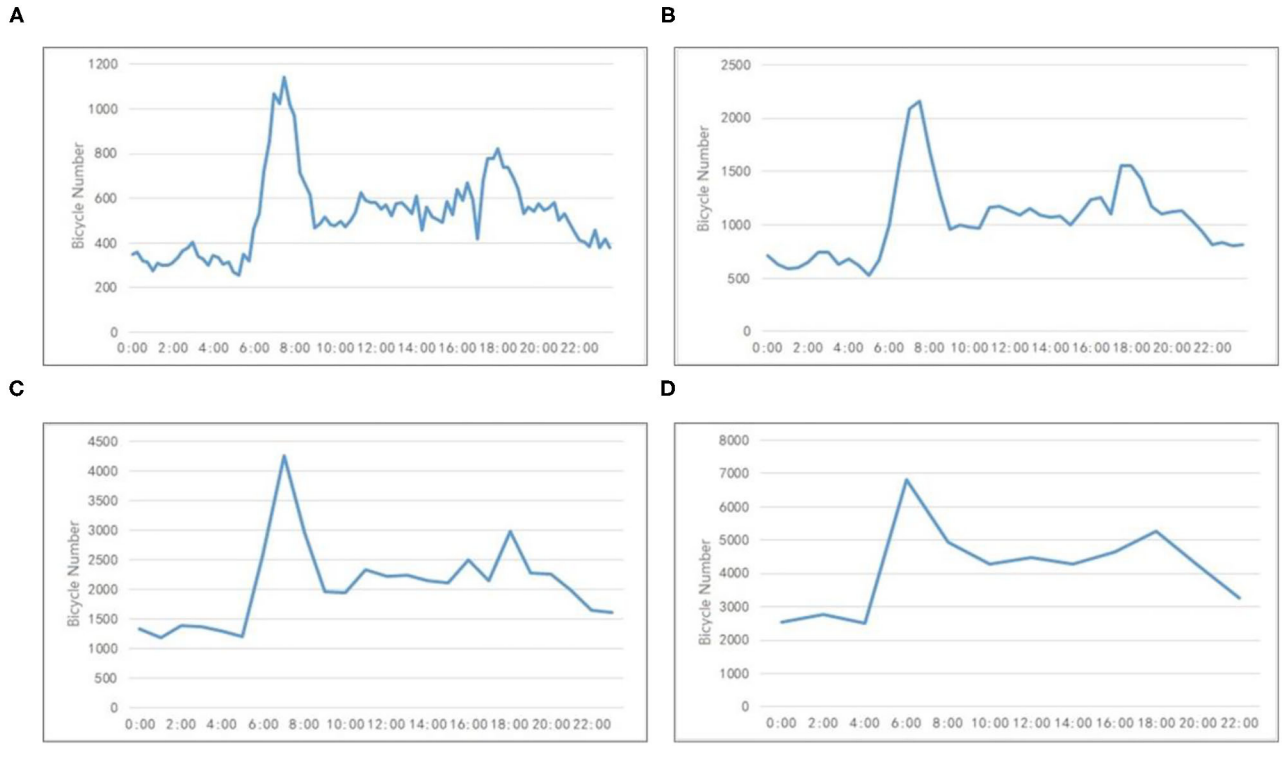

FIGURE 2 | The curves of bicycle numbers at different intervals. **(A)** 15 min. **(B)** 30 min. **(C)** 60 min. **(D)** 120 min.

curve is smoother than the time interval of 15 and 30 min. When the interval is >60 min, there are some difficulties in discovering the number changes of bicycle trips in 1 day. Therefore, this article takes 1 h as the time interval during the experiment to alleviate the impact of possible data loss on the overall law and effectively reduce the calculation rate.

Similarities in Different Types of AOIs

The possible trend similarity is explored to reflect the similar trends of cycling in different types of AOIs in the same time period. The cosine similarity can measure the trend similarity by comparing two vectors in a vector space. It evaluates the similarity between two vectors by calculating the cosine of the angle between them; thus it is not related to the specific value and is only affected by the angle of the two vectors. Formula (1) is used to calculate the cosine similarity $\cos\theta$ (50).

$$\cos\theta = \frac{\sum_{i=1}^{n} A_i B_i}{\sqrt{\sum_{i=1}^{n} (A_i)^2}\sqrt{\sum_{i=1}^{n} (B_i)^2}} \quad (1)$$

where $\cos\theta$ is the cosine similarity; A_i and B_i represent the components of vectors A and B, respectively; and n is the number of samples.

Table 2 lists the calculated cosine similarities among the AOIs of residential areas, commercial buildings and scenic areas. A higher cosine similarity indicates that the variation trend in the number of bicycle trips is similar within the same type of AOI. In contrast, a lower cosine similarity indicates that the variation trend in the number of bicycle trips is different in various types of AOIs, which are located in different urban function regions.

Daily Correlation

The daily changes in the number of bicycle trips on weekdays and weekends are considered to be different. The Pearson correlation coefficient is applied to calculate the daily correlation of the numbers of bicycle rides every 2 days in a week from March 12 to March 18. Formula (2) can calculate the Pearson correlation coefficient $\rho_{X,Y}$ (51).

$$\rho_{X,Y} = \frac{\sum_{i=1}^{n} (X_i - \overline{X})(Y_i - \overline{Y})}{\sqrt{\sum_{i=1}^{n} (X - \overline{X})^2}\sqrt{\sum_{i=1}^{n} (Y - \overline{Y})^2}} \quad (2)$$

where X, Y are 2 days; n is the number of hours in each day, which is 24; X_i, Y_i are the number of bicycles at the ith hour corresponding to X, Y; and $\overline{X}, \overline{Y}$ are the average values of X, Y. When $\rho_{X,Y}$ is -1, it means that X, Y are completely negatively correlated; when $\rho_{X,Y}$ is 1, it means that X, Y are completely positively correlated; when $\rho_{X,Y}$ is 0, it means that X, Y have no correlation.

As shown in **Table 3**, the correlation coefficients between weekdays are higher than 0.9. However, the correlation coefficients between weekdays and weekends are lower, ranging from 0.8 to 0.9. The correlation coefficient between Saturday and Sunday is 0.973, showing a high correlation. The results show that the daily cycling regularity is similar among weekdays and between weekends, but it is slightly different between weekends and weekdays.

Above all, the time interval for shared bicycle location data is determined to be 1 h in the constructed QPSO-LSTM model. In addition, due to the different regularity of changes, the number of bikes on weekdays and that on weekends need to be predicted separately, as does that in different AOIs.

MODEL CONSTRUCTION

The QPSO-LSTM model for predicting the OD quantity of shared bicycles is constructed as shown in **Figure 3**. The model is trained by using a training set and then is used to predict the number of shared bicycle trips in the future by using a test set. The model implementation process consists of three parts: data processing, the prediction model based on LSTM, and QPSO optimization.

First, the acquired cycling data were classified according to different AOI types to form cycling data with an interval of 1 h. Temperature, wind speed and precipitation were selected as the influencing factors of cycling and incorporated into the cycling data. The data underwent normalization, supervised learning and dataset division processing before model training and prediction. In particularly, 80% of the data were used as the training set and 20% were used as the validation set (52). Then, as a deep learning algorithm for sequential data prediction, LSTM is the core algorithm of the prediction model QPSO-LSTM. It was used to predict the OD quantity of shared bicycles by building a multilayer LSTM network. Finally, QPSO was applied to solve the optimization problem of the hyperparameters of the prediction model. By using QPSO, the hyperparameter combination suitable for the prediction model can be determined quickly to effectively improve the accuracy of the model.

Prediction Network Based on LSTM

The structure of the LSTM network of QPSO-LSTM is shown in **Figure 4** below. Its input data are bicycle and meteorological data, and the output data are the number of bicycles needed in the future. The horizontal line through the entire memory cell is similar to a conveyor belt, indicating the state of the cell. There are three types of gates in LSTM: the forget gate, input gate and output gate. The forget gate determines how much information should be removed from the cell state at the last moment, as shown in the red box in **Figure 4**. The new input information is determined by the input gate in the cell state, as shown in the yellow box. The parts of the cell state that are utilized to generate the final output of the memory cell are decided by the output gate, as shown in the green box (54–56). In addition, the pink circle in the memory cell represents the point operation, while the yellow rectangle represents the activation function, and they are all used to compute the gates and the memory cell output.

QPSO Optimization

QPSO hyperparameter optimization mainly includes determining the parameters to be optimized, selecting the

TABLE 3 | Daily correlation in 1 week.

Similarity	Monday	Tuesday	Wednesday	Thursday	Friday	Saturday	Sunday
Monday	1	0.970	0.965	0.957	0.974	0.848	0.788
Tuesday		1	0.940	0.918	0.957	0.811	0.723
Wednesday			1	0.954	0.970	0.819	0.759
Thursday				1	0.971	0.878	0.849
Friday					1	0.879	0.824
Saturday						1	0.973
Sunday							1

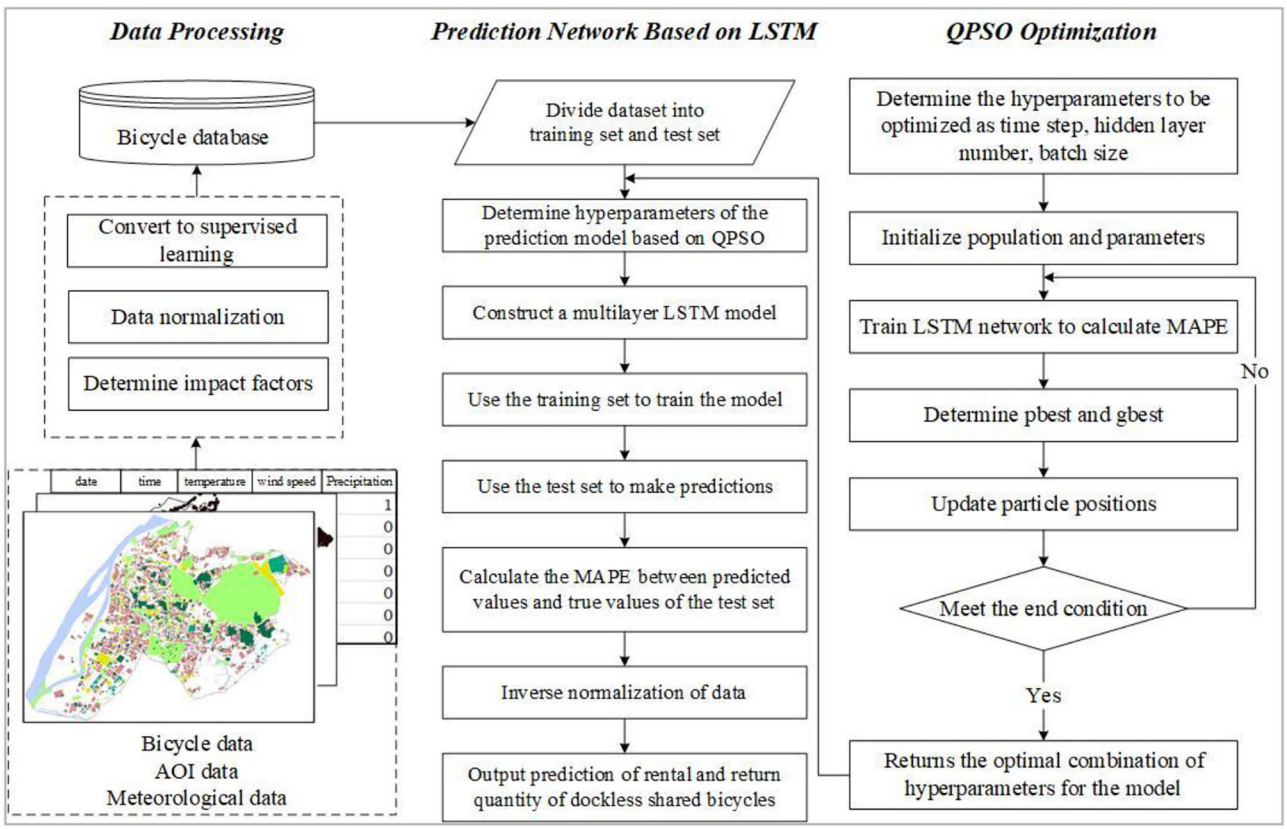

FIGURE 3 | QPSO-LSTM flowchart.

fitness function, and determining and updating the optimal positions of particles.

As shown in **Figure 5**, the time step, batch size and the numbers of nodes in the network hidden layers are selected as the parameters to be optimized in the prediction network, and each has an arrow pointing to it. The time step parameter determines the number of previous data moments in the model input at a certain moment. The batch size can effectively improve memory utilization and model training speed after optimization. A reasonable number of hidden layer nodes can avoid as much of the model over fitting phenomenon during training as possible. The change in the number of shared bicycle trips has a daily characteristic, so the value range of the time step is determined to be [1, 24]. The number of hidden layer nodes is determined according to the empirical rule (25), as shown in Formula (3).

$$u=\sqrt{m+n}+a \tag{3}$$

where m, n are the number of input and output layers of the network, respectively, and a is any integer between 3 and 10. The number of hidden layers ranges from [5, 50], and the range of the batch size is set to [1, 30].

QPSO needs to determine the objective function to determine the pros and cons of the current particle. Commonly used evaluation indicators for regression models include root mean

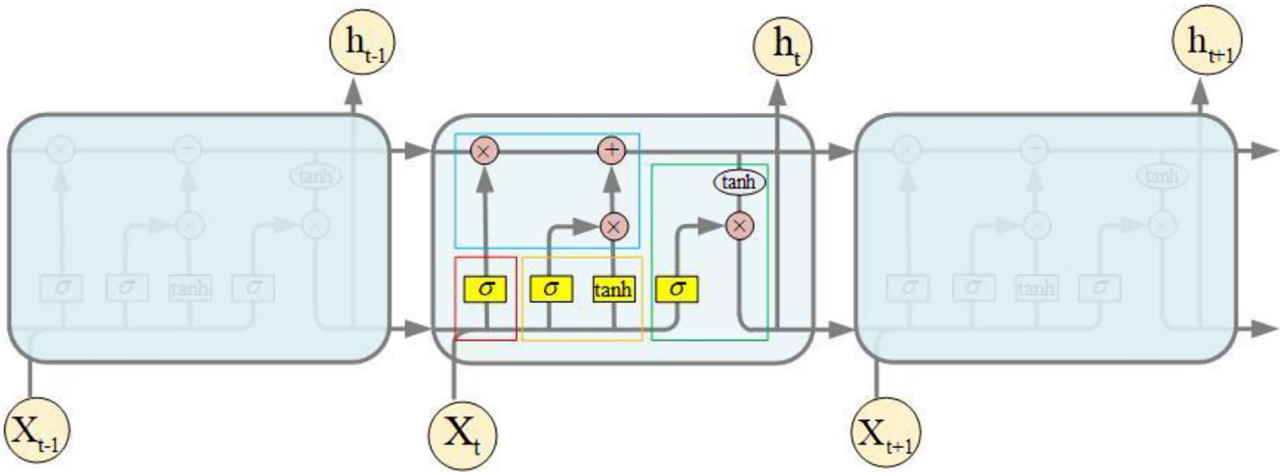

FIGURE 4 | Prediction network of QPSO-LSTM: Redrawn and extended from Li et al. (53).

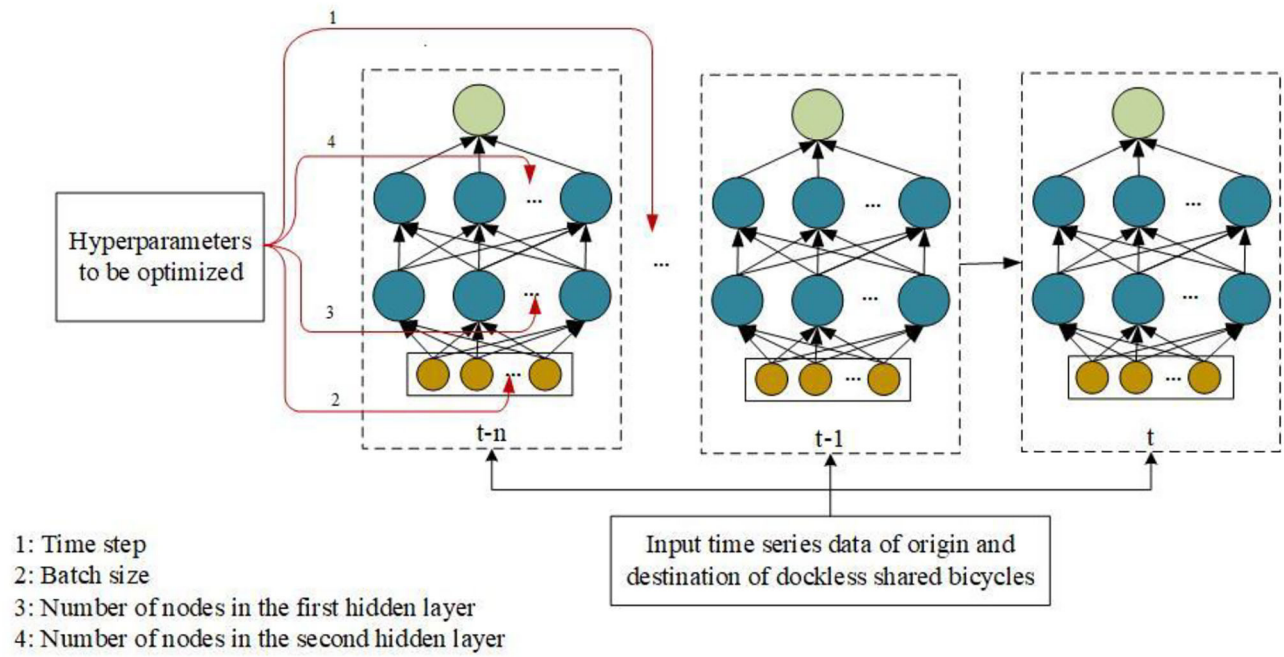

FIGURE 5 | Parameters to be optimized in the prediction network: 4 parameters are selected to be optimized.

square error (RMSE), mean absolute error (MAE) and mean absolute percentage error (MAPE) (57). Formulas (4–6) below are used to calculate these evaluation indicators.

$$RMSE = \sqrt{\frac{1}{m}\sum_{i=1}^{m}\left[h\left(x_i\right) - y_i\right]^2} \tag{4}$$

$$MAE = \frac{1}{m}\sum_{i=1}^{m}\left|h\left(x_i\right) - y_i\right| \tag{5}$$

where m, $h\left(x_i\right)$, and y_i are the length, predicted value and true value of the verification set, respectively.

When using QPSO to optimize the hyperparameters of our prediction network, MAPE is selected as the fitness function of the particle, which is defined by Formula (6).

$$MAPE = \frac{1}{m}\sum_{i=1}^{m}\left|\frac{h\left(x_i\right) - y_i}{y_i}\right| \tag{6}$$

According to the fitness function, the objective function value, the MAPE between the predicted value and the true value of the model, at each position is calculated. The smaller the objective function value is, the better the position.

In the whole learning process, the optimal position found by individual particles is $pbest_i$, and the mean value of the best position of individual particles is *mbest*. The objective function values of all particles in the population are calculated many times during the learning process to determine the global optimal position *gbest* of each particle in all the learning processes. Formulas (7–9) can be used to calculate these values (35).

$$x_i = P_i \pm \alpha \left| mbest - x_i \right| \ln\left(\frac{1}{u}\right) \tag{7}$$

$$P_i = \varnothing pbest_i + (1 - \varnothing)\, gbest \tag{8}$$

$$mbest = \frac{1}{M}\sum_{i-1}^{M} pbest_i \tag{9}$$

where M is the size of the particle group; x_i is the position of the ith particle; α is the innovation parameter; and $\varnothing$ and u are uniformly distributed values on (0, 1).

MODEL APPLICATION AND VERIFICATION

Model Results and Typical Case Analysis

The prediction models of different AOIs obtained after model training can be applied to predict the OD quantity of bicycles for all types of AOIs in the whole study area. According to the QPSO optimization results, the time step is 4, which means that the model uses the number of bicycles in the previous 4 moments to predict the number of bicycles in the next moment. In addition, the batch size and the node numbers of the first hidden layer and the second hidden layer are set to 28, 10, and 16, respectively.

For each AOI, the model to which it belongs is applied to predict the number of bicycles in each hour. For example, the prediction results of the OD quantities of bicycle rides at 8 am on March 14 are shown in **Figure 6**. At 8 A.M. in the study area, the bicycle OD quantities of the different regions are slightly different, which fully reflects the characteristics of residents' trips and verifies the effectiveness of the prediction model. As shown in the **Figure 6**, there are more origin points than destination points in residential areas. The AOI area of scenic areas accounts for the largest proportion of the total area of the study area, ∼40.2%. Due to their larger area, there are more bikes in scenic areas, such as Purple Mountain and Xuanwu Lake, which are generally shown in red in the **Figure 6**.

Two typical areas, including residential areas and commercial buildings, are selected to use the corresponding model to predict the OD quantity of bicycles. The typical residential area selected is Huaxincheng, which is located near Yuantong station of subway Line 1 and Line 2, and leisure and entertainment facilities such as Hexi Central Park and Nanjing Famous Taiwan Goods City are around it. Taking it as an example, its bicycle OD data on the weekday of March 14 are selected to predict the supply and demand of bicycles by using the prediction model of residential area AOIs. The prediction of bicycle OD numbers in Huaxincheng is shown in **Figure 7**. The results show that bicycle OD numbers are higher in the morning and evening peak hours, but their changes are different. The peak value of the number of origin points in the morning peak period is greater than that in the evening peak period, while the peak value of the destination points in the evening peak period is higher than that in the morning peak period. This prediction conforms to the daily regularity of cycling for residents commuting to work.

The typical commercial building selected is Fenghuang Square located at No. 1, Hunan Road and is an innovative commercial mall. The cycling OD data of this area on March 14 are selected to predict the supply and demand of shared bicycles by using O and D models of commercial building AOIs. The predicted bike OD numbers of Fenghuang Square are shown in **Figure 8**. The result also reflects the characteristics of the morning and evening peaks. The number of bicycle destination points in the morning peak hours was slightly higher than that of origin points, while the number of origin points in the evening peak hours was much higher. This prediction is in line with the regularity of the use of bicycles near commercial buildings.

Model Evaluation

Bicycles have different cycling patterns in different types of AOIs. Using the constructed prediction model, bicycle supply and demand prediction models suitable for different types of AOIs, including residential areas, commercial buildings, scenic spot areas, science, education and cultural areas, and other service areas, are obtained after model training. The data used in model training are the series data of each type of AOI in the whole study area, with a total of 32 days of data, 80% of which is 25 days in total as the training set, and 20% of which is 7 days in total as the test set.

Figure 9 verifies the prediction accuracy of the OD distribution models of the residential areas. When verifying the model, the data from the week from March 12th to March 18th are selected as input. Each day consists of 24 h of data, with a total of 7*24, 168 pieces of input data. Since the time step set in the training model is 4, a total of 168*4 inputs are formed after conversion to supervised learning, and the range of predicted results is from 3 o'clock on March 12 to 23 o'clock on March 18. The results show that the predicted value and the true value of the QPSO-LSTM models are relatively consistent, as well as the change trend in the values. The peak times appearing each day are consistent, and the peak values are similar. In addition, residents have strong cycling regularity on weekdays but no obvious cycling regularity on weekends. There are several obvious morning peaks and evening peaks within a week, but the use of bicycles on weekends is greatly reduced. Specifically, for the origin points of the residential areas, as shown in **Figure 9A**, morning peaks are significantly higher than evening peaks, while for the destination points, as shown in **Figure 9B**, the comparison results are the opposite. The above conclusions are in line with the cycling characteristics of urban residents and verify the performance of the QPSO-LSTM prediction model.

The BP network, RNN network and ARIMA model are applied to predict the number of bicycle origin points of residential areas from 4:00 on March 12 to 23:00 on March 18. The comparison results between the true value and prediction of these three models are shown in **Figure 10**. Comparing the prediction results of the three models with the true value, the

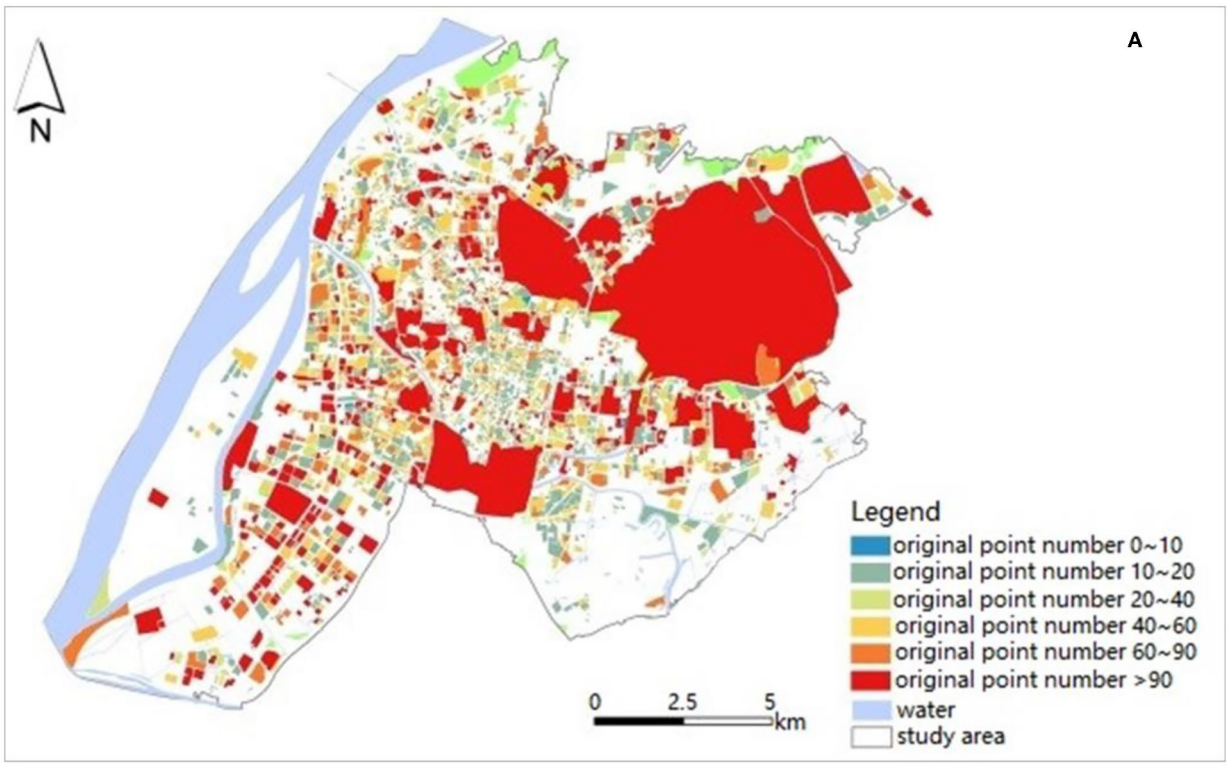

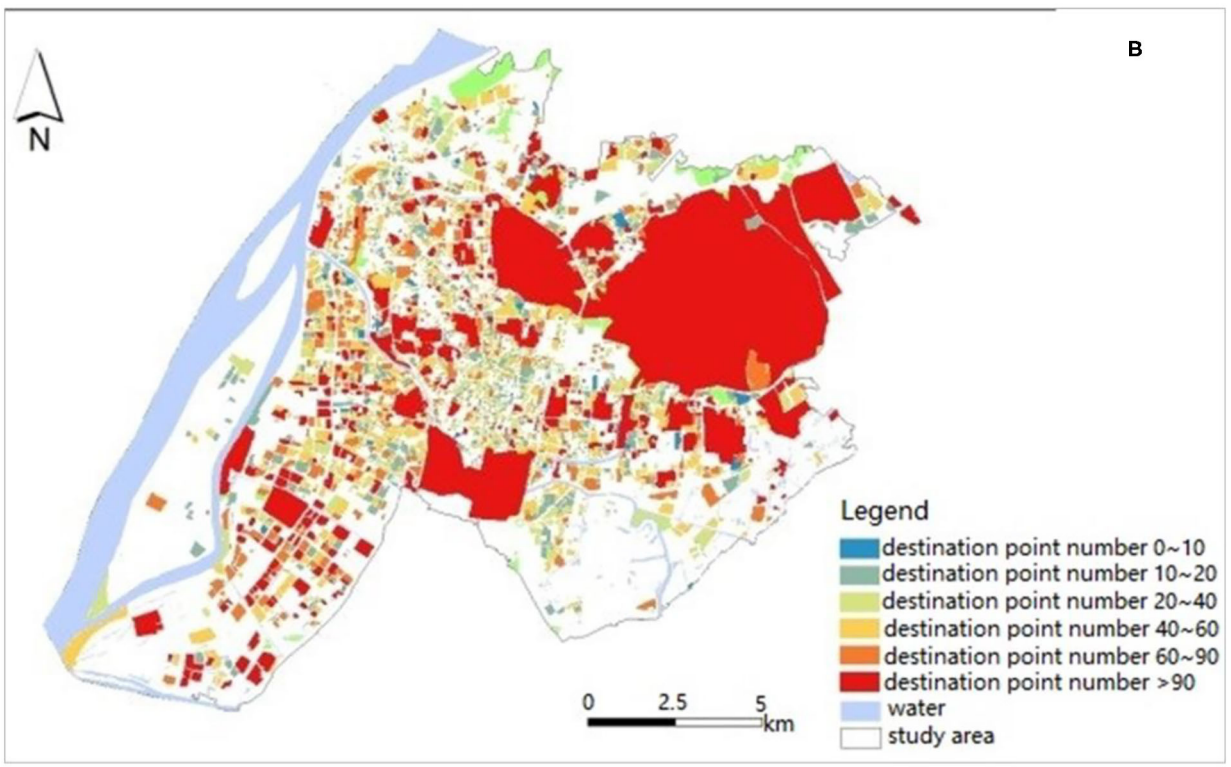

FIGURE 6 | Prediction results at 8 am of study area. **(A)** Origin points. **(B)** Destination points.

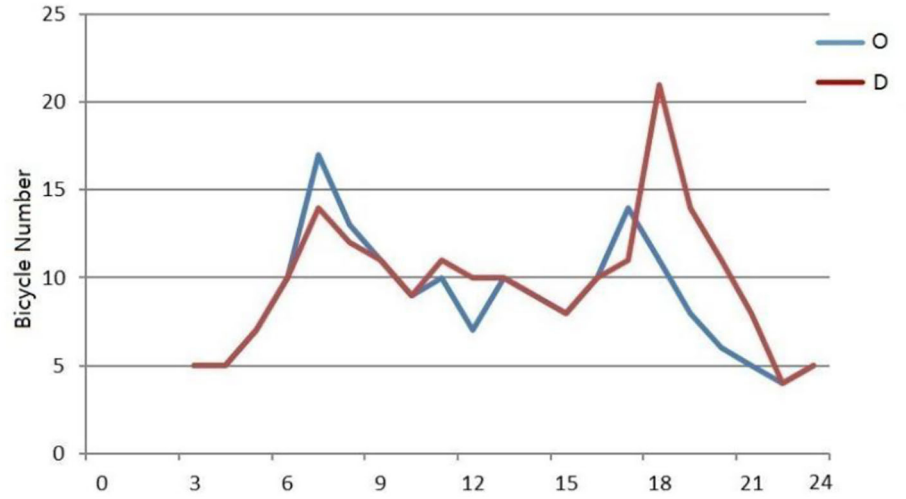

FIGURE 7 | Prediction of bicycle OD quantity in Huaxincheng.

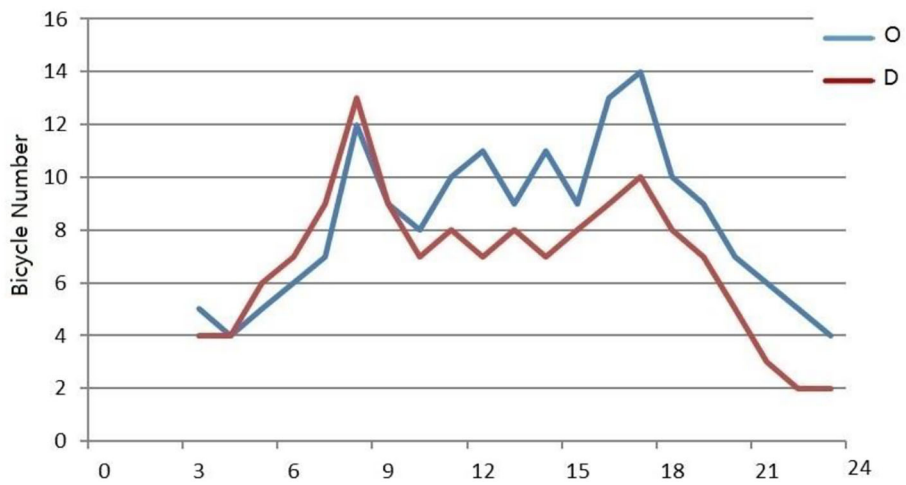

FIGURE 8 | Prediction of bicycle OD quantity in Fenghuang Square.

change trends are roughly the same, and they all perform well at predicting the number of bicycles between peaks. However, there are some differences in the predictions for the periods around the peaks. The predicted values of ARIMA during these periods are closer to the true values than the other two models, especially in the periods near the low peaks. For example, from 0:00 to 6:00 every day, the ARIMA prediction is closer to the true value, while the prediction values of RNN and BP are significantly higher. In addition, compared with the predictions of BP and RNN, BP performs slightly better than RNN. As a result, ARIMA has the best prediction effect, followed by BP and finally RNN.

To verify the accuracy of the QPSO-LSTM model, a verification set is used to compare and verify the prediction accuracy of the other models constructed, including the BP network, RNN network, and ARIMA model, as shown in **Table 4**. Whether RMSE, MAE, or MAPE is used as the evaluation index, the error of the QPSO-LSTM model is smaller than that of RMSE, MAE, or MAPE, which means that the prediction accuracy of the QPSO-LSTM model is higher than that of theirs. Taking MAPE as an example, the QPSO-LSTM model has the lowest error value, which is 0.087. Conversely, it has the highest accuracy, which is up to ∼91%. The error values of the other three models are all >0.1, which means that their accuracy is <90%. As a result, the QPSO-LSTM model is confirmed to have better accuracy and to be able to reasonably predict the supply and demand of shared bicycles of different AOIs.

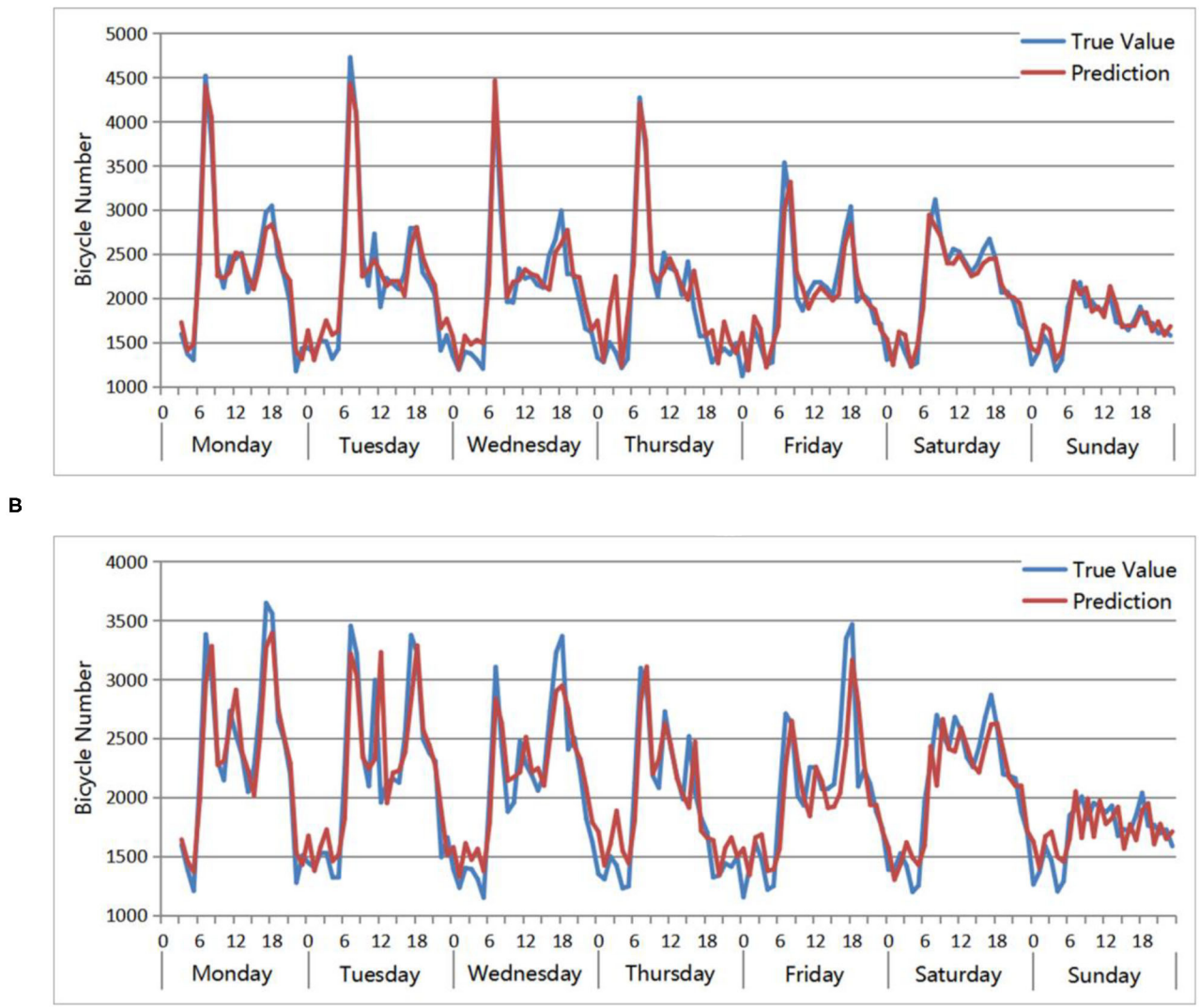

FIGURE 9 | Accuracy evaluation: true value and prediction of QPSO-LSTM in residential areas. **(A)** Origin points number. **(B)** Destination points number.

CONCLUSIONS

The travel mode is a factor influencing environmental and public health that cannot be ignored (58, 59). Shared bicycles, as a healthy and environmentally sustainable travel mode, should be conveniently accessed by the public. Thus, it is necessary to predict the demand for shared bicycles and optimize the supply of shared bicycles in different urban regions. In this article, a bicycle prediction model called QPSO-LSTM is established, which aims to predict the number of bicycles at OD points in different regions. It is trained with the same dataset as BP, RNN, and ARIMA, and the result shows that QPSO-LSTM significantly outperforms the other models. Furthermore, the model is also applied to predict the bicycle numbers in two typical areas, and the prediction results validate the availability of the model.

Since QPSO-LSTM can predict the future supply and demand for shared bicycles of each analysis unit (AOI), the future distribution of shared bicycles can be rebalanced based on the prediction results. By designing scheduling schemes that optimize resource allocation, idle bikes can be dispatched in a timely manner to areas with large demand, so that the number of shared bicycles tends to be reasonable. Reasonable scheduling optimization can rebalance the distribution of shared bicycles, meet the needs of users for using bikes, improve user satisfaction, and ensure that the shared bicycle system is in a state of dynamic balance. Optimization of bicycle layout according to the actual demand and time series regularity can effectively guide the planning of urban green travel.

Although the QPSO-LSTM has been verified to be a useful method to predict the demand for shared bicycles, some limitations remain.

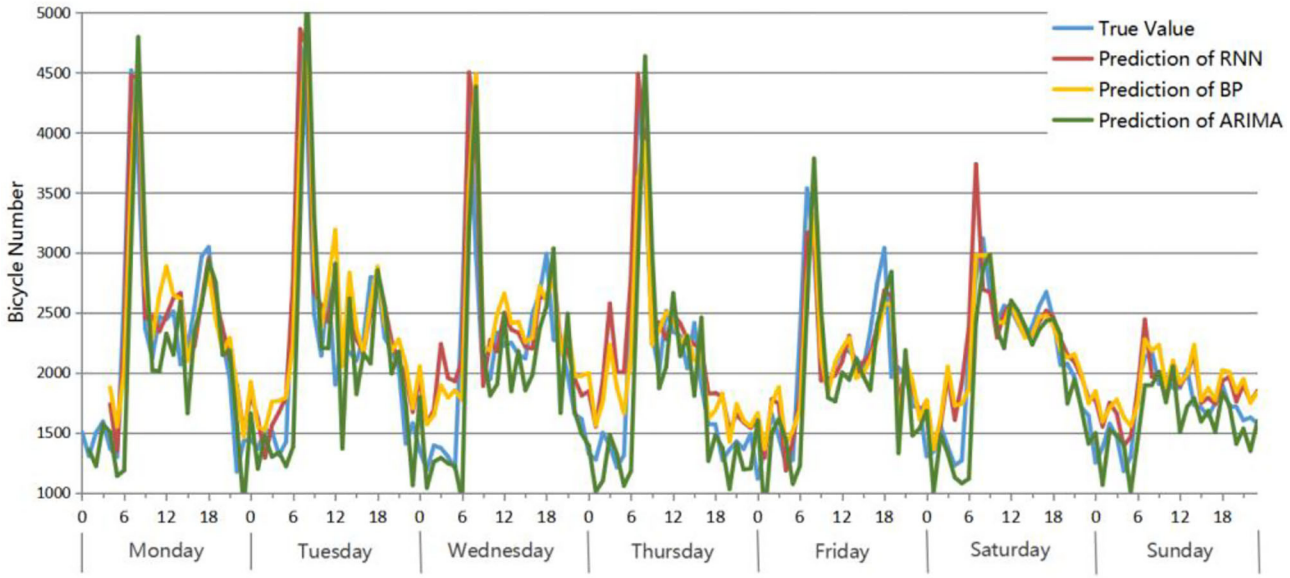

FIGURE 10 | Accuracy evaluation: True value and prediction results of 3 models for the residential area bicycle origin point number from 4:00 on March 12 to 23:00 on March 18.

TABLE 4 | Accuracy comparison of different models.

Type	RMSE	MAE	MAPE
BP Network	354.58	247.99	0.131
RNN Network	346.47	266.01	0.145
ARIMA Model	314.13	193.12	0.104
QPSO-LSTM Model	224.63	160.40	0.087

(1) The current QPSO-LSTM mainly used cycling data, and the weather data (e.g., temperature, wind speed and precipitation) were incorporated into the cycling data. However, other factors such as road networks, visibility in foggy weather, and seasonal changes in the weather might also affect the public's willingness to use bicycles and cause differences in OD distributions. Thus, these factors should also be taken into account in the prediction model.

(2) The performance of QPSO-LSTM was evaluated by using data from Nanjing. However, whether the model is a good choice for other similar cities still needs to be tested. In addition, the characteristics of dockless shared bicycle OD trips need to be analyzed to discover the driving mechanism of these characteristics.

(3) The prediction of the OD distribution provides opportunities for optimizing shared bicycle allocation. However, there is still a long way to go to keep the demand and supply of shared bicycles in a dynamic balance. The optimization of the layout of shared bicycles based on the prediction results is expected to be explored in further studies.

DATA AVAILABILITY STATEMENT

The data and codes that support the findings of this study are available in GitHub with the identifier: https://github.com/SharingBikeNNU/QPSO-LSTM.

AUTHOR CONTRIBUTIONS

MC: conceptualization, investigation, writing, and funding acquisition. YL: methodology and validation. YZ: methodology. GL: project administration. ZM: investigation and writing—review and editing. All authors contributed to the article and approved the submitted version.

FUNDING

This study was supported by the National Natural Science Foundation of China (Grant Nos. 41671385, 41622108, and 41871178), the Priority Academic Program Development of Jiangsu Higher Education Institutions (No. 164320H116).

ACKNOWLEDGMENTS

We thank the editor and reviewers who provided helpful suggestions on ways to improve the paper.

REFERENCES

1. DeMaio P. Bike-sharing: History, impacts, models of provision, and future. *J Public Transport.* (2009) 12:41–56. doi: 10.5038/2375-0901.12.4.3
2. Fu C, Guo Q. Road traffic injuries in shared bicycle riders in China. *Lancet Public Health.* (2018) 3:e111. doi: 10.1016/S2468-2667(18)30024-0
3. Beairsto J, Tian Y, Zheng L, Zhao Q, Hong J. Identifying locations for new bike-sharing stations in Glasgow: an analysis of spatial equity and demand factors. *Ann GIS.* (2021). doi: 10.1080/19475683.2021.1936172
4. Fishman E. Bikeshare: A review of recent literature. *Transport Rev.* (2016) 36:92–113. doi: 10.1080/01441647.2015.1033036
5. Ding D, Jia Y, Gebel K. Mobile bicycle sharing: the social trend that could change how we move. *Lancet Public Health.* (2018) 3:e215. doi: 10.1016/S2468-2667(18)30066-5
6. de Chardon CM. The contradictions of bike-share benefits, purposes and outcomes. *Transport Res Part A: Policy Pract.* (2019) 121:401–19. doi: 10.1016/j.tra.2019.01.031
7. Maas S, Attard M, Caruana MA. Assessing spatial and social dimensions of shared bicycle use in a Southern European island context: The case of Las Palmas de Gran Canaria. *Transport Res Part A: Policy Pract.* (2020) 140:81–97. doi: 10.1016/j.tra.2020.08.003
8. Kang Y, Zhang F, Gao S, Lin H, Liu Y. A review of urban physical environment sensing using street view imagery in public health studies. *Ann GIS.* (2020) 26:261–75. doi: 10.1080/19475683.2020.1791954
9. Murphy E, Usher J. The role of bicycle-sharing in the city: Analysis of the Irish experience. *Int J Sustain Transport.* (2015) 9:116–25. doi: 10.1080/15568318.2012.748855
10. Lee IM, Shiroma EJ, Lobelo F, Puska P, Blair SN, Katzmarzyk PT, et al. Effect of physical inactivity on major non-communicable diseases worldwide: an analysis of burden of disease and life expectancy. *Lancet*. (2012) 380:219–29. doi: 10.1016/S0140-6736(12)61031-9
11. Woodcock J, Tainio M, Cheshire J, O'Brien O, Goodman A. Health effects of the London bicycle sharing system: health impact modelling study. *BMJ.* (2014) 348:g425. doi: 10.1136/bmj.g425
12. Heinen E, Kamruzzaman M, Turrell G. The public bicycle-sharing scheme in Brisbane, Australia: Evaluating the influence of its introduction on changes in time spent cycling amongst a middle-and older-age population. *J Transport Health.* (2018) 10:56–73. doi: 10.1016/j.jth.2018.07.003
13. Fishman E, Washington S, Haworth N. Barriers and facilitators to public bicycle scheme use: A qualitative approach. *Transport Res Part F: Traffic Psychol Behav.* (2012) 15:686–98. doi: 10.1016/j.trf.2012.08.002
14. Zhang Y, Mi Z. Environmental benefits of bike sharing: A big data-based analysis. *Appl Energy.* (2018) 220:296–301. doi: 10.1016/j.apenergy.2018.03.101
15. Chen Z, van Lierop D, Ettema D. Exploring dockless bikeshare usage: A case study of Beijing, China. *Sustainability.* (2020) 12:1238. doi: 10.3390/su12031238
16. Hua M, Chen J, Chen X, Gan Z, Wang P, Zhao D. Forecasting usage and bike distribution of dockless bike-sharing using journey data. *IET Intelligent Trans Syst.* (2020) 14:1647–56. doi: 10.1049/iet-its.2020.0305
17. Bao J, Yu H, Wu J. Short-term FFBS demand prediction with multi-source data in a hybrid deep learning framework. *IET Intelligent Transport Syst.* (2019) 13:1340–7. doi: 10.1049/iet-its.2019.0008
18. Mooney SJ, Hosford K, Howe B, Yan A, Winters M, Bassok A, et al. Freedom from the station: Spatial equity in access to dockless bike share. *J Transport Geography.* (2019) 74:91–96. doi: 10.1016/j.jtrangeo.2018.11.009
19. Shaheen SA, Guzman S, Zhang H. Bikesharing in Europe, the Americas, and Asia: past, present, and future. *Transport Res Rec.* (2010) 2143:159–67. doi: 10.3141/2143-20
20. Jiang J, Lin F, Fan J, Lv H, Wu J. A destination prediction network based on spatiotemporal data for bike-sharing. *Complexity.* (2019) 2019:7643905. doi: 10.1155/2019/7643905
21. Shen J, Liu X, Chen M. Discovering spatial and temporal patterns from taxi-based Floating Car Data: A case study from Nanjing. *GIScience Remote Sensing.* (2017) 54:617–38. doi: 10.1080/15481603.2017.1309092
22. Chen M, Voinov A, Ames DP, Kettner AJ, Goodall JL, Jakeman AJ, et al. Position paper: Open web-distributed integrated geographic modelling and simulation to enable broader participation and applications. *Earth-Sci Rev.* (2020) 207:103223. doi: 10.1016/j.earscirev.2020.103223
23. Chen M, Lv G, Zhou C, Lin H, Ma Z, Yue S, et al. Geographic modeling and simulation systems for geographic research in the new era: Some thoughts on their development and construction. *Sci China Earth Sci.* (2021) 64:1207–23. doi: 10.1007/s11430-020-9759-0
24. Salih-Elamin R, Al-Deek H. Short-term prediction for bike share systems' travel time under the effects of weather conditions. *Adv Transport Stud.* (2020) 50:81–94. doi: 10.4399/97888255317326
25. Liu Q, Xue Y, Wu J. Forecast of bicycle sharing demand using BP neural network based on improved brain storm optimization. In: *EITCE 2019: 3rd International Conference on Electronic Information Technology and Computer Engineering; 2019 Oct 18; Xiamen, China*. IEEE (2019). doi: 10.1109/EITCE47263.2019.9095056
26. Lin F, Wang S, Jiang J, Fan W, Sun Y. Predicting public bicycle rental number using multi-source data. In: *IJCNN 2017: International Joint Conference on Neural Networks; 2017 May 14; Anchorage, AK, USA*. IEEE. (2017). doi: 10.1109/IJCNN.2017.7966030
27. Lingras P, Sharma S, Zhong M. Prediction of recreational travel using genetically designed regression and time-delay neural network models. *Transport Res Rec.* (2002) 1805:16–24. doi: 10.3141/1805-03
28. Van Lint JW, Hoogendoorn SP, van Zuylen HJ. Freeway travel time prediction with state-space neural networks: modeling state-space dynamics with recurrent neural networks. *Transport Res Rec.* (2002) 1811:30–9. doi: 10.3141/1811-04
29. Gers FA, Schmidhuber J, Cummins F. Learning to forget: Continual prediction with LSTM. *Neural Comput.* (2000) 12:2451–71. doi: 10.1162/089976600300015015
30. Gers F. *Long Short-Term Memory in Recurrent Neural Networks*. [dissertation]. [Lausanne]: École Polytechnique Fédérale De Lausanne (2001).
31. Hochreiter S, Schmidhuber J. Long short-term memory. *Neural Comput.* (1997) 9:1735–80. doi: 10.1162/neco.1997.9.8.1735
32. Xu C, Ji J, Liu P. The station-free sharing bike demand forecasting with a deep learning approach and large-scale datasets. *Transport Res Part C: Emerg Technol.* (2018) 95:47–60. doi: 10.1016/j.trc.2018.07.013
33. Ai Y, Li Z, Gan M, Zhang Y, Yu D, Chen W, et al. A deep learning approach on short-term spatiotemporal distribution forecasting of dockless bike-sharing system. *Neural Comp App.* (2019) 31:1665–77. doi: 10.1007/s00521-018-3470-9
34. Li Y, Shuai B. Origin and destination forecasting on dockless shared bicycle in a hybrid deep-learning algorithms. *Multimedia Tools App*. (2020) 79:5269–80. doi: 10.1007/s11042-018-6374-x
35. Kennedy J, Eberhart R. Particle swarm optimization. In: *Proceedings of ICNN'95-International Conference on Neural Networks; 1995 Nov 27; Perth, WA, Australia*. IEEE. (1995).
36. Sun J, Feng B, Xu W. Particle swarm optimization with particles having quantum behavior. In: *Proceedings of the 2004 Congress on Evolutionary Computation; 2004 Jun 19; Portland, OR, USA*. IEEE (2004).
37. Wang M, Wan Y, Ye Z, Lai X. Remote sensing image classification based on the optimal support vector machine and modified binary coded ant colony optimization algorithm. *Inform Sci.* (2017) 402:50–68. doi: 10.1016/j.ins.2017.03.027
38. Fan Y, Wang G, Lu X, Wang G. Distributed forecasting and ant colony optimization for the bike-sharing rebalancing problem with unserved demands. *PLoS ONE.* (2019) 14:e0226204. doi: 10.1371/journal.pone.0226204
39. Luo C, Huang C, Cao J, Lu J, Huang W, Guo J, et al. Short-term traffic flow prediction based on least square support vector machine with hybrid optimization algorithm. *Neural Process Lett.* (2019) 50:2305–22. doi: 10.1007/s11063-019-09994-8
40. Zhang ZG, Yin JC, Wang NN, Hui ZG. Vessel traffic flow analysis and prediction by an improved PSO-BP mechanism based on AIS data. *Evolving Syst.* (2019) 10:397–407. doi: 10.1007/s12530-018-9243-y
41. Zhang SQ, Lin KP. Short-term traffic flow forecasting based on data-driven model. *Mathematics.* (2020) 8:152. doi: 10.3390/math8020152
42. Zeng C, Hua C, Lei T, Xiao X. Short-term traffic flow prediction on campus based on modified PSOBP neural network. In: *ICPMS2020: The Third International Conference on Physics; 2020 May 20-22; Kunming, China*. IOP Publishing. (2020). doi: 10.1088/1742-6596/1592/1/012071

43. García-Palomares JC, Gutiérrez J, Latorre M. Optimizing the location of stations in bike-sharing programs: A GIS approach. *Appl Geography.* (2012) 35:235–46. doi: 10.1016/j.apgeog.2012.07.002
44. Imani AF, Eluru N. Analyzing destination choice preferences in bicycle sharing systems: an investigation of Chicago's Divvy System. *J Transport Geography.* (2015) 44:53–64. doi: 10.1016/j.jtrangeo.2015.03.005
45. Wang X, Lindsey G, Schoner JE, Harrison A. Modeling bike share station activity: Effects of nearby businesses and jobs on trips to and from stations. *J Urban Plann Dev.* (2016) 142:04015001. doi: 10.1061/(ASCE)UP.1943-5444.0000273
46. Zhang Y, Thomas T, Brussel M, Van Maarseveen M. Exploring the impact of built environment factors on the use of public bikes at bike stations: case study in Zhongshan, China. *J Transport Geography.* (2017) 58:59–70. doi: 10.1016/j.jtrangeo.2016.11.014
47. El-Assi W, Mahmoud MS, Habib KN. Effects of built environment and weather on bike sharing demand: a station level analysis of commercial bike sharing in Toronto. *Transportation.* (2017) 44:589–613. doi: 10.1007/s11116-015-9669-z
48. Du M, Cheng L. Better understanding the characteristics and influential factors of different travel patterns in free-floating bike sharing: Evidence from Nanjing, China. *Sustainability.* (2018) 10:1244. doi: 10.3390/su10041244
49. Scott DM, Ciuro C. What factors influence bike share ridership? An investigation of Hamilton, Ontario's bike share hubs. *Travel Behav Soc.* (2019) 16:50–8. doi: 10.1016/j.tbs.2019.04.003
50. Bhopale AP, Tiwari A. Swarm optimized cluster based framework for information retrieval. *Expert Syst App.* (2020) 154:113441. doi: 10.1016/j.eswa.2020.113441
51. Bommisetty RM, Prakash O, Khare A. Keyframe extraction using Pearson correlation coefficient and color moments. *Multimedia Syst.* (2019) 26:267–99. doi: 10.1007/s00530-019-00642-8
52. Sohrabi S, Ermagun A. Dynamic bike sharing traffic prediction using spatiotemporal pattern detection. *Transport Res Part D: Transport Environ.* (2021) 90:102647. doi: 10.1016/j.trd.2020.102647
53. Li YY, Van Do T, Nguyen HT. A comparison of forecasting models for the resource usage of MapReduce applications. *Neurocomputing.* (2020) 418:36–55. doi: 10.1016/j.neucom.2020.07.059
54. Moon T, Ahn TI, Son JE. Long short term memory for a model free estimation of macronutrient ion concentrations of root zone in closed loop soilless cultures. *Plant methods.* (2019) 15:59. doi: 10.1186/s13007-019-0443-7
55. Zhao Y, Liu Q, Zhang Z, Bi Z, Bai Y, Zhou Y, et al. Estimating the Q-marker concentrations of Salvia miltiorrhiza via a long short-term memory algorithm using climatic factors and metabolic profiling. *Indus Crops Products.* (2020) 156:112883. doi: 10.1016/j.indcrop.2020.112883
56. Lipton ZC, Berkowitz J, Elkan, C. A critical review of recurrent neural networks for sequence learning. *arXiv[Preprint].arXiv:1506.00019.* (2015). doi: 10.48550/arXiv.1506.00019
57. Peng Y, Xiang W. Short-term traffic volume prediction using GA-BP based on wavelet denoising and phase space reconstruction. *Phys A: Statist Mech App.* (2020) 549:123913. doi: 10.1016/j.physa.2019.123913
58. Wu L, Wang W, Jing P, Chen Y, Zhan F, Shi Y, et al. Travel mode choice and their impacts on environment—a literature review based on bibliometric and content analysis, 2000–2018. *J Clean Product.* (2020) 249:119391. doi: 10.1016/j.jclepro.2019.119391
59. Zhu R, Anselin L, Batty M, Kwan MP, Chen M, Luo W, et al. The effects of different travel modes and travel destinations on COVID-19 transmission in global cities. *Sci Bull.* (2022) 67:588–92. doi: 10.1016/j.scib.2021.11.023

Conflict of Interest: The authors declare that the research was conducted in the absence of any commercial or financial relationships that could be construed as a potential conflict of interest.

frontiers | Frontiers in Public Health

ORIGINAL RESEARCH
published: 02 May 2022
doi: 10.3389/fpubh.2022.870403

Green Space Cooling Effect and Contribution to Mitigate Heat Island Effect of Surrounding Communities in Beijing Metropolitan Area

Wei Liu[1†], *Haiyue Zhao*[1†], *Shibo Sun*[2], *Xiyan Xu*[3], *Tingting Huang*[1] *and Jianning Zhu*[1*]

[1] School of Landscape Architecture, Beijing Forestry University, Beijing, China, [2] Department of Horticulture, Beijing Vocational College of Agriculture, Beijing, China, [3] School of Chemistry and Chemical Engineering, Beijing Institute of Technology, Beijing, China

OPEN ACCESS

Edited by:
Chuanrong Zhang,
University of Connecticut,
United States

Reviewed by:
Si Chen,
Hubei University, China
Xufeng Cui,
Zhongnan University of Economics and Law, China
Huali Xiang,
Zhongnan University of Economics and Law, China

***Correspondence:**
Jianning Zhu
blzjn@vip.sina.com

[†]These authors have contributed equally to this work and share first authorship

Specialty section:
This article was submitted to Environmental health and Exposome, a section of the journal Frontiers in Public Health

Received: 06 February 2022
Accepted: 04 April 2022
Published: 02 May 2022

Citation:
Liu W, Zhao H, Sun S, Xu X, Huang T and Zhu J (2022) Green Space Cooling Effect and Contribution to Mitigate Heat Island Effect of Surrounding Communities in Beijing Metropolitan Area. Front. Public Health 10:870403. doi: 10.3389/fpubh.2022.870403

With the rapid process of urbanization and global warming, many metropolises are vulnerable to high temperatures in summer, threatening the health of residents. However, green spaces can generate a cooling effect to mitigate the urban heat island effect in big cities. They can also help to improve the living quality and wellbeing of surrounding residents. In this paper, we utilized the radiative transfer equation algorithm, k-means clustering algorithm, big data crawling, and spatial analysis to quantify and map the spatial distribution, cooling capacity, and cooling contribution for surrounding communities of 1,157 green spaces within Beijing Fifth Ring Road, a typical metropolitan area. The findings showed that (1) the area proportion of the heat island in the study area is larger than that of the cooling island. Accounting for only about 30% area in the study area, the green spaces reduce the average land surface temperature by 1.32°C. (2) The spatial features of green space, such as area and shape complexity, have a significant influence on its cooling effect. (3) Four clusters of green spaces with specific spatial features and cooling capacity were identified. And there were differences among these clusters in green space cooling contribution for the surrounding communities. (4) The differences in green space cooling contribution also existed in different urban zones. Specifically, the middle zone performed significantly better than the inner and outer zones. (5) We furthered in finding that some green spaces with medium and high cooling contributions need to improve their cooling capacity soon, and some green spaces with low cooling contributions or no contributions have a good potential for constructing new communities in the future. Our study could help planners and government understand the current cooling condition of green spaces, to improve their cooling capacity, mitigate the urban heat island effect, and create a comfortable and healthy thermal environment in summer.

Keywords: green space, cooling effect, cooling contribution, metropolitan area, urban thermal environment, resident health

INTRODUCTION

With the rapid development of urbanization and global warming, urban expansion in the past led to a dramatic change in the underlying surface (1, 2). The problems of the urban thermal environment, such as the urban heat island (UHI) effect and extreme weather events, arose worldwide (3). Additionally, in recent years, the development pattern of smart growth made some metropolitan areas of high density and intensive, where the urban and environmental problems caused by high temperature also became more serious (4). According to some studies, high temperature leads to an increase in some health risks, diseases, and even mortality of the public (5–7). It also brings a vicious circle of 'high temperature—energy consumption—"greenhouse effect"—high temperature,' which makes the urban environmental health and the ecological condition deteriorate rapidly (8). However, as an essential part of green infrastructure (GI), the urban green spaces have many ecosystem services. They can play a significant role in mitigating the UHI and promoting thermal environment health, especially in metropolitan areas, which has been confirmed by many studies (9, 10). Therefore, in the context of climate change and urbanization, how to utilize the green spaces' cooling capacity to reduce the influence of extreme heat weather in summer and improve the thermal comfort of the environment has become a hot issue for relevant scholars.

So far, the research on the green space cooling effect roughly has contained 2 aspects: the macro and the micro. The macro studies primarily focused on the spatial-temporal distribution of cooling islands (11, 12), landscape or green space spatial pattern (13, 14), and influencing factors or drivers of the green space cooling effect (15, 16). Li and Zhou found that the green space patch intensity and mean patch shape are negatively correlated with UHI intensity, while green space edge density is positively correlated with it in Illinois-Indiana-Ohio, United States (17). Zhao et al. mapped the land surface temperature (LST) and land cover of Shenyang, China, and indicated that among all types of land cover, the highest mean LST is buildings and roads, while the lowest is water. The temperature of farmland is higher than that of green space. They also emphasized that although the water and the green space have a good cooling effect, the capacity is not obvious if their area is small (3). And some researchers are focusing on the cooling effect of a certain land cover or element, such as water (18), forests (19, 20), and wetlands (21–23). Wang et al. found that LST is affected by water, and the cooling effect of water varies according to different land covers (24). In the micro aspect, most of the previous studies focused on the influencing factors of the park cooling effect in a city or the simulation of green space cooling effect in a small area (25, 26). Jaganmohan et al. measured mobile air temperature in 62 parks and forests of Leipzig, Germany, and found that the cooling quality of forests is better than that of parks. And with size increasing and shape complex decreasing, the cooling effect of parks and forests increases (27). Chen et al. defined the different aspects of parks' cooling capacities, such as cooling efficiency, cooling gradient, cooling area, and cooling intensity, and found the inequity in accessing park cooling service in Wuhan, China (28).

However, it can be seen from the previous studies that most macro studies focused on the scale of the entire city or built-up area, while the micro studies focused on the individual or group scale of green spaces. No transition appeared between the macro studies and micro studies. In addition, some macro studies ignored regional disparities in the green space cooling effect between the urban core and the suburbs, which is caused by the difference between the urban and rural structure of the underlying surface and land cover. Thus, there is a demand for mesoscale research on the cooling effect on a specific geographical area of the city. Besides, some micro research about parks' cooling effect selected fewer samples (dozens of parks), which might make the results of these studies quite inconsistent with each other in the same study area (29). And there are many green spaces in the city that are not parks, which still have a perfect cooling service for the surrounding residents. They should be included in the study samples to increase the quantity of analysis and improve the accuracy of the results. Finally, a few studies paid attention to the green space cooling contribution to the community (GCC), which partly reflects the well-being and value of green space ecosystem services. And it also can help the government and planners in a deep understanding and better management of our city.

In this paper, we selected a typical metropolitan area on mesoscale, within the 5th Ring Road of Beijing as the study area. This region with the most diverse land use, functions, and vitality in the whole city is more vulnerable to extremely high-temperature disasters. So, in this specific area, the green space cooling effect was focused on, which has great scientific value and practical significance. Then, in this paper, we quantified the cooling effect indicators and landscape indicators of 1,157 green spaces with more than 1 hm^2 in the study area, classified them into 4 clusters with different cooling characteristics, and defined and mapped the green space cooling contribution to the surrounding communities for the first time. Our study aims to: (1) quantify and obtain the overall characteristics and spatial distribution of LST and cooling-heat islands in the study area; (2) quantify the green space cooling effect and find the spatial features of the green spaces with higher cooling capacity; (3) based on the green space spatial features and characteristics of green space cooling effect, identify different clusters of green spaces, and compare their cooling capacity and advantages; (4) quantify the spatial distribution of green space cooling contribution to communities' green spaces and assess their performance in different clusters and zones.

STUDY AREA

Beijing (115.7°-117.4°E, 39.4°-41.6°N) is the capital of China, located in the north of North China Plain, adjacent to Hebei Province and Tianjin city. It covers an area of 16,410 km^2, with a population of 218.9 million in 2020 (30). And it is dominated by a warm temperate semi-humid and semi-arid monsoon climate, with hot and rainy in summer and cold and dry in winter. The annual average temperature of the city is 11–13°C, and the annual extreme high temperature is around 35–40°C.

The study area is within the Fifth Ring Expressway in Beijing, including the whole or part of the area of the six administrative districts, which are Dongcheng, Xicheng, Haidian, Chaoyang, Shijingshan, and Fengtai (**Figure 1**). This area undertakes the four core functions of the capital according to the *Beijing Master Plan (2016–2035)*, such as the political center, cultural center, science and technology center, and also international exchange center (31). In addition, our study area is densely populated and is also the core of the highly-urbanized religions of Beijing. The dwelling population in this area accounts for 48.9% of the whole city, while it covers a total area of 66,655 hm^2, accounting for only 4.1% of Beijing. Moreover, according to the "figure-ground relation" of the city and urban development history, we divide the study area into three zones: the inner zone within the 2nd Ring Road, the middle zone from the 2nd Ring Road to the 4th Ring Road, and the outer zone from the 4th Ring Road to the 5th Ring Road.

MATERIALS AND METHODS

Retrieving Land Surface Temperature and Classification of Cooling-Heat Islands

The Landsat 8 TIRS image (path/row: 123/32, cloud cover: 1%, and no cloud in the study area) was obtained at 02:53:37 GMT on 12 September 2017. We downloaded the remote sensing data from the Geospatial Data Cloud (www.gscloud.cn), and preprocessed the image on the ENVI 5.3, including radiometric calibration and atmospheric correction of thermal infrared data and multispectral data to eliminate the errors from sensors and atmosphere. Then, we selected a suitable algorithm to retrieve the LST using the remote sensing image. At present, there are 4 methods: radiative transfer equation algorithm (RTE) (32), split window algorithm, single-channel algorithm, and multi-channel algorithm. Many previous studies utilized RTE and obtained accurate results (33–35). Thus, we determined the RTE method to retrieve the LST of the study area. According to the steps of the method, we converted the digital number of all the satellite image bands to at-satellite reflectance using the gray value of the raw data first. Then, we calculated the Normalized Difference Vegetation Index (NDVI) (36) and retrieved the brightness temperature of the blackbody using RTE. Finally, the LST map was obtained by the Planck formula (**Figure 2A**), and 5 zones showing the spatial distribution of heat and cooling islands in **Figure 2B** were classified using the mean-standard deviation method (37).

Classification of Land Use

The land use data used in this paper are the global land cover in 2017 of 10 m accuracy published by the Tsinghua University (38). The acquisition time of the data is the same as that of remote sensing data used to retrieve LST. The data cover 10 categories of land use, and the study area involves 8 of them. Then, we combined farmland, forest, shrubland, and grassland into a new green land layer, combined water and wetland into a new water layer, and combined impervious surface and bare land into a new impervious surface layer (**Figure 3A**). After that, we merged the new green land layer and the new water layer within 30 m into the green space layer. Previous research indicated that the minimum area of the parks with a cooling effect in Beijing is around 1–3 hm^2 (39). To eliminate interference, the green spaces with the area below 1 hm^2 were deleted. In addition, the Summer Palace in the northwest of the study area is connected with Haidian Park, Liangshan Park, and some orchards, becoming a vast green space with an area of more than 1,900 hm^2. The size of this green space is much larger than other green spaces. To make mathematical statistics more scientific, the green space was deleted. Finally, 1,243 green spaces were selected as the study objects (**Figure 3B**).

Definition of Cooling Indicators and Landscape Features

The cooling capacity of green space is evaluated by several indicators. Reflecting the amplitude of reducing LST of the surrounding impervious surfaces, green space cooling intensity (GCI) is one of the core indicators. We used the buffer method (25, 40) to define the GCI. We set 10 ring buffers with 60 m width for each green space from their boundary, and the average LST of impervious surface in each buffer was calculated. It is worth noting that we did not calculate the average LST of the entire buffers as in some previous studies to reduce the impact of other green spaces in the buffers on LST. Then, the curve was drawn in **Figure 4A** based on the data of a certain green space. The horizontal axis is the distance between the green space boundary and the buffer. And the vertical axis is the average LST of the green space and the impervious surface in a buffer. According to previous studies (41–43), we quantified the maximum distance of the green space cooling effect (L_{MAX}) and the green space cooling intensity (GCI). L_{MAX} was confirmed as the distance from the first turning point of LST to the green space boundary; GCI was defined as the difference between the impervious surface temperature at L_{MAX} and the average LST of the green space. According to the definition, 1,157 green spaces' cooling intensity was calculated as shown in **Figure 4B**. Besides, we also defined and quantified other indicators reflecting green space cooling capacity or landscape features, such as the green space cooling area (GCA) (28), the green space cooling efficiency (GCE) (44), the green space cooling gradient (GCG) (28), and the green space shape index (GSI), as can be seen in **Table 1**.

Identification of Green Space Clusters Based on Cooling Effect and Spatial Feature

We used the K-means clustering algorithm to identify different green space clusters with different cooling effects or spatial features. First, we normalized the 5 selected factors to ensure the accuracy of the subsequent calculations. Then, we found the appropriate K-value before analysis. Yuan and Yang indicated that compared with other methods of finding K-value, the Elbow method has a faster speed for less and uncomplicated data with the same accuracy (45). Therefore, this paper used python programming to obtain the K-value by the Elbow method. The result showed that when the K-value is 4, the sum of squared

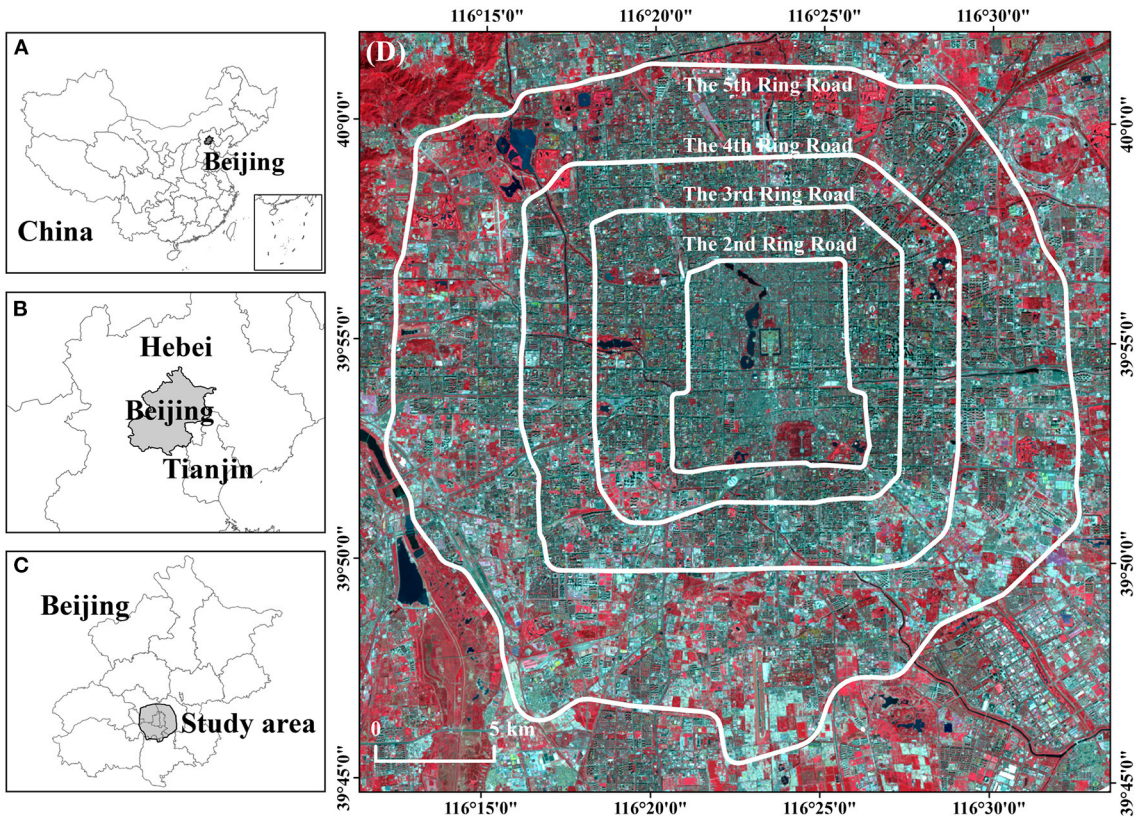

FIGURE 1 | Location of the study area in Beijing metropolitan area, China **(A–C)**. The Landsat8 remote sensing image **(D)** is displayed in false color mode, which is composed of band 5 (near-infrared), band 4 (red), and band 3 (green).

errors (SSE) is smaller. Finally, we took 4 as the suitable K-value and divided 1,157 green spaces into 4 clusters with different cooling effects and spatial features.

Analysis of the Green Space Cooling Contribution to Surrounding Communities

To explore whether the cooling effect of green spaces is enjoyed by surrounding communities, we defined the concept of green space cooling contribution for community residents (GCC) for the first time. The GCC is the product of the community population per unit of green space cooling area (GCA) and green space cooling intensity (GCI). The community population, located in cooling coverage, is the product of the total number of households in communities and the average population per household. We used big data crawling software, Octoparse, to obtain the total number of households and detailed addresses of all communities in our study area from the Anjuke website (https://beijing.anjuke.com), which is the largest online real estate trading website in China. Then, through python programming, we utilized Baidu Geocoder API to convert the detailed addresses of communities into coordinates recognized by ArcGIS. Finally, the community points data with the total number of households and the accurate spatial location was obtained. It is worth noting that all spatial data, such as remote sensing images, land use data, the community points data, all used the WGS-1984 coordinate system to be calculated seamlessly together in ArcGIS.

$$GCC = \frac{N_h \times N_P \times GCI}{GCA} \quad (1)$$

Where N_h is the total number of households located in cooling coverage; N_P is the average population per household. According to the *Beijing statistical yearbook 2018*, the N_P of the study area is 2.52 (46). And **GCI** is the green space cooling intensity; **GCA** is green space cooling area.

RESULTS

General Characteristics of LST and Its Corresponding Land Use

Combined with the LST of the study area in **Figure 2A** and cold-hot islands distribution in **Figure 2B**, we identified many hot spots which are mainly distributed in the old town, industrial and logistics areas, such as the central and southern part of the 2nd Ring Road, the southeast part of the 3rd Ring Road to the 5th Ring Road, and the southwest part of the 4th Ring Road to the 5th Ring Road. The LST in these areas is 35–40°C, and in some regions, its LST is above 45°C, which showed

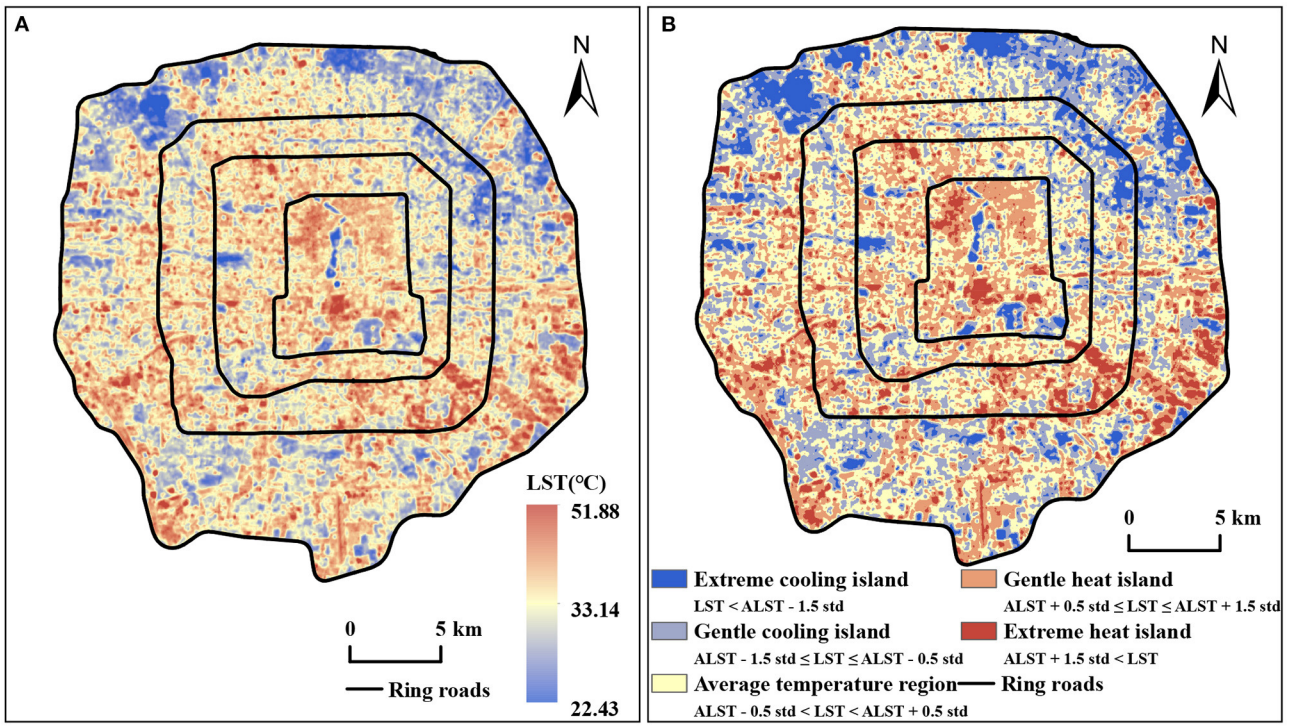

FIGURE 2 | Spatial distribution of LST **(A)** and cold-hot islands at different levels **(B)** in the study area. Where ALST is the average LST; std is the standard deviation of LST in the study area.

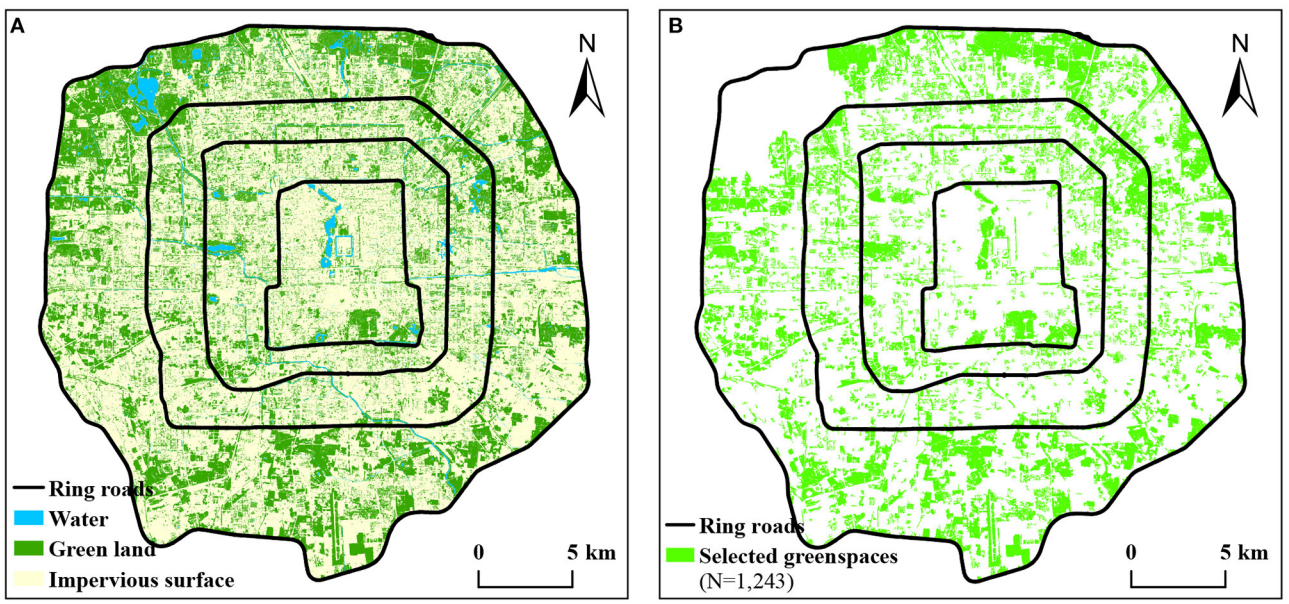

FIGURE 3 | Spatial distribution of land use in the study area **(A)**, green spaces selected as the study objects **(B)**.

that the health condition of the urban thermal environment was worrying. Moreover, we found that the LST in the north and northwest of the study area is significantly lower. The low LST was also found in the northeast from the 4th Ring Road to the 5th Ring Road. Some parks, golf courses, and nursery gardens are distributed in these areas. In addition, there are many cold spots scattered in the city, mainly some comprehensive parks, riverside parks, and gardens adjacent to large buildings or

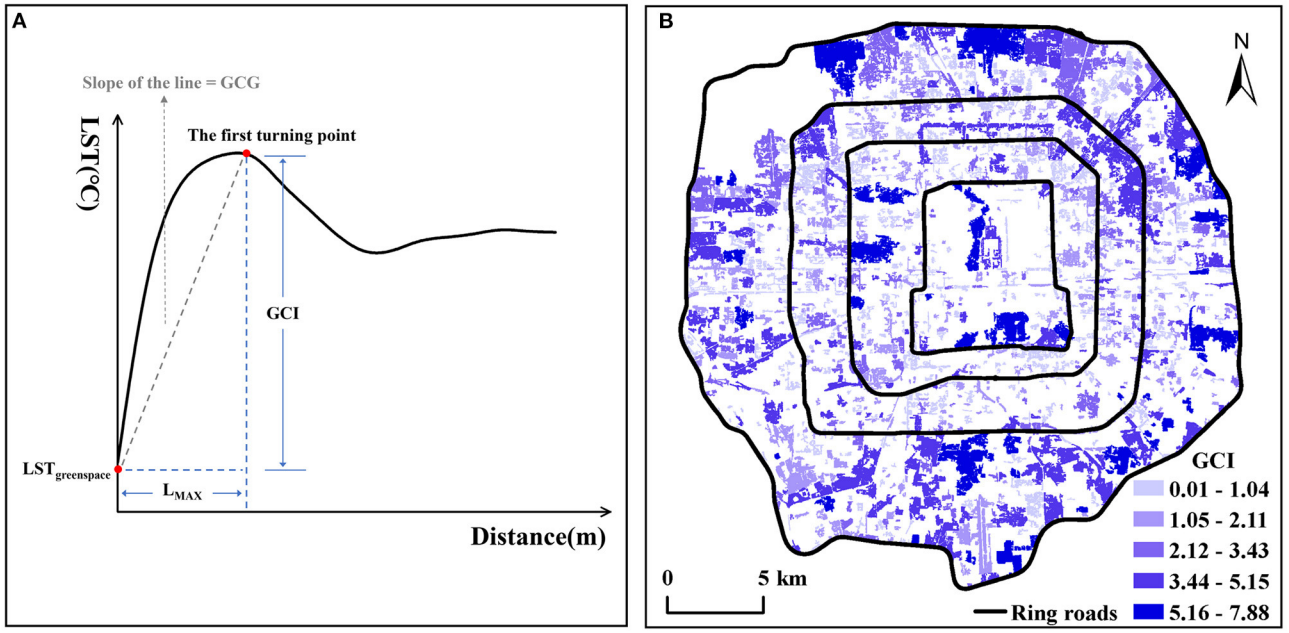

FIGURE 4 | Average LST schematic diagram of green space and surrounding impervious surface **(A)**, the spatial distribution of 1,157 green spaces with different degrees of GCI **(B)**.

communities. These areas are cool and comfortable for residents in summer.

According to the statistics in ArcGIS, we found that the average LST of the study area is 33.14°C, while the maximum LST is 51.88°C, and the minimum LST is only 22.43°C. The standard deviation (std) is 3.30. And in terms of the proportion of cold-hot islands area, the average temperature region accounted for the largest proportion which is 39.28% and the heat islands area accounted for 30.89% which is also higher than that of cold islands (29.83%). In addition, from the perspective of land use, the average LST of green spaces is significantly lower than that of impervious surfaces. The average LST of pure green land (about 20,257.29 hm^2) is 31.09°C; the average LST of water (about 915.21 hm^2) is 27.83°C and the average LST of impervious surface (about 45,375.93 hm^2) is 34.46°C. It suggested that the green space, accounting for only 30% of the study area, reduces the average LST of the whole area by 1.32°C. So, it can be seen that urban green spaces have a strong cooling effect and benefit the thermal environment health of the city.

Correlation Between Spatial Features and Cooling Effect

Previous studies showed that the spatial features of green spaces were correlated with their cooling effect (27, 47, 48). To verify the conclusion, Spearman's correlation analysis between them was performed. We selected the area (GA), shape index (GSI), and perimeter (C_G) to describe the spatial features of green spaces; the cooling area (GCA), cooling intensity (GCI), cooling gradient (GCG), and the maximum cooling distance (L_{MAX}) to describe the cooling effect of green spaces. The results of the correlation analysis are shown in **Table 2**.

There is a significantly positive correlation ($p < 0.01$) between GA and GCI, indicating that the larger the green space area, the larger the cooling temperature, which is consistent with Li et al. (49). But the fitting curve in **Figure 5A** showed that with the increase of GA, the change rate of GCI gradually decreases. That is, after reaching a certain degree (about 50 hm^2), if GA continues to increase, the change of GCI will be no longer obvious. Due to the scarcity of land in metropolitan areas, the size of green spaces is not recommended to be more than 50 hm^2. C_G also exerts a positive effect on GCI ($p < 0.01$), but the relationship between them is weak (rho < 0.4), which indicated that the green space perimeter has little influence on the degree of cooling temperature. However, GSI is negatively correlated with GCI ($p < 0.01$), which showed that the more complex the green space shape, the smaller the cooling temperature. In **Figure 5B**, when the GSI value is larger than 17, the GCI reaches 0, and the green space cooling effect disappears.

GA and C_G are significantly in positive correlation with GCA ($p < 0.01$), which shows that the larger the green space size, the larger the cooling coverage in **Figures 5C,D**. GCA is also significantly negatively correlated with GSI ($p < 0.01$), suggesting the more complex the green space shape, the less the cooling coverage (**Figure 5E**).

GA is also positively correlated with GCG ($p < 0.01$), and GSI is negatively correlated with GCG ($p < 0.01$), indicating the larger the green space area and the more regular of green space shape, the larger the cooling gradient. That is, if green space is larger and regular in shape, it will be more likely to cool the surrounding temperature quickly and efficiently (**Figures 5F,G**). But there is no obvious positive correlation between C_G and GCG ($p < 0.01$, rho < 0.4), which suggests that green spaces

TABLE 1 | Definition of cooling and landscape indices.

Cooling indicators and landscape features	Abbreviation	Definitions	Meaning	Unit
The maximum distance of green space cooling effect	L_{MAX}	L_{MAX} is the distance from the green space boundary to the buffer with the first turning point	Cooling range of the green space	*m*
Green space cooling intensity	*GCI*	*GCI* is the difference between the impervious surface temperature at L_{MAX} and the average *LST* of the green space $\mathbf{GCI = T_{LMAX} - T_G}$ Where, T_{LMAX} is the impervious surface temperature (°C) at L_{MAX}; T_G is the average *LST* of the green space	Amplitude of lowering temperature of surrounding impervious surface	°C
Green space cooling area	*GCA*	*GCA* is the buffer area with the maximum cooling distance from green space boundary	Cooling coverage	m^2
Green space cooling efficiency	*GCE*	*GCE* is the ratio of the green space cooling area to green space area $\mathbf{GCE = \frac{GCA}{GA}}$ Where, *GA* is the green space area (m^2)	Area cooled by per unit area of green space	/
Green space cooling gradient	*GCG*	*GCG* is the ratio of green space cooling intensity to the maximum distance of green space cooling effect $\mathbf{GCG = \frac{GCI}{L_{MAX}}}$	Temperature cooled per unit distance of green space cooling effect	°C/m^2
Green space shape index	*GSI*	*GSI* is the ratio of perimeter to area of green space $\mathbf{GSI = \frac{C_G}{GA}}$ Where, C_G is the perimeter (*m*) of green space	Shape complexity of green space	m^{-1}

TABLE 2 | Correlation analyses between cooling indicators and spatial features of green space.

	GCI (°C)	GCA (hm^2)	GCG (°C/m)	L_{MAX} (m)
GA (hm^2)	0.473**	0.875**	0.505**	0.367**
GSI (m^{-1})	−0.650**	−0.456**	−0.549**	−0.477**
C_G (m)	0.370**	0.820**	0.358**	0.214**

***, *indicate significant at the 1 and 5% levels, respectively.*

with large or small perimeters have the same influence on their cooling gradient.

Only GSI has a significantly negative correlation with L_{MAX} ($p < 0.01$), which suggests that the more regular the green space shape, the longer the cooling distance (**Figure 5H**). GA and C_G have a positive influence on L_{MAX}, but the relationship between them is weak ($p < 0.01$, rho < 0.4). So, the green spaces with larger or small areas and perimeters have the same influence on their cooling distance.

In sum, green space area (GA) and shape index (GSI) possess an obvious influence on green space cooling capacity, especially on cooling intensity (GCI), cooling area (GCA), and cooling gradient (GCG). Green space perimeters (C_G) have a weak correlation with cooling capacity except for GCA. The maximum cooling distance (L_{MAX}) is only significantly correlated with GSI. Thus, it can be seen that the green spaces with larger areas and more regular shapes probably possess a better cooling capacity.

Green Space Clusters With Different Spatial Features and Cooling Effects

GCI, GCA, and GCG, the core indicators of reflecting green space cooling capacity, together with GA and GSI, which have a higher correlation with the 3 core cooling indicators above, were selected as classification metrics. After the k-means method identification, 4 clusters (**Figure 6A**) were obtained from 1,157 green spaces and their features are shown in **Table 3**.

Cluster 1 has the most green spaces, up to 476. These green spaces with an average area of 7.55 hm^2 are mainly some large residential green spaces, greenbelts, and some small theme parks (**Figure 6B**). Their cooling indicators perform poorly: the average GCI is low, the cooling coverage is small, and the cooling distance is also close. But the GCE is higher. We believe that this cluster of green spaces is suitable for regions that possess some area for green space construction. And there is a comfortable thermal environment and low cooling demand.

Cluster 2 is mainly moderate-area parks, with an average area of 26.70 hm^2 and smaller GSI (**Figure 6C**). The parks are evenly distributed in the study area. The GCI, GCA, L_{MAX}, and GCG of these green spaces are higher, indicating that they can have

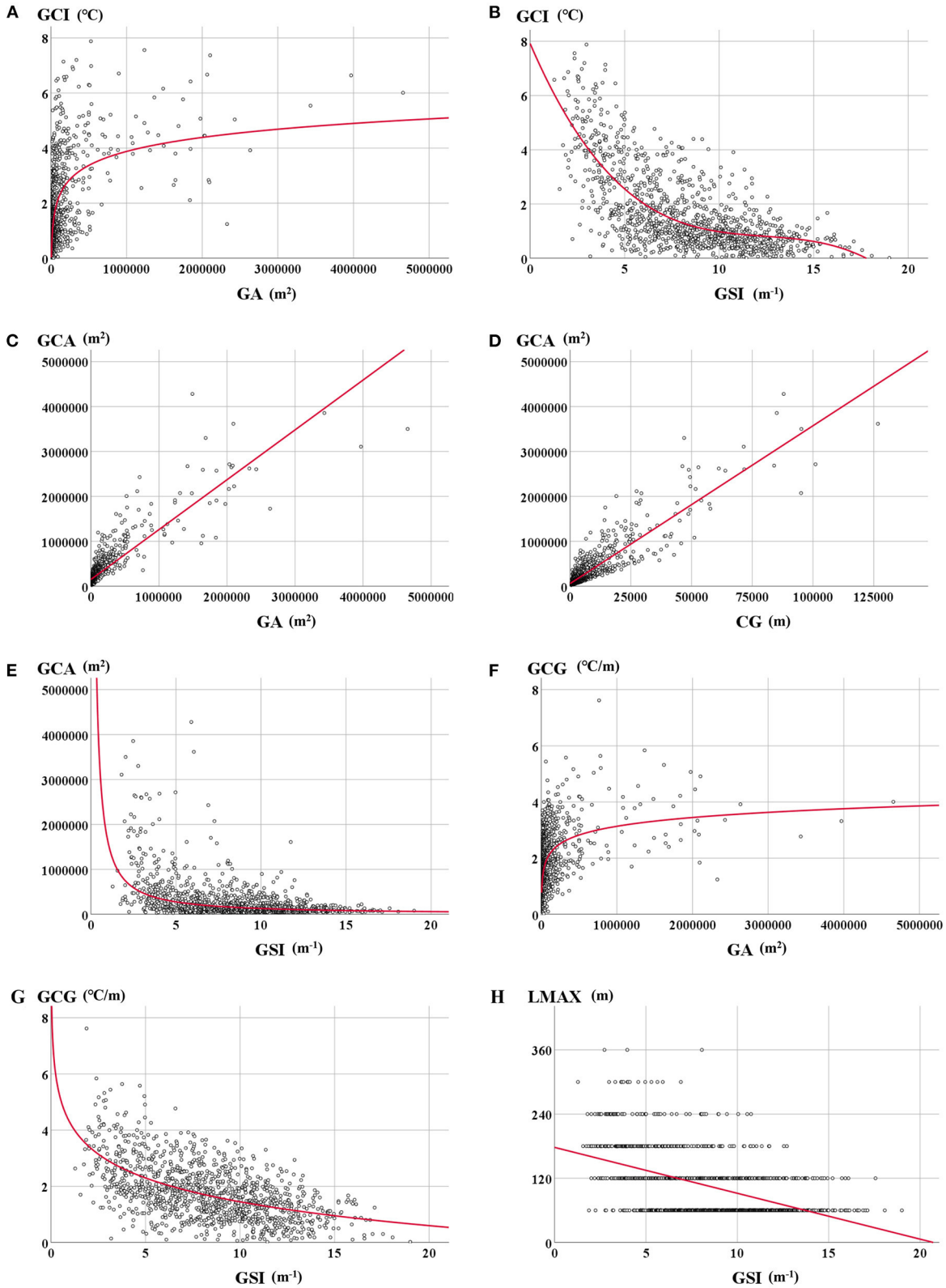

FIGURE 5 | Relationship between dependent (GCI) and independent [GA: **(A)**, GSI: **(B)**], relationship between dependent (GCA) and independent [GA: **(C)**, C_G: **(D)**, GSI: **(E)**], relationship between dependent (GCG) and independent [GA: **(F)**, GSI: **(G)**], relationship between dependent (L_{MAX}) and independent [GSI: **(H)**]. The regression line using the ordinary least squares method is presented in red. The regression models were selected among linear, logarithmic, and power functions with the largest R^2 value.

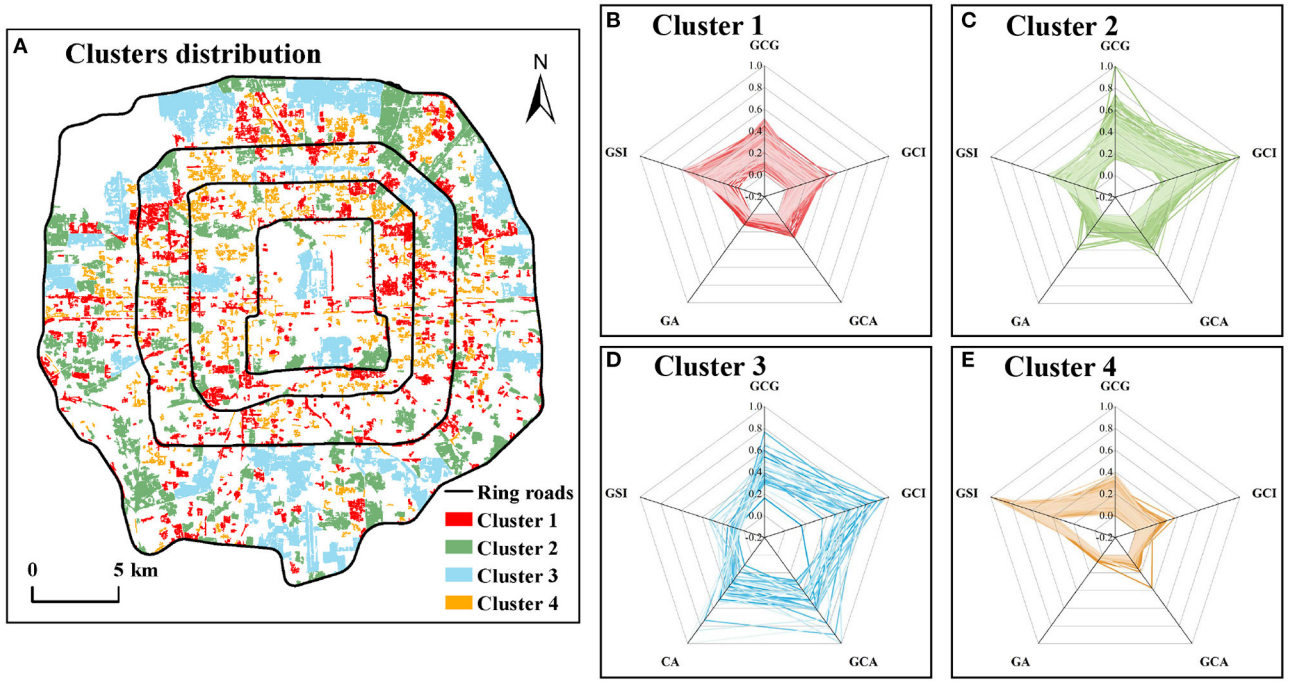

FIGURE 6 | Spatial distribution of 4 clusters green spaces in different cooling effect **(A)**, Radar diagrams of landscape and cooling metrics for 4 clusters green spaces **(B–E)**.

TABLE 3 | Average characteristics of 4 green space clusters.

	Green space quantity	GA (hm^2)	GCA (hm^2)	GSI (m^{-1})	GCI (°C)	GCG (°C/m)	L_{MAX} (m)	GCE
Cluster 1	476	7.55	21.02	7.13	1.46	1.91	76.44	2.78
Cluster 2	189	26.70	59.62	4.47	4.07	2.90	140.34	2.23
Cluster 3	32	182.02	237.26	3.23	5.01	3.30	151.82	1.30
Cluster 4	460	3.76	14.66	11.56	0.70	1.10	63.64	3.90

an excellent cooling effect on the surrounding areas and create a more comfortable thermal environment for the metropolitan areas. But their GCE is relatively low. These green spaces need relatively adequate land and space, and they are recommended to be set in the areas with high UHI.

Cluster 3 is mainly large parks, with an average area of 182.02 hm^2 (**Figure 6D**). They are primarily comprehensive or ecological parks distributed in the outer zone of the study area, and a small number of green spaces are historical gardens located in the inner and middle zones of our study area. These green spaces of the cluster have the largest GCI, GCG, GA, GCA, and L_{MAX}, suggesting they, with the perfect cooling capacity, can reduce LST over long distances and can rapidly mitigate UHI of the surroundings. However, the GCE and the GSI are the smallest among all clusters, indicating most green spaces are more regular in shape, and the cooling efficiency is the lowest. In short, these green spaces have an excellent cooling effect, but the size is enormous, which is suitable for the region with more considerable cooling demand and sufficient area for green space construction.

Cluster 4 is mainly attached green space with the smallest area, including residential green space, green belts, green space attached to urban roads, and so on (**Figure 6E**). These green spaces are dominated by GSI and GCE, and other indicators perform poorly, such as GCA, GCI, GCG, and L_{MAX}. They are the smallest among all clusters, suggesting their cooling capacity is extremely limited. Therefore, these green spaces are recommended to be located where needs little cooling demand.

Green Space Cooling Contribution to Communities

Characteristics of Different Levels of Green Space Cooling Contribution

According to the formula in formula 1, the cooling contribution for the community of 1,157 green spaces (GCC) was obtained, of which 489 green spaces have no community in their cooling coverage. That is, they do not have any GCC for communities. The rest of the green spaces were divided into three categories: low GCC, medium GCC, and high

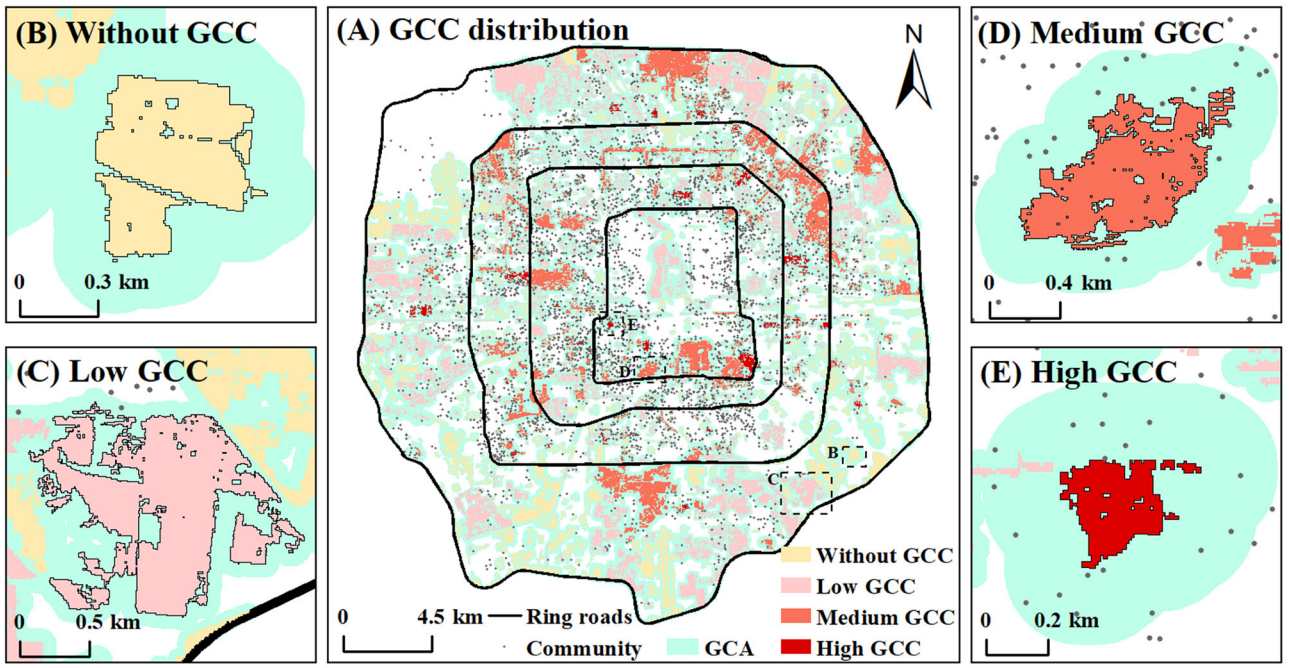

FIGURE 7 | Spatial distribution of green spaces with different GCC levels **(A)**, examples of green spaces with different GCC levels **(B–E)**.

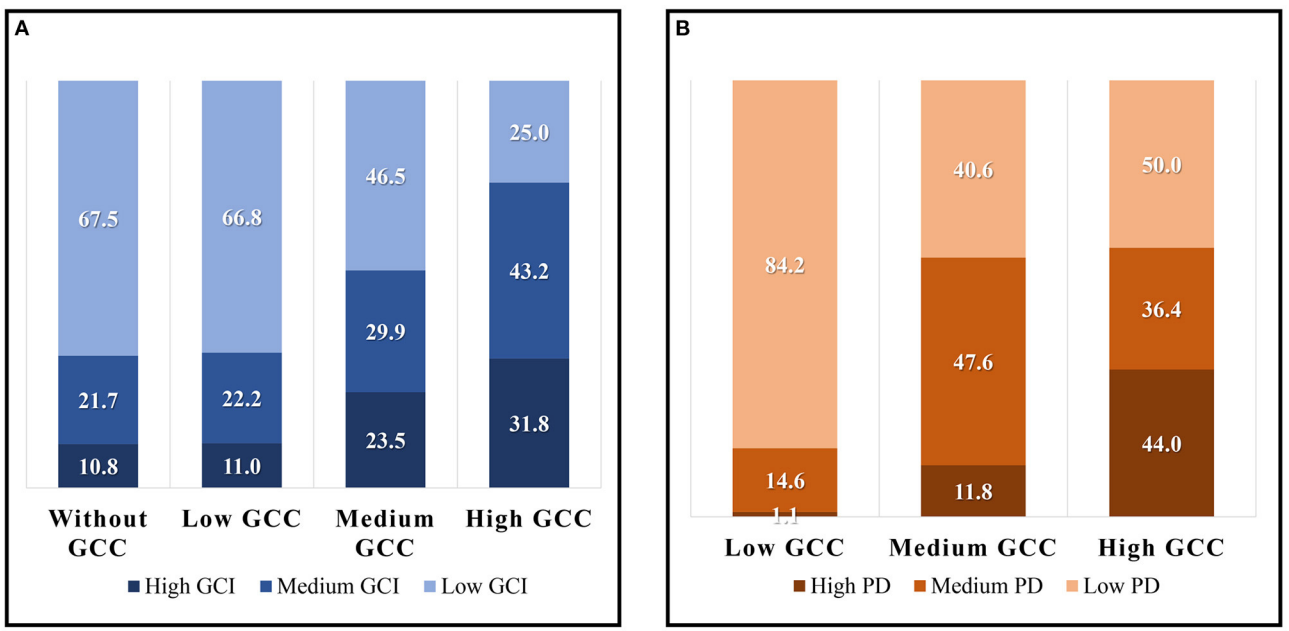

FIGURE 8 | The proportion of green space with low, medium, and high GCI in different GCC groups **(A)**, the proportion of green space serving low, middle, and high population density in different GCC groups **(B)**.

GCC according to the Natural Breaks (Jenks) method (**Figures 7A**, **8**).

The 489 green spaces without contribution are mainly distributed in the east, southeast, and south of the outer zone in the study area. Their average area is small, only 8.25 hm^2, which leads to their poor cooling capacity. The GCA and the L_{MAX} of the green spaces are the smallest among all categories, and their GCI is also smaller. For example. 67.5% of these green spaces possess low GCI in **Figure 8A**. Therefore, except no distribution of communities around the green spaces, the poor cooling effect

and small cooling coverage might be the important reasons why they do not have any cooling contribution. Besides, there are 32.5% green spaces with middle or high GCI, suggesting that they possess a great cooling capacity and might become potential areas for new community construction. For example, Haitang Park (**Figure 7B**), located in the southeast of the outer zone, has an excellent cooling capacity and more extensive cooling coverage, but there was no community around it in 2017. According to the plan, several new communities will be distributed around it in the future.

There are 473 green spaces with low GCC, of which the larger ones are distributed in the outer zone, and the smaller ones are mainly distributed in the inner zone and middle zone. The average area of these green spaces is large, but their cooling capacity performs poorly. The GCI and L_{MAX} of most green spaces are very low, and they also serve smaller communities. So the low cooling contribution of these green spaces might be due to the lower amplitude of reducing LST as well as the small population of the surrounding communities. Significantly, 15.7% of the green spaces are surrounded by large communities and residents, but their cooling capacity is very weak. The cooling effect of these green spaces is the key that needs to be improved in the future. While 33.2% of the green spaces with middle or high GCI, such as Hongbo Park in **Figure 7C**, have only a few residents around them. They might play an important role in cooling the temperature for new communities in the future.

There are 187 green spaces with a moderate cooling contribution to the surrounding communities. And they are mainly distributed in the middle zone. The average area and GCA of these green spaces are the largest among all categories, and GCI and L_{MAX} are large too, which indicates that most of these green spaces have a perfect cooling performance. At the same time, a lot of communities are distributed around them, such as Taoranting Park in **Figure 7D**, thus, they have a good performance on cooling contribution to the surrounding communities. But there is still 46.5% of these green spaces needing to improve their cooling capacity to serve the surrounding communities better.

Only 44 green spaces have a high cooling contribution to the surrounding communities, and their spatial distribution is relatively scattered. Xuanwu Art Park is a typical green space with high GCC (**Figure 7E**). Although the area of these green spaces is the smallest, only 8.02 hm^2, they have the perfect cooling performance. The GCI, GCE, and L_{MAX} of 75% of these green spaces perform perfectly among all green spaces. However, 11 green spaces surrounded by a large number of residents have a weak cooling effect, which should be improved in the future. Meanwhile, there are 6 green spaces with the highest cooling capacity with a few residents around, so they can become the potential areas to provide cooling services for new communities in the future.

Characteristics of Green Space Cooling Contribution in Different Urban Areas

Generally, there are 668 green spaces with GCC (**Figure 9A**). The GCC performance of the green spaces in the middle zone is the best, slightly better than that in the outer zone, and the worst in the inner zone. It is worth noting that the median value of the inner zone is lower than the bottom value of the middle zone and outer zone, indicating that the GCC of most green spaces in the inner zone performs very poorly. In terms of dispersion, the middle zone is also the largest, and the inner zone is slightly larger than the outer zone.

From the proportion of various levels of GCC in each zone (**Figure 9B**), the sum of levels of low GCC and no GCC accounts for more than 70% in all zones of which the value of the outer zone is the highest up to 87.1%. In addition, the quantity of green spaces with high GCC and low GCC accounts for the most in the inner zone; the quantity of green spaces with medium GCC accounts for the most in the middle zone; while the quantity of green spaces with no GCC accounts for the most in the outer zone up to 56.8%. It is concluded that most green spaces in the inner zone are with GCC, but the most value is lower. About 70% of the green spaces in the middle zone are with GCC, and the proportion of the medium and high levels of GCC is the largest, so the GCC performance in the middle zone is the best. However, due to more than half of the green spaces in the outer zone are not with GCC and the proportion of medium and high GCC is the least, the GCC performance of the outer zone is the worst.

Characteristics of Different Clusters' Green Space Cooling Contribution

Among the 668 green spaces with GCC (**Figure 10A**), the GCC of cluster 2 is the highest, while the GCC of cluster 3 is slightly smaller than that of cluster 1, and the GCC of cluster 4 is the worst. Specifically, the reason the GCC of cluster 4 is worse than that of cluster 1 might be a small size, poor cooling intensity, and small cooling area of green spaces in cluster 4. Therefore the cooling capacity is so small not to mitigate the heat island effect of surrounding communities. In addition, although the size and cooling capacity of cluster 3 are larger than that of cluster 2, most of the green spaces of cluster 3 are distributed in the outer zone and serve a small number of communities and populations, so its GCC performance is not as good as that of cluster 2.

From the distribution of different levels of GCC in each cluster, nearly half of the green spaces in cluster 1 are not with GCC, and the value also reaches about 40% in cluster 2 and cluster 4 (**Figure 10B**). Only cluster 3 is relatively low—just 15.6%. Moreover, more green spaces in cluster 2 and cluster 3 are with medium- and high-level GCC. But cluster 4 has the least green spaces with medium and high GCC. In short, cluster 3 performed best in the cooling contribution for communities, followed by cluster 2, cluster 1, and cluster 4. It can be seen that the green space cooling contribution varies with spatial feature and cooling capacity.

DISCUSSION

The Cooling Effect of Green Space in the Metropolitan Area

This paper found that urban green space can produce a cooling effect and significantly mitigate UHI, which has been confirmed by many studies (50, 51). However, it is worth noting that the cooling effect of green space is related to the distance from the green space boundary. That is, with the increase of the

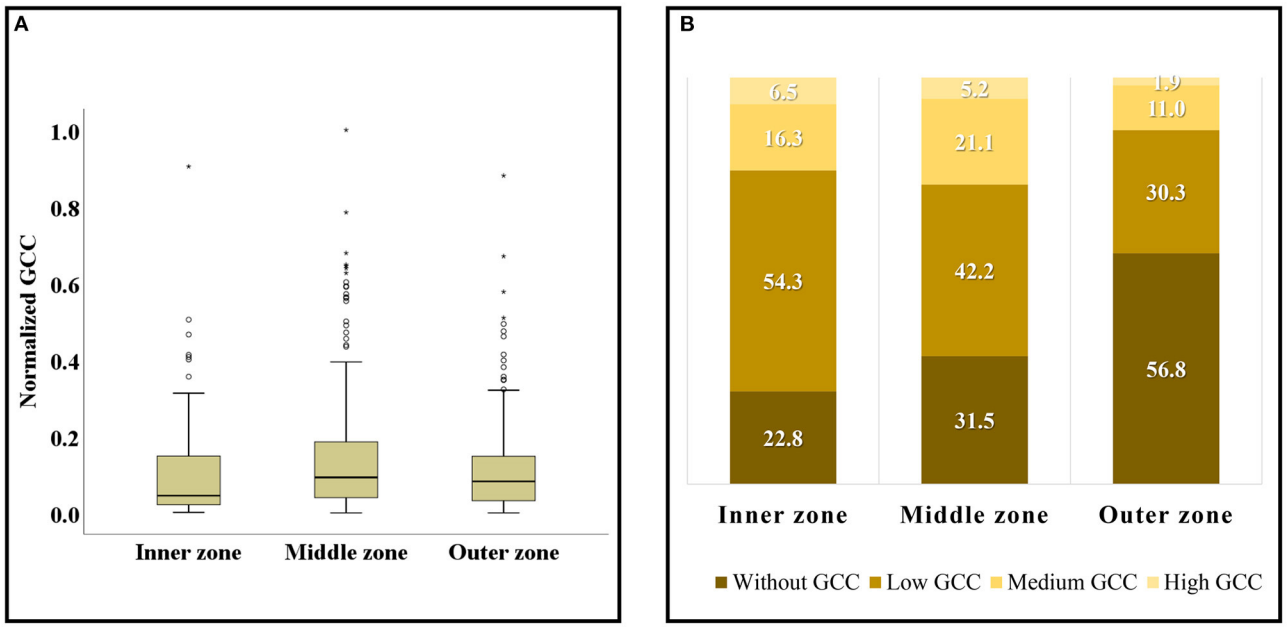

FIGURE 9 | The box diagram of GCC distribution in different urban zones **(A)**, proportion of green spaces with different levels of GCC in different zones **(B)**. Hollow circles ○ represent mild outliers; asterisks * represent extreme outliers.

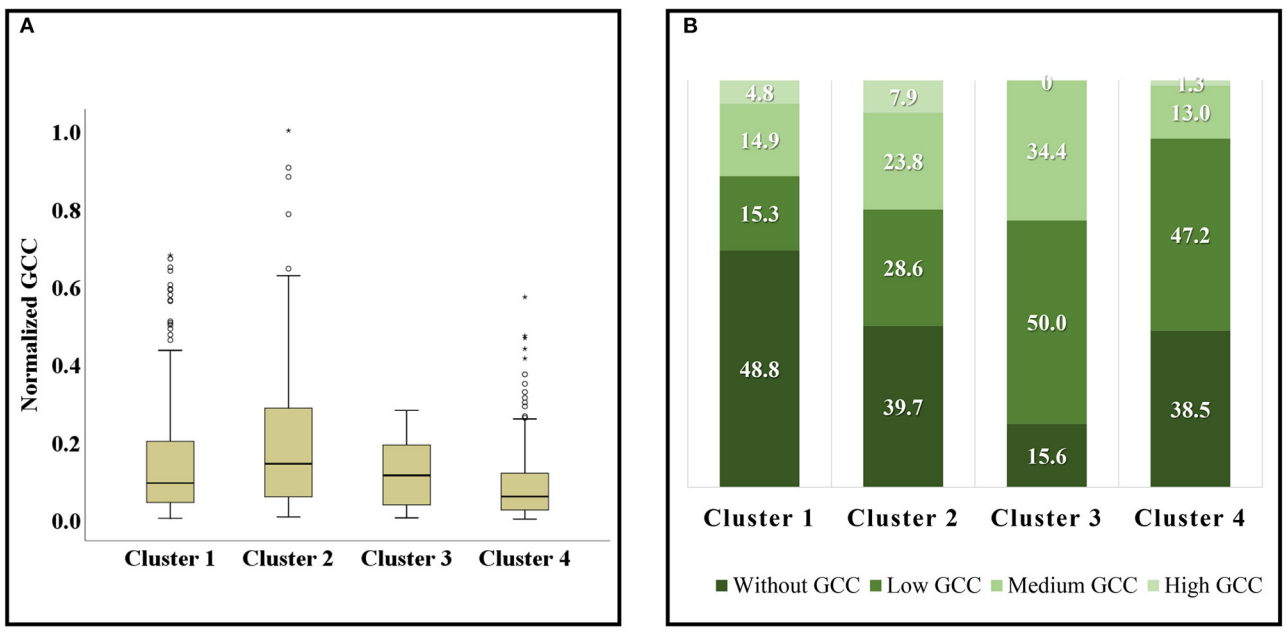

FIGURE 10 | The box diagram of GCC distribution in different clusters **(A)**, the proportion of green spaces with different levels of GCC in different clusters **(B)**. Hollow circles ○ represent mild outliers; asterisks * represent extreme outliers.

distance, the change of the effect becomes lower and lower. When the turning point of distance appears, the cooling effect changes to zero. It showed that the cooling range of green space is not infinite, which is consistent with other research results (25). Besides, we also found that GA and GSI were significantly correlated with GCI, which is consistent with Qiu et al. (39) and Shah et al. (44). But some studies believed that there was no apparent relationship between them. The number of samples analyzed in these studies is only several dozens (28, 48). The lack of adequate samples may affect the accuracy of the studies and lead to the inconsistency of these results. These studies also pointed out that green spaces with small size, a high proportion of water area, and high NDVI usually possess higher GCI than those large green spaces with only forest and grass (34, 43, 50).

Our research also confirms the view at the case level. The GCI of the Xuanwu Art Park (7.8 hm^2) with water accounting for 20% of the area and dense vegetation is much higher than that of some large-sized nurseries (more than 100 hm^2) in the southwest and southeast of the study area, where the vegetation is sparse and growing.

This paper also confirmed that GA and C_G are positively correlated with GCA, which was consistent with Lin et al. (52). The larger the area and perimeter, the larger the contact area between the green space and the surrounding impervious surface, boosting the heat exchange, thus, increasing the cooling coverage. After that, GA and GSI are also significantly correlated with GCG, which is different from Chen et al. (28) and Qiu et al. (53). They believed that GCG is related more to the water area. In conclusion, we believe that green space planning and rebuilding should take the specific cooling needs of the region into consideration, such as cooling coverage, cooling intensity, and cooling gradient. Based on the specific cooling needs, the spatial features and construction elements of green space should be scientifically arranged to effectively alleviate the UHI and create a comfortable and healthy thermal environment in summer.

Rational Spatial Arrangement and Optimization of 4 Green Space Clusters

We found that the green space with a larger area and more regular shape possesses higher GCI, GCA, GCG, and L_{MAX} except for GCE. However, due to the scarcity of land in large cities, especially in metropolitan areas, it is necessary to weigh the relationship between the size of green space and the cost of green space planning and construction (54, 55). With the premise of enjoying good green cooling services, we would like to save funds and costs as much as possible. Therefore, it is necessary to fully understand and make the most of the cooling advantages and features of different green space clusters to adjust and optimize the spatial distribution of green space to realize the optimal green space cooling effect. For example, in densely populated urban fringe areas with large cooling demands and sufficient construction space, it is recommended to build large ecological parks, like the green spaces in cluster 3. These green spaces have the best cooling capacity to mitigate UHI effectively, and also possess important ecosystem service functions. Moreover, in large commercial office areas, communities, and industrial areas with high cooling demands and limited available land, some medium-sized urban parks can be arranged, like the green spaces in cluster 2. These green spaces can be designed with a certain area of water and dense forest vegetation, which not only have a better cooling effect and benefit the health of the surrounding thermal environment to a great extent but also provide entertainment benefiting citizens' mental health. After that, for some communities and office areas lacking available land and large green spaces, some fragmented green spaces in these areas can be integrated into a blue-green infrastructure with several hectares and relatively regular shape, which can also give a good cooling effect, like the green spaces in cluster 1. In sum, the cooling demand of citizens and the cooling supply of different green space clusters should be considered and matched in urban green space planning and construction (56, 57).

The Different Performance of Green Space Cooling Contribution to Surrounding Communities

From the perspective of different levels of GCC, we found that many green spaces were with low GCC or without GCC, but the surrounding of some of these green spaces was the potential location for new communities in the future. Meanwhile, despite the high value in GCC, some green spaces still need to improve their cooling capacity to meet the cooling requirement. Thus, in the process of green space planning and repairing, GCC should be improved according to the green space conditions, cooling demand from residents, and the reasons for this phenomenon.

According to the above results, more than 80% of the green spaces were without GCC or with low GCC. We believe that there are mainly two reasons for this phenomenon. First, there might be no community distribution within a certain distance around the green spaces or the size of the community population is small, that is, the green space cooling effect served too few residents. Second, there are communities around, but the performance of the cooling capacity of these green spaces is very poor. To be specific, these green spaces' cooling range cannot cover enough surrounding communities and their cooling intensity is also weak. Based on the two reasons, we proposed the following strategies to improve GCC. For the first reason, we recommended that according to urban planning, the surrounding of the green spaces with excellent cooling effects can be used as a potential site for new communities. For the second reason, we advised that the green spaces should improve their cooling capacity by modifying their spatial or landscape features to promote their cooling contribution. According to the above results and other studies, it can be enhanced effectively *via* increasing the green space area (GA), water area (58), living vegetation volume (LVV) (59), and the area proportion of dense trees and shrubs (60), and reducing boundary complexity (GSI). Moreover, as the above illustrated, there were also some green spaces with middle and high GCC that need to be worthy of attentions. They are surrounded by a high-density population and perform poorly in cooling capacity. We recommended these green spaces should refer to the promotion methods of the second reason to advance their GCC by increasing their cooling effect. Finally, we suggested that the level of GCC should be taken into consideration in future green space planning and construction, and GCC can be taken as one of the evaluation indicators of whether the green space should be repaired and whether the surrounding of the green space can be suitable to build new communities.

From the perspective of different city zones, we found that there is a variance in green space cooling contribution among these regions. That is, the performance of GCC in the middle zone is the best and the performance of the inner zone is slightly better than that of the outer zone. Previous studies also confirmed that real regional differences have existed in the green space cooling effect (14), which indicated potential unfairness in green space cooling services among city zones. We guessed the reasons

for this phenomenon might be related to the history of urban development. As an old town, the inner zone was saturated before 2000. The green space construction at that time did not receive enough attention. Many green spaces with small or medium size and worse cooling capacity are surrounded by communities, which leads to many green spaces with low GCC appearing in the inner zone. However, the middle zone is the key construction area from 2000 to 2015. With the rapid increase of population in Beijing and the improvement of people's demand for urban green spaces, the government began to pay attention to the scientific construction of urban green spaces. Therefore, there are many modern parks and residential green spaces with larger sizes and good cooling capacity, which makes them perform better in cooling contribution. The outer zone is the key area of current urban construction. Although some green spaces have a large size and perfect cooling effect, the population density in this area is relatively low. Meanwhile, there are still many regions remaining to be developed and exploited. Thus, many green spaces are not with GCC.

Therefore, we suggest that the government and managers attach enough importance to the invisible and potential imbalance and unfairness and bridge it (61). The inner zone can make full use of the current urban renewal policy, and integrate the small green spaces around the community to form urban green infrastructure on a larger scale to produce a cooling effect fully. As for the green spaces in the middle zone, we should further improve the green space cooling contribution purposefully according to the evaluation results of the cooling effect. As for the outer zone, the results of GCC can be used as an essential basis for selecting the new community locations to improve the resident density around the green space with an excellent cooling effect.

Research Limitations and Future Directions

Our research still exerts some limitations in the following aspects. First, the LST retrieved from the remote sensing data is the surface temperature at a specific static moment. In the future, if we obtain dynamic remote sensing data (or LST data) and population distribution data, we will get the GCC of the whole day, and have a deeper understanding of the green space cooling capacity and cooling services. Second, due to the limitation of fine resident distribution data, we replaced it with point data of the community from the real estate trading website. In the future, we will try to obtain more accurate population distribution data or vector data of communities and buildings including population information to make our research more scientific. Finally, the study only focused on the green space cooling service to the community. In the future, all regions with high-density populations in our study area also can be selected for research.

CONCLUSION

So far, many studies have discussed the influencing factors of the cooling effect of green space (15, 29, 62). But few studies have discussed whether the cooling effect of green spaces is enjoyed by residents. Therefore, from a humanistic perspective, this study furthers our understanding of how the different locations in urban zones and different spatial features of green spaces affect their cooling effect and cooling contribution to the surrounding communities, which is crucial to improving the cooling capacity of green spaces in summer and creating a comfortable urban thermal environment.

Thus, we first investigated the overall characteristics and spatial distribution of LST in the study area by using the radiative transfer equation method. The results showed that the old town and industrial and logistics areas possessed the highest LST, while the parks and water possessed the lowest. And the area of the urban heat island is larger than that of the cooling island and the LST of water among all types of land use is the lowest (27.83°C). Accounting for only about 30% area of the study area, green spaces reduced the LST of the whole study area by 1.32°C. Then, we explored the correlation between the spatial features of green spaces and their cooling capacity. The results showed that the GA and GSI are significantly correlated with their cooling capacity, indicating that the green spaces with large areas and regular shapes generally have a good cooling effect. However, there is a threshold for the GA, which is about 50 hm^2. Next, according to the spatial characteristics and cooling effect, 1,157 green spaces with cooling capacity are divided into 4 clusters. And the cooling supply of the 4 clusters was also discussed, respectively. Finally, we defined and mapped the green space cooling contribution to the surrounding community, and discussed the methods of green spaces with different levels of GCC to improve their contribution. It was found that 32.5% of green spaces without cooling contribution, 33.2% of green spaces with low contribution, and 23.5% of green spaces with medium contribution have good cooling capacity, but the surrounding population density is low, which is the potential area set for the new communities in the future; 25.7% of green spaces with low contribution and 11.8% of green spaces with medium contribution served a large population. But these green spaces' cooling capacity is poor, so it is vital to improve their cooling effect. Lastly, based on the urban spatial pattern and the distribution of green space cooling contribution, we further discussed the performance characteristics of GCC in different urban zones and different green space clusters. The study found that the GCC in the middle of the Beijing metropolitan area is significantly better than that of the inner and the outer zones. The green space clusters with moderate scale and high cooling effect have a higher GCC. In the future, the community layout could take green space cooling contribution into consideration to make full use of the optimal efficiency of the green space cooling effect on the health of the community thermal environment.

The study helps guide the green space planning in metropolitan areas to a certain extent and allows the government and planners to deeply understand the actual situation of the cooling effect of green spaces and their cooling contribution to the communities. In addition, it has certain practical significance for improving the ecosystem service of urban blue-green infrastructures and community health and wellbeing.

DATA AVAILABILITY STATEMENT

The datasets presented in this study can be found in online repositories. The names of the repository/repositories and

accession number(s) can be found at: https://www.gscloud.cn/home; http://data.ess.tsinghua.edu.cn/fromglc2017v1.html; https://beijing.anjuke.com/community/?from=navigation.

AUTHOR CONTRIBUTIONS

HZ put forward the ideas, conducted experiments, wrote and modified the manuscript, and drew all figures and tables. WL perfected the initial ideas, provided guidance and suggestions, and did some checking. JZ provided guidance and suggestions. SS and XX solved some technical problems and provided suggestions. TH polished the writing of the manuscript. All authors contributed to the article and approved the submitted version.

FUNDING

This study was supported by the MOE (Ministry of Education in China) Project of Humanities and Social Sciences (Grant No. 18YJC850016) and the Fundamental Research Funds for the Central Universities (2019ZY43).

ACKNOWLEDGMENTS

We are grateful to the foundation of the Project of Humanities and Social Sciences and the Fundamental Research Funds for the Central Universities. And special thanks to the anonymous reviewers and the editor for their constructive comments. Finally, thanks to Guodong Zhu from Liaocheng University and Mengzhu Yan from Beijing Forestry University for their advice on the writing of the manuscript.

REFERENCES

1. Rauf S, Pasra MM, Yuliani. Analysis of correlation between urban heat islands (UHI) with land-use using sentinel 2 time-series image in Makassar city. *IOP Conf Ser Earth Environ Sci.* (2020) 419:12088. doi: 10.1088/1755-1315/419/1/012088
2. Zhao J, Yan Y, Deng H, Liu G, Shao G. Remarks about landsenses ecology and ecosystem services. *Int J Sust Dev World Ecol.* (2020) 27:1–6. doi: 10.1080/13504509.2020.1718795
3. Zhao ZQ, He BJ, Li LG, Wang HB, Darko A. Profile and concentric zonal analysis of relationships between land use/land cover and land surface temperature: case study of Shenyang, China. *Energy Build.* (2017) 155:282–95. doi: 10.1016/j.enbuild.2017.09.046
4. Wang J, Chen Y, Liao W, He G, Tett SFB, Yan Z, et al. Anthropogenic emissions and urbanization increase risk of compound hot extremes in cities. *Nat Clim Change.* (2021) 11:1084–9. doi: 10.1038/s41558-021-01196-2
5. Martiello MA, Giacchi MV. High temperatures and health outcomes: a review of the literature. *Scand J Public Health.* (2010) 38:826–37. doi: 10.1177/1403494810377685
6. Maimaitiyiming M, Ghulam A, Tiyip T, Pla F, Latorre-Carmona P, Halik Ü, et al. Effects of green space spatial pattern on land surface temperature: implications for sustainable urban planning and climate change adaptation. *ISPRS J Photogramm.* (2014) 89:59–66. doi: 10.1016/j.isprsjprs.2013.12.010
7. Deschenes O. Temperature, human health, and adaptation: a review of the empirical literature. *Energy Econ.* (2014) 46:606–19. doi: 10.1016/j.eneco.2013.10.013
8. Hirano Y, Fujita T. Evaluation of the impact of the urban heat island on residential and commercial energy consumption in Tokyo. *Energy.* (2012) 37:371–83. doi: 10.1016/j.energy.2011.11.018
9. Algretawee H, Rayburg S, Neave M. Estimating the effect of park proximity to the central of Melbourne city on urban heat island (UHI) relative to land surface temperature (LST). *Ecol Eng.* (2019) 138:374–90. doi: 10.1016/j.ecoleng.2019.07.034
10. Aram F, Solgi E, García EH, Mosavi A, Várkonyi-Kóczy AR. The cooling effect of large-scale urban parks on surrounding area thermal comfort. *Energies.* (2019) 12:3904. doi: 10.3390/en12203904
11. Msab D, Zllc D, Fn D, Bhtab E, Pei LC, Hua W, et al. Spatiotemporal pattern and long-term trend of global surface urban heat islands characterized by dynamic urban-extent method and MODIS data. *ISPRS J Photogramm Remote Sens.* (2022) 183:321–35. doi: 10.1016/j.isprsjprs.2021.11.017
12. Farshid, Aram, Ester, Higueras, García, Ebrahim, et al. Urban green space cooling effect in cities. *Heliyon.* (2019) 5:1339. doi: 10.1016/j.heliyon.2019.e01339
13. Kong F, Yin H, James P, Hutyra LR, He HS. Effects of spatial pattern of green space on urban cooling in a large metropolitan area of eastern China. *Landscape Urban Plan.* (2014) 128:35–47. doi: 10.1016/j.landurbplan.2014.04.018
14. Srivanit M, Iamtrakul P. Spatial patterns of green space cool islands and their relationship to cooling effectiveness in the tropical city of Chiang Mai, Thailand. *Environ Monit Assess.* (2019) 191:580–1. doi: 10.1007/s10661-019-7749-9
15. Cheng X, Wei B, Chen G, Li J, Song C. Influence of park size and its surrounding urban landscape patterns on the park cooling effect. *J Urban Plan Dev.* (2015) 144:A4014002. doi: 10.1061/(ASCE)UP.1943-5444.0000256
16. Huang X, Wang Y. Investigating the effects of 3D urban morphology on the surface urban heat island effect in urban functional zones by using high-resolution remote sensing data: a case study of Wuhan, Central China. *ISPRS J Photogramm Remote Sens.* (2019) 152:119–31. doi: 10.1016/j.isprsjprs.2019.04.010
17. Li X, Zhou W. Optimizing urban green space spatial pattern to mitigate urban heat island effects: extending understanding from local to the city scale. *Urban Urban Green.* (2019) 41:255–63. doi: 10.1016/j.ufug.2019.04.008
18. Du H, Song X, Jiang H, Kan Z, Wang Z, Cai Y. Research on the cooling island effects of water body: a case study of Shanghai, China. *Ecol Indic.* (2016) 67:31–8. doi: 10.1016/j.ecolind.2016.02.040
19. Brugger P, Roo FD, Krniger K, Rotenberg E, Tatarinov F, Yaki R D, et al. Contrasting turbulent transport regimes explain cooling effect in a semi-arid forest compared to surrounding shrubland. *Agric For Meteorol.* (2019) 15:269–70; 19–27. doi: 10.1016/j.agrformet.2019.01.041
20. Gianelle D, Sottocornola M. Forest have a long-term cooling effect during heat waves. *Nat Geosci.* (2011) 3:722–7. doi: 10.1038/ngeo950
21. Sun R, Chen A, Chen L, Lue Y. Cooling effects of wetlands in an urban region: the case of Beijing. *Ecol Indic.* (2012) 20:57–64. doi: 10.1016/j.ecolind.2012.02.006
22. Xue Z, Hou G, Zhang Z, Lyu X, Jiang M, Zou Y, et al. Quantifying the cooling-effects of urban and peri-urban wetlands using remote sensing data: case study of cities of Northeast China. *Landscape Urban Plan.* (2019) 182:92–100. doi: 10.1016/j.landurbplan.2018.10.015
23. Wu S, Yang H, Luo P, Luo C, Cheng Y. The effects of the cooling efficiency of urban wetlands in an inland megacity: a case study of Chengdu, Southwest China. *Build Environ.* (2021) 204:108128. doi: 10.1016/j.buildenv.2021.108128
24. Wang Y, Zhan Q, Ouyang W. How to quantify the relationship between spatial distribution of urban waterbodies and land surface temperature? *Sci Total Environ.* (2019) 671:1–9. doi: 10.1016/j.scitotenv.2019.03.377
25. Peng J, Dan Y, Qiao R, Liu Y, Wu J. How to quantify the cooling effect of urban parks? Linking maximum and accumulation perspectives. *Remote Sens Environ.* (2021) 252:112135. doi: 10.1016/j.rse.2020.112135
26. Lin BS, Lin CT. Preliminary study of the influence of the spatial arrangement of urban parks on local temperature reduction. *Urban Urban Green.* (2016) 20:348–57. doi: 10.1016/j.ufug.2016.10.003

27. Jaganmohan M, Knapp S, Buchmann CM, Schwarz N. The bigger, the better? The influence of urban green space design on cooling effects for residential areas. *J Environ Qual.* (2016) 45:134. doi: 10.2134/jeq2015.01.0062
28. Chen M, Jia W, Yan L, Du C, Wang K. Quantification and mapping cooling effect and its accessibility of urban parks in an extreme heat event in a megacity. *J Clean Product.* (2021) 334:130252. doi: 10.1016/j.jclepro.2021.130252
29. Zhao-Wu YU, Guo QH, Sun RH. Impacts of urban cooling effect based on landscape scale: a review. *Chin J Appl Ecol.* (2015) 26:636–42. doi: 10.13287/j.1001-9332.20141031.003
30. Beijing Municipal Bureau Statistics. *Beijing Statistical Yearbook 2021. Report.* Beijing: Beijing Municipal Bureau Statistics (2021). Available online at: http://nj.tjj.beijing.gov.cn/nj/main/2021-tjnj/zk/indexeh.htm
31. Beijing Municipal Commission of Planning and Natural Resources. *Beijing Master Plan (2016-2035). Report.* Beijing Municipal Commission of Planning and Natural Resources (2017). Available online at: http://www.beijing.gov.cn/gongkai/guihua/wngh/cqgh/201907/t20190701_100008.html
32. Jiménez-Muñoz JC, Sobrino JA, Skoković D, Mattar C, Cristóbal J. Land surface temperature retrieval methods from landsat-8 thermal infrared sensor data. *IEEE Geosci Remote Sens.* (2014) 11:1840–3. doi: 10.1109/LGRS.2014.2312032
33. Feyisa GL, Dons K, Meilby H. Efficiency of parks in mitigating urban heat island effect: an example from Addis Ababa. *Landsc Urban Plan.* (2014) 123:87–95. doi: 10.1016/j.landurbplan.2013.12.008
34. Yu Z, Fan H, Yang G, Liu TY, Vejre H. How to cool hot-humid (Asian) cities with urban trees? An optimal landscape size perspective. *Agr For Meteorol.* (2019) 265:338–48. doi: 10.1016/j.agrformet.2018.11.027
35. Du H, Cai W, Xu Y, Wang Z, Wang Y, Cai Y. Quantifying the cool island effects of urban green spaces using remote sensing data. *Urban Urban Green.* (2017) 27:24–31. doi: 10.1016/j.ufug.2017.06.008
36. Sobrino JA, Jiménez-Muoz JC, Paolini L. Land surface temperature retrieval from LANDSAT TM 5. *Remote Sens Environ.* (2004) 90:434–40. doi: 10.1016/j.rse.2004.02.003
37. Yang C, He X, Yan F, Yu L, Bu K, Yang J, et al. Mapping the influence of land use/land cover changes on the urban heat island effect—a case study of Changchun, China. *Sustainability.* (2017) 9:312. doi: 10.3390/su9020312
38. Gong P, Liu H, Zhang M, Li C, Wang J, Huang H, et al. Stable classification with limited sample: transferring a 30-m resolution sample set collected in 2015 to mapping 10-m resolution global land cover in 2017. *Sci Bull.* (2019) 64:370–3. doi: 10.1016/j.scib.2019.03.002
39. Qiu KB, Jia BQ, Cheng JF. Cool island effect of urban parks and its influencing factors within the Fifth Ring in Beijing. *Chin J Ecol.* (2017) 9:1–17. doi: 10.13292/j.1000-4890.201707.027
40. Yu Z, Guo X, J Rgensen G, Vejre H. How can urban green spaces be planned for climate adaptation in subtropical cities? *Ecol Indic.* (2017) 82:152–62. doi: 10.1016/j.ecolind.2017.07.002
41. Chang CR, Li MH, Chang SD. A preliminary study on the local cool-island intensity of Taipei city parks. *Landsc Urban Plan.* (2007) 80:386–95. doi: 10.1016/j.landurbplan.2006.09.005
42. Xin C, Onishi A, Chen J, Imura H. Quantifying the cool island intensity of urban parks using ASTER and IKONOS data. *Landsc Urban Plan.* (2010) 96:224–31. doi: 10.1016/j.landurbplan.2010.03.008
43. Sugawara H, Narita KI, Mikami T. Vertical structure of the cool island in a large urban park. *Urban Clim.* (2021) 35:100744. doi: 10.1016/j.uclim.2020.100744
44. Shah A, Garg A, Mishra V. Quantifying the local cooling effects of urban green spaces: evidence from Bengaluru, India. *Landsc Urban Plan.* (2021) 209:104043. doi: 10.1016/j.landurbplan.2021.104043
45. Yuan C, Yang H. Research on K-value selection method of K-means clustering algorithm. *Multidisci Sci J.* (2019) 2:226–35. doi: 10.3390/j2020016
46. Beijing Municipal Bureau Statistics. *Beijing Statistical Yearbook 2018. Report.* Beijing: Beijing Municipal Bureau Statistics (2018). Available online at: http://nj.tjj.beijing.gov.cn/nj/main/2018-tjnj/zk/indexch.htm
47. Yu Z, Yang G, Zuo S, Jrgensen G, Vejre H. Critical review on the cooling effect of urban blue-green space: a threshold-size perspective. *Urban Urban Green.* (2020) 49:126630. doi: 10.1016/j.ufug.2020.126630
48. Gunawardena KR, Wells MJ, Kershaw T. Utilising green and bluespace to mitigate urban heat island intensity. *Sci Total Environ.* (2017) 584–5:1040–55. doi: 10.1016/j.scitotenv.2017.01.158
49. Li H, Wang G, Tian G, Jombach S. Mapping and analyzing the park cooling effect on urban heat island in an expanding city: a case study in Zhengzhou City, China. *Land.* (2020) 9:1–17. doi: 10.3390/land9020057
50. Yu ZW, Yao Y, Yang G, Wang X, Vejre H. Strong contribution of rapid urbanization and urban agglomeration development to regional thermal environment dynamics and evolution. *Forest Ecol Manag.* (2019) 446:214–25. doi: 10.1016/j.foreco.2019.05.046
51. Yu ZW, Gao J, Wang L, Vejre H. Suitability of regional development based on ecosystem service benefits and losses: a case study of the Yangtze river delta urban agglomeration, China. *Ecol Indic.* (2019) 107:105579. doi: 10.1016/j.ecolind.2019.105579
52. Lin W, Yu T, Chang X, Wu W, Zhang Y. Calculating cooling extents of green parks using remote sensing: method and test. *Landsc Urban Plan.* (2015) 134:66–75. doi: 10.1016/j.landurbplan.2014.10.012
53. Qiu K, Jia B. The roles of landscape both inside the park and the surroundings in park cooling effect. *Sustain Cities Soc.* (2020) 52:101864. doi: 10.1016/j.scs.2019.101864
54. Du H, Cai Y, Zhou F, Jiang H, Xu Y. Urban blue-green space planning based on thermal environment simulation: a case study of Shanghai, China. *Ecol Indic.* (2019) 106:105501. doi: 10.1016/j.ecolind.2019.105501
55. Cheng S, Chenniu Y, Shuaiwang L. Study on the mitigation effect of parks on the urban heat island effect - taking Shenzhen as an example. *Chin Landsc Architect.* (2019) 35:6. doi: 10.19775/j.cla.2019.10.0040
56. Yang G, Yu ZW, Jrgensen G, Vejre H. How can urban blue-green space be planned for climate adaption in high-latitude cities? A seasonal perspective. *Sustain Cities Soc.* (2020) 53:101932. doi: 10.1016/j.scs.2019.101932
57. Yun HH, Qin J, Chan Y. Micro-scale thermal performance of tropical urban parks in Singapore. *Build Environ.* (2015) 94:467–76. doi: 10.1016/j.buildenv.2015.10.003
58. Shi L, Zhao M. Cool island effect of urban parks and impact factors in summer: a case study of Xi'an. *J Arid Land Resourc Environ.* (2020) 34:154. doi: 10.13448/j.cnki.jalre.2020.139
59. Hua L, Sun F, Chen J, Tang L. Quantifying the cool-island effects of urban parks using Landsat-8 imagery in a coastal city, Xiamen, China. *Acta Ecologica Sinica.* (2020) 40:11. doi: 10.5846/stxb202003140536
60. Wang X, Feng X, Chen K, Gao X. Study on the cooling effect of urban parks base on the case of Changzhou, Jiangsu, China. *China Environ Sci.* (2021) 41:8. doi: 10.19674/j.cnki.issn1000-6923.20210603.002
61. Wu L, Kim SK. Does socioeconomic development lead to more equal distribution of green space? Evidence from Chinese cities. *Sci Total Environ.* (2020) 757:143780. doi: 10.1016/j.scitotenv.2020.143780
62. Martins T, Adolphe L, Bonhomme M, Bonneaud F, Guyard W. Impact of urban cool Island measures on outdoor climate and pedestrian comfort: simulations for a new district of Toulouse, France. *Sustain Cities Soc.* (2016) 26:9–26. doi: 10.1016/j.scs.2016.05.003

Conflict of Interest: The authors declare that the research was conducted in the absence of any commercial or financial relationships that could be construed as a potential conflict of interest.

frontiers | Frontiers in Public Health

ORIGINAL RESEARCH
published: 17 May 2022
doi: 10.3389/fpubh.2022.890175

Conflict or Coordination? Spatiotemporal Coupling of Urban Population–Land Spatial Patterns and Ecological Efficiency

Ling Shan, Yuehua Jiang, Cuicui Liu, Jing Zhang, Guanghong Zhang and Xufeng Cui**

School of Business Administration, Zhongnan University of Economics and Law, Wuhan, China

The coordinated relationship between urban population–land spatial patterns (UPLSPs) and ecological efficiency (EE) is conducive not only to the rational utilization of resources and environment and the sustainable development of society, but also to the provision of a living environment that benefits public health. Identifying the coupling relationship of urban development and EE can provide critical information for urban planning. Previous studies have mainly focused on the coupling relationship between urban population and land, urbanization, and ecological development, while ignoring that between UPLSPs and EE. This study integrates several models to construct a novel framework for coupling UPLSPs and EE. Taking Hubei Province as the research area, we calculate the UPLSPs, EE, and their coupling coordination degree for 12 cities from 2000 to 2019. The paper offers several conclusions. (1) the urban population–land spatial matching degree increased, but the overall matching level was not high; the average value of EE showed an "N"-shaped change trajectory, and its overall level was low, with small changes and obvious regional differences. (2) The average value of the coupling coordination degree between UPLSPs and EE was a slow upward trend, with a radial distribution high in the middle and low in the periphery. There was conflict between the spatial patterns and EE, and the former restricted the development of the latter. (3) There were strong correlations between coordination degree and various indicators of UPLSPs and EE. While we should revitalize the stock of construction land and optimize the upgrading of the industrial structure, we also must coordinate human and land resources and the ecological environment, and narrow regional development differences. This study provides a new framework for urban environmental assessment and urban planning decision-making.

Keywords: ecological efficiency, coupling, Hubei Province, China, urbanization

OPEN ACCESS

Edited by:
Hongtao Yi,
The Ohio State University, United States

Reviewed by:
Bin Yang,
China University of Mining and Technology, China
Sha Chen,
Zhejiang University of Finance and Economics, China

****Correspondence:***
Guanghong Zhang
z0001297@zuel.edu.cn
Xufeng Cui
cxf@zuel.edu.cn

Specialty section:
This article was submitted to Environmental health and Exposome, a section of the journal Frontiers in Public Health

Received: *05 March 2022*
Accepted: *21 April 2022*
Published: *17 May 2022*

Citation:
Shan L, Jiang Y, Liu C, Zhang J, Zhang G and Cui X (2022) Conflict or Coordination? Spatiotemporal Coupling of Urban Population–Land Spatial Patterns and Ecological Efficiency. Front. Public Health 10:890175. doi: 10.3389/fpubh.2022.890175

INTRODUCTION

Urbanization has become an important trend in global development (1). Currently, 55% of the world's population lives in urban areas, a proportion that is expected to increase to 68% by 2050. Overall growth could add another 2.5 billion people to urban areas by 2050, with close to 90% of this increase taking place in Asia and Africa (2). China has experienced the largest and fastest urbanization process in the history of the world. At the end of 2019, China's urbanization rate reached 60.60%, an increase of 49.96 percentage points since 1949, and an average annual

increase of 0.71 percentage points (3). Urbanization is undoubtedly an important driving force for China's economic development (4). However, the rapid development of cities has also spawned some inevitable problems, such as the reduction of biodiversity, the unreasonable allocation of urban resources, deterioration of the ecological environment, and urban emergencies (5–10), and so on, which have placed enormous pressure on China's public health, social economy, resources, and environment. To solve these problems, it is necessary to guide urban construction with the concept of ecological civilization, and to coordinate the relationship between urban development and ecological efficiency (EE).

The most important aspects of urbanization are population and land (11, 12). The urban population–land spatial patterns (UPLSPs) is the form of spatial agglomeration of urbanization elements. EE is the efficient use of ecological resources to meet human needs. It involves not only the unity of economic benefits and resources with environmental benefits, but also the essential embodiment of green and sustainable development (13). As an important grain production base and ecological barrier in the central region, Hubei Province has a superior location and a strong economy. It is a strategic support in the rise of central China. However, the contradictions between population agglomeration, urban land expansion, and ecological environment and economic development in this region have become increasingly prominent, threatening public health and the sustainable development of the city. How to deal with the relationship between the UPLSPs and EE and realize the rational utilization of resources and the sustainable development of society is an important task. What is the relationship between the UPLSPs and EE in Hubei Province? Is it one of conflict or coordination? These issues deserve in-depth study.

The concept of EE was first put forward by Schaltegger and Sturm in (14), and its original meaning was the ratio of economic value added to environmental impact. Subsequently, the World Business Council for Sustainable Development expanded the meaning to include obtaining products and services that could meet the needs of human life at the cost of minimizing resource consumption and environmental impact. At present, much research on urbanization and EE has been carried out, but these studies mainly focus on a single dimension of the topic. Most scholars believe that current urbanization features uncoordinated growth and is excessive (15). Relevant research mainly focuses on three aspects: (1) the spatial distribution differences of urban populations and land (16); (2) the calculation of coupling coordination degree between urban populations and land; and (3) uncoordinated factors of urban populations and land. Moreover, research on the coordination between population and land urbanization uses the coupling coordination model (17–20), the elastic coefficient model (21), and the Tapio decoupling model (22), among others. Scholars have proposed that location factors, economic development level, household registration systems, and land financialization (23, 24) all have important impacts on urban populations and land.

Moreover, academic research on EE has been growing and mainly focuses on three aspects. First, some studies explore the measurement index system and method of EE, mainly by using measurement index systems, such as "input + desirable output + undesirable output" (25, 26) and "resource consumption input + environmental impact input + output" (27, 28). Scholars also use the data envelopment analysis (DEA) method (29–31), slacks-based measure (SBM) model (32, 33), stochastic frontier approach (34, 35), Malmquist productivity index approach (36, 37), and ecological footprint model (38, 39) to calculate EE; among these, the DEA method and the SBM model are the most widely used. Second, scholars have analyzed evolution in the spatiotemporal patterns of EE across regions using methods such as spatial autocorrelation, Markov chain models, and the Theil index (40, 41). Third, research has applied Tobit models, spatial econometric models, system GMM methods, and other approaches to study the effects of urbanization, technological innovation, industrial structure, energy consumption, natural resource endowments, environmental regulation, foreign direct investment, economic development level (27, 42–44), and other factors on EE.

The research on both urbanization and EE mainly focuses on their spatiotemporal coupling characteristics (45, 46) and the impact of urban construction on EE (44). The unit of analysis of most studies is typically a whole country, urban agglomerations, or provinces. For example, at the scale of the whole country, Liu et al. (6, 45) analyzed the comprehensive urbanization level, energy EE, and their coupling coordination degree in 281 prefecture-level cities in China over the past 11 years. At the scale of urban agglomerations, Zhou et al. (47) focused on the impact of urbanization level and population urbanization lags on EE in the Bohai-rim urban agglomeration. At the province level, Yao et al. (44) used the spatial Durbin model to explore the multi-dimensional impact mechanism of urbanization in 30 provinces in China from 2008 to 2017, along with the internal structural effect of each dimension on EE. However, these studies have paid little attention to the relationship between the UPLSPs and EE.

Therefore, taking Hubei Province as the research area, this study first calculates the UPLSPs, EE, and their coupling coordination degree for 12 cities in Hubei Province from 2000 to 2019 by constructing a spatial matching evaluation model, super-efficiency SBM model, and coupling coordination degree model. Then, spatial autocorrelation and gray relational analysis methods are used to explore the spatiotemporal evolution and driving factors of the coupling coordination degree between the UPLSPs and EE. Finally, on this basis, policy recommendations are made for new urbanization development and ecological civilization construction in Hubei Province. Further, this study provides a new framework for urban environmental assessment and urban planning decision-making. The research framework is shown in **Figure 1**.

STUDY AREA

Hubei Province is located in the middle of China (**Figure 2**) and spans east longitude 108°21'42"−116°07'50" and north latitude 29°01'53"−33°6'47". It is about 740 kilometers from east to west and 470 kilometers from north to south. Hubei Province has 12 prefecture-level cities, three provincial municipalities, one

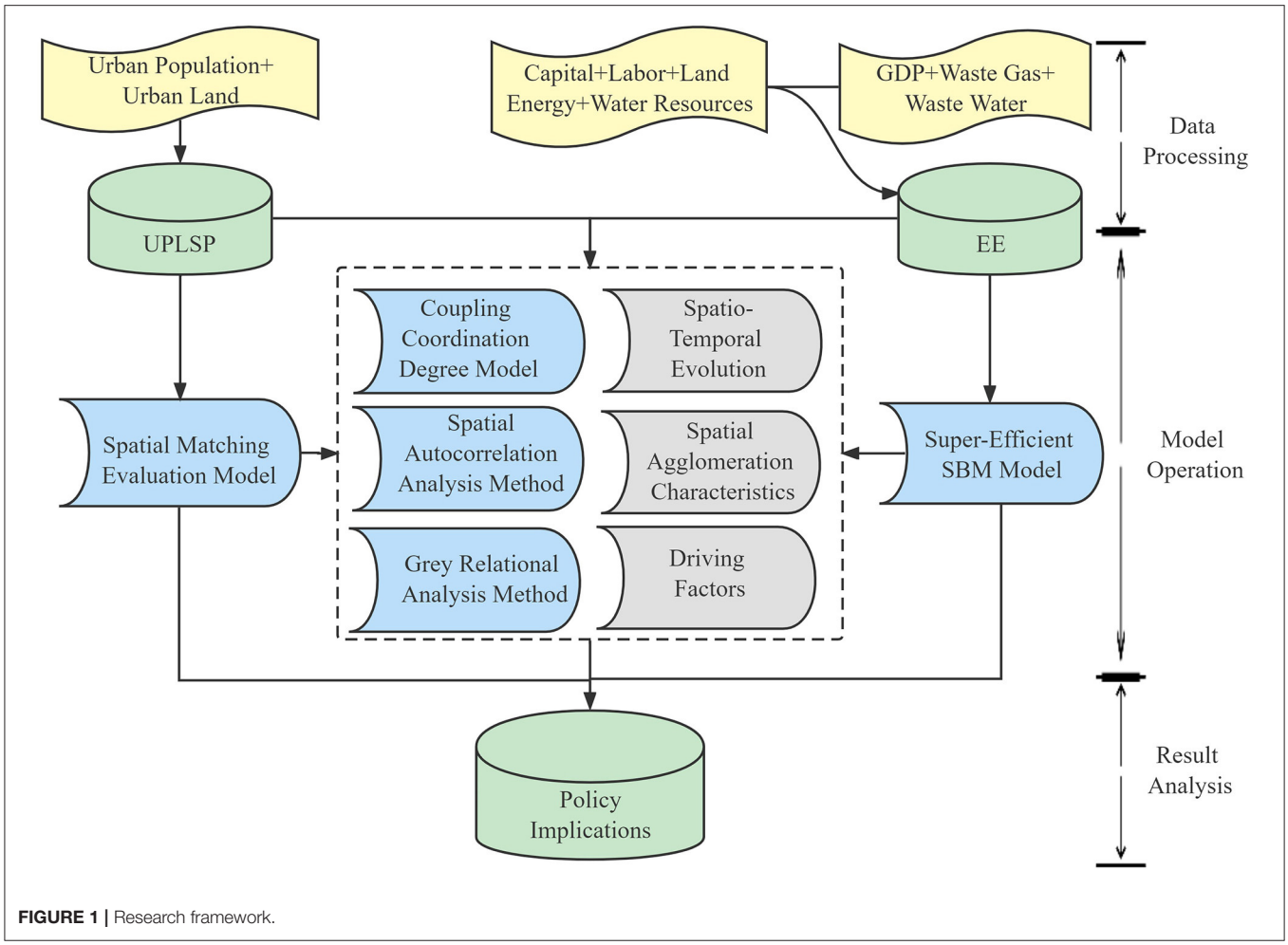

FIGURE 1 | Research framework.

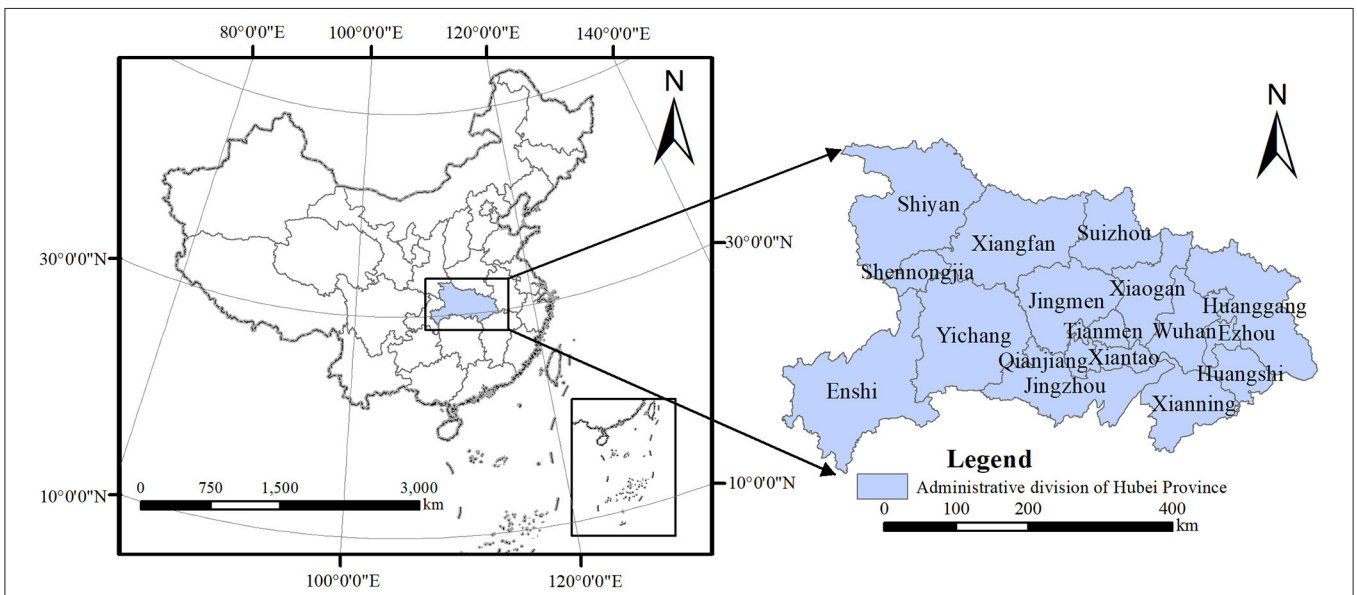

FIGURE 2 | Study area (Source of base map: the open source map data service provided by the National Platform for Common GeoSpatial Information Services: https://www.tianditu.gov.cn).

autonomous prefecture, and one forest district. By the end of 2019, the permanent resident population of Hubei Province was 59.27 million, accounting for 4.23% of the national population. The total land area of the province was 185,900 square kilometers, accounting for 1.94% of the nation's total area (3).

Hubei Province has superior geographical conditions and is a powerful economic province in China. As an important part of the national development strategy of the Yangtze River Economic Belt and the rise of central China, it is necessary to actively promote the construction of new urbanization and ecological civilization. However, with the accelerated development of urbanization and industrialization, the contradiction between humans and land, economic development and environmental protection, in Hubei Province becomes more apparent. Therefore, this paper selects Hubei Province as the research area, and the findings have reference value for other cities. Moreover, due to the functional attributes of the city and the suitability of the research, this study considers 12 prefecture-level cities in Hubei Province.

DATA AND METHODS

Data Sources and Processing

The data come from the *China Urban Construction Statistical Yearbook* (2000–2019), the *China City Statistical Yearbook* (2001–2020), and the *Hubei Statistical Yearbook* (2001–2020). Based on the data on adjacent years, the missing data for individual cities are reconstructed using the moving average and trend extrapolation methods.

The EE indicators constructed in this paper include input, desired output, and undesired output, as shown in **Table 1**. The input indicators include capital, labor, land, energy, and water resources; the desired output indicators are captured with regional gross domestic product (GDP) and deflating GDP, with 2000 identified as the baseline to eliminate the impact of price factors. The undesired output indicators include both waste gas and waste water. In addition, since the capital stock cannot be obtained directly from the statistical yearbook, this paper uses the capital stock, calculated through the continuous inventory method, as the capital investment; the formula is as follows:

$$\mathrm{K\_it} = \mathrm{K\_(it-1)}(1-\delta) + \mathrm{I\_it} \tag{1}$$

where K represents the capital stock, i represents the region, t represents the period, δ represents the depreciation rate, and I represents the total investment in fixed assets in the whole country. Following prior research (50), the depreciation rate is 9.6%. The total investment in fixed assets in the whole country in 2000 is divided by 10% as the initial capital stock *K_0*. According to the investment in fixed assets price index, the total investment in fixed assets in the whole country is converted into the constant price based on the year 2000.

In the multi-index evaluation system, each evaluation indicator usually has different dimensions and orders of magnitude, owing to its different attributes. Therefore, this paper uses the min-max normalization method to standardize the original data (51, 52), as follows:

$$\text{positive indicators}: \ \mathrm{Z_{ij}} = \frac{X_{ij} - min\left(X_{ij}\right)}{max\left(X_{ij}\right) - min\left(X_{ij}\right)} \tag{2}$$

$$\text{negative indicators}: \ \mathrm{Z_{ij}} = \frac{max\left(X_{ij}\right) - X_{ij}}{max\left(X_{ij}\right) - min\left(X_{ij}\right)} \tag{3}$$

where Z_{ij} is the standard value of the index j in the i^{th} year, X_{ij} is the original data of the index j in the i^{th} year, and $\max\left(X_{ij}\right)$ and $\min\left(X_{ij}\right)$ are the maximum and minimum values of the j^{th} index, respectively.

Methods

Spatial Matching Evaluation Model

Referring to the research on spatial matching and spatial agglomeration (53), this paper constructs the urban population–land spatial matching evaluation model, and uses the spatial density of the urban population and land to describe the coordinated relationship between people and land in the urbanization system. The model is as follows:

$$Match_i = \left(Pop_i / \sum_{i=1}^{n} Pop_i\right) \times \left(Land_i / \sum_{i=1}^{n} Land_i\right)^{-1} - 1 \tag{4}$$

where $Match_i$ is the urban population–land spatial mismatching degree in the i^{th} area, and Pop_i and $Land_i$ are the evaluation values for the urban population and urban land in the i^{th} area. The urban population and land measures are constructed using urban population size data and data on the built-up area, respectively; all data are obtained from the *China Urban Construction Statistical Yearbook*.

The absolute value of $Match_i$ illustrates the urban population–land spatial matching degree, and $abs\left(Match_i\right) \in [0, +\infty)$. When the value of $abs\left(Match_i\right)$ gradually increases, the urban population–land spatial matching degree tends to weaken; this means that the urban population and land in this region are uncoordinated in the spatial dimension. In contrast, when $abs\left(Match_i\right)$ gradually decreases, the urban population–land spatial matching degree tends to increase; this indicates that the urban population and land in this region are coordinated.

According to the sign on $Match_i$, the types of UPLSPs can be divided into "urban population concentration," "urban land concentration," and "urban population–land relative matching." Urban population concentration indicates that the urban population is more concentrated than the land in this area, while urban land concentration suggests the reverse. Finally, urban population–land relative matching indicates that the spatial distribution of the two components is balanced. To judge the strength of the urban population–land spatial matching degree, the grades of UPLSPs are divided into "relative matching," "low mismatch," "moderate mismatch," and "high mismatch," as shown in **Table 2**.

Based on the above urban population–land spatial matching evaluation model, the regional comprehensive mismatching

TABLE 1 | Evaluation index system of EE.

Target level	Criterion level	Indicator level	Literature source
Input	Capital	Total investment in fixed assets in the whole country/100 million yuan (Y1)	(25, 26, 33, 46, 48, 49)
	Labor	Number of employees at the end of the period/10,000 people (Y2)	(25, 26, 33, 46, 48, 49)
	Land	Built-up area/km^2 (Y3)	(26, 33, 49)
	Energy	Annual electricity consumption/100 million kW.h (Y4)	(33, 48, 49)
	Water resources	Total water resources/100 million cu.m^3 (Y5)	(26, 27, 48, 49)
Desired output	Economic growth	GDP/100 million yuan (Y6)	(25–27, 46, 48, 49)
Undesired output	Waste water	Industrial wastewater discharge/10,000 tons (Y7)	(26, 27, 33, 46, 48, 49)
	Waste gas	Industrial SO_2 emissions/ton (Y8)	(27, 33, 48, 49)
		Industrial smoke (powder) dust emissions/ton (Y9)	(26, 27, 33, 46, 48, 49)

TABLE 2 | Types and grades of UPLSPs.

UPLSPs type	UPLSPs grade	Value range	UPLSPs type	UPLSPs grade	Value range
Urban land concentration	High mismatch	$Match < -0.5$	Urban population concentration	Low mismatch	$0.1 \leq Match < 0.3$
Urban land concentration	Moderate mismatch	$-0.5 \leq Match < -0.3$	Urban population concentration	Moderate mismatch	$0.3 \leq Match < 0.5$
Urban land concentration	Low mismatch	$-0.3 \leq Match < -0.1$	Urban population concentration	High mismatch	$Match \geq 0.5$
Urban population–land relative matching	Relative matching	$-0.1 \leq Match < 0.1$			

degree evaluation model is defined as:

$$Zmatch = \left[\frac{\left(\sum_{i=1}^{n} Match_i{}^2 \right)}{n} \right]^{\frac{1}{2}} \tag{5}$$

where *Zmatch* is the urban population–land comprehensive mismatching degree of the upper-level region, and $Match_i$ is the same for the lower-level region. *Zmatch* is a comprehensive measure of the degree of urban population–land mismatching in the upper-level region containing the lower-level region. For $Zmatch \in [0, +\infty$, the larger the *Zmatch* value, the higher the comprehensive mismatch of the upper region, and the more unbalanced the spatial distribution of the urban population and land in this region.

Super-Efficient SBM Model

The common EE measurement method is the DEA model. However, traditional DEA models are mostly radial or angular and do not consider the problem of factor relaxation. Therefore, Tone proposed a non-radial and non-angular SBM model (54, 55), which considered not only the proportional improvement between the current state of the invalid DMU and the strong target value, but also the relaxation improvement. However, it is still a problem that the effective units cannot be further sorted and distinguished. Therefore, this study adopts the super-efficiency SBM model; that is, the SBM model is extended by considering the changes in production technology that occurred each year during the study period (56). The efficiency is estimated in a non-ray manner. Equation (6) shows this expression:

$$\rho = \min \frac{1 - \frac{1}{m} \sum_{i=1}^{m} \frac{s_h^-}{x_{hk}}}{1 + \frac{1}{q_1+q_2} \left(\sum_{r=1}^{q_1} \frac{s_r^-}{y_{rk}} + \sum_{t=1}^{q_2} \frac{s_t^{b-}}{y_{hk}^b} \right)} \tag{6}$$

$$s.t. \sum_{j=1, j \neq k}^{n} x_{h1}\lambda_1 - s_h^- \leq x_{ik}; \sum_{l=1, l \neq k}^{n} y_{hl}^b \lambda_1 - s_r^{b-} \leq y_{rk}$$

$$1 + \frac{1}{q_1 + q_2} \left(\sum_{r=1}^{q_1} \frac{s_r^-}{y_{rk}} + \sum_{t=1}^{q_2} \frac{s_t^{b-}}{y_{hk}^b} \right) > 0$$

$$\lambda_h, s_h^-, s_r^+ \geq 0$$

where ρ denotes EE; x_{hk}, y_{rk}, and y_{hk}^b denote the h^{th} input factor, the r^{th} desired output, and the h^{th} undesired output of the k^{th} prefecture-level city, respectively; s_h^-, s_r^-, and s_t^{b-} denote slack variables of the input factors, desired output, and undesired output, respectively; λ_1 denotes the constraint condition; and $h = 1, 2, \ldots, q_1$; $t = 1, 2, \ldots, q_2$; and $l = 1, 2, \ldots, n(j \neq k)$.

Coupling Coordination Degree Model

Coupling coordination degree refers to the degree of benign coupling in the interaction relationship; it can be used to characterize whether the functions promote each other at a high level or restrict each other at a low level (57, 58). This study uses it to measure the coordinated relationship between the UPLSPs and EE.

Coupling Degree Model

Based on the relevant research results (59, 60), the coupling degree model of UPLSPs and EE is constructed as follows:

$$C = \left[\frac{f(x) \times g(y)}{\left(\frac{f(x)+g(y)}{2} \right)^2} \right]^{\frac{1}{2}} \tag{7}$$

where C is the coupling degree between UPLSPs and EE, and $C \in [0, 1]$. When the value of C is smaller, the mutual interaction between UPLSPs and EE is lower, and vice versa. When $C = 1$, the optimal coordination state of the two is achieved. The functions $f(x)$ and $g(y)$ are UPLSPs and EE, respectively.

Coupling Coordination Degree Model

The coupling coordination index is introduced to construct the coupling coordination degree model of UPLSPs and EE, and the model is as follows (61, 62):

$$D = \sqrt{C \times T} \tag{8}$$

$$T = \alpha f(x) + \beta g(y) \tag{9}$$

where D is the coupling coordination degree of UPLSPs and EE, C is the coupling degree of UPLSPs and EE, T is the comprehensive coordination index of UPLSPs and EE, and α and β are the contributions of UPLSPs and EE to urban development, respectively. Considering the same contribution, $\alpha = \beta = 0.5$.

As in previous studies (63, 64), the coupling coordination degree of UPLSPs and EE is divided into three intervals (imbalanced recession interval, transitional harmonic interval, and coordinated development interval) and ten types, as shown in **Table 3**.

Spatial Autocorrelation Analysis Model

Spatial autocorrelation is an important indicator that tests whether the attribute value of a certain element is significantly associated with the attribute value of its adjacent spatial points. It is divided into global spatial autocorrelation and local spatial autocorrelation (65, 66). Global spatial autocorrelation is used to measure whether there is agglomeration or dispersion in the spatial distribution of element attribute values. It is usually expressed by the global Moran's I index, the calculation of which is as follows (15, 44, 67):

$$I = \frac{\sum_{i=1}^{n} \sum_{j=1}^{n} W_{ij} \left(x_i - x \right) \left(x_j - x \right)}{S^2 \sum_{i=1}^{n} \sum_{j=1}^{n} W_{ij}} \tag{10}$$

where I is the global Moran's I index; n is the number of prefecture-level cities; x_i and x_j are the coupling coordination degrees of UPLSPs and EE in regions i and j, respectively; x is the average value of the coupling coordination degree of UPLSPs and EE; S^2 is the sample variance; and $S^2 = \frac{1}{n} \sum_{i=1}^{n} \left(x_i - x \right)^2$. $W_{ij}$is the spatial weight matrix of regions i and j (when regions i and j are adjacent, W_{ij} =1; when regions i and j are not adjacent, $W_{ij=}$0). The value of Moran's I index is in the range of [−1,1]. Moran's I index values greater than zero indicate a positive spatial correlation, less than zero indicate a negative spatial correlation, and equal to zero indicate no spatial correlation.

Local spatial autocorrelation is used to measure the correlation of each spatial element attribute in the local position. It is usually expressed by the local Moran's I index, the calculation of which is as follows (68):

$$I_i = \frac{(x_i - \bar{x})}{S^2} \sum_{j=1}^{n} W_{ij} \left(x_j - \bar{x} \right) \tag{11}$$

where I_i is the local Moran's I index; the meanings of n, x_i, x_j, $\bar{x}$, S^2, and $W_{ij}$are shown above. A value of $I_i > 0$ indicates the spatial aggregation of similar values (high–high or low–low) around the unit in the area, and a value <0 indicates the spatial aggregation of dissimilar values (high–low or low–high).

Gray Relational Analysis Method

Gray system theory is a method proposed by Deng (69) in the 1980's to study the uncertainty problem with little data and poor information. Gray relational analysis is a quantitative method used to judge whether the corresponding sequences are closely related according to the geometric similarity of sequence curves, which can measure the degree of association between factors. The calculation steps are as follows (70, 71):

(1) Determine the reference sequence and comparison sequence, and use the mean normalization method for data standardization. This study selects the coupling coordination degree of UPLSPs and EE in Hubei Province as the reference sequence, denoted as $X_O(k)$, and the driving factors as the comparison sequence, denoted as $X_i(k)$. The normalized reference sequence and comparison sequence are $X_O{}'(k)$ and $X_i{}'(k)$ $(i = 1, 2, 3, \ldots, n)$.

(2) Calculate the relational coefficient $\zeta_i(k)$.

$$\zeta_i(k) = \frac{\min_i \min_k \left| X_O{}'(k) - X_i{}'(k) \right| + \rho \max_i \max_k \left| X_O{}'(k) - X_i{}'(k) \right|}{\left| X_O{}'(k) - X_i{}'(k) \right| + \rho \max_i \max_k \left| X_O{}'(k) - X_i{}'(k) \right|} \tag{12}$$

$$X_i{}'(k) = \frac{X_i(k)}{\bar{X}_i(k)} \bar{X}_i(k) = \frac{1}{n} \sum_{k=1}^{n} X_i(k)$$

where $\left| X_O{}'(k) - X_i{}'(k) \right|$ is the minimum absolute value of two levels of two sequences, $\left| X_O{}'(k) - X_i{}'(k) \right|$ is the maximum absolute value of two levels of two sequences; ρ is the resolution coefficient; and $\rho = 0.5$.

(3) Calculate the relational degree r_i:

$$r_i = \frac{1}{n} \sum_{k=1}^{N} \zeta_i(k), i = 1, 2, 3, \ldots, n \tag{13}$$

TABLE 3 | Classification of the coupling coordination degree.

D	Coupling coordination type	Coupling coordination interval	*D*	Coupling coordination type	Coupling coordination interval
$0 \leq D < 0.1$	Extremely imbalanced	Imbalancedrecession interval	$0.5 \leq D < 0.6$	Primary coordination	Coordinated development interval
$0.1 \leq D < 0.2$	Moderately imbalanced		$0.6 \leq D < 0.7$	Intermediate coordination	
$0.2 \leq D < 0.3$	slightly imbalanced		$0.7 \leq D < 0.8$	good coordination	
$0.3 \leq D < 0.4$	barely harmonic coordination	Transitional harmonic interval	$0.8 \leq D < 0.9$	high-quality coordination	
$0.4 \leq D < 0.5$	harmonic coordination		$0.9 \leq D \leq 1$	extreme coordination	

TABLE 4 | Classification of the relational degree.

Grade	No correlation	Low correlation	Moderate correlation	High correlation	Strong correlation	Complete correlation
r_i	0	(0, 0.35)	(0.35, 0.65)	(0.65, 0.85)	(0.85, 1)	1

The value range of the relational degree r_i is [0, 1]; the larger the value of r_i, the greater the correlation between the indicators and the stronger the coupling. In addition, as in the literature (72, 73), the relational degree of the coupling coordination degree of UPLSPs and EE is divided into six types, as shown in **Table 4**.

RESULTS

Spatiotemporal Evolution of UPLSPs in Hubei Province

This study uses cross-sectional data from 2000, 2005, 2010, 2015, and 2019 to analyze the UPLSPs of Hubei Province along the time and space dimensions based on the spatial matching evaluation model. The results are shown in **Table 5**. The comprehensive mismatching degree of Hubei Province shows an overall downward trend, from 0.3228 in 2000 to 0.2530 in 2019, and the type of UPLSPs is always urban population concentration. This indicates that the level of urban population–land spatial matching has been gradually increasing. The main reason for this is because, with the development of the social economy and the improvement of living standards, more people have moved from rural areas to cities, resulting in an increase of the urban population and population density.

At the city level, the urban population–land spatial matching degree in Hubei Province from 2000 to 2019 increased in Wuhan, Shiyan, Xiangyang, Ezhou, Jingmen, Huanggang, Xianning, and Suizhou. It decreased in Huangshi, Yichang, Xiaogan, and Jingzhou. In 2000, Shiyan, Yichang, Xiangyang, Ezhou, Jingmen, Xiaogan, Huanggang, and Xianning were classified as urban land concentration, Wuhan and Suizhou were urban population concentration, and Huangshi and Jingzhou were urban population–land relative matching. In 2019, Shiyan, Yichang, Ezhou, Huanggang, Xianning, and Suizhou were urban land concentration; Wuhan, Huangshi, Xiaogan, and Jingzhou were urban population concentration; and Xiangyang and Jingmen were matched. The UPLSPs type in Hubei Province is mainly urban land concentration, and there has been a transformation from concentrations of urban land to urban populations.

TABLE 5 | UPLSPs in Hubei Province from 2000 to 2019.

Number	City	2000	2005	2010	2015	2019
1	Wuhan	0.4270	0.4288	0.2169	0.1027	0.1224
2	Huangshi	−0.0190	−0.2064	0.1287	0.4855	0.1354
3	Shiyan	−0.3792	−0.3557	−0.1882	−0.1431	−0.2460
4	Yichang	−0.1046	−0.1954	−0.1805	−0.2847	−0.3411
5	Xiangyang	−0.1523	−0.1304	−0.1276	−0.1332	−0.0652
6	Ezhou	−0.4224	−0.3897	−0.2073	−0.1453	−0.3260
7	Jingmen	−0.4628	−0.3417	−0.2068	−0.0389	0.0692
8	Xiaogan	−0.4170	−0.5412	−0.3374	0.2901	0.4528
9	Jingzhou	−0.0011	0.2730	0.0777	0.1243	0.3045
10	Huanggang	−0.1921	−0.0221	−0.0415	−0.2662	−0.1050
11	Xianning	−0.3107	−0.4261	−0.5044	−0.2696	−0.2683
12	Suizhou	0.4356	0.7369	−0.2239	0.1478	−0.2484
Comprehensive mismatching degree of Hubei Province		0.3228	0.3840	0.2345	0.2333	0.2530

Figure 3 shows the evolution of the spatial pattern of UPLSPs. There were seven cities with a moderate mismatch in 2000, which reduced to four in 2019. Three cities has a low mismatch in 2000, which increased to six in 2019. The number of matched cities was relatively stable, with two in 2000, 2010, and 2019, and only one in other years. This indicates that urban population–land spatial matching has spatial heterogeneity. Moreover, the overall matching level is not high but shows an upward trend annually.

Spatiotemporal Evolution of EE in Hubei Province

This study uses the super-efficiency SBM model and MATLAB software to calculate the EE of 12 cities in Hubei Province in 2000, 2005, 2010, 2015, and 2019. According to **Table 6**, the average value of EE in Hubei Province increased from 0.6459 in 2000 to 0.6618 in 2019, with an average annual growth rate of 0.1281%. The change is "N"-shaped—first rising, then decreasing, and then rising—and the overall level of EE is low, but the changes are not large.

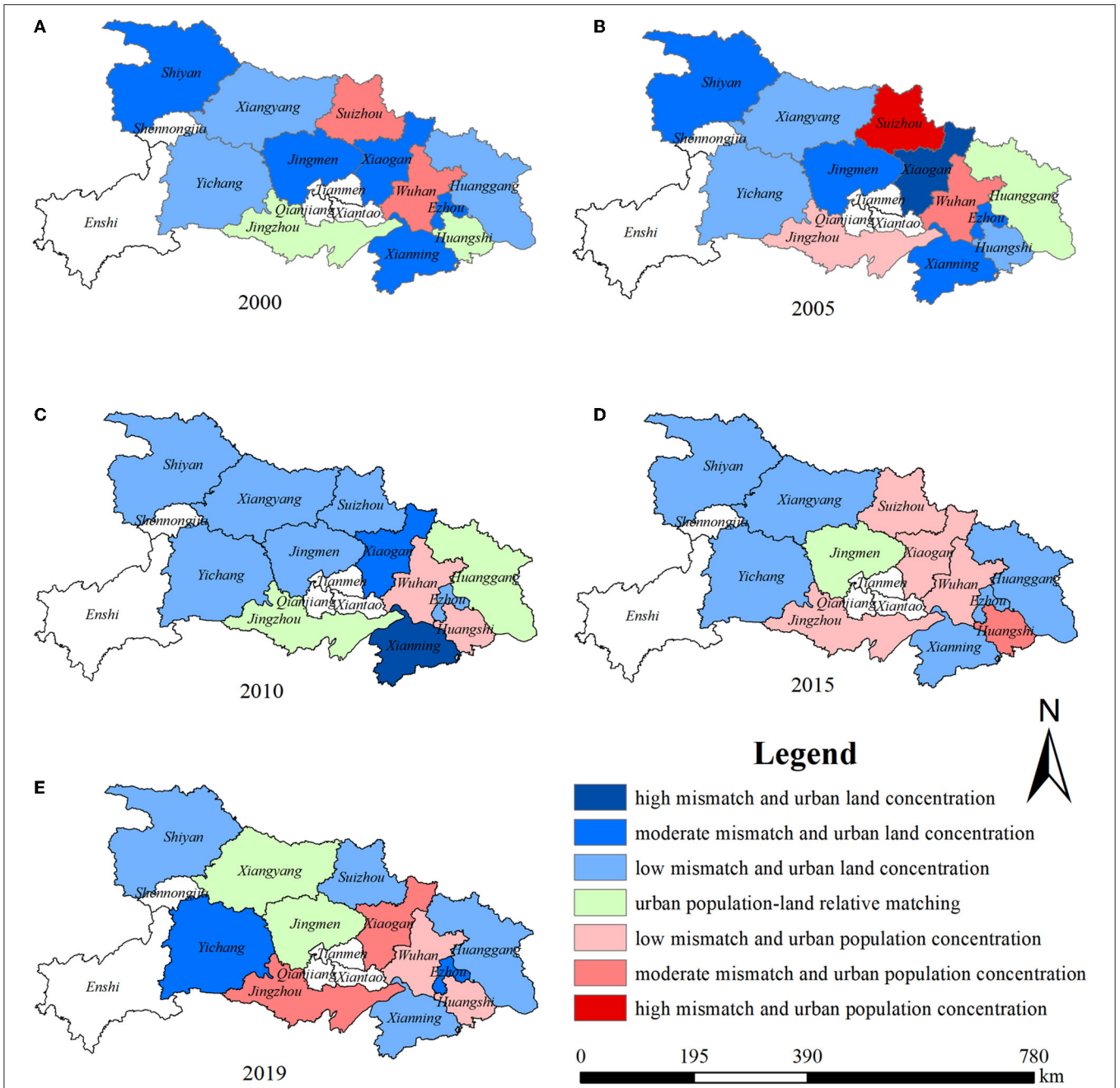

FIGURE 3 | (A–E) Spatial distribution of UPLSPs in Hubei Province from 2000 to 2019 (Source of base map: the open source map data service provided by the National Platform for Common GeoSpatial Information Services: https://www.tianditu.gov.cn).

At the city level, the EE values for Huangshi, Shiyan, Ezhou, Jingmen, and Jingzhou increased slightly from 2000 to 2019, and the average annual growth rates of Huangshi and Ezhou were higher, at 3.0152% and 4.8789%, respectively. The EE values of Wuhan, Yichang, Xiangyang, Xiaogan, Huanggang, Xianning, and Suizhou decreased from 2000 to 2019, and the average annual growth rates of Xiaogan, Huanggang, Suizhou, and Xianning were higher: −2.2396%, −2.3611%, −1.9344%, and −1.8018%, respectively.

Subsequently, using the natural breaks method, the EE value of Hubei Province is divided into five types: 0–0.4 is low, 0.4–0.6 is medium-low, 0.6–0.8 is medium, 0.8–1.0 is medium-high, and 1.0–2.0 is high. **Figure 4** depicts the results, and the level of EE shows a gradual upward trend. There were three cities with a high level of EE in 2000; this increased to four by 2019. No city was

TABLE 6 | EE in Hubei Province from 2000 to 2019.

Number	City	2000	2005	2010	2015	2019	Average value	Average annual growth rate (%)
1	Wuhan	1.2294	1.3761	1.0453	1.1646	1.2163	1.2063	−0.0564
2	Huangshi	0.4425	0.5912	0.4595	0.5795	0.7781	0.5702	3.0152
3	Shiyan	0.4330	0.6057	0.4596	0.4653	0.5031	0.4933	0.7929
4	Yichang	0.3877	0.4024	0.2845	0.2717	0.3185	0.3330	−1.0295
5	Xiangyang	0.3703	0.4451	0.2847	0.2536	0.3571	0.3422	−0.1909
6	Ezhou	0.4581	0.6117	0.6084	1.0097	1.1325	0.7641	4.8789
7	Jingmen	1.0397	1.1617	1.0021	0.6944	1.1066	1.0009	0.3287
8	Xiaogan	0.4718	0.5897	0.3402	0.2285	0.3068	0.3874	−2.2396
9	Jingzhou	0.4216	0.5983	0.4032	0.4201	0.5149	0.4716	1.0577
10	Huanggang	0.3905	0.5382	0.1905	0.2056	0.2480	0.3146	−2.3611
11	Xianning	0.3954	0.5413	0.2466	0.2597	0.2799	0.3446	−1.8018
12	Suizhou	1.7104	1.4495	1.4708	1.2866	1.1801	1.4195	−1.9344
	Hubei	0.6459	0.7426	0.5663	0.5699	0.6618	0.6373	0.1281

included in the medium-high group in 2000, but this increased to one in 2019. Five cities were at the medium-low level of EE, which reduced to two by 2019. A the low level of EE, there were four cities in 2000 and five by 2019. In addition, there are obvious regional differences in EE across Hubei Province, with high levels found in the center of the region and low levels around the periphery. In 2000, only Wuhan, Jingmen, and Suizhou in central Hubei Province had high level of EE. In 2019, Wuhan, Ezhou, Jingmen, and Suizhou were coded high, and the EE levels of other cities were low, with a radial distribution from the center to the surrounding areas. The main reason for this may be that the cities in the central plain have a higher level of economic development, better transportation options, and higher levels of technological innovation, which promote the improvement of EE.

Spatiotemporal Evolution of the Coupling Coordination Degree Between UPLSPs and EE in Hubei Province

The results obtained using the coupling coordination degree model are shown in **Table 7** and **Figure 5**. Based on **Table 3**, the relationship between UPLSPs and EE is classified into conflict and coordination. If the coupling coordination degree is <0.7, the relationship is considered conflictual; if it is >0.7, the relationship is considered one of coordination.

The average coupling coordination degree of UPLSPs and EE in Hubei Province from 2000 to 2019 exhibits a slow upward trend, increasing from 0.5820 in 2000 to 0.6938 in 2019. This translates to a shift from primary coordination to intermediate coordination, with an average annual growth rate of 0.9294%. In addition, there is a conflictual relationship between UPLSPs and EE in Hubei Province, and the population–land spatial matching degree is lower than the EE. Therefore, the UPLSPs of Hubei Province restricted the development of EE during this period.

At the city level, the coupling coordination degree of UPLSPs and EE shows an overall upward trend from 2000 to 2019, including in Wuhan, Huangshi, Shiyan, Yichang, Xiangyang, Ezhou, Jingzhou, Xianning, and Suizhou. The areas with a downward trend include Jingmen, Xiaogan, and Huanggang. From 2000 to 2019, Jingmen had the highest average value of coupling coordination (0.8343), which is considered high-quality coordination; Huanggang had the lowest average value (0.5356), which is considered primary coordination. In 2009, only Jingmen had a coordination relationship, while the other cities were classified as exhibiting conflict, and the population–land spatial matching degrees were all lower than the EE values. Clearly, the UPLSPs in regions other than Jingmen constrained the development of EE. In 2019, the UPLSPs and EE of Wuhan, Huangshi, Shiyan, Ezhou, Jingmen, and Suizhou featured coordination relationships, while Yichang, Xiangyang, Xiaogan, Jingzhou, Huanggang, and Xianning exhibited conflictual relationships. The population–land spatial matching degree of Xiaogan was higher than the EE value, indicating that EE in this area restricted the development of UPLSPs. The patterns in the other cities were the opposite.

Figure 6 indicates that from 2000 to 2019, the coupling coordination degree of UPLSPs and EE in Hubei Province has improved: in 2000, there were eight cities with primary coordination, three with intermediate coordination, and one with high-quality coordination. In 2019, once city had barely harmonic coordination, three had primary coordination, two had intermediate coordination, two had good coordination, two had high-quality coordination, and two had extreme coordination. The spatial distribution of the coupling coordination degree of UPLSPs and EE is similar to that of EE; that is, higher values are found in the middle, with lower values found around the periphery. In 2000, Jingmen, in the central region of Hubei Province, had the highest coupling coordination degree, which involved high-quality coordination. By 2019, Suizhou and Ezhou featured extreme coordination, and Wuhan and Jingmen were coded as high-quality coordination. The main reason for this may be that the spatial distributions of population and land in these areas are relatively balanced, and the level of EE is high. UPLSPs and

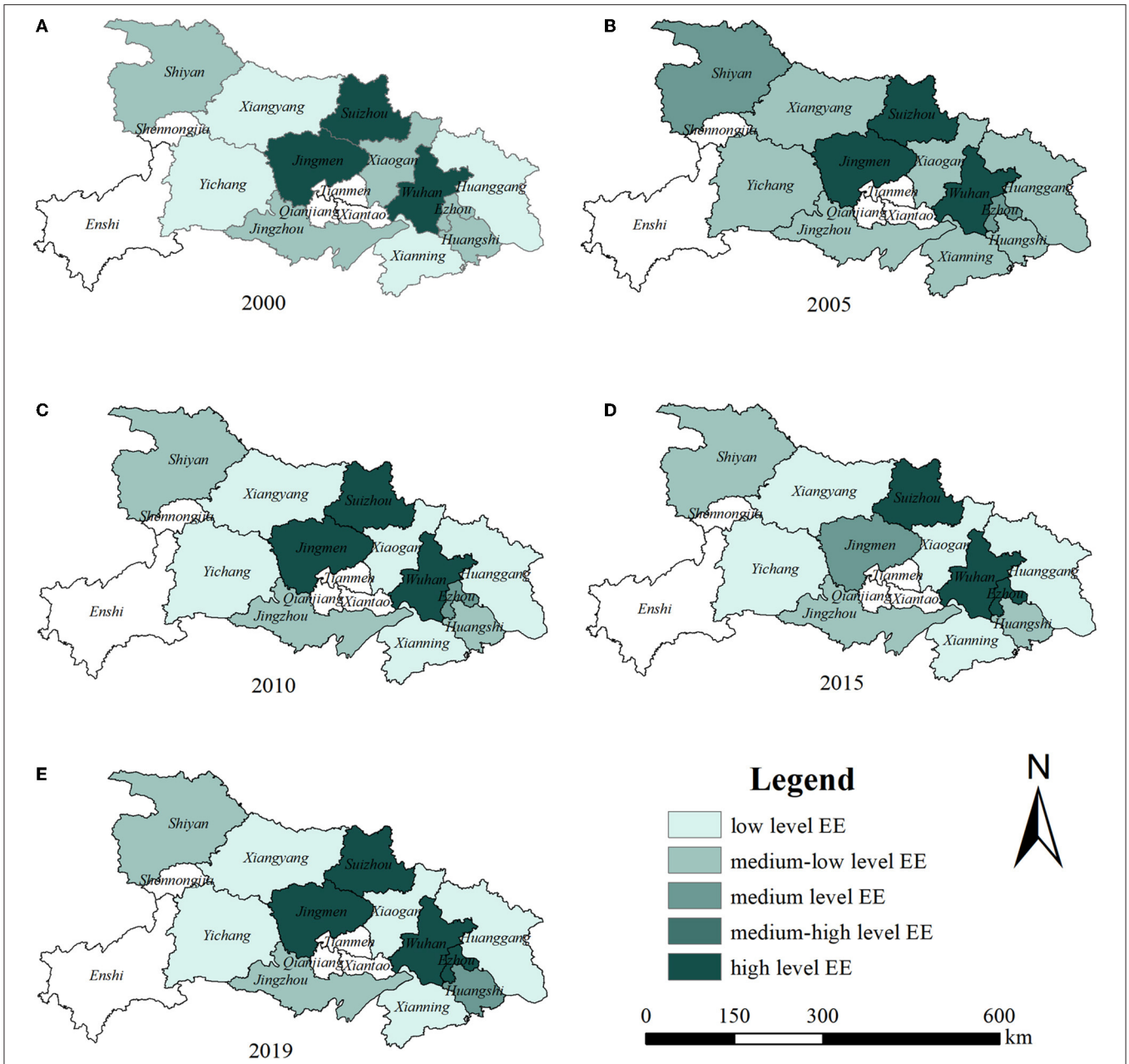

FIGURE 4 | (A–E) Spatial distribution of EE in Hubei Province from 2000 to 2019 (Source of base map: the open source map data service provided by the National Platform for Common GeoSpatial Information Services: https://www.tianditu.gov.cn).

EE promote and influence each other, showing a high state of coupling.

Using Geoda software, the spatial autocorrelation analysis of the coupling coordination degree of UPLSPs and EE in Hubei Province is carried out using the geographical distance spatial weight matrix. The results are shown in **Table 8**. The global Moran's I index of the coupling coordination degree of each city was negative from 2000 to 2019. Except for 2015, the results are statistically significant at the 5% level, showing a significant negative spatial correlation. That is, the spatial distribution illustrates that cities with high coupling coordination are surrounded by cities with low coupling coordination, while cities with low coupling coordination are surrounded by those with high coupling coordination. Specifically, the global Moran's I index shows a trend of first decreasing, then increasing, and again decreasing, from −0.361 in 2000 to −0.438 in 2019. This reflects the gradual growth of spatial dispersion of coupling coordination degree across cities, as well as the gradual expansion of the difference in this degree.

TABLE 7 | The coupling coordination degree between UPLSPs and EE in Hubei Province from 2000-2019.

Number	City	2000	2005	2010	2015	2019	Average value	Average annual growth rate (%)
1	Wuhan	0.5208	0.7382	0.5145	0.8374	0.8300	0.6882	2.4836
2	Huangshi	0.5359	0.6691	0.4964	0.4503	0.7225	0.5748	1.5847
3	Shiyan	0.6007	0.6991	0.6469	0.7167	0.7406	0.6808	1.1078
4	Yichang	0.5173	0.5244	0.5609	0.6275	0.6378	0.5736	1.1081
5	Xiangyang	0.5123	0.5583	0.5448	0.5826	0.6100	0.5616	0.9224
6	Ezhou	0.6249	0.7071	0.7056	0.8959	0.9757	0.7818	2.3725
7	Jingmen	0.8610	0.8968	0.8058	0.7753	0.8325	0.8343	−0.1771
8	Xiaogan	0.6329	0.7147	0.6349	0.4446	0.3527	0.5560	−3.0311
9	Jinzhou	0.5185	0.5817	0.5112	0.6175	0.5527	0.5563	0.3362
10	Huanggang	0.5364	0.6089	0.4533	0.5593	0.5202	0.5356	−0.1612
11	Xianning	0.5610	0.6701	0.6111	0.6144	0.5873	0.6088	0.2412
12	Suizhou	0.5623	0.5623	0.8979	0.8386	0.9643	0.7651	2.8793
	Hubei Province	0.5820	0.6609	0.6153	0.6633	0.6938	0.6431	0.9294

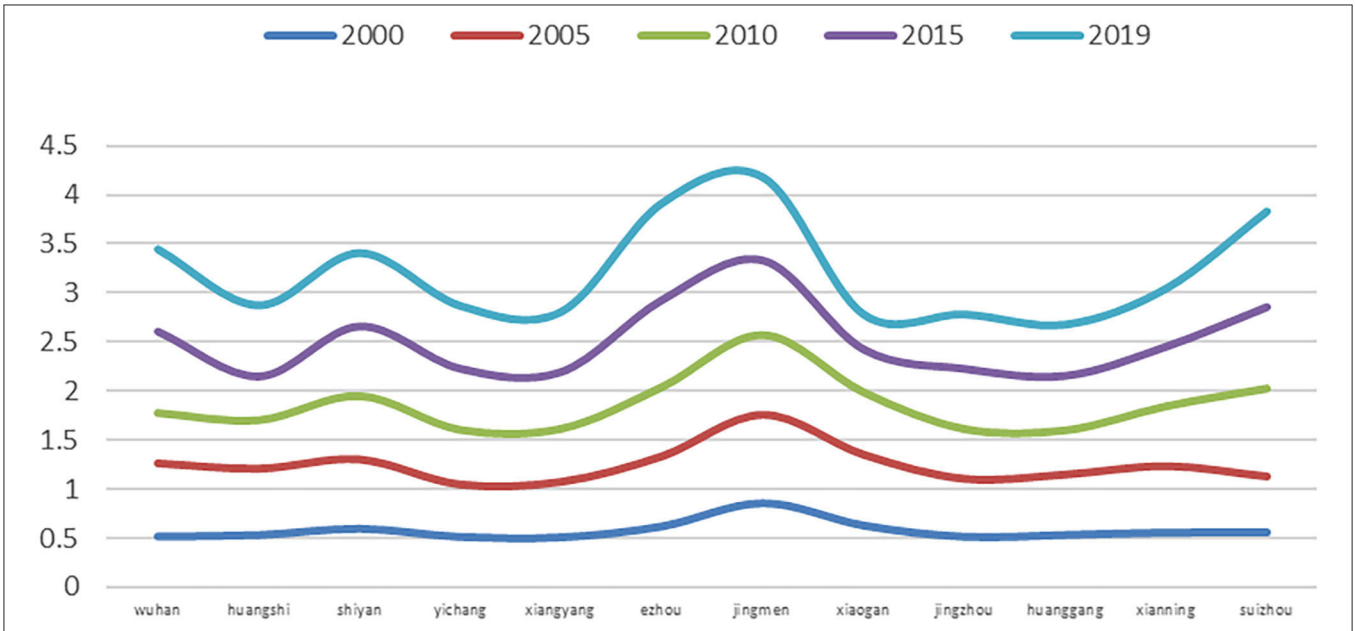

FIGURE 5 | The coupling coordination degree between UPLSPs and EE in Hubei Province.

The global Moran's I index only reveals the overall agglomeration type of the study area, and it is necessary to further identify the local spatial correlations and the spatial pattern distribution of the coupling coordination degree using a Moran scatterplot. The Moran scatterplot classifies the coupling coordination degree of UPLSPs and EE into four types, which fall in different quadrants. Quadrant I is the high–high agglomeration (H-H), indicating that the level of coupling coordination between the region and its surrounding areas is relatively high, and the degree of spatial difference between the two is small. Quadrant II is the low–high agglomeration (L-H), indicating that the region has a low level of coupling coordination, the surrounding areas are higher, and the degree of spatial difference between the two is relatively large. Quadrant III represents the low–low agglomeration (L-L), indicating that the level of coupling coordination between the region and the surrounding areas is low, and the spatial difference between the two is relatively small. Finally, Quadrant IV is the high–low agglomeration (H-L), indicating that the level of coupling coordination in the region is relatively high, while the surrounding areas are relatively low, and the degree of spatial difference between the two is relatively large.

According to **Figure 7** and **Table 9**, most cities in Hubei Province fell into Quadrants II and IV in 2000 and 2019. This suggests a significant negative spatial correlation between the coupling coordination degree of UPLSPs and EE, which has the characteristics of a discrete distribution; that is, the cites with high coupling coordination are adjacent to those with low

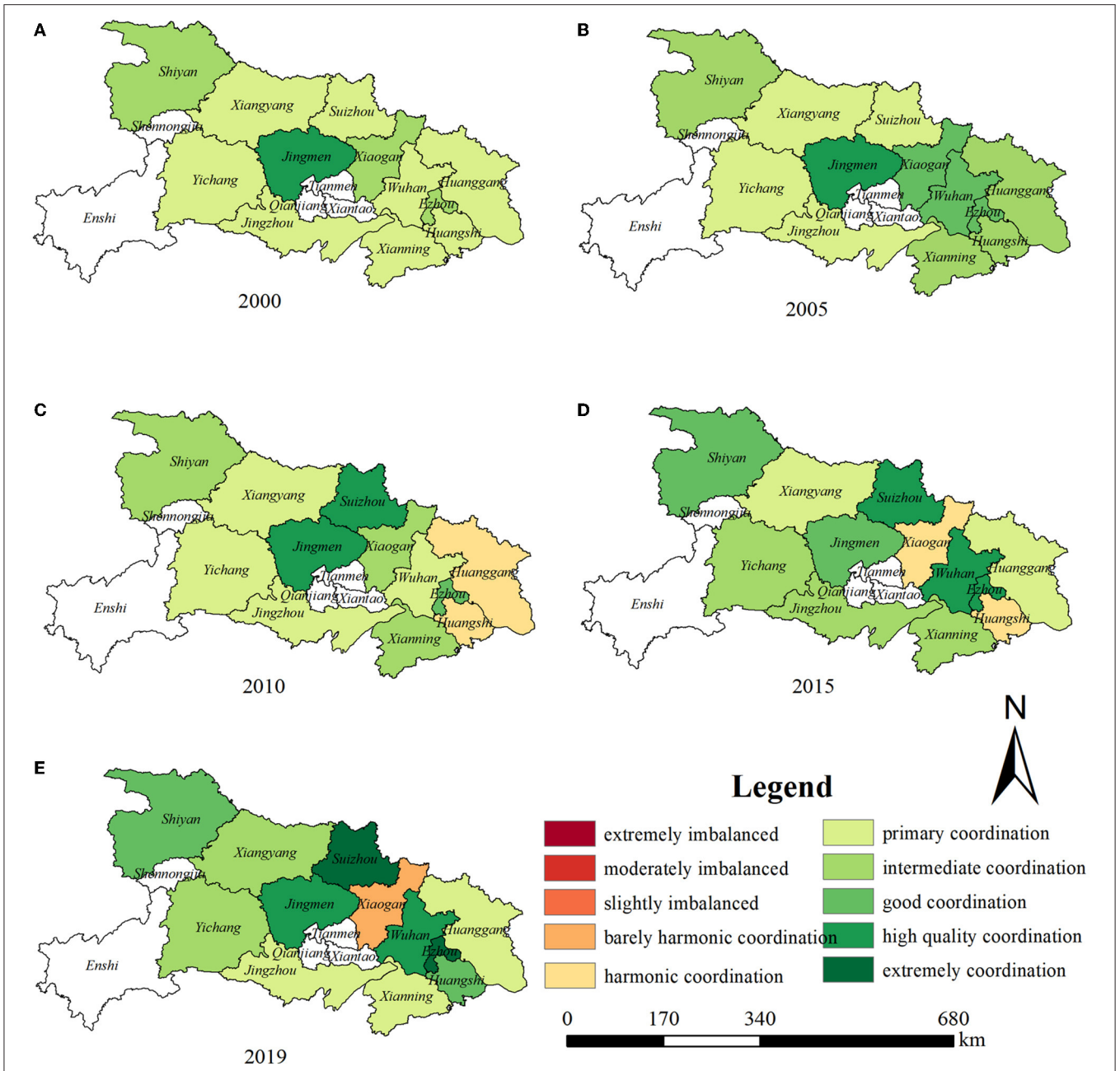

FIGURE 6 | (A–E) Spatial distribution of the coupling coordination degree between UPLSPs and EE (Source of base map: the open source map data service provided by the National Platform for Common GeoSpatial Information Services: https://www.tianditu.gov.cn).

coupling coordination. Cities in Quadrant II are L-H, indicating that the natural resource endowments of each city have strong heterogeneity and the gap in economic development is large, so the spatial connection is weak. Cities in Quadrant IV are H-L, indicating that these areas do not have a strong driving effect on the surrounding cities, and they even absorb the advantageous resources around them to vigorously develop themselves.

Based on the gray relational model, this study calculates the driving factors of the coupling coordination degree between UPLSPs and EE in Hubei Province, as shown in **Table 10**. The relational degree between the coupling coordination degree and the indicators of UPLSPs and EE is basically above 0.5, which indicates the close relationship between them. According to **Table 10**, the driving factors of coupling coordination in Hubei Province are ranked from strong to weak: total water resources > built-up area > industrial wastewater discharge > number of employees at the end of the period > GDP > industrial SO_2 emissions > annual electricity

TABLE 8 | Moran's I index of the coupling coordination degree between UPLSPs and EE from 2000-2019.

	2000	2005	2010	2015	2019
Moran's I	−0.361	−0.462	−0.048	−0.425	−0.438
Z value	−1.9800	−2.0155	0.2677	−1.6054	−1.6991
P value	0.027**	0.014**	0.354	0.034**	0.033**

****p<0.01, **p<0.05, *p<0.1. The statistical inferences on the table are based on 999 random permutations proposed by Ansen Lin.*

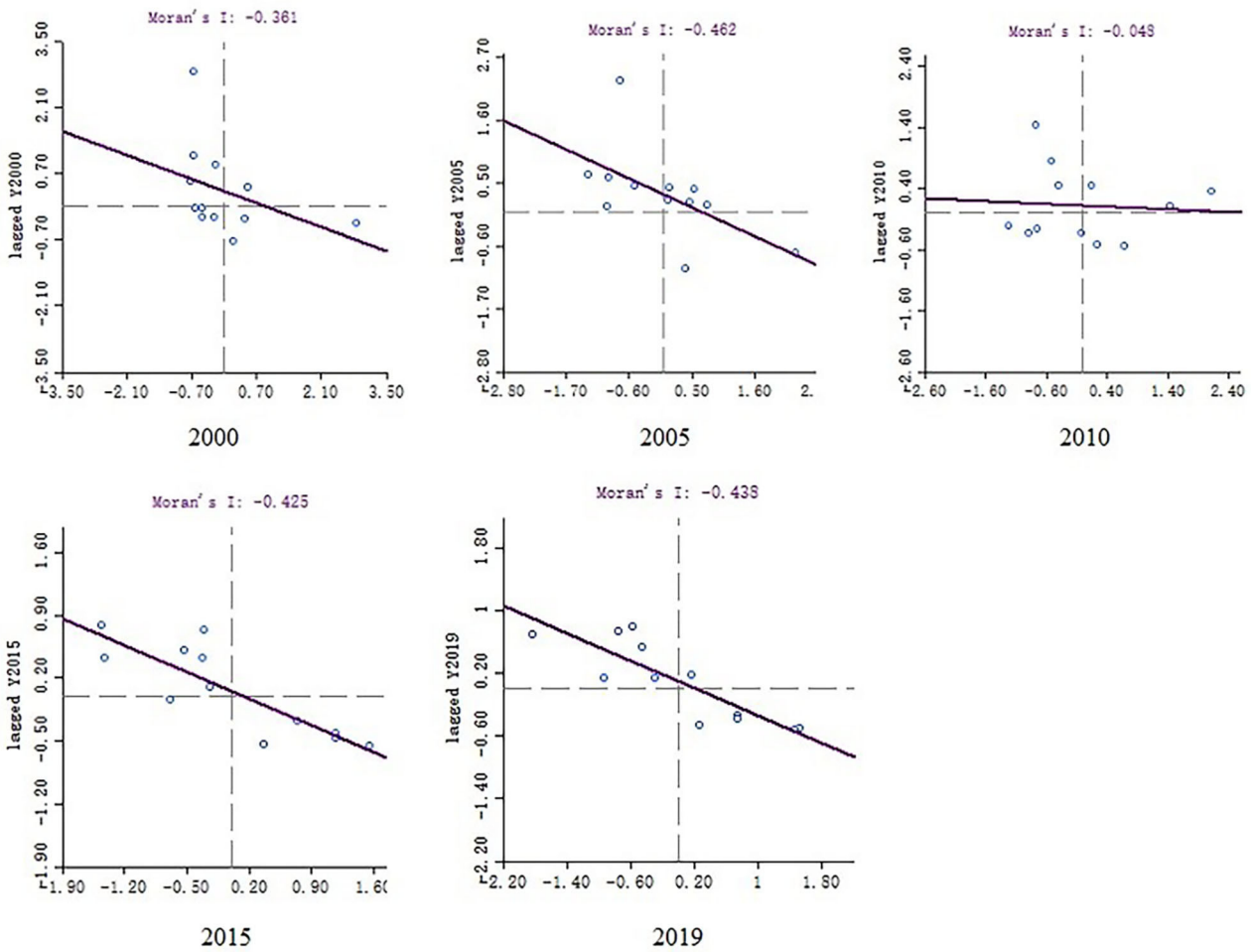

FIGURE 7 | Moran scatterplot of the coupling coordination degree between UPLSPs and EE in Hubei Province from 2000-2019.

consumption > industrial smoke (powder) dust emissions > UPLSPs > total investment in fixed assets in the whole country. This shows that the key factor restricting the coupling coordination of UPLSPs and EE in Hubei Province is the total water resources.

At the city level, Wuhan, Ezhou, and Suizhou have the highest correlations between the coupling coordination degree and the number of employees at the end of the period, which are 0.8873, 0.9425, and 0.9294, respectively. Huangshi and Jingmen have the highest correlations between the coupling coordination degree with the built-up area: 0.8940 and 0.8649, respectively. Shiyan, Yichang, Jingzhou, Huanggang, and Xianning have the highest correlations between the coupling coordination degree with the total water resource: 0.9175, 0.8136, 0.9035, 0.9035, and 0.8767, respectively. Xiangyang has the highest correlation between the coupling coordination degree and the UPLSPs, equal to 0.8334. Finally, Xiaogan has the highest correlation between the coupling coordination degree and industrial smoke (powder) dust emissions, which is 0.8975.

In view of the factors restricting the coordinated development of UPLSPs and EE in Hubei Province, Wuhan, Ezhou, and

TABLE 9 | Agglomeration pattern of the coupling coordination degree between UPLSPs and EE in Hubei Province.

	H-H agglomeration	L-H agglomeration	L-L agglomeration	H-L agglomeration
2000	Xiaogan	Jingzhou Yichang Xiangyang Suizhou	Wuhan Huanggang Xianning Huangshi	Jingmen Ezhou Shiyan
2005	Xianning Huangshi Xiaogan Ezhou Wuhan	Jingzhou Yichang Suizhou Xiangyang Huanggang	None	Shiyan Jingmen
2010	Suizhou Jingmen Xiaogan	Yichang Xiangyang Jingzhou	Huanggang Huangshi Wuhan Xianning	Shiyan Suizhou
2015	None	Yichang Xianning Xiangyang Jingzhou Xiaogan Huangshi	Huanggang	Shiyan Jingmen Suizhou Wuhan Ezhou
2019	Huangshi	Xiaogan Huanggang Jingzhou Xianning Xiangyang Yichang	None	Shiyan Jingmen Wuhan Suizhou Ezhou

Suizhou should promote the orderly flow of labor elements, deepen the reform of the household registration system, smooth the social flow channels of labor and talents, strengthen the introduction of employees, and improve the level of labor market allocation. Huangshi and Jingmen need to pay attention to make full use of the existing land resources, optimize the structure of urban land use and improve the level of the intensive use of land resources. Shiyan, Yichang, Jingzhou, Huanggang, and Xianning ought to highly value regional water resources protection, enhance residents' awareness of environmental protection, prevent water pollution, and promote the rational allocation of water resources, conservation, and management protection. Xiangyang requires leaders to focus on the spatial distribution of the urban population and land. The city is classified as urban population–land relative matching, so a mechanism should be established to assess the spatial pattern of the urban population and land. Xiaogan demands that we strengthen the protection of the ecological environment. Its EE is low, so it should optimize upgrading the industrial structure and take a green and low-carbon development path.

DISCUSSION

The results of this study showed that from 2000 to 2019 in Hubei Province, UPLSPs exhibited a medium-low mismatch and urban population concentration, and EE was at a medium-low level.

TABLE 10 | The correlation between coupling coordination degree and UPLSPs?EE in Hubei Province.

City	X	Y_1	Y_2	Y_3	Y_4	Y_5	Y_6	Y_7	Y_8	Y_9
Wuhan	0.5999	0.6324	0.8873	0.6792	0.7109	0.8652	0.6760	0.6769	0.6180	0.5947
Huangshi	0.6341	0.6762	0.8266	0.8940	0.8031	0.7435	0.7903	0.8794	0.8043	0.7915
Shiyan	0.7317	0.5213	0.6918	0.7578	0.7091	0.9175	0.6705	0.7217	0.7016	0.6244
Yichang	0.7502	0.4969	0.6328	0.6590	0.5401	0.8136	0.6123	0.6690	0.5743	0.6240
Xiangyang	0.8334	0.5212	0.6437	0.7263	0.6362	0.7775	0.6737	0.7143	0.6255	0.6882
Ezhou	0.6592	0.5252	0.9425	0.8030	0.7136	0.4945	0.6709	0.6953	0.5750	0.6372
Jingmen	0.5922	0.5103	0.6637	0.8649	0.6280	0.8601	0.6555	0.7335	0.7974	0.7323
Xiaogan	0.4328	0.6584	0.7522	0.7892	0.7418	0.8844	0.7593	0.8590	0.8123	0.8975
Jingzhou	0.6129	0.5299	0.7270	0.8723	0.6713	0.9035	0.6864	0.7889	0.6633	0.6810
Huanggang	0.6399	0.5148	0.6011	0.7399	0.5920	0.9322	0.6764	0.7642	0.6518	0.7472
Xianning	0.8470	0.5182	0.6817	0.7598	0.6430	0.8767	0.6713	0.8148	0.6602	0.7900
Suizhou	0.5074	0.6840	0.9294	0.8475	0.7942	0.9067	0.8157	0.8338	0.7409	0.7294
Hubei Province	0.6534	0.5657	0.7483	0.7827	0.6819	0.8313	0.6965	0.7626	0.6854	0.7115

X is the UPLSPs.

The coupling coordination degree between the two was slowly increasing, but it was still low, with strong heterogeneity across regions. The total water resources were the most important factor affecting the coupling coordination between the two. In addition, UPLSPs and EE in Hubei Province had a conflictual relationship, and UPLSPs restricted the development of EE.

First, the UPLSPs of Hubei Province from 2000 to 2019 is classified as urban population concentration, but most cities are considered urban land concentration. There is a phenomenon of urban land concentration transforming to urban population concentration, which is consistent with some previous research (74). This may be because, in the process of urbanization, most local governments have equated urbanization with urban construction, overemphasized the expansion of the urban built-up area, and ignored the implementation of urban population agglomerations and social security after agglomeration, resulting in problems such as the land urbanizing faster than the population. However, to promote the development of new urbanization is essentially to shift from the "land urbanization" mode, which relies on land finance, construction of industrial development zones, and industrial and real estate development in new urban areas, to "population urbanization," which is oriented to the settlement of the migrating population. Therefore, the evaluation mechanism of urban population–land spatial matching should be established to optimize the flow of elements between the two systems (7, 73). In addition, different measures can be used for different types of cities. For cities that feature an urban land concentration, such as Shiyan, Yichang, Ezhou, Huanggang, Xianning, and Suizhou, we should revitalize the stock of construction land and strictly control its incremental expansion to meet the land demands of urban development and to curb the horizontal expansion of the urban scale. For cities with an urban population concentration, such as Wuhan, Huangshi, Xiaogan, and Jingzhou, we should optimize the upgrading of industrial structure and promote the equalization of public services to meet the land demands of urban population growth and avoid the deterioration of the urban environment through growing traffic congestion caused by increasing limitations on space.

Second, the overall level of EE in Hubei Province is low but with little variation, and there are obvious regional differences, which is consistent with previous research (48). This may be because, with the continuous expansion of the economy and the continuous increase of the population in Hubei Province, the consumption demand for energy resources in the region is increasing, and the production of various pollutants is also increasing, resulting in the increase of ecological pressure and prominent environmental problems; therefore, the level of EE is low. Upgrading the industrial structure should be optimized, and green and low-carbon development needs to be pursued (26). As for cities with high EE, such as Wuhan, Jingmen, and Suizhou, we should actively play the leading role and promote the improvement of EE in surrounding cities by sharing the experiences of ecological environment governance.

Finally, UPLSPs and EE are in conflict, and the UPLSPs of urban land concentration constrains the development of EE, which is consistent with some previous findings (72). This is likely because, with the rapid urbanization of Hubei Province, many people are gathering in cities, urban population density is increasing, and the demand for resources by urban residents have damaged the environment, thus limiting the level of EE. Therefore, it is necessary to strengthen the regional coordination mechanism, clarify the resource endowment advantages and main functions of each city, and vigorously promote the free flow and optimal allocation of production factors within the region (75). Cities with high coupling coordination, such as Suizhou and Wuhan, should give play to the spatial spillover effect, and promote the synergistic development of surrounding cities; cities with low coupling coordination, such as Xiaogan and Huanggang, should transform their development models and take the needs of economic development and the ecological environment into consideration.

The main contributions of this study are several. First, it discusses the dynamic relationship between UPLSPs and EE. Second, the urban population–land spatial matching evaluation model and super-efficient SBM model are constructed to measure UPLSPs and EE, respectively. Finally, the gray relational analysis method is used to analyze the driving factors affecting the coupling coordination degree of UPLSPs and EE in Hubei Province to provide a theoretical reference for regional governments to implement differentiation strategies. However, there are some research limitations. (1) This study constructs the index system of EE based on "input + desired output + undesired output," but the index selection of the EE input–output system may also contain some other indicators that need to be further explored. This is an aspect that needs detailed research in the future. (2) This study examines the coupling coordination degree between UPLSPs and EE at the city level, and does not investigate the urban agglomeration or county levels. In future research, more in-depth studies need to be carried out along multiple scales and dimensions.

CONCLUSION

This study takes Hubei Province as the research area to explore UPLSPs, EE and their degree of coupling coordination in 12 cities from 2000 to 2019. These measures are calculated by constructing a spatial matching evaluation model, super-efficiency SBM model, and coupling coordination degree model. Then, spatial autocorrelation analysis and gray relational analysis methods are used to explore the spatiotemporal evolution characteristics and driving factors of the coupling coordination between UPLSPs and EE. The purpose of this is to guide the rational allocation of urban populations and land and the construction of ecological civilizations in Hubei Province. The results include a few important points. First, the urban population–land spatial matching degree shows a gradual upward trend from 2000 to 2019, but the overall matching level is not high; the average value of EE takes an "N"-shaped trajectory, and its overall level is low, with obvious regional differences. Second, the average value of the coupling coordination degree between UPLSPs and EE exhibits a slow upward trend, with a radial distribution such that levels are high in the middle and low along the periphery. There is a conflictual relationship between UPLSPs and EE, and the former restricts the development of the latter. Finally, there is

a strong correlation between the degree of coupling coordination and various indicators of UPLSPs and EE.

DATA AVAILABILITY STATEMENT

The raw data supporting the conclusions of this article will be made available by the authors, without undue reservation.

AUTHOR CONTRIBUTIONS

XC designed the research framework. GZ revised the whole paper. LS analyzed the data and written the main sections. LS, YJ, CL, and JZ collected the data and discussed the results. All authors read and approved the final manuscript.

FUNDING

The Fundamental Research Funds for the Central Universities, Zhongnan University of Economics and Law (CN) (NO. 2722022BY014); the Hubei Provincial Department of Education Project of Philosophy and Social Sciences (CN) (No. 21G015).

REFERENCES

1. Xia C, Li Y, Li R. Research on coordination relationship between ecological environment and urbanization in Kunming based on Coupling Model. *Int J Environ Sci Dev.* (2019) 10:216–22. doi: 10.18178/ijesd.2019.10.7.1176
2. United Nation, *Department of Economic and Social Affairs*. World Urbanization Prospects 2018: *Highlights*. (2019).
3. National Bureau of Statistics. *China Statistical Yearbook*. China Statistics Press: Beijing, China. (2020).
4. Liang L, Wang Z, Li J. The effect of urbanization on environmental pollution in rapidly developing urban agglomerations. *J Clean Prod.* (2019) 237:117649. doi: 10.1016/j.jclepro.2019.117649
5. Dadi D, Azadi H, Senbeta F, Abebe K, Taheri F, Stellmacher T. Urban sprawl and its impacts on land use change in Central Ethiopia. *Urban Forestry and Urban Greening.* (2016) 16:132–41. doi: 10.1016/j.ufug.2016.02.005
6. Lin Y, Zhong P, Chen T. Association between socioeconomic factors and the COVID-19 outbreak in the 39 well-developed cities of China. *Front Public Health.* (2020) 8:546637. doi: 10.3389/fpubh.2020.546637
7. Cui X, Liu C, Shan L, Lin J, Zhang J, Jiang Y, et al. Spatial-temporal responses of ecosystem services to land use transformation driven by rapid urbanization: a case study of Hubei Province, China. *Int J Environ Res Public Health.* (2021) 19:178. doi: 10.3390/ijerph19010178
8. Jiang T, Deng Z, Zhi Y, Cheng H, Gao Q. The effect of urbanization on population health: evidence from China. *Front Public Health.* (2021) 9:706982. doi: 10.3389/fpubh.2021.706982
9. Kassouri Y. Monitoring the spatial spillover effects of urbanization on water, built-up land and ecological footprints in sub-Saharan Africa. *J Environ Manage.* (2021) 300:113690. doi: 10.1016/j.jenvman.2021.113690
10. Li F, Liu J, Chen Z, Huang J, Liu C, Qu Z. Navigating to urban environmental health: Professionalized and personalized healthy living assistant based on intelligent health risk management. *Urban Clim.* (2021) 40:101020. doi: 10.1016/j.uclim.2021.101020
11. Yu D, Li X, Yu J, Shi X, Liu P, Tian P. Whether urbanization has intensified the spread of infectious diseases—Renewed question by the COVID-19 pandemic. *Front Public Health.* (2021) 9:699710. doi: 10.3389/fpubh.2021.699710
12. Ding T, Chen J, Fang Z, Chen J. Assessment of coordinative relationship between comprehensive ecosystem service and urbanization: a case study of Yangtze River Delta urban Agglomerations, China. *Ecol Indic.* (2021) 133:108454. doi: 10.1016/j.ecolind.2021.108454
13. Han Y, Zhang F, Huang L, Peng K, Wang X. Does industrial upgrading promote eco-efficiency? –a panel space estimation based on Chinese evidence. *Energy Policy.* (2021) 154:112286. doi: 10.1016/j.enpol.2021.112286
14. Schaltegger S, Andreas S. 6kologische Rationalität: Ansatzpunkte Zur Ausgestaltung von Ökologieorientierten Managementinstrumenten. *Die Unternehmung.* (1990) 4:273–90. Available online at: http://www.jstor.org/stable/24180467
15. Bao H, Shan L, Wang Y, Jiang Y, Lee C, Cui X. How does local real estate investment influence neighborhood $PM_{2.5}$ concentrations? A spatial econometric analysis. *Land.* (2021) 10:518. doi: 10.3390/land10050518
16. Cui X. Population urbanization and land urbanization in Ethnic Minority areas: Disequilibrium and spatial heterogeneity. *China Popul Resour Environ.* (2014) 24:63–72.
17. Ma L, Cheng W, Qi J. Coordinated evaluation and development model of oasis urbanization from the perspective of new urbanization: a case study in Shandan County of Hexi Corridor, China. *Sustain Cities Soc.* (2018) 39:78–92. doi: 10.1016/j.scs.2018.02.007
18. Lv T, Wang L, Zhang X, Xie H, Lu H, Li H, et al. Coupling coordinated development and exploring its influencing factors in Nanchang, China: from the perspectives of land urbanization and population urbanization. *Land.* (2019) 8:178. doi: 10.3390/land8120178
19. Han H, Li H. Coupling coordination evaluation between population and land urbanization in Ha-Chang urban agglomeration. *Sustainability.* (2020) 12:357. doi: 10.3390/su12010357
20. Shan L, Jiang Y, Liu C, Wang Y, Zhang G, Cui X, et al. Exploring the multi-dimensional coordination relationship between population urbanization and land urbanization based on the MDCE model: a case study of the Yangtze River Economic Belt, China. *PLoS ONE.* (2021) 16:e0253898. doi: 10.1371/journal.pone.0253898
21. Qu Y, Zhan L, Jiang G, Ma W, Dong X. How to address "population decline and land expansion (PDLE)" of rural residential areas in the process of urbanization: A comparative regional analysis of human-land interaction in Shandong Province. *Habitat Int.* (2021) 117:102441. doi: 10.1016/j.habitatint.2021.102441
22. Shi L, Wang Y. Evolution characteristics and driving factors of negative decoupled rural residential land and resident population in the Yellow River Basin. *Land Use Policy.* (2021) 109:105685. doi: 10.1016/j.landusepol.2021.105685
23. Ji L, Zhang W. Fiscal incentives and sustainable urbanization: evidence from China. *Sustainability.* (2019) 12:103. doi: 10.3390/su12010103
24. Ji Y, Guo X, Zhong S, Wu L. Land financialization, uncoordinated development of population urbanization and land urbanization, and economic growth: Evidence from China. *Land.* (2020) 9:481. doi: 10.3390/land9120481
25. Xia B, Dong S, Li Y, Li Z, Sun D, Zhang W, et al. Evolution characters and influencing factors of regional eco-efficiency in a developing country: Evidence from Mongolia. *Int J Environ Res Public Health.* (2021) 18:10719. doi: 10.3390/ijerph182010719
26. He J, Hu S. Ecological efficiency and its determining factors in an urban agglomeration in China: the Chengdu-Chongqing urban agglomeration. *Urban Clim.* (2022) 41:101071. doi: 10.1016/j.uclim.2021.101071
27. Yasmeen H, Tan Q, Zameer H, Tan J, Nawaz K. Exploring the impact of technological innovation, environmental regulations and urbanization on ecological efficiency of China in the context of COP21. *J Environ Manage.* (2020) 274:111210. doi: 10.1016/j.jenvman.2020.111210
28. Chen X, Zhou H. (2019). Dynamic coordinated relationships and interactive effects between urban smart development and ecological efficiency: a case study of 276 cities at prefecture level and above in China. *Geogr Res.* (2019) 38:2653–2665. (in Chinese). doi: 10.11821/dlyj020180674

29. Picazo-Tadeo AJ, Gómez-Limón JA, Reig-Martínez E. Assessing farming eco-efficiency: a data envelopment analysis approach. *J Environ Manage.* (2011) 92:1154–64. doi: 10.1016/j.jenvman.2010.11.025
30. Amowine N, Li H, Boamah KB, Zhou Z. Towards ecological sustainability: assessing dynamic total-factor ecology efficiency in Africa. *Int J Environ Res Public Health.* (2021) 18:9323. doi: 10.3390/ijerph18179323
31. Moutinho V, Madaleno M. A two-stage DEA model to evaluate the technical eco-efficiency indicator in the EU Countries. *Int J Environ Res Public Health.* (2021) 18:3038. doi: 10.3390/ijerph18063038
32. Du Y, Jiang J, Li C. Ecological efficiency evaluation of marine ranching based on the Super-SBM model: a case study of Shandong. *Ecol Indic.* (2021) 131:108174. doi: 10.1016/j.ecolind.2021.108174
33. Qin M, Sun M, Li J. Impact of environmental regulation policy on ecological efficiency in four major urban agglomerations in eastern China. *Ecol Indic.* (2021) 130:108002. doi: 10.1016/j.ecolind.2021.108002
34. Yang Y, Deng X. The spatio-temporal evolutionary characteristics and regional differences in affecting factors analysis of China's urban eco-efficiency. *Sci Geogr Sin.* (2019) 39:1111–8. (in Chinese). doi: 10.13249/j.cnki.sgs.2019.07.009
35. Gu R, Zhu Y. Spatial-temporal characteristics and influencing factors of ecological efficiency in Jiangsu Province: Testing of stochastic frontier production function and spatial econometrics. *Areal Res Dev*. (2020) 39:166–170+176. (in Chinese)
36. Ma X, Wang C, Yu Y, Li Y, Dong B, Zhang X, et al. Ecological efficiency in China and its influencing factors—a super-efficient SBM metafrontier-Malmquist-Tobit model study. *Environ Sci Pollut Res.* (2018) 25:20880–98. doi: 10.1007/s11356-018-1949-7
37. Li Y, Zhang J, Yang X, Wang W, Wu H, Ran Q, et al. The impact of innovative city construction on ecological efficiency: a quasi-natural experiment from China. *Sustain Prod Consumpt.* (2021) 28:1724–35. doi: 10.1016/j.spc.2021.09.012
38. Yang L, Yang Y. Evaluation of eco-efficiency in China from 1978 to 2016: based on a modified ecological footprint model. *Sci Total Environ.* (2019) 662:581–90. doi: 10.1016/j.scitotenv.2019.01.225
39. Ke H, Dai S, Yu H. Spatial effect of innovation efficiency on ecological footprint: city-level empirical evidence from China. *Environ Technol Innov.* (2021) 22:101536. doi: 10.1016/j.eti.2021.101536
40. Shen Y, Sun S, Yue S, Sun X. Ecological development efficiency index of tropics and subtropics in China. *Environ Sci Pollut Res.* (2020) 27:14160–74. doi: 10.1007/s11356-020-07844-y
41. Fan Z, Deng C, Fan Y, Zhang P, Lu H. Spatial-temporal pattern and evolution trend of the cultivated land use eco-efficiency in the National Pilot Zone for ecological conservation in China. *Int J Environ Res Public Health.* (2021) 19:111. doi: 10.3390/ijerph19010111
42. Luo Y, Lu Z, Muhammad S, Yang H. The heterogeneous effects of different technological innovations on eco-efficiency: evidence from 30 China's provinces. *Ecol Indic.* (2021) 127:107802. doi: 10.1016/j.ecolind.2021.107802
43. Tan J, Wang R. Research on evaluation and influencing factors of regional ecological efficiency from the perspective of carbon neutrality. *J Environ Manage.* (2021) 294:113030. doi: 10.1016/j.jenvman.2021.113030
44. Yao J, Xu P, Huang Z. Impact of urbanization on ecological efficiency in China: an empirical analysis based on provincial panel data. *Ecol Indic.* (2021) 129:107827. doi: 10.1016/j.ecolind.2021.107827
45. Liu W, Zhan J, Zhao F, Wei X, Zhang F. Exploring the coupling relationship between urbanization and energy eco-efficiency: a case study of 281 prefecture-level cities in China. *Sustain Cities Soc.* (2021) 64:102563. doi: 10.1016/j.scs.2020.102563
46. Ren F, Yu X. Coupling analysis of urbanization and ecological total factor energy efficiency —— a case study from Hebei province in China. *Sustain Cities Soc.* (2021) 74:103183. doi: 10.1016/j.scs.2021.103183
47. Zhou Y, Kong Y, Wang H, Luo F. The impact of population urbanization lag on eco-efficiency: A panel quantile approach. *J Clean Prod.* (2020) 244:118664. doi: 10.1016/j.jclepro.2019.118664
48. Chen M, Liu W, Wang S, Liu Y. Spatial-temporal differentiation of urban eco-efficiency in the Yangtze River Economic Belt and its driving factors. *China Popul Resour Environ*. (2020) 30:121–7. (in Chinese). doi: 10.12062/cpre.20200433
49. Tian P, Wang H, Li J, Cao L, Hu Q. Eco-efficiency evaluation and influencing factors analysis of county-level cities in the East China Sea coastal zone. *Geographical Research*. (2021) 40:2347–66. (in Chinese). doi: 10.11821/dlyj020200810
50. Zhang J, Wu G, Zhang J. The estimation of China's provincial capital stock:1952-2000. *Econ Res J*. (2004) 10:35–44. (in Chinese).
51. Sun Y, Zhao T, Xia L. Spatial-temporal differentiation of carbon efficiency and coupling coordination degree of Chinese county territory and obstacles analysis. *Sustain Cities Soc.* (2022) 76:103429. doi: 10.1016/j.scs.2021.103429
52. Cai Z, Li W, Cao S. Driving factors for coordinating urbanization with conservation of the ecological environment in China. *Ambio*. (2021) 50:1269–80. doi: 10.1007/s13280-020-01458-x
53. Yin Z, Zhu T. A study of the spatial matching relationship between China's provincial supporting resources for elderly and aged population. *J Jiangxi Univ Finance Econ.* (2019) 4:82–90. (in Chinese). doi: 10.13676/j.cnki.cn36-1224/f.2019.04.008
54. Tone K. A slacks-based measure of efficiency in data envelopment analysis. *Eur J Oper Res.* (2001) 130:498–509. doi: 10.1016/S0377-2217(99)00407-5
55. Tone K. *Dealing With Undesirable Outputs in DEA: A Slacks-Based Measure (SBM) Approach*. North American Productivity Workshop (2004). pp. 44−5.
56. Tone K. A slacks-based measure of super-efficiency in data envelopment analysis. *Eur J Oper Res.* (2002) 143:32–41. doi: 10.1016/S0377-2217(01)00324-1
57. Li C, Gao X, He B, Wu J, Wu K. Coupling coordination relationships between urban-industrial land use efficiency and accessibility of highway networks: evidence from Beijing-Tianjin-Hebei urban agglomeration, China. *Sustainability.* (2019) 11:1446. doi: 10.3390/su11051446
58. Yang C, Zeng W, Yang X. Coupling coordination evaluation and sustainable development pattern of geo-ecological environment and urbanization in Chongqing municipality, China. *Sustain Cities Soc.* (2020) 61:102271. doi: 10.1016/j.scs.2020.102271
59. Ariken M, Zhang F, Chan NW, Kung HE. Coupling coordination analysis and spatio-temporal heterogeneity between urbanization and eco-environment along the Silk Road Economic Belt in China. *Ecol Indic.* (2021) 121:107014. doi: 10.1016/j.ecolind.2020.107014
60. Li W, Wang Y, Xie S, Cheng X. Coupling coordination analysis and spatiotemporal heterogeneity between urbanization and ecosystem health in Chongqing municipality, China. *Sci Total Enviro.* (2021) 791:148311. doi: 10.1016/j.scitotenv.2021.148311
61. Cai B, Shao Z, Fang S, Huang X, Huq ME, Tang Y, et al. Finer-scale spatiotemporal coupling coordination model between socioeconomic activity and eco-environment: a case study of Beijing, China. *Ecol Indic.* (2021) 131:108165. doi: 10.1016/j.ecolind.2021.108165
62. Wang R, Tan J. Exploring the coupling and forecasting of financial development, technological innovation, and economic growth. *Technol Forecast Soc Change.* (2021) 163:120466. doi: 10.1016/j.techfore.2020.120466
63. Cai J, Li X, Liu L, Chen Y, Wang X, Lu S. Coupling and coordinated development of new urbanization and agro-ecological environment in China. *Sci Total Enviro.* (2021) 776:145837. doi: 10.1016/j.scitotenv.2021.145837
64. Zhang D, Chen Y. Evaluation on urban environmental sustainability and coupling coordination among its dimensions: a case study of Shandong Province China. *Sustain Cities Soc.* (2021) 75:103351. doi: 10.1016/j.scs.2021.103351
65. Hu X, Ma C, Huang P, Guo X. Ecological vulnerability assessment based on AHP-PSR method and analysis of its single parameter sensitivity and spatial autocorrelation for ecological protection – a case of Weifang City, China. *Ecol Indic.* (2021) 125:107464. doi: 10.1016/j.ecolind.2021.107464
66. Jin G, Deng X, Zhao X, Guo B, Yang J. Spatio-temporal patterns of urban land use efficiency in the Yangtze River Economic Zone during 2005-2014. *Acta Geogr Sin*. (2018) 73:1242–52. (in Chinese). doi: 10.11821/dlxb201807005
67. Di D, Wu Z, Wang H, Zhang F. Spatial pattern analysis on the functions of water resources economic–social–ecological complex system. *J Clean Prod.* (2022) 336:130323. doi: 10.1016/j.jclepro.2021.130323
68. Ke X, Wang X, Guo H, Yang C, Zhou Q, Mougharbel A. Urban ecological security evaluation and spatial correlation research—–based on

data analysis of 16 cities in Hubei Province of China. *J Clean Prod.* (2021) 311:127613. doi: 10.1016/j.jclepro.2021.127613
69. Deng J. Grey control system. *J Huazhong Univ Sci Technol.* (1982) 3:9–18.
70. Tan X, Deng J. Grey relational analysis: a new method of multi-factor statistical analysis. *Stat Res.* (1995) 3:46–8.
71. Peng X, Tang X, Chen Y, Zhang J. Ranking the healthcare resource factors for public satisfaction with health system in China—based on the grey relational analysis models. *Int J Environ Res Public Health.* (2021) 18:995. doi: 10.3390/ijerph18030995
72. Qiu M, Yang Z, Zuo Q, Wu Q, Jiang L, Zhang Z, et al. Evaluation on the relevance of regional urbanization and ecological security in the nine provinces along the Yellow River, China. *Ecol Indic.* (2021) 132:108346. doi: 10.1016/j.ecolind.2021.108346
73. Liang S, Lv X, Zhang Y. Temporal and spatial characteristics of the coupling evolution of population structure and industrial structure upgrading: Grey correlation analysis based on time series and provincial panel data. *Reform Econ Syst*. (2019) 2:54–61. (in Chinese).
74. Li Q, Ding C, Song G. Urban sprawl and productivity: promotion or suppression? Analysis based on night light data. *J Manag Sci China.* (2021) 24:45–62. doi: 10.19920/j.cnki.jmsc.2021.03.004
75. Dong L, Shang J, Ali R, Rehman, R. The coupling coordinated relationship between new-type urbanization, eco-environment and its driving mechanism: A case of Guanzhong, China. *Front Environ Sci.* (2021) 9:638891. doi: 10.3389/fenvs.2021.638891

Conflict of Interest: The authors declare that the research was conducted in the absence of any commercial or financial relationships that could be construed as a potential conflict of interest.

Publisher's Note: All claims expressed in this article are solely those of the authors and do not necessarily represent those of their affiliated organizations, or those of the publisher, the editors and the reviewers. Any product that may be evaluated in this article, or claim that may be made by its manufacturer, is not guaranteed or endorsed by the publisher.

frontiers | Frontiers in Public Health

DATA REPORT
published: 12 July 2022
doi: 10.3389/fpubh.2022.908760

The Provincial Baseline of $PM_{2.5}$ in China and Its Hierarchical Management Strategy

Doudou Jin[1], Shaojie Kong[2], Changhong Ou[2], Anwei Chen[1] and Fei Li[2]**

[1] College of Resources and Environment, Hunan Agricultural University, Changsha, China, [2] School of Information and Safety Engineering, Zhongnan University of Economics and Law, Wuhan, China

Keywords: cumulative frequency curve method, $PM_{2.5}$ baseline, hierarchical management strategy, China, air quality

OPEN ACCESS

Edited by:
Mohiuddin Md. Taimur Khan, Washington State University Tri-Cities, United States

Reviewed by:
Shani Tiwari, Council of Scientific and Industrial Research (CSIR), India
Junyuan Guo, Chengdu University of Information Technology, China

***Correspondence:**
Anwei Chen
a.chen@hunau.edu.cn
Fei Li
lifei@zuel.edu.cn

Specialty section:
This article was submitted to Environmental health and Exposome, a section of the journal Frontiers in Public Health

Received: *31 March 2022*
Accepted: *17 June 2022*
Published: *12 July 2022*

Citation:
Jin D, Kong S, Ou C, Chen A and Li F (2022) The Provincial Baseline of $PM_{2.5}$ in China and Its Hierarchical Management Strategy. Front. Public Health 10:908760. doi: 10.3389/fpubh.2022.908760

INTRODUCTION

Atmospheric $PM_{2.5}$ pollution has become a challenge worldwide, especially in some developing countries (1–3). $PM_{2.5}$ has become the primary pollutant in most cities in China (4) and attacked more and more scholars' attention (5–8). In recent years, although the $PM_{2.5}$ pollution in some areas of China shows a slight decrease, which does not alleviate this serious problem (9). If more accurate and effective control measures are taken, the $PM_{2.5}$ concentration (population-weighted) will gradually reduce to 35 $\mu g/m^3$ (China's current air quality standard) in 2030 (10). Although the Chinese government has taken many ways to deal with $PM_{2.5}$ pollution, air quality is still not optimistic, especially in winter (4). The definitions of pollution in China are based on the air quality standard value (10 $\mu g/m^3$) formulated by the World Health Organization (WHO) or national level I concentration limit (15 $\mu g/m^3$) and national secondary concentration limit (35 $\mu g/m^3$). However, the size of the human population and their activities, and the level of economic development in each region are quite different. Therefore, using the "One-Size Fits All" policy for $PM_{2.5}$ control on a relatively large scale is obviously unscientific (11, 12).

The introduction of baseline value in $PM_{2.5}$ control can effectively overcome the shortcomings mentioned above. The baseline is the upper limit of element content in a certain area under the influence of human activities (calculated under low human activities). There are similarities and differences between baseline, background, and standard values. The background value is the statistical average of the quality parameters obtained from monitoring relatively clean areas in a region. The standard value is formulated by relevant national laws and regulations to protect and improve the living environment and ecological environment to ensure human health. However, environmental standards cannot replace the baseline due to the different geological conditions, geochemical characteristics, and human activities in different regions. In baselines investigation, the methods in geochemical baseline investigation are widely referenced. However, the geochemical background and geochemical baseline are often confused or replaced by each other in concept and application in many situations. For many people, the differences between them are ignored. Cannon, head of the Yellowstone geochemical baseline research project in the United States, once pointed out that the geochemical background represents the concentration of elements in natural substances, excluding the impact of human activities (13). On the contrary, the baseline represents the concentration of elements measured in time in some places in areas disturbed by human activities, which is usually not the actual background. A geochemical baseline is a natural change in the concentration of chemical elements in the earth's surface materials. However, this natural change does not exclude the impact of human activities. It aims to describe the current supergene environmental conditions and is a benchmark material to measure future environmental changes.

It has greater practical significance and can provide an essential basis for future environmental risk assessment. The normalization method and cumulative frequency curve method are the most commonly used methods for determining geochemical baseline (14). At first, many scientists used the normalization method to study the concentration of elements in marine and estuarine sediments. Later, it was introduced into the study of geochemical baseline, so its scope of application is limited. The cumulative frequency curve method has a long history. It can determine the baseline value of any substance. Therefore, this paper uses the cumulative frequency curve method to explore determining the Chinese baseline values of $PM_{2.5}$ on a provincial scale.

The primary aims of this work are to establish the baseline values of $PM_{2.5}$ in 31 provinces across China using the cumulative frequency curve method. Then, the provinces are classified according to the relationship between baseline values, monitoring values, and standard values. Finally, the $PM_{2.5}$ hierarchical management strategy is proposed for the three types of provinces obtained.

METHODS OF THE CUMULATIVE FREQUENCY CURVE

Bauer et al. devised the cumulative frequency curve approach to assess geochemical baselines (15, 16). The method involves plotting the distribution curve on the decimal axis with the element concentration as the X-axis and the cumulative frequency as the Y-axis. A curve usually has one or two inflection points (points where the curve has a significant deflection). Below the inflection point represents the lower limit of human activities, and the baseline value was obtained by averaging the data less than the inflection point. If the cumulative frequency curve was nearly straight without an inflection point, the average of all data was utilized as the baseline value (17). Certainly, when the cumulative frequency curve method is used in establishing the $PM_{2.5}$ baseline, some uncertainties or differences need to be explained. Firstly, according to the relevant research, the calculation of element geochemical baseline value using this method requires long time-series data. While, due to Spatio-temporal pollution characteristics of $PM_{2.5}$, the daily data for 2018 and 2019 is preliminarily selected and the effect of time series length can be further discussed. Secondly, this work selected the provincial scale, so we should later consider whether the application details of this method will change if the scale changes under different environmental control decision needs.

DATA SOURCES

$PM_{2.5}$ data are obtained from China National Environmental Monitoring Center (http://www.cnemc.cn/). Due to the unavailability of data from Hong Kong, Macao, and Taiwan, data from 31 provinces on the mainland were analyzed.

$PM_{2.5}$ DETERMINATION OF BASELINE VALUE

The first step is to draw the cumulative frequency curve. The second step is gradually calculating the fitting curve's determination coefficient between each point and the first point. Then, a chart was obtained using the ordinal number as the x-axis and the determination coefficient as the y-axis. First, the determination coefficient will fluctuate and then reach the relatively high point (higher than the data surroundings), the first inflection point of the cumulative frequency curve. Subsequently, the determination coefficient may reach the highest point and the second inflection point again. Take Beijing and Jiangsu for examples (**Figures 1C,D**). Beijing's coefficient of determination began with a series of fluctuations and then gradually rose to the highest point, the first inflection point of Beijing's cumulative frequency curve. Starting from the first inflection point, the second inflection point can be obtained in the same way. The coefficient of determination of Jiangsu also has a series of fluctuations at first and then increases to a maximum point, and then there is no increase in fluctuation. Therefore, the cumulative frequency curve of Jiangsu has only one inflection point. The cumulative frequency curves of Beijing and Jiangsu are shown in **Figures 1A,B**.

After determining the inflection point, the next step is to determine which inflection point is used as the upper limit of the baseline value. When the cumulative frequency curve has only one inflection point, the average value of all points below the inflection point shall be taken as the baseline value. When the cumulative frequency curve has two inflection points, compare the similarity between the frequency distribution between the two inflection points and the frequency distribution before and after the first inflection point. If it is close to the first inflection point, select the first inflection point as the upper limit of the calculated baseline value. Otherwise, select the second inflection point.

It can be seen from **Table 1** that the cumulative frequency curve of 93.55% of provinces (29 provinces) has two inflection points, indicating that human activities have a significant impact on $PM_{2.5}$ emission. It can be known from the provincial population data (which could be found from the data availability link), that the population of these provinces in 2018 and 2019 is also relatively large. The annual average concentrations limit of China air quality standard (GB3095-2012) and WHO phase I target (IT1) are 35 $\mu g/m^3$. Comparing the baseline value, monitoring value, and the standard value of each province one by one, it is found that the average value of 2-year monitoring value of 61.29% of provinces and the baseline value of 29.03% of provinces exceed this value. All baseline values are lower than the average value of the 2-year monitoring value. Based on this, it is very unscientific to adopt the same standard requirements for different provinces. In addition, since the baseline value is obtained under the condition of low human activities, it is tough to directly require $PM_{2.5}$ emissions to be reduced to the same standard value for some provinces where the baseline value exceeds the standard value. For example, the baseline value of Anhui Province (39.44 $\mu g/m^3$) is greater than the standard

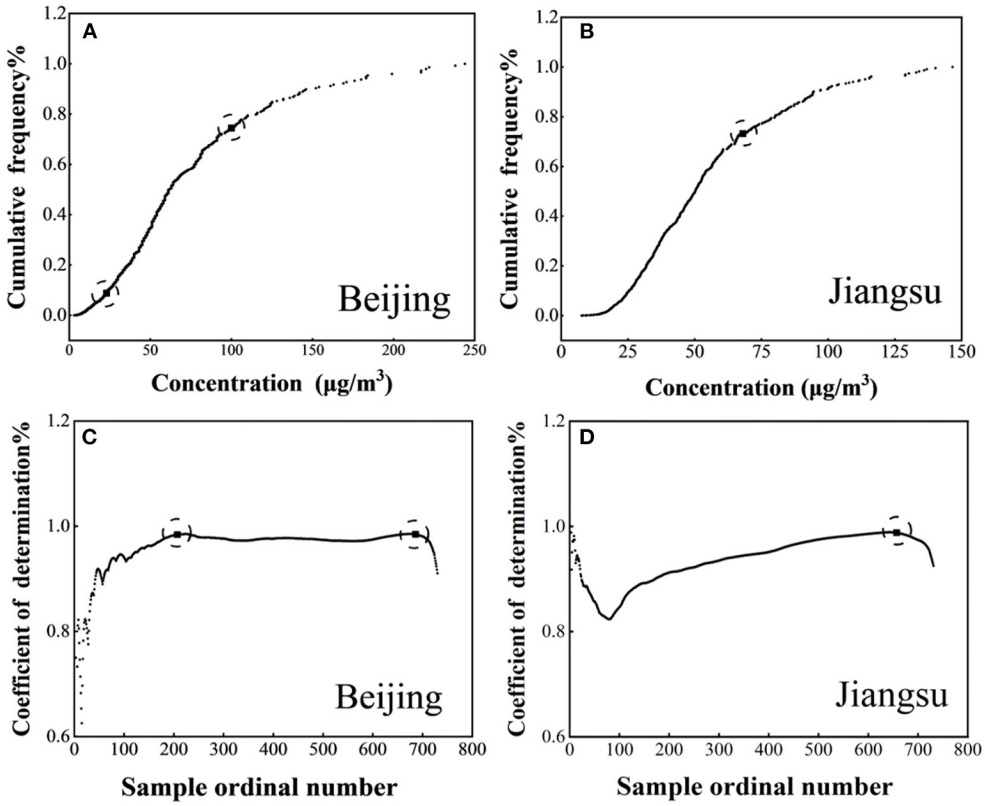

FIGURE 1 | Cumulative frequency distribution **(A,B)** and inflection point **(C,D)** of Beijing and Jiangsu.

value. Therefore, it is being challenged to directly require it to reduce $PM_{2.5}$ emissions to the standard value. Anhui Province can implement "step-by-step" measures to reduce the emission of $PM_{2.5}$ to the baseline value first and then to the standard value.

CLASSIFICATION CONTROL BASED ON THREE VALUES

According to the relationship between baseline, monitoring, and standard values, 31 provinces are divided into three categories for classified control (**Figure 2**). As shown in **Figure 2**, Guangxi, Zhejiang, Gansu, Jilin, Guangdong, Inner Mongolia, Guizhou, Qinghai, Fujian, Yunnan, Hainan, and Tibet belong to the first category. Henan, Tianjin, Hebei, Shanxi, Anhui, Beijing, Jiangsu, and Shandong belong to the second category; Shaanxi, Liaoning, Hubei, Hunan, Jiangxi, Xinjiang, Ningxia, Chongqing, Sichuan, Shanghai, and Heilongjiang belong to the third category. The first category's monitoring value and baseline value are all lower than the standard value. Among them, the baseline value of Zhejiang, Guangdong, Fujian, and Tibet is not much different from the average value of the 2 years. Therefore, while these provinces continue to maintain this state, they can further move closer to the baseline value and strive to minimize the emission of $PM_{2.5}$. The baseline value and monitoring value of the second category are all higher than the standard value. Combined with the above, it can be seen that the baseline value is calculated under low human activities. If these provinces are directly required to reduce the emission of $PM_{2.5}$ to the standard value, it is complicated and unscientific. Therefore, provinces belonging to this category can implement "step-by-step" measures, that is, reduce to the baseline value first and then reduce to the standard value. For provinces belonging to the third category, it is necessary to reduce the emission of $PM_{2.5}$ to the national standard first and then strive to promote the green and high-quality development of the economy further to reduce the emission of $PM_{2.5}$ to the baseline value.

CONCLUSION

The baseline value of $PM_{2.5}$ is determined by the cumulative frequency curve method. According to the relationship between baseline value, monitoring value, and national standard value (35 $\mu g/m^3$), the $PM_{2.5}$ hierarchical management strategy is proposed. Ninety-three percent of the provinces' $PM_{2.5}$ emissions are significantly affected by different degrees of human activities. The provinces are divided into three categories, and different compliance requirements are put forward. The monitoring

TABLE 1 | $PM_{2.5}$ in each province baseline and two-year mean ($\mu g/m^3$).

Province	Inflection point	Baseline value	Average annual value	Difference	Province	Inflection point	Baseline value	Average annual value	Difference
Guangxi	2	26.70	33.52	6.82	Anhui	2	39.48	47.64	8.16
Zhejiang	2	30.23	33.04	2.81	Beijing	2	37.38	46.12	8.74
Gansu	2	28.78	32.01	3.23	Jiangsu	1	36.41	43.48	7.07
Jilin	2	23.22	31.67	8.45	Shandong	2	36.01	45.91	9.9
Guangdong	2	27.40	28.95	1.55	Shaanxi	1	34.94	47.79	12.85
Inner Mongolia	2	23.31	27.24	3.93	Liaoning	2	34.42	39.45	5.03
Guizhou	2	23.56	26.95	3.39	Hubei	2	34.41	45.12	10.71
Qinghai	2	22.87	26.07	3.2	Hunan	2	32.92	40.65	7.73
Fujian	2	23.37	24.78	1.41	Jiangxi	2	32.17	36.12	3.95
Yunnan	2	19.22	22.67	3.45	Xinjiang	2	46.77	50.51	3.74
Hainan	2	13.07	15.86	2.79	Ningxia	2	30.94	34.65	3.71
Tibet	2	11.74	13.32	1.58	Chongqing	2	31	38.31	7.31
Henan	2	42.64	60.68	18.04	Sichuan	2	30.04	36.09	6.05
Tianjin	2	41.17	51.5	10.33	Shanghai	2	27.61	34.42	6.81
Hebei	2	40.78	52.91	12.13	Heilongjiang	2	21.68	37.97	16.29
Shanxi	2	39.77	50.64	10.87					

1-one inflection point, 2-two inflection points; the difference between the baseline value and the annual mean value.

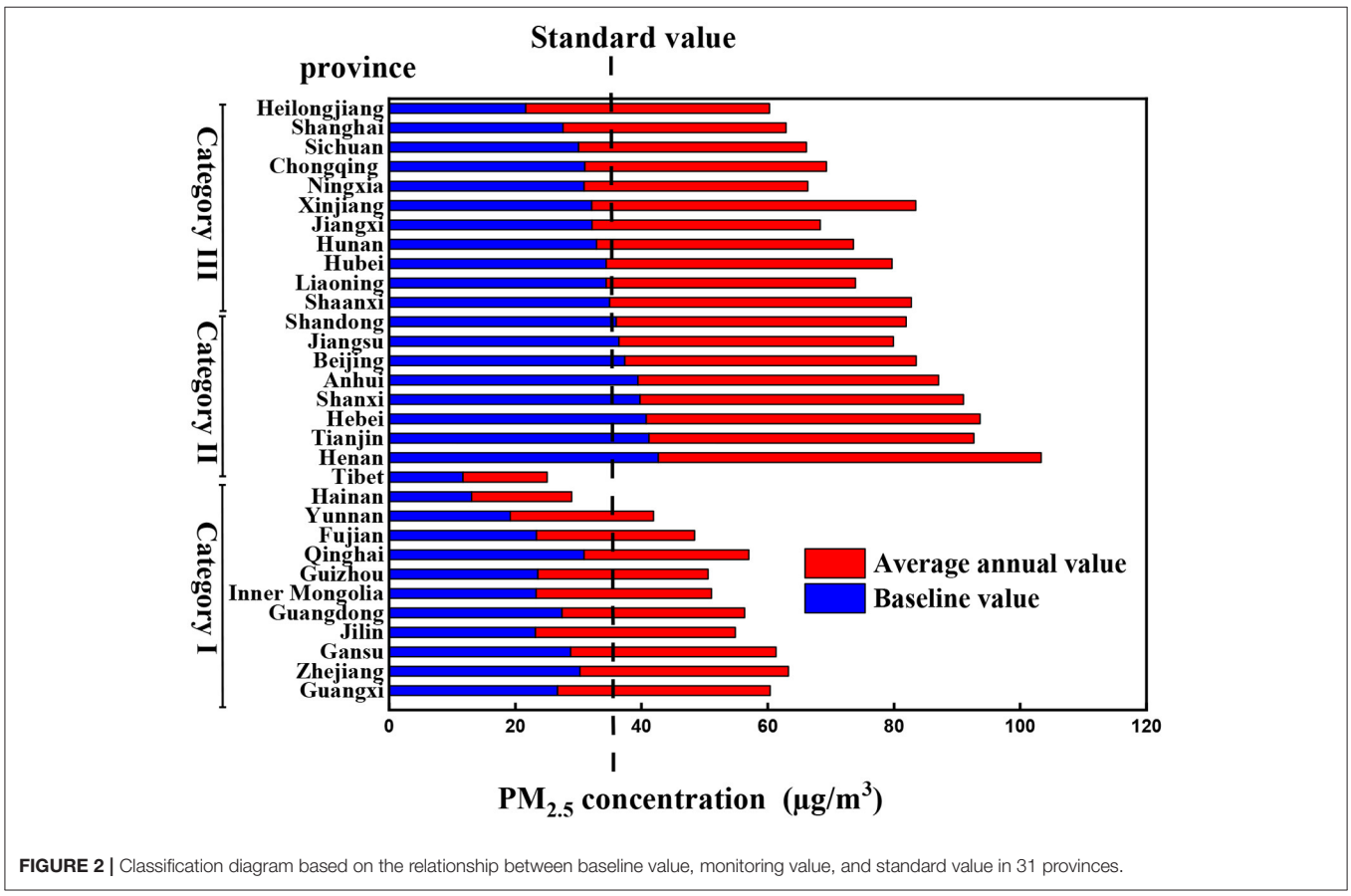

FIGURE 2 | Classification diagram based on the relationship between baseline value, monitoring value, and standard value in 31 provinces.

value and baseline value of the first category of provinces are all lower than the standard value. While these provinces continue to maintain this state, they can further move closer to the baseline value and strive to minimize the emission of $PM_{2.5}$. The baseline value and monitoring value of the second category of provinces are higher than the standard

value. Provinces in this category can implement "step-by-step" measures that are first reduced to the baseline value and then reduced to the standard value. The baseline value for the third category of provinces is lower than the standard value, while the monitoring value is higher. These provinces can first reduce the emission of $PM_{2.5}$ to the national standard and then strive to promote the development of a green and high-quality economy to reduce the emission of $PM_{2.5}$ further to reach the baseline value.

DATA AVAILABILITY STATEMENT

The original contributions presented in the study are publicly available. This data can be found here: https://doi.org/10.6084/m9.figshare.19779688.v1.

AUTHOR CONTRIBUTIONS

DJ and SK structured and wrote the manuscript. CO and SK analyzed the data and contributed with descriptive analysis. FL and AC reviewed the manuscript. All authors contributed to manuscript revision, read, and approved the submitted version.

FUNDING

This study was funded by the National Natural Science Foundation of China (51879105), Hubei Provincial Outstanding Young Science and Technology Innovation Team Project (T2021032), and Fundamental Research Funds for the Central Universities from Zhongnan University of Economics and Law (2722021AJ007, 202151414, 202151408).

REFERENCES

1. Maji KJ, Arora M, Dikshit AK. Premature mortality attributable to $PM_{2.5}$ exposure and future policy roadmap for "air apocalypse" affected Asian megacities. *Process Safe Environ*. (2018) 118:371–83. doi: 10.1016/j.psep.2018.07.009
2. Zhou Z, Tan ZB, Yu XH, Zhang RT, Wei YM, Zhang MJ, et al. The health benefits and economic effects of cooperative $PM_{2.5}$ control: a cost-effectiveness game model. *J Clean Prod*. (2019) 228:1572–85. doi: 10.1016/j.jclepro.2019.04.381
3. Chen XY, Li F, Zhang JD, Zhou W, Wang XY, Fu HJ. Spatiotemporal mapping and multiple driving forces identifying $PM_{2.5}$ variation and its joint management strategies across China. *J Clean Prod*. (2020) 250:119–534. doi: 10.1016/j.jclepro.2019.119534
4. Li JC, Gao QX, Li L, Zheng YF, Gao WK. Enlightenment and suggestions on the air quality of Beijing Tianjin and Hebei were revealed by primary pollutants. *Res Environ Sci*. (2018) 31:1651–61. doi: 10.13198/j.issn/1001-6929.2018.07.07
5. Fan H, Zhao CF, Yang YK, Yang XC. Spatio-temporal variations of the $PM_{2.5}/PM_{10}$ ratios and its application to air pollution type classification in China. *Front Environ Sci*. (2021) 9:218. doi: 10.3389/fenvs.2021.692440
6. An Z, Huang RJ, Zhang R, Tie X, Li G, Cao J, et al. Severe haze in Northern China: a synergy of anthropogenic emissions and atmospheric processes. *Proc Natl Acad USA*. (2019) 116:8657–66. doi: 10.1073/pnas.1900125116
7. Chen R, Yang C, Li P, Wang JW, Liang Z, Wang WZ, et al. Long-term exposure to ambient $PM_{2.5}$ sunlight and obesity: a nationwide study in China. *Front Endocrinol*. (2021) 12:790294. doi: 10.3389/fendo.2021.790294
8. Mao LX, Wang L, Pan X, Zhang M, Wu X, Zhang W. A study on the dynamic spatial spillover effect of urban form on $PM_{2.5}$ concentration at county scale in China. *Atmos Res*. (2022) 269:2022269. doi: 10.1016/j.atmosres.2022.106046
9. Zhang YH, Yang XY, Cheng H, Zhang LH, Zhao AM, Zhou CY, et al. Remote sensing monitoring and analysis of $PM_{2.5}$ and NO_2 concentration changes in China and key regions in the first quarter of 2018–2020. In: *Proceedings of the Annual Conference of Science and Technology of the Chinese Society of Environmental Sciences (Volume I)*. Nanjing (2020). p. 1239–44.
10. Yue H, He C, Huang Q, Yin D, Bryan BA. The stronger policy is required to substantially reduce deaths from $PM_{2.5}$ pollution in China. *Nat Commun*. (2020) 11:1–10. doi: 10.1038/s41467-020-15319-4
11. Chen J, Zhou CS, Wang SJ, Hu JC. Identifying the socioeconomic determinants of population exposure to particulate matter ($PM_{2.5}$) in China using geographically weighted regression modeling. *Environ Pollut*. (2018) 241:494–503. doi: 10.1016/j.envpol.2018.05.083
12. Wang JY, Wang SJ, Li SJ. Examining the spatially varying effects of factors on $PM_{2.5}$ concentrations in Chinese cities using geographically weighted 34 regression modeling. *Environ Pollut*. (2019) 248:792–803. doi: 10.1016/j.envpol.2019.02.081
13. Darnley A G. A global geochemical reference network: the foundation for geochemical baselines. *J Geochem Explor*. (1997) 60:1–5. doi: 10.1016/S0375-6742(97)00020-4
14. Xuan H, Teng YG, Ni SJ, Wang JS, Zhang CJ. Potential ecological risk assessment on heavy metal in the soil of indexing area based on the geochemical baseline. *Mineral Rock*. (2005) 4: 69–72. doi: 10.19719/j.cnki.1001-6872.2005.04.011
15. Teng YG, Ni SJ. *Theory and Practice of Geochemical Baseline*. Beijing: Chemical Industry Press (2007).
16. Bauer I, Bor J. Lithogene, geogene und anthropogene Schwermetallgehalte von Lößböden an den Beispielen von Cu, Zn, Ni, Pb, Hg und Cd. *Mainzer Geowiss Mitt*. (1995) 24:47–70.
17. Wei CY, Wen HL. Geochemical baselines of heavy metals in the sediments of two large freshwater lakes in China: implications for contamination character and history. *Environ Geochem Health*. (2012) 34:737–48. doi: 10.1007/s10653-012-9492-9

Conflict of Interest: The authors declare that the research was conducted in the absence of any commercial or financial relationships that could be construed as a potential conflict of interest.

Advantages of publishing in Frontiers

OPEN ACCESS
Articles are free to read for greatest visibility and readership

FAST PUBLICATION
Around 90 days from submission to decision

HIGH QUALITY PEER-REVIEW
Rigorous, collaborative, and constructive peer-review

TRANSPARENT PEER-REVIEW
Editors and reviewers acknowledged by name on published articles

Frontiers
Avenue du Tribunal-Fédéral 34
1005 Lausanne | Switzerland

Visit us: www.frontiersin.org
Contact us: frontiersin.org/about/contact

REPRODUCIBILITY OF RESEARCH
Support open data and methods to enhance research reproducibility

DIGITAL PUBLISHING
Articles designed for optimal readership across devices

FOLLOW US
@frontiersin

IMPACT METRICS
Advanced article metrics track visibility across digital media

EXTENSIVE PROMOTION
Marketing and promotion of impactful research

LOOP RESEARCH NETWORK
Our network increases your article's readership